Generation of a CRHR1-specific *Cre*-driver mouse line to address CRH/CRHR1-related neurocircuits

von Claudia Kühne

Inaugural-Dissertation zur Erlangung der Doktorwürde der Tierärztlichen Fakultät der Ludwig-Maximilians-Universität München

Generation of a CRHR1-specific *Cre*-driver mouse line to address CRH/CRHR1-related neurocircuits

von Claudia Kühne

aus Neustadt/Aisch

München 2018

Aus dem Zentrum für Klinische Tiermedizin der Tierärztlichen
Fakultät der Ludwig-Maximilians-Universität München

Lehrstuhl für Allgemeine Pathologie

und Pathologische Anatomie

Arbeit angefertigt unter der Leitung von
Univ.-Prof. Dr. Kaspar Matiasek

Angefertigt am
Max-Planck-Institut für Psychiatrie, München
Mentor: Dr. Jan Deussing

Gedruckt mit Genehmigung der Tierärztlichen Fakultät

der Ludwig-Maximilians-Universität München

Dekan:	Univ.-Prof. Dr. Reinhard K. Straubinger, Ph.D.
Berichterstatter:	Univ.-Prof. Dr. Kaspar Matiasek
Korreferent/en:	Priv.-Doz. Dr. Ivica Međugorac
	Univ.-Prof. Dr. Eckhard Wolf
	Univ.-Prof. Dr. Bernd Kaspers
	Univ.-Prof. Dr. Hermann Ammer

Tag der Promotion:

27.Juli 2018

To my parents

Parts of the presented results have been published:

Kühne C, Puk O, Graw J, Hrabě de Angelis M, Schütz G, Wurst W, Deussing JM. *Visualizing corticotropin-releasing hormone receptor type 1 expression and neuronal connectivities in the mouse using a novel multifunctional allele*. J Comp Neurol. 2012 Oct 1;520(14):3150-80.

Dedic N, Kühne C, Jakovcevski M, Hartmann J, Genewsky AJ, Gomes KS, Anderzhanova E, Pöhlmann ML, Chang S, Kolarz A, Vogl AM, Dine J, Metzger MW, Schmid B, Almada RC, Ressler KJ, Wotjak CT, Grinevich V, Chen A, Schmidt MV, Wurst W, Refojo D, Deussing JM. *Chronic CRH depletion from GABAergic, long-range projection neurons in the extended amygdala reduces dopamine release and increases anxiety*. Nat Neurosci. 2018 Jun;21(6):803-807.

Table of Contents

List of Abbreviations

3V	third ventrile
4V	fourth ventricle
7	nucleus facialis
12	nucleus hypoglossus
AAV	adeno-associated virus
AC	adenylyl cyclase
Aca	anterior commissure
AcbC	nucleus accumbens core
AcbSh	nucleus accumbens shell
ACTH	adrenocorticotropic hormone
Amb	nucleus ambiguus
AON	nucleus olfactorius anterior
AP	area postrema
Apit	anterior pituitary
ARH	arcuate nucleus
ATP	adenosine triphosphate
AVP	arginine vasopressin
Bar	Barrington's nucleus
BLA	basolateral amygdaloid nucleus
BNST	bed nucleus of the stria terminalis
CA1	field CA1 of hippocampus
CA2	field CA2 of hippocampus
CA3	field CA3 of hippocampus
cAMP	cyclic adenosine monophosphate
cc	corpus callosum
CeA	central amygdala
Cereb	cerebellum
cg	cingulate cortex
CingCx	cingulate cortex
Cl	claustrum
Cpu	caudate putamen (striatum)
CREB	cAMP response element
CRF	corticotropin releasing factor
CRH	corticotropin releasing hormone
Ctx	cortex
DA	dopamine
DAG	diacylglycerine
DEPC	diethylpyrocarbonate
DG	dentate gyrus
DGPo	polymorph layer dentate gyrus
DR	dorsal raphe nucleus
Ec	external capsule
Ect	ectorhinal cortex
Ent	entorhinal cortex
ERK	extracellular signal-regulated kinase
FSC	frontal-subcortical circuits
GABA	γ-aminobutyric acid
GAD	glutamic acid decarboxylase
Gcc	genu of corpus callosum
Gl	glomerular layer of the olfactory bulb
GP	globus pallidus
gr	granule layer, cerebellum
GR	glucocorticoid receptor
GRK	G protein-coupled kinase
GrO	granule cell layer of the olfactory bulb
Hyg	hygromycin
HPA	hypothalamic-pituitary-adrenal axis
IC	internal capsule
ICV	intracerebroventricular
IF	interfascicular nucleus
INL	inner nuclear layer
IP3	inositol 1, 4, 5-triphosphate
IPL	inner plexiform layer
IRES	internal ribosomal entry site
ISO	isocortex
LC	locus coeruleus
LDTg	laterodorsal tegmental nucleus
LHA	lateral hypothalamic area
LHB	lateral habenula
LS	lateral septal nucleus
LV	lateral ventricle
MD	mediodorsal thalamic nucleus
MeA	medial amygdaloid nucleus
Mfb	medial forebrain bundle
MG	medial geniculate nucleus
Mi	mitral cell layer of the olfactory bulb
Mlf	medial longitudinal fasciculus
MM	medial mammillary nucleus
mol	molecular layer, cerebellum
MPB	medial parabrachial nucleus
NA	noradrenaline
NAc	nucleus accumbens
Neo	neomycin
NS	nigrostriatal bundle
NT	neurotransmitter
NTS	nucleus solitary tract
OB	olfactory bulb
ON	overnight
opt	optic tract
OT	olfactory tubercle
P	Purkinje cell
PAG	periaqueductal grey
PBP	parabrachial pigmented nucleus
PFC	prefrontal cortex
PG	pontine grey
PIF	parainterfascicular nucleus

PIP2	phosphatidylinositol-bisphosphate
Pir	piriform cortex
PKA	protein kinase A
PKC	protein kinase C
PLC	phospholipase C
PN	paranigral nucleus
POMC	pro-opiomelanocortin
PP	perforant path
PVN	paraventricular nucleus
Py	pyramidal cell layer
RMC	red nucleus, magnocellular part
RMCE	recombinase mediated cassette exchange
Rt	reticular thalamic nucleus
RT	room temperature
scp	superior cerebellar peduncle
SNC	substantia nigra, compact part
SNR	substantia nigra, reticular part
SSR	site specific recombinase
TH	tyrosine hydroxylase
Tu	olfactory tubercle
UCN	urocortin
VLUT	vesicular glutamate transporter
VP	ventral pallidum
VTA	ventral tegmental area

1 Introduction

All living organisms depend on adapting to changing environmental demands. The body's ability to maintain a complex equilibrium, also referred to as "Homeostasis" is essential for survival (*1*). The challenge of homeostasis by internal or external factors is referred to as "stress", which leads to different adaptive physiological reactions in an organism (*2*). This so called "stress response" encompasses neuroendocrine (activation of the hypothalamic-pituitary-adrenal (HPA) axis), autonomic (increased cardiovascular and respiratory activity) and behavioral (arousal, defense/escape or "fight"-response) changes and aims to reconstitute the initial homeostasis by a process called allostasis, meaning achieving stability through physiological or behavioral change ("remaining stable by being variable") (*3*). Sustained over-activation of allostatic systems as well as failure to shut off or inadequate response of the system, referred to as "allostatic load" can lead to the development of stress-related psychopathologies such as anxiety and depression.

In vertebrates, the main stress response system is the brain (*4*), because it determines what is stressful and orchestrates the stress response via two coherent systems: the autonomic sympathetic nervous system (SNS) and the neuroendocrine hypothalamic-pituitary axis. Various molecules ("stress mediators") are released in response to stress, which comprise in particular monoamines, neuropeptides and steroids. Whereas neurotransmitters are important for the immediate ("fight-or-flight") response to the stressor, corticosteroids are responsible for promoting the adaptive components (*5*). The discovery of the neuropeptide corticotropin-releasing hormone (CRH) in 1981 by the group of Wylie Vale (*6*) was a major breakthrough for the understanding of the neurobiological mechanisms controlling the stress response. CRH plays a central role in coordinating the endocrine, autonomic and behavioral responses to stress. CRH displays a dual capacity acting as a secretagogue within the scope of the HPA system and as an important integrator of the stress response through modulating synaptic transmission in the central nervous system. The biological activity of CRH is predominantly mediated via CRH receptor type 1 (CRHR1), a G-protein coupled, 7-transmembrane receptor, which is widely expressed in various brain structures, where it integrates the processing of sensory information and motor control and in the pituitary where it mediates the release of adrenocorticotropic hormone (ACTH) subsequent to binding of CRH. Numerous

pharmacological and genetic studies published during the last decades clearly support a causative role of CRH/CRHR1 overactivation in stress-related psychiatric disorders and led to the development of CRHR1 antagonists for the treatment of chronic anxiety disorders and depression. Up to now – although anxiolytic and antidepressant effects were reported in animal experiments and human clinical trials - none of these compounds has successfully passed all clinical trials and therefore failed to reach market maturity (*7*). These discrepancies could potentially be related to a lack of consideration of the dimension of circuit- and cell-type specificity regarding CRH/CRHR1-mediated modulation of the stress response. Multiple interconnected brain regions, such as hippocampus, prefrontal cortex, amygdala and ventral tegmental area (VTA) are associated with stress-related pathophysiology and functional impairment/imbalance can independently develop in distinct neuroanatomical circuits, resulting in subsequent dysfunction of other brain regions/circuits. Moreover, recent findings suggesting that the net effect of CRHR1 activation depends on cell-type specific receptor-neurotransmitter interactions, adds another level of complexity (*8*).

In the past decades the molecular and genetic “toolbox” targeting CRH system components has evolved rapidly and genetic dissection of the CRH system via conventional and conditional gene targeting approaches in the mouse has increased our understanding of CRH/CRHR1 function within the line of the organism's stress response and furthermore revealed bidirectional CRH/CRHR1 neurocircuitries which are relevant for adaptive emotional behavior in response to stress (*9*). The future challenge is to unravel the distinct pathways, cell-types and molecular mechanisms by which the CRH/CRHR1-system translates stressful stimuli into the final adaptive and maladaptive behavioral response. Gene-specific promoter driven *Cre* mouse lines provide experimental access to specific cell types and neuronal populations that are the basic units of neural circuits. Therefore, we aimed to generate a CRHR1 *Cre*-driver mouse line, which will complement the existing genetic tools and facilitate further dissection of CRH/CRHR1 related neurocircuits, cell-types and downstream molecular pathways.

2 Literature

2.1 The central CRH system and neuropathology of stress

According to the latest estimates by the World Health Organization (WHO), neuropsychiatric disorders including depression, bipolar affective disorder, schizophrenia, dementia, anxiety disorders and epilepsy, are leading courses of disability worldwide with devastating social and economic consequences. Mental, neurological and substance use disorders account for 13% of the total global burden of disease with anxiety and depressive disorders being among the single largest contributors to disability worldwide (World Health Organization, 2015) (*10*). A large amount of basic and clinical studies link dysregulation of the HPA stress axis and hyperactive/imbalanced corticotropin-releasing hormone (CRH) circuits within the hippocampus, nucleus accumbens, lateral septum, bed nucleus of stria terminalis, amygdala and VTA to the pathophysiology of stress-related mood disorders such as major depressive disorder or bipolar disorder (*10*-*16*).

The physician and endocrinologist Hans Selye first defined the term stress in 1936 as a nonspecific response of the body to any internal or external demand threatening homeostasis. He was also the first who described the system through which the body copes with stress, the HPA axis (*2, 17*). The key structures of the HPA axis are the paraventricular nucleus of the hypothalamus (PVN) which contains neuroendocrine, hypophyseotropic neurons that synthesize and secrete CRH, the anterior lobe of the pituitary and the adrenal glands. Under normal, unstressed conditions the HPA axis coordinates diurnal events (sleep/wake activity, food intake) resulting in a peak of glucocorticoid hormone secretion at the onset of the diurnal activity period. In response to physical or psychological stimuli (this expression contains the awareness that not all impulses that activate the HPA axis are considered as stressful, e.g., appetitive/rewarding stimuli, sexual encounter), CRH, also known as corticotropin-releasing factor (CRF), synthesized in neurons of the parvocellular subdivision of the PVN, is released from neurosecretory nerve terminals into hypophyseal portal vessels that access the anterior pituitary. Binding of CRH to its corresponding CRHR1, stimulates the synthesis and release of adrenocorticotropic hormone (ACTH) into the systemic circulation. ACTH reaches the adrenal glands via the central blood flow where it binds to its specific receptor in the zona fasciculata of the adrenal cortex. ACTH stimulation leads to the synthesis and release of

glucocorticoids (cortisol in humans, corticosterone in rodents; peaking 15-30 minutes after onset of acute stress) into the blood circulation. Glucocorticoids are the downstream effectors of the HPA axis that mediate an array of physiological and metabolic effects to prepare the organism for acute reactions to the stressor, e.g., increasing cardiovascular tone, energy mobilization, anti-inflammatory properties, inhibition of digestion and reproduction (*18-21*). In order to restore the HPA axis or prevent excessive activation, e.g., of the cardiovascular, immune and gastrointestinal organ system, autoregulatory feedback mechanisms occur at several sites of the axis in the brain and pituitary, thereby inhibiting secretion of CRH and ACTH. The negative feedback is mediated by the glucocorticoid (GR) and the mineralocorticoid receptor (MR) which are widely expressed in stress-responsive brain regions, with the PVN and hippocampus being of particular importance (*22*). Glucocorticoids inhibit the mRNA expression of CRH and vasopressin in the PVN via binding to the glucocorticoid receptors being expressed on the peptide–synthesizing neurons themselves (*23*). Additionally, as both receptors are highly expressed in the hippocampus, there is considerable evidence that this brain structure inhibits basal and stress induced HPA axis activity (*24*). Negative feedback on basal and induced ACTH secretion occurs also at the level of the adenohypophysis where glucocorticoids decrease levels of mRNA encoding for the ACTH precursor protein pro-opiomelanocortin (POMC) (*25*). Dysfunction of the HPA system resulting in increased ACTH and cortisol levels is by far the most robust finding in patients with major depression (*13*). Long lasting HPA axis hyperactivity/dysregulation can lead to cortisol-mediated epigenetic modifications of the glucocorticoid receptor, permanent morphological changes in the hippocampus and abnormalities in neuroplasticity and neurogenesis (*26*). Thus, the integrity of the HPA axis is critical to restore or maintain homeostasis and inadequate or excessive activation can lead to a wide array of stress-related disorders including autoimmune disease (*27*), hypertension, anxiety and affective disorders such as major depression (Figure 1). In addition to its role as main physiological regulators of basal and stress-induced HPA axis activity it was shown that CRH and CRH receptor 1 are widely expressed in many extrahypothalamic sites of the brain including the limbic system, the mesencephalic dopamine system and the locus coeruleus/noradrenaline (LC/NA) system in the brainstem (*8, 28-30*). CRH/CRHR1 modulate synaptic transmission via interacting with central neurotransmitters affecting their excitatory and inhibitory activity and

thereby mediate the behavioral and autonomic components of the stress response. Numerous animal studies revealed that intracerebroventricular (icv) administration of CRH results in increased anxiety-like behavior, arousal, altered locomotor activity, decreased food consumption, sleep disturbances and declined sexual behavior-just to name a few. These behavioral responses mimic those observed when an animal faces a stressor. It is important to mention that most of these behavioral effects are also present after hypophysectomy and are thus mediated by central CRH controlled pathways and are independent of HPA-axis activation (*31*). Many studies in humans point to centrally hyperactive CRH neurons and impaired negative glucocorticoid-mediated feedback loops in neuropathologies associated with stress (*14, 32-34*).

The core effectors within the stress system are highly interconnected and comprise the hypothalamic hormones arginine vasopressin (AVP), CRH and NA within the locus coeruleus in the brainstem and other noradrenergic cell groups within the central autonomic/sympathetic nervous system. The targets of these stress mediators are downstream systems such as the cognitive, fear, reward, gastrointestinal, metabolic, immune, cardiorespiratory and reproductive systems as well as the wake-sleep centers of the brain. In general neural pathways mediating arousal, alertness and cognition are promoted whereas more vegetative pathways such as feeding, reproduction and immunity are inhibited (*35*). The AVP/CRH and LC/NA “control centers” of the stress system are connected in a reciprocal positive feedback loop, for example, activation of one system in parallel activates the other as well. Furthermore, other excitatory and inhibitory pathways are able to activate both systems. For example, visceral and somatic stress stimuli (catecholaminergic/noradrenergic afferents from the sympathetic and parasympathetic nervous system) are integrated in the so-called “central autonomic network” including hypothalamic nuclei such as the PVN, the lateral hypothalamic area and the mammillary nucleus as well as extrahypothalamic structures like the LC and the raphe nuclei. Discharged LC neurons activate the peripheral sympathetic nervous system, which is responsible for the autonomic component of the stress response, such as increase in heart rate, increased blood pressure and respiratory rate, increased gluconeogenesis and lipolysis. In addition, studies have shown that CRH-containing terminals arising from the PVN (distinct from those projecting to the median eminence and initiating the HPA axis response), bed nucleus of stria terminals (BNST), Barrington’s nucleus and the central nucleus of the amygdala

synapse on noradrenergic LC neurons and that locally administered CRH increases the firing rate of LC neurons, increases c-fos expression and noradrenaline release in LC projection target sites (*36*) such as the forebrain, cortex and hippocampus. Given the roles of these areas in cognitive and memory consolidation functions, these neurocircuits may be involved in facilitating spontaneous and/or intuitive behavioral responses to stressful stimuli. Dysregulated noradrenaline circuits have been associated with cognitive and sensory signal-processing deficits that have been found in schizophrenia, dementia, Alzheimer's and Parkinson's disease, as well as stress-related disorders such as depression and anxiety (*37*). In this context, it is worth mentioning that some of the current drugs used to treat depression and anxiety disorders target the noradrenergic system (noradrenaline reuptake inhibitors; NRIs).

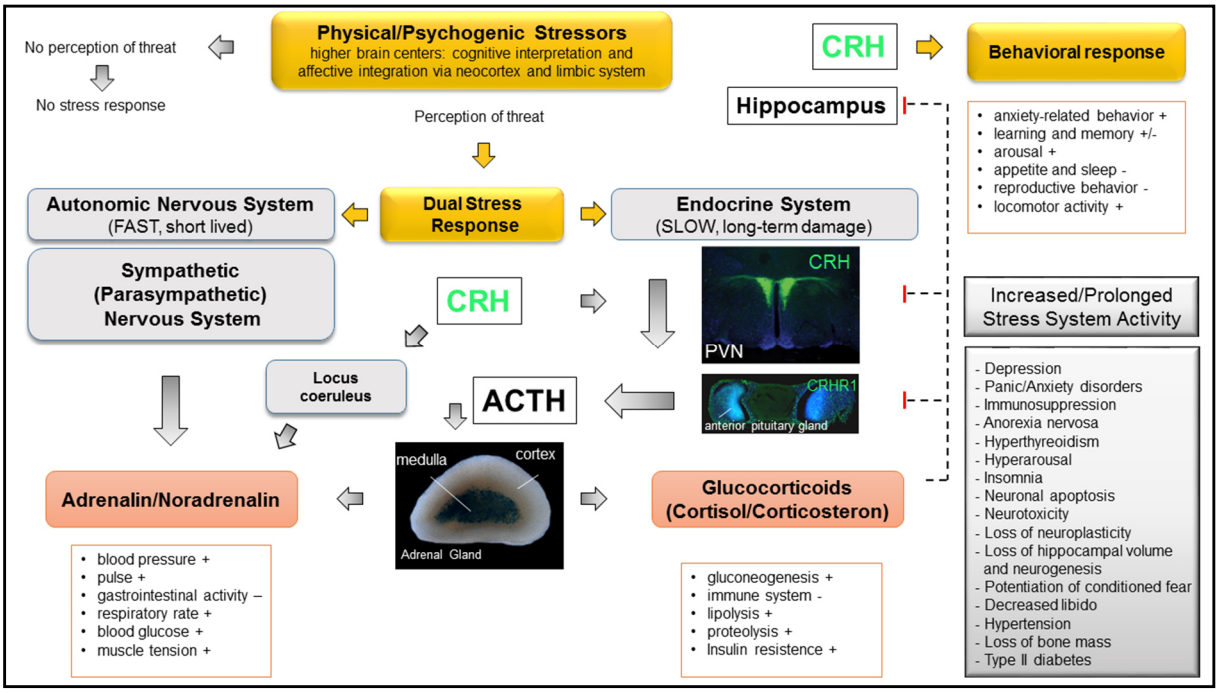

Figure 1: CRH mediates endocrine, autonomic and behavioral adaptational responses to stress

Simplified schematic illustration of the dual stress response and the role of CRH as a secretagogue within the line of the HPA axis and as a central neuromodulator. For details, see text. Pictures depict reporter gene expression in the PVN of *Crh-IRES-Cre* mice crossed with *GFP* reporter mice and in the pituitary of *CRHR1*^{Cre} mice crossed with *Sun1 sfGFP* reporter mice. Transversal view of an X-Gal stained adrenal gland from *R26R*^{NatCre} mice with reporter gene expression in noradrenaline transporter expressing cells of the adrenal medulla.

Other extrahypothalamic brain sites and pathways that are activated during stress challenges include the mesocortical and mesolimbic dopamine system, which links the VTA to the prefrontal cortex, the nucleus accumbens and the extended

amygdala/hippocampus circuit, the latter being involved in the generation of fear/anxiety (amygdala) and memory consolidation (hippocampus). The hippocampus was the first brain structure beside the hypothalamus to be recognized as stress responsive and the effects of CRH on hippocampal function (learning and memory processes) and neuronal structure has been subject of numerous investigations in recent years (*38, 39*). Generally speaking, it is not surprising that stress modulates hippocampal function since remembering and learning from critical life events entails an evolutionary advantage. CRH expression in the hippocampus is well established- it is expressed in a subset of GABAergic interneurons within the pyramidal cell layers of areas CA1 and CA3 as well as in strata radiatum and oriens and in the dentate gyrus hilar region (*40*). The corresponding receptor (CRHR1) is mainly expressed on excitatory glutamatergic pyramidal cells and on dentate hilar mossy cells (*29, 41*). Based on electrophysiological *ex vivo* studies it was demonstrated that CRH, via CRHR1 amplifies neuronal excitation on its passage from the dentate gyrus to the CA1 field and modulates voltage-gated ion currents thereby increasing excitability of CRHR1 expressing CA1 pyramidal neurons (*42, 43*). Furthermore, the MR and GR receptors for adrenal steroids are highly expressed in all hippocampal subfields (CA1, CA2, CA3) including the dentate gyrus and subiculum (*44*). *In situ* hybridization studies revealed increased hippocampal *Crh* mRNA expression after stressful stimuli (*45*) and it depends on time and severity how stress influences hippocampal function and structure. CRH-induced acute activation of principal neurons augment memory and related cellular processes whereas prolonged and repeated exposure to elevated CRH levels results in dendritic spine atrophy and reduced synaptic plasticity which causes learning deficits and cognitive decline (*40, 46-48*). There is a striking spatial difference regarding long-term potentiation (the cellular correlate of synaptic strength and learning and memory, respectively): acute stress causes facilitation of LTP in the ventral hippocampus and the opposite (depression of LTP) in the dorsal hippocampus. As the hippocampus is interconnected with a variety of different brain structures this spatial bidirectionality may underlie the selective stress dependent routing, e.g., facilitation of the efferent output from the ventral hippocampus to the amygdala versus suppression of the dorsal connectivity to the cortex. (*49*). Neuroimaging studies in patients with stress-related disorders such as major depression have shown volume reduction (reduction in neuropil) in various subfields of the hippocampus and in the posterior division,

respectively, which is virtually connected to poor memory performance - one of the main impairments in cognitive function of depressed patients (*50*). Furthermore, many studies revealed stress-mediated suppressed hippocampal neurogenesis and neuronal differentiation of progenitor cells in the hippocampus (*51*). CRH is expressed in the neurogenic hippocampal granular zone and *in vitro* as well as *in vivo* studies provide evidence that CRH through its receptor CRHR1 is implicated in neurogenesis and has the potential for neuroprotection regarding the damaging effects of glucocorticoids on neuronal progenitor cells (*52, 53*).

Within the central amygdala (CeA) and the bed nucleus of the stria terminalis (BNST) *Crh* mRNA is upregulated after exposure to stress (*48*). A number of studies in rodents and humans demonstrate that both highly connected brain regions form a functional interrelated circuit that plays a key role in integrating potentially threat-relevant information, as well as in acquisition of fear memory and promotion of feelings of fear and anxiety (*54-57*). At this point it is essential to mention that in the literature there is no uniform classification of the terms fear and anxiety as well as of the underlying brain circuits (*58*). An early working model by Davis and colleagues supports the view that fear (here defined as stimulus–specific short-term response) and anxiety (here defined as stimulus-unspecific sustained type of response) are mediated independently (fear-CeA vs anxiety-BNST) (*59*). Later on this hypothesis was further refined: the CeA mediates immediate (“phasic”) responses (phasic fear) to threats via projections originating in the medial part of the CeA (CeA_M) to the hypothalamus and brainstem, whereas projections from the lateral part (CeA_L) to the BNST are responsible for the sustained responses (sustained fear) to diffuse/less predictable cues (*60*). Recently, Shackman and colleagues reviewed latest studies of rodents, monkeys and humans and provide new insights, which are in contrast to the earlier hypotheses: both, the CeA and BNST integrate aversive challenges and play an important role in the development of states of fear and anxiety. (*57*).

CRH is highly expressed in the lateral part of the central amygdala where it mediates contextual fear memory (*61*) and facilitates conditioned fear acquisition at low threat levels via the CRHR1 (*62*). Site-specific genetic manipulation of CRH in the CeA via lentiviral-based knockdown or overexpression revealed stress-induced effects on anxiety-like behaviors as well as the impact of CeA CRH on regulating basal HPA axis activity (higher levels of basal plasma corticosterone in CRH knockdown

animals) (*63-65*). There is considerable evidence from human studies that link altered amygdala function to anxiety disorders and that treatment with anxiolytics reduces activation of the amygdala in a dose-dependent manner (*66, 67*)

Beside the amygdala a region often referred to as “extended” amygdala, the bed nucleus of the stria terminalis, has garnered attention with regard to stress response, anxiety and addiction, the latter being highly comorbid with psychiatric disorders. As the BNST is interconnected with stress responsive brain regions like amygdala, hippocampus, hypothalamus and brain reward centers such as the nucleus accumbens shell and VTA, it represents a central node in both fear and reward neurocircuitries (*68*). CRH is highly expressed in the dorsal (oval nucleus) and ventral (fusiform nucleus) subdivisions of the BNST (*69, 70*) and immunohistochemistry studies in adult mice revealed the GABAergic identity of these neurons (*71*). Stressful stimuli increase CRH expression within the dorsolateral and ventrolateral subdivisions of the BNST and lentiviral-mediated chronic over-expression of CRH within BNST neurons (thereby mimicking a state of physiologically CRH hyperactivity) modulates conditioned anxiety-like behaviors and decreases CRHR1 receptor density probably by altering CRH signaling cascades in local BNST microcircuits (*72*). The fear-potentiated startle response in humans (modeling conditioned anxiety in rodents) is selectively enhanced in post-traumatic stress patients and patients with panic disorders and is sensitive to treatment with benzodiazepines and SSRIs (selective serotonin reuptake inhibitors) (*60*). More recent studies revealed the possibility of two stress-related opposing circuits (anxiogenic and anxiolytic) within the BNST. Stress and drug abuse can upset the balance of these distinct pathways towards a pathological state (*73*). Recently, a BNST-VTA CRH circuit was described which controls binge ethanol consumption in mice via signaling at the CRHR1 within the VTA (*74*). Latest findings from human studies based on ultra-high resolution magnetic resonance imaging (7T fMRI) provide evidence for the involvement of the BNST in both stress-related illnesses namely anxiety disorders and addiction (*75*). Temporally-extended threat monitoring processes in more highly trait anxious individuals are mediated by an exaggerated response of the BNST (*76*). Patients with spider phobia display elevated BNST activity (*77*) and functional MRI scans in patients with generalized anxiety disorders showed increased activity in the BNST during conditions of uncertainty (*78*). Alcoholic patients exhibit increased functional neural connectivity between amygdala

and BNST which may contribute to stress-induced relapse (*79*). Deep brain stimulation of the BNST has turned out to be a promising treatment for obsessive-compulsive disorders (OCD) (*80*). In the recent past, the BNST has gained attention as treatment target for anxiety and addiction due to its bidirectional connectivity with the VTA (the key node within the brain's reward system) and the significant co-morbidity between mood/anxiety disorders and substance use disorders.

Historically the HPA axis and the LC-noradrenaline system were the main brain networks that have been in focus studying the stress response, whereas the dopamine (DA) system was considered as the drug-and natural-reward circuit of the brain. Over the past few years, numerous studies clearly demonstrated that also acute and repeated stress and aversive events activate dopaminergic neurons within the mesocorticolimbic pathway and can induce neuroadaptations resulting in intensified neuronal responses to later aversive and rewarding stimuli (*81, 82*). Dysregulation in dopaminergic neurocircuitries has been linked to many psychiatric and neurological disorders such as Parkinson's disease, schizophrenia, drug abuse and depression. It is hypothesized that the origin of pathology lies within the complex afferent modulation of neuronal activity in this brain region (*83*). The VTA and substantia nigra pars compacta (SNC) include a group of adjacent neurons located in the ventral midbrain that represent the majority of dopaminergic cell bodies in the brain and the origin of the mesocorticolimbic circuit and other dopamine pathways. Initially, electrophysiological and behavioral studies have led to the conclusion that these DA neurons constitute a homogenous neuronal population which is uniformly activated by natural (e.g., food, sex, social interactions) and artificial rewarding (e.g., drug abuse), as well as reinforcing processes or reward-predictive cues (*84*). Several studies called this simplified acceptance into question as it was shown that dopamine neurons are potently excited in response to aversive stimuli and stressful events. For example, stress stimulates the release of CRH into the VTA and leads to increased dopamine neuron firing via CRHR1 dependent activation of the PLC–PKC signaling pathway (*85*). In addition, physical/psychological stress induces dopamine release in VTA projecting regions such as striatum, nucleus accumbens and medial frontal cortex (*86, 87*). The implementation of technical advances in optogenetics, mouse genetics and viral-mediated tracing techniques in combination with behavioral studies enable the dissection of neuronal cell types and connectivities within the midbrain dopaminergic system with unprecedented precision. Neurons within the VTA differ in

their cytoarchitecture, dopaminergic content, electrophysiological properties and connectivity within the reward circuitry (*88*). The VTA is made up of a mixture of ~70% dopaminergic (identified by the expression of tyrosine hydroxylase protein), but also ~30% γ-aminobutyric-acid (GABA) neurons (specified by their expression of glutamic acid decarboxylase (GAD) 65 or 67 mRNA or vesicular GABA transporter (VGAT) mRNA) and a small population (~2-3%) of glutamatergic neurons (expressing the vesicular glutamate transporters (VGLUTs) mRNA). Moreover, subpopulations of VTA neurons were identified which are capable of releasing two neurotransmitters (DA and GABA, or DA and glutamate) and it seems likely that this multiplexed neurotransmission underlies heterogeneous responses of distinct VTA neurons (*89, 90*). Furthermore, the rostral and caudal subnuclei of the VTA possess clear topographical differences with respect to connectivities and behavioral outputs (*91*). One potential mediator that links the brain reward and stress system is CRH and its receptors CRHR1/CRHR2. Recently Grieder and colleagues could identify a subpopulation of dopaminergic neurons in rodents and humans (highest density in the posterior VTA) that express CRH which is released after chronic exposure to nicotine and blocks nicotine-induced activation of GABAergic input onto dopaminergic neurons via the CRHR1 (*92*). *In vivo* microdialysis demonstrated dynamic extracellular CRH changes in different subregions of the VTA during acute and repeated stress, which promotes increased cocaine taking and -seeking (*88*). These results demonstrate that the two systems (Dopamine and CRH) interact with each other in the VTA and that CRH is able to modulate dopaminergic neurotransmission. With regard to the drug addiction field, it is hypothesized that the brain stress system impacts key elements of the addiction cycle, particularly in the withdrawal state. Drug abuse may sensitize the dopaminergic system to the actions of CRH and continuous cycles of drug abuse/withdrawal lead to hyperactivation of the CRH/CRHR1 system, which provokes a negative emotional state that predominates the acute positive hedonic effect of drug abuse (pleasure, contentment). This allostatic load is then responsible for the transition to drug dependence and relapse because the drug abuse alleviates the CRH/CRHR1-mediated counter regulatory negative emotional symptoms of withdrawal (*93, 94*).

In recent years, several studies linked the brain's reward regions to mood disorders such as depression and anxiety, partly because of the fact that most depressed patients exhibit anhedonia (reduced ability to feel pleasure), appetite disturbances

and loss of motivation - core symptoms that involve alterations in reward signaling (*95*). Studies in mice using viral mediated locally overexpression of a dominant negative mutant K^+ channel - thereby exciting all VTA neurons regardless of projection or cell-type - resulted in social defeat stress-induced social avoidance and anhedonia and point towards the involvement of hyperactive dopaminergic neurons in stress-induced behavioral pathology (*96*). By using circuit-specific optogenetic tools Chaudhury and colleagues could demonstrate that increased phasic firing of dopaminergic VTA-nucleus accumbens (NAc) projecting neurons mediates stress susceptibility (*97*). Other studies indicate a possible bidirectional role of VTA dopamine neurons in the stress response, depending on the strength and nature of the stressor. For example, chronic cold stress (a relative mild stressor compared to above mentioned social defeat stress) decreases the activity of dopaminergic neurons in the VTA in contrast to restraint stress that increases DA neuron activity (*98*). Cell-type specific genetic deletion of CRHR1 in midbrain dopaminergic neurons increases anxiety-like behavior and reduces dopamine release in the prefrontal cortex, suggesting an anxiolytic role for CRHR1 in this specific neuronal subpopulation (*99*). Dedic and colleagues identified a subset of CRH expressing GABAergic BNST-VTA projecting neurons that target the CRHR1 on dopaminergic neurons and modulate emotional behavior by positively regulating dopamine release (*100*). So far the existing studies highlighted the complexity and heterogeneity of the mesolimbic dopaminergic circuits and suggest that CRH might differently modulate dopaminergic neurotransmission under basal and stress conditions (*101*). Future research depicting the specific molecular pathways within the mesolimbic and other dopaminergic circuits, which regulate mood and motivation, will open up new avenues for the development of antidepressant medications. New molecular targets in brain reward circuits represent potential therapeutic objectives also for treatment of drug abuse, as there is a high rate of co-morbidity between depression and addiction (*81, 102*). The first studies in humans have found encouraging antidepressant effects of deep brain stimulation of the medial forebrain bundle (MFB) - a white matter tract that mediates, among other regions, connectivity between the VTA and nucleus accumbens (NAc) (*103*).

2.2 The CRH family and their respective receptors

Corticotropin-releasing hormone, also known as corticotropin-releasing factor or corticoliberin is a 41-amino acid neuropeptide in mammals derived from a 196-amino acid preprohormone, that was originally isolated and described in 1981 by Vale and colleagues (*6*). Initially it was considered to name the newly discovered peptide "Amunine" (Greek word for "to defend") to emphasize that the CRH-mediated activation of the hypothalamic-pituitary-axis reflects an "acute defense of homeostasis" (*104*). Even at that time the Vale group sensed an important role for CRH beyond stimulation of ACTH secretion and it did not take long until Nemeroff and associates published experimental evidence for elevated CRH levels in the cerebrospinal fluid of patients with major depression (*11*) and reduced CRH binding sites in the frontal cortex of suicide victims (*12*). Subsequent studies found *Crh* mRNA and protein to be widely expressed in the central nervous system and to some extent in peripheral tissues (e.g., skin, placenta, thymus, gastrointestinal tract). In the brain, the main site of CRH production is the parvocellular division of the PVN, which projects to the median eminence. Furthermore, it is expressed in the olfactory bulb, cortex, nucleus accumbens, central nucleus of the amygdala (CeA) - mainly in the lateral subdivision (CeA_L), bed nucleus of the stria terminalis (BNST), interstitial nucleus of the posterior limb of the anterior commissure (IPAC), hippocampus (only scattered interneurons), lateral hypothalamic area, medial geniculate nucleus, periaqueductal grey, raphe magnus, Barrington's nucleus, medial vestibular nucleus and inferior olive (*69, 71, 105, 106*). CRH is also expressed in the spinal cord, indicating a role in the peripheral stress response (*6, 107*). In summary, it can be said that CRH is the main regulator of HPA axis activity during stress, thereby coordinating the neuroendocrine response. In addition, the presence of *Crh* mRNA in the other brain regions, mainly limbic and related to the stress response, such as BNST, CeA, cerebral cortex and dorsal root ganglion neurons of the spinal cord suggests that this peptide also modulates neuronal activity. It thereby acts as a neuromodulator and plays an important role in controlling behavioral and autonomic responses to stress (*108*).

The characterization of CRH was followed in 1995 by the identification of urocortin 1 (UCN1) (*109*), another mammalian CRH-related peptide (45% sequence identity) involved in the stress response. More recently two additional members of the CRH-

family, namely urocortin 2 (UCN2, also called “stresscopin-related-peptide”) and urocortin 3 (UCN3, also called “stresscopin”) were discovered, representing a distinct evolutionary branch within the family (*110, 111*). Recent phylogenetic studies revealed that the “CRH-family” evolved from one ancestral gene, developing into two branches (CRH/UCN1 and UCN2/UCN3) through an early gene duplication event (*112, 113*). Compared to the more widespread distribution of CRH, the expression of the urocortins is restricted to particular brain areas and some peripheral organs. The main expression site for UCN1 is the Edinger-Westphal nucleus, where it is assumed that UCN1 expressing neurons contribute to some stress-related effects (*114, 115*). Central UCN2 is detectable in the PVN, supraoptic nucleus, brainstem nuclei and LC (*110*). Highest levels of peripheral UCN2 expression have been reported in skeletal muscle and skin (*116*). UCN3 is expressed in the medial amygdala, BNST, superior paraolivary nucleus, nucleus parabrachialis and the premammillary nucleus. In the periphery UCN3 expression has been detected in the small intestine (mucosal cells in the intestinal crypts and goblet cells) and in pancreatic beta-cells (*117*).

CRH and its related peptides exert their biological activity via two subtypes of G protein-coupled heptahelical receptors, CRHR1 and CRHR2, which were discovered in 1993 (*118*) and 1995, respectively (*119*). In humans and rodents CRHR1α represents the main and fully functional isoform of the CRHR1 (*120*), whereas the CRHR2 gene encodes for three functional splice variants (variant a, b, c in humans; variant a and c in rodents) (*118, 119, 121, 122*). G protein–coupled receptors (GPCRs), also known as seven-transmembrane domain receptors, constitute a superfamily of receptors that transduce extracellular signals across the cell membrane and activate intracellular signal transduction pathways. GPCRs dysfunction/dysregulation has been linked to several human diseases and because of their role in cell signaling and the high number of receptors that are potentially druggable, this receptor family represents an important pharmaceutical target, estimated to be the objective of more than 40% of the drugs used in modern clinical medicine today (*123, 124*).

2.2.1 CRHR1 signal transduction

CRHR1 and CRHR2 belong to the class B1 or secretin family of GPCRs and consist of a large extracellular N-terminus (ECD1) and three extracellular loops (extracellular

domain ECD2-4), seven transmembrane domains (TM1-7), three intracellular loops (intracellular domain ICD1-3) and the C-terminal intracellular tail including a class I PDZ-binding motif (ICD4) (*125*). The seven transmembrane and intracellular domains of both receptors show the highest degree of sequence conservation (85-90% identity), especially the ICD3 which is 100% conserved in all CRH receptors and represents the putative coupling site for G proteins (*104*) (Figure 2).

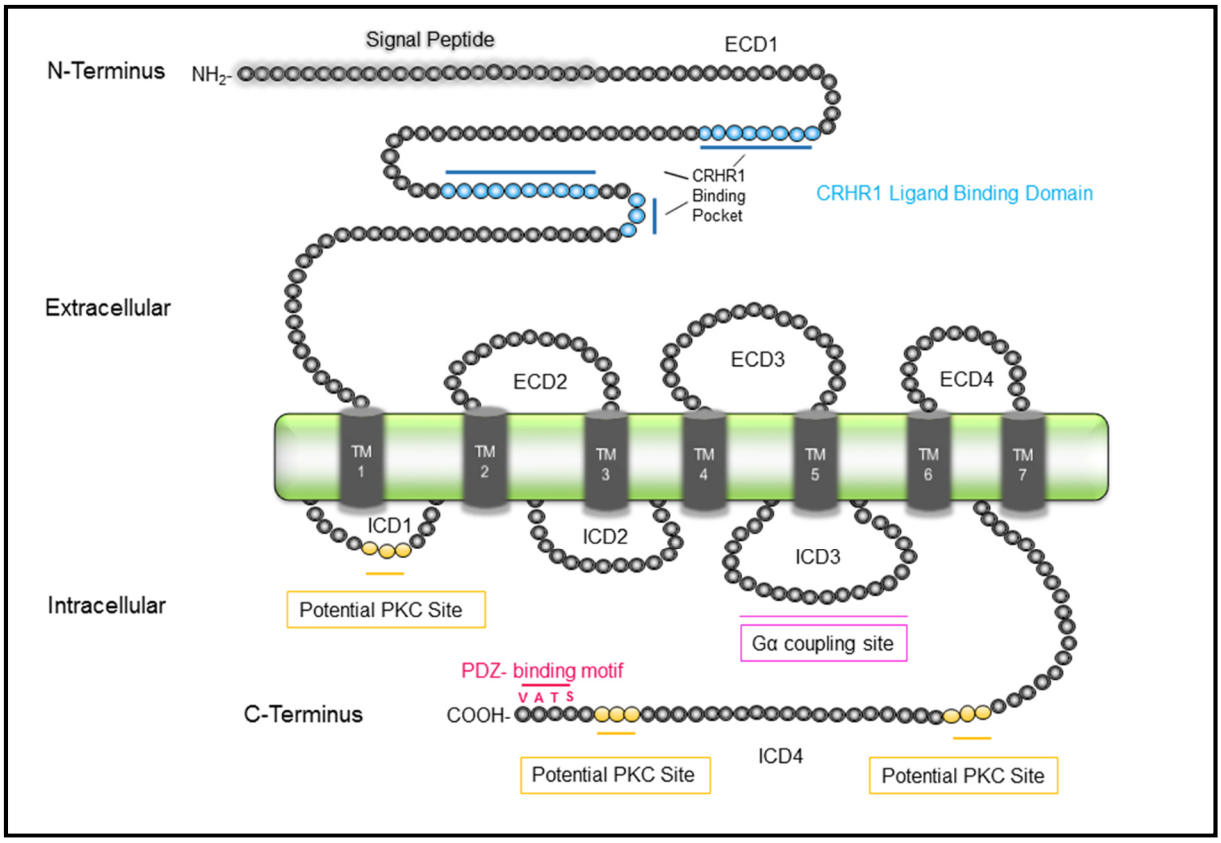

Figure 2: Schematic representation of the corticotropin-releasing hormone receptor type 1 (CRHR1)

The CRHR1 belongs to the secretin family (subfamily B1) of G protein-coupled receptors that consist of an extracellular N-terminus, seven transmembrane spanning segments (TM1-7) connected by three extra- and intracellular loops/domains (ECD, ICD) and an intracellular C-terminus. For details, see text.

The N-terminal ECD1 represents the major ligand binding site of the receptors where binding of CRH/Urocortins leads to receptor activation in a two-step mechanism, the so called “two-domain” model: the C-terminus of the ligand binds the extracellular N-terminus of the receptor, thereby promoting interaction of the N-terminal ligand segment with the receptor’s juxtamembrane domains resulting in a conformational active signaling state with increased affinity for stimulatory heterotrimeric GTP binding proteins (Gs and Gq). Subsequently the Gsα subunit couples to the receptor’s third intracellular loop resulting in an activation of the transmembrane

adenylyl cyclase (tmACs), which increases the level of the second messenger cyclic AMP (cAMP) and produces a ~1300 fold increase in the receptor's affinity for CRH/UCNs. Recently, Silberstein and colleagues provide evidence for a separate cAMP source, produced by the soluble adenylyl cyclase (sAC), which is distributed throughout the cell and activated by CRHR1-induced intracellular calcium increase and after receptor internalization (*126*). Through activation of protein kinase A (PKA) CRHR agonists can activate cytosolic downstream events such as cAMP response element-binding protein (CREB) and extracellular signal-regulated kinase (ERK1/2) phosphorylation which in turn initiate events in the nucleus at the level of gene transcription via CREB (*127, 128*). Furthermore, CRHR1 receptors can activate the phospholipase C (PLC) - protein kinase C (PKC) pathway via coupling to the Gqα subunit. Activation of the CRHR1 has been shown to increase formation of other second messengers, such as triphosphoinositol (IP3), diacylglycerine (DAG) and to increase intracellular Ca^{2+} levels via PLC mediated hydrolysis of phosphatidylinositol-bisphosphate (PIP2). There is evidence that PKC-mediated phosphorylation is involved in CRHR desensitization depending on the cellular context (*129*). Beside above described signaling cascades, CRHRs have also been shown to activate a variety of other pathways such as the NO/cGMP pathway (involved in the control of vascular tone), the Akt/protein kinase B (PKB) pathway, the caspase pro-apoptotic pathway, the NF-κB- and Nur1/Nur77 pathway and other transcription factor pathways (*129, 130*). To prevent cellular overstimulation different intracellular mechanisms, such as receptor phosphorylation by second messenger-activated PKA/PKC or G protein-coupled receptor kinases (GRKs), homologous desensitization via uncoupling from G-proteins and lysosomal degradation have been described (*131*). GRK3 is the major regulator of CRHR1 phosphorylation and requires G$\beta\gamma$-subunits for its recruitment and association with the C-terminus of the receptor. Receptor phosphorylation leads to translocation of β-arrestins to the plasma membrane and binding to the receptor which initiates receptor uncoupling, internalization and desensitization of signaling (*132*). In a recent publication Bender and colleagues provide experimental evidence for an interaction of the C-terminal PDZ binding motif (amino acids S^{412}-T^{413}-A^{414}-V^{415}) of CRHR1 with members of the membrane-associated guanylate kinase (MAGUK) family, such as MAGI2 (*125*). MAGUK proteins can attenuate CRHR1 internalization and endocytosis of CRHR1 upon stimulation with CRH by interfering with β-arrestin recruitment to the receptor

(*133*). Recently the crystal structure of the CRHR1-transmembrane domain has been published which will enable structure-based approaches to drug design (*134*). Moreover, it has become apparent that many GPCRs exist in a constitutively active state, where activation of the receptor and stimulation of intracellular signaling pathways occurs ligand- independent (*135*). Constitutively active mutant receptors are useful experimental tools for academic and industrial research; e.g., replacing the N-terminal domain of the CRHR1 by the amino-terminal residues (1-16) of CRH resulted in a chimeric receptor which displays significant levels of constitutive activation, measured by increased levels of intracellular cAMP (*136*). By applying this approach it was demonstrated that local CRH signaling onto adult-born neurons promotes/stabilizes chemical synapses in the rodent olfactory bulb (*137*). By using structural modeling and mutagenesis Yin and colleagues could identify two key structural elements that stabilize the inactive state of GPCRs and mutations in this conserved polar core next to TM6 of the CRHR1 induces constitutive G-protein signaling (*138*). Dissecting CRHR1-signaling complexity and regulatory mechanisms of tissue- and agonist-specific cellular responses is an essential prerequisite for exploiting the potential of CRHRs as novel therapeutic/drug targets (Figure 3).

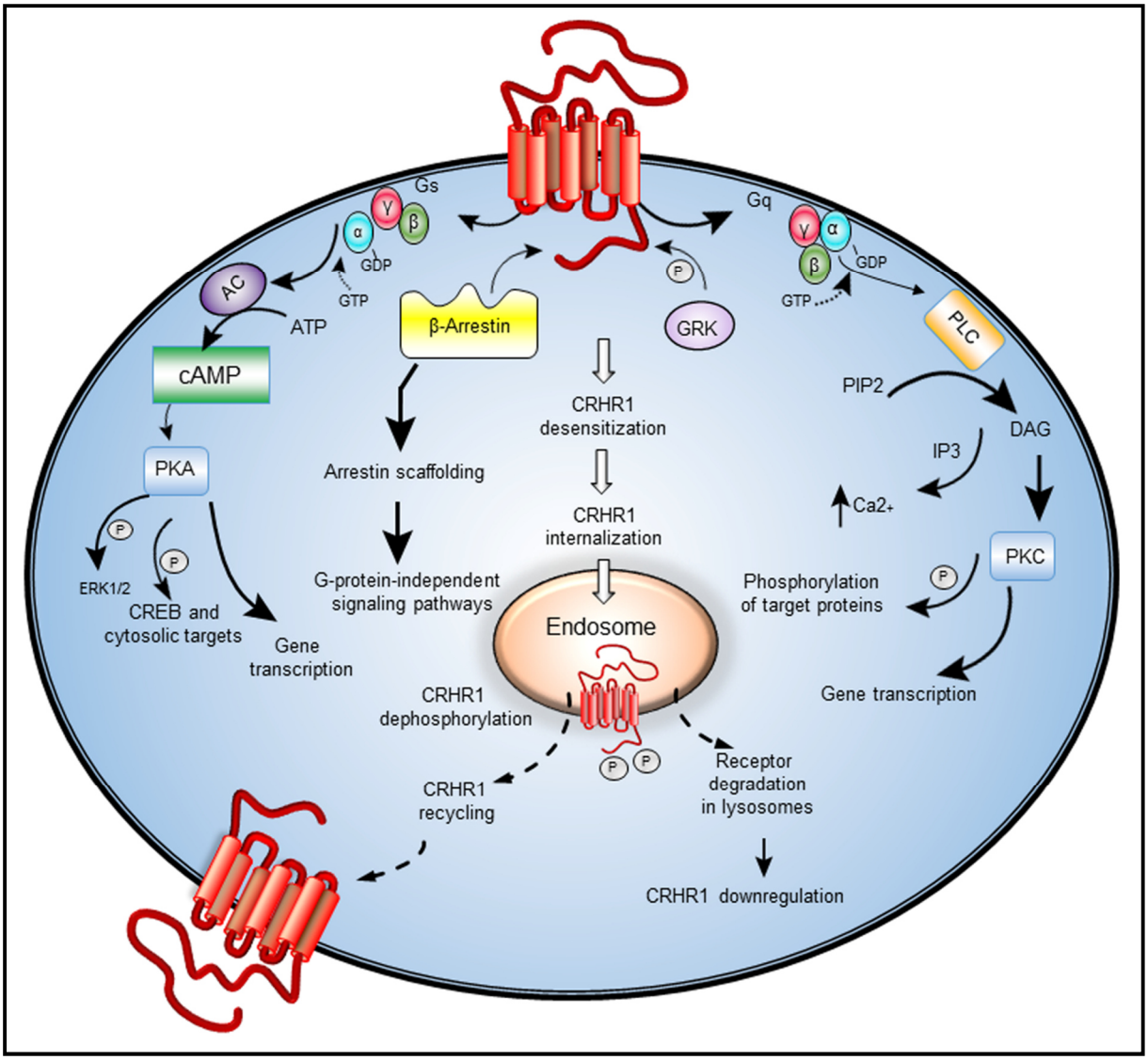

Figure 3: Major CRHR1 downstream signaling and trafficking pathways

For details, see text. Abbreviations: (AC) adenylyl cyclase; (ATP) adenosine triphosphate; (cAMP) cyclic adenosine monophosphate; (CREB) cAMP response element-binding protein; (DAG) 1,2-diacylglycerol; (ERK1/2) extracellular signal-regulated kinase; (GDP) guanosine diphosphate; (IP3) triphosphoinositol; (GRK) G protein-coupled receptor kinase; (GTP) guanosine triphosphate; (PIP2) phosphatidylinositol-bisphosphate; (PKA) protein kinase A; (PKC) protein kinase C; (PLC) phospholipase C

2.2.2 Distribution and expression of CRHRs

Although both receptors share ~70% amino acid identity, they differ in their tissue specific distribution as well as in their binding affinities. CRHR1 displays highest affinity for CRH and UCN1, binding both with similar affinity. In contrast to CRHR2, whose binding affinities to CRH-related peptides can be ranked as follows: UCN1>UCN2>UCN3>>CRH (*129, 139*). Additionally, the biological effects of CRH and UCN1 are not only controlled by CRH receptors, but also via a 37kDa glycoprotein, the CRH-binding protein (CRH-BP). Latest studies support the thesis that CRH-BP plays an inhibitory role via binding CRH, UCN1 and to a lesser extent UCN2, thereby sequestering them away from their respective receptors CRHR1 and CRHR2 resulting in decreased action at hormonal and synaptic levels (*140, 141*).

Both receptors are widely expressed in a number of tissues, however the CRHR1 is predominantly found in the CNS compared to CRHR2, which is detected to a greater degree in the periphery. A number of studies based on mRNA *in situ* hybridization and high-affinity radioligand binding (mainly in rodents), have indicated that CRHR1 is found throughout the brain, for instance in the olfactory bulb, cerebral cortex (high levels of expression in cortical layer IV), hippocampus (CA1, CA2 and polymorph layer of the dentate gyrus), BNST, basolateral amygdala, reticular thalamic nucleus, globus pallidus, VTA, raphe nucleus and cerebellum (*29, 142*). A more detailed analysis revealed CRHR1 expression in distinct neurotransmitter systems, e.g., receptor expression in glutamatergic neurons of cortex, hippocampus and basolateral amygdala, in GABAergic neurons in the reticular thalamic nucleus, globus pallidus, septum and BNST, dopaminergic neurons in the VTA and SNC and 5-HT neurons in the raphe nuclei (*99*). It is also detectable at high levels in the anterior pituitary, where CRH/CRHR1 interaction initiates the synthesis and release of ACTH. Additionally, it can be found in a number of peripheral tissues, e.g., skin, eye, female reproductive tract, adrenal gland and gastrointestinal tract. Expression of the receptor in the spinal cord points towards a role in peripheral stress adaptive processes (*41, 143*). In contrast, expression of CRHR2 is more restricted in the brain, compared to CRHR1. The predominant expressions sites comprise the dorsal and median raphe nuclei, lateral septum, BNST, ventromedial hypothalamic nucleus and the choroid plexus. In the periphery the receptor has been found in the heart, lung, gastrointestinal tract, adrenal gland, skeletal muscle and male reproductive system (*139*) (Figure 4).

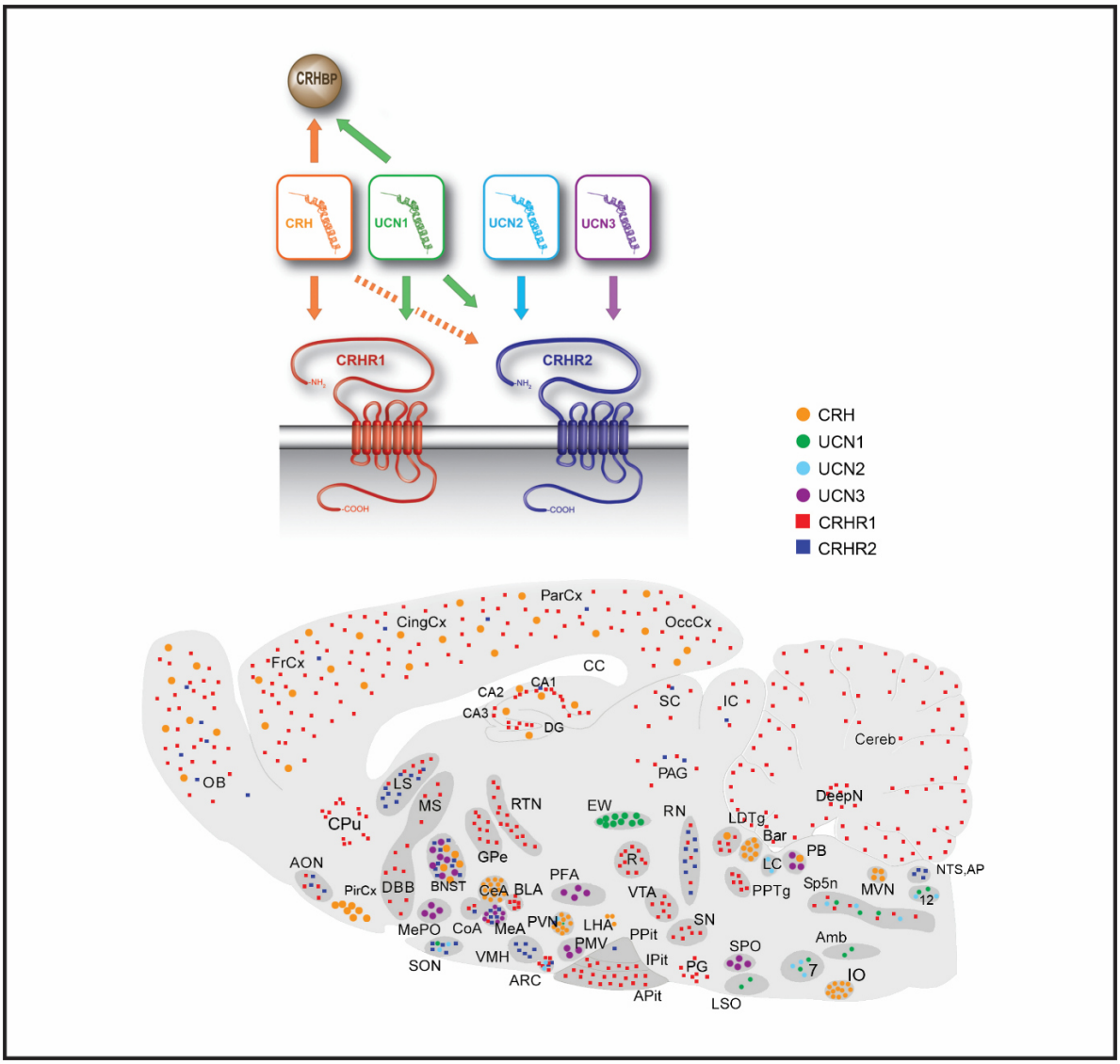

Figure 4: Schematic illustration of the CRH family and their cognitive receptors

Top: binding affinities of CRHRs and CRH-BP for CRH and the urocortins (dashed arrow indicates lower affinity); CRH binds with higher affinity to CRHR1 compared to UCN1. UCN2 and UCN3 are selective ligands for CRHR2. CRH binding protein (CRH-BP) can “sequester” CRH and UCN1 thereby regulating the availability of the peptides.
Bottom: spatial distribution of the “CRH ligand family” and their receptors; Abbreviations: (7) nucleus facialis; (12) nucleus hypoglossus; (Amb) nucleus ambiguus; (AON) nucleus olfactorius anterior; (AP) area postrema; (Apit) anterior pituitary; (ARC) nucleus arcuatus; (BLA) basolateral amygdala; (BNST) bed nucleus of stria terminalis; (CA1-3) field CA1-3 of hippocampus; (CC) corpus callosum; (CeA) central amygdala; (Cereb) cerebellum; (CingCx) cingulate cortex; (CoA) cortical amygdalar nucleus; (CPu) caudate putamen; (DBB) diagonal band of Broca; (Deep N) deep nuclei cerebellum; (DG) dentate gyrus; (FrCx) frontal cortex; (IC) inferior colliculus; (IO) inferior olive; (Ipit) intermediate lobe pituitary; (LC) locus coeruleus; (LDTg) laterodorsal tegmental nucleus; (LSO) lateral superior olivary complex; (MeA) medial amygdala; (MePO) medial preoptic nucleus; (MS) medial septum; (NTS) nucleus solitary tract; (OB) olfactory bulb; (OccCx) occipitale cortex; (PAG) periaqueductal grey; (ParCx) parietal cortex; (PFA) perifornical area; (PG) pontine grey; (Ppit) posterior pituitary; (PPTg) pedunculopontine nucleus; (PVN) paraventricular hypothalamic nucleus; (R) nucleus ruber; (RN) raphe nuclei; (SC) superior colliculus; (SN) substantia nigra; (SON) supraoptic nucleus; (Sp5n) nucleus spinalis trigemini; (SPO) superior paraolivery nucleus. With permission from Dr.Jan Deussing.

2.3 The role of CRH receptor 1 in stress-related disorders

Over the past few years many studies including pharmacological approaches, conditional and conventional mouse models for the CRH/CRHR1 system and viral-based methods have been conducted, which clearly support a role for CRH/CRHR1 in neuroendocrine, autonomic and behavioral changes, which are implicated in stress-related disorders with a strong emotional component, e.g., anxiety, depression and post-traumatic stress disorders (*16, 144, 145*). Many clinical findings such as elevated CRH levels in the cerebrospinal fluid of patients with depression or with posttraumatic stress disorders, reduced CRH binding sites in the forebrain of depressed suicide victims, elevated number of CRH secreting neurons in the PVN of patients with depression and a blunted ACTH response to exogenous CRH application have supported the assertion that abnormal CRH neuromodulation and CRHR1 signal transduction play a leading role in the pathophysiology of stress-related disorders (*14, 15*). Several human genetic association studies suggest an interaction between genetic CRHR1 variations (single nucleotide polymorphisms, SNPs) and the risk for stress-related disorders including depression and anxiety. Two SNPs (rs878886 in the 3' UTR of the CRHR1 gene and rs28632197 in the vasopressin 1B receptor, AVPR1B) are significant associated with panic disorder (*146*). Several studies reported an association of SNPs within the CRHR1 with response to antidepressant treatment in patients with anxious depression (*147, 148*). Another set of studies analyzing gene x environment interactions demonstrated a strong relation of intronic CRHR1 SNP rs4792887 and stressful life events in terms of suicide attempts in depression (*149*). The SNP rs1876831 links negative life events and adolescent alcohol consumption (*15, 150*). It is likely, that the sum of genetic variants within the CRH system and interactions with environmental factors influence the susceptibility to stress-related psychiatric disorders potentially by altering the impact of stress on epigenetic signatures.

In addition to human genetic studies a large number of rodent studies in which CRH was either injected into the brain (via intracerebroventricular administration) or genetically overexpressed, thereby modeling the same etiology that triggers human depression, clearly demonstrated that CRH accounts for behavioral changes related to affective disorders: increased anxiety and arousal, decreased sexual interest and appetite, sleep disturbances and others (*151*). Importantly, chronic hypercortisolism

alone is not sufficient to explain altered anxiety-related behavior as has been proved by a genetic mouse model discriminating direct effects of centrally hypersecreted CRH from those resulting from HPA axis hyperactivity. In general, central CRH hyperdrive on its own or in synergism with elevated glucocorticoid levels is responsible for enhanced anxiety-related behavior (*152*). Centrally administered CRHR1 antagonist or *Crhr1* antisense mRNA decrease stress-elicited anxiety-related behavior and therefore strongly point towards a role of CRHR1 in mediating these behavioral changes (*153*). However, questions regarding the specificity of the antagonist and the antisense mRNA, as well as the fact that acute administration of exogenous peptides does not mimic long-lasting CRH effects prompted the generation of transgenic mice overexpressing (gain-of-function mutants) or lacking (loss-of-function mutants) the CRHR1 and further members of the “CRH-family” and provided valuable insights into the underlying brain neurocircuits (*9, 154*).

2.3.1 Loss-of-function mouse models targeting the CRHR1

In 1998, two independently generated conventionally CRHR1 knockout mouse lines consistently supported that CRHR1 mediates anxiogenic behavior (*155, 156*). Behavioral studies in both lines revealed reduced anxiety-related behavior under basal conditions. However, this targeting strategy has two drawbacks: first, due to the conventional targeting approach also anterior pituitary corticotrophs are lacking a functional active receptor, resulting in disrupted HPA axis activity, including reduced basal and stress-induced corticosterone levels. For this reason, it cannot be excluded that the altered glucocorticoid levels in these mouse lines are the main reason for the observed behavioral effects. Second, the ablation of a gene during embryogenesis might lead to compensatory mechanisms that can mask the direct effects of the receptor (*157*). To overcome the limitations a conditional CRHR1 knockout mouse line was generated, using the *Cre*/*loxP* system to dissect CRH/CRHR1 pathways responsible for the behavioral phenotype, from those controlling neuroendocrine functions (*158*). In this mouse model *Cre* recombinase expression under the control of the Camk2a promoter leads to a postnatal deletion of CRHR1 in limbic forebrain regions such as the hippocampus, cortex, amygdala and BNST. As expected basal plasma glucocorticoid and ACTH levels were normal, but disruption of CRH/CRHR1 pathways in limbic neurocircuits significantly reduced anxiety-related behavior.

Further studies revealed that CRHR1 in forebrain limbic neurocircuits not only modulates emotional but also cognitive responses (*159, 160*). In addition to genetic loss-of-function studies, viral-mediated knockdown of *Crhr1* mRNA expression is another useful technique to study neuronal function in the rodent brain in a spatial- and time- dependent manner. Sztainberg and colleagues targeted the CRHR1 in the basolateral amygdala (BLA) and in the external segment of the globus pallidus (GPe) via stereotactic delivery of lentiviral vectors expressing small interfering RNA directed against the receptor mRNA. Consistent with the results from genetic knockout mice outlined above, downregulation of the CRHR1 in the BLA significantly decreases anxiety-related behavior, whereas knockdown of CRHR1 in the GPe revealed a previously unexpected anxiolytic role of the receptor by modulating release of enkephalin from the striatum to the GPe (*161, 162*). More recently, the role of CRHR1 regarding the link between stress, addiction and reward was investigated via knockdown of the receptor in the VTA. CRHR1 knockdown within the VTA is not critical regarding self-administration behavior for cocaine or sucrose but effectively blocked stress- and cue-induced reinstatement of cocaine seeking (*163*). In addition, it was shown that the knockdown of the receptor enhances tone-conditioned fear most probably via modulation of GABAergic signaling (*164*). Future studies designed to dissect the specific CRH inputs to VTA subnuclei as well as the subcellular localization of the receptor are necessary to unravel the underlying neurocircuits that modulate aversive learning and memory.

Nevertheless, one question remained unanswered for some time: which are the CRH/CRHR1-controlled neurotransmitter (NT) circuits that adjust stress-related behavior (see following chapter).

2.3.2 Dissecting CRH/CRHR1-dependent neurocircuitries in the central nervous system

To address the question of neurotransmitter identity a dual approach using double *in situ* hybridization and double immunohistochemistry was chosen to circumvent the lack of specific antibodies for CRHR1 (*99*). With these methods expression of *Crhr1* mRNA was detected/confirmed in forebrain glutamatergic neurons of the hippocampus and cortex, in dopaminergic neurons of the VTA and SNpc, in GABAergic neurons of the reticular thalamic nucleus (Rt), globus pallidus (GP) and

septum and in very few serotonergic (5-HT) neurons of the dorsal and median raphe nucleus. To dissect the underlying neurocircuits, a conditional CRHR1 knockout mouse line in which the exons 9 to 13 are flanked by *loxP* sites (*158*) was bred to a selection of neurotransmitter-specific *Cre*-driver lines, thereby deleting CRHR1 in forebrain glutamatergic (*Nex-Cre*), forebrain GABAergic (*DLX5/6-Cre*), midbrain dopaminergic (*Dat-CreER*^{T2}) and hindbrain serotonergic (*ePet-Cre*) neurons. Disruption of CRH/CRHR1 signaling in glutamatergic neurocircuits resulted in an anxiolytic phenotype, a result that is in line with the forebrain-specific knockout line described above. No anxiety-related phenotype was observed in intercepted GABAergic and serotonergic circuits. On the contrary, an increased anxiety-like phenotype was observed when specifically deleting the receptor from midbrain dopaminergic neurons in the VTA and SNC. These results uncover a previously unrecognized bidirectional role of the CRHR1 with regards to anxiety, meaning that CRH/CRHR1 controlled anxiogenic glutamatergic and anxiolytic dopaminergic neurocircuits orchestrate adaptive emotional responses to stressful challenges in an antagonistic manner to keep the system balanced. In this context, it is important to note that the predominant view that CRH acts as a generally “aversive” neuropeptide with regard to stressful stimuli has to be reconsidered (*8*). This insight has also been supported by Lemos and colleagues who demonstrated a switch-over of CRH action in the nucleus accumbens from appetitive to aversive after stress (*101*). A most recent study further supports the existence of an “anxiolytic” CRH/CRHR1 circuit. The study revealed a novel population of CRH-expressing long range projecting neurons localized in the BNST and CeA targeting CRHR1-expressing dopaminergic neurons in the VTA/SNC that positively modulate dopaminergic neurotransmission in the prefrontal cortex and thereby decrease anxiety-related behavior (*100*). To summarize, the role of the CRH/CRHR1 system in HPA axis regulation as well as regulation of emotional behavior is well characterized (reviewed in Dedic et al., 2017) (Figure 5). Future challenges in this research field such as dissecting “aversive” versus “appetitive” CRH/CRHR1 pathways require more sophisticated tools enabling, e.g., bidirectional control of neuronal activity or anterograde/retrograde *Cre* dependent tracing strategies to visualize ligand/receptor connectivities in specific brain circuitries.

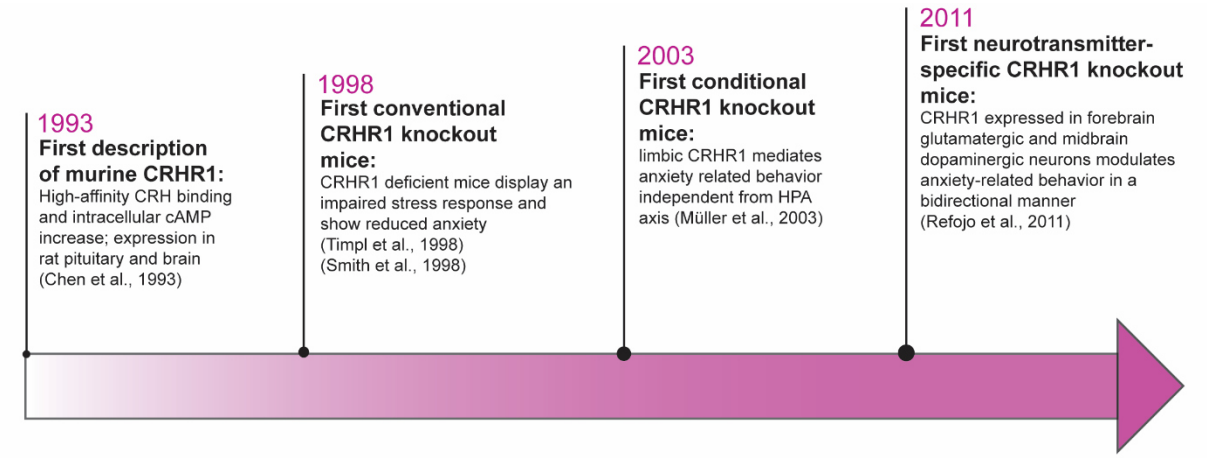

Figure 5: Summary of pioneering genetic mouse models targeting the CRH receptor type 1

2.4 *Cre*-driver mouse lines for neural circuit mapping

Since the first isolation of CRH in 1981 and its high affinity receptor CRHR1 in 1993, there has been remarkable progress in the field of stress research. Recently, two comprehensive studies dissected the neurochemical identity of CRH- and CRHR1-expressing neurons in the mouse brain and revealed a bidirectional role of the CRH/CRHR1 system in modulating anxiety-related behavior (*99, 100*). Unraveling the underlying neurocircuits represents a major challenge in the future and requires additional genetic tools that allow for labeling, modulation of gene expression and manipulation of cellular activity in specific cell types and/or anatomical regions (*165, 166*). To date genetically engineered mouse lines and viral vectors represent popular strategies in psychiatric research. In mice, the *Cre/loxP* recombinase system from the bacteriophage P1 has evolved as a powerful tool for cell-type specific manipulations. *Cre* (“causes recombination”) belongs to the integrase family of site specific DNA recombinases and recognizes a 34bp nucleotide sequence named *loxP* (“locus of crossing over”), thereby catalyzing recombination between two *loxP* sites depending on their orientation (*167*). A *loxP* site is composed of two 13bp-inverted repeats flanking an 8bp asymmetric spacer that determines directionality of the site. *Cre*-mediated recombination between two directly repeated *loxP* sites will finally result in the deletion of the intervening sequence. In contrast, opposing orientation of *loxP* sites lead to continuous inversion of the *loxP* flanked (“floxed”) DNA. In addition *Cre* can also exchange sequences distal to *loxP* sites present on two linear DNA

molecules and integrate DNA sequences from a circular DNA molecule (*168*). If the *Cre* recombinase gene is placed downstream of a specific promoter and combined with “inducible” conditional tools, then cell type-specific genomic manipulations are possible. In the past, many gene-specific *Cre*-driver mouse lines have been generated by either conventional- or bacterial artificial chromosome (BAC) transgenic- or knock-in approaches. In general the latter technique reflects endogenous gene expression more precisely compared to random transgenic insertion (*169*). Regardless which approach is selected, a detailed characterization of *Cre* expression is mandatory as various caveats to the functionality of *Cre*-driver mouse lines ,e.g., mosaic deletion activity, ectopic expression, sex differences and *Cre* toxicity have been reported (*170*). Regarding the members of the “CRH-family” various *Cre*-driver mouse lines have been generated in the past: three *CRHR2-Cre*, two *UCN3-Cre* lines and six CRH *Cre*-driver lines (reviewed by Dedic et al., 2017) (overview see Table 1; modified from Dedic et al., 2017).

Table 1: Summary of *Cre*-driver lines targeting the CRH/UCN system

Transgenic Line	Targeting Strategy	Expression/Phenotype	Reference
CRFp3.0Cre	**Transgenic:** 3.0kb of CRH regulatory elements upstream of the START codon were cloned in front of the *Cre* coding sequence and a mouse line was generated via pronuclear injection of the linearized construct	*Cre* expression pattern matched CRH expression in a subset of neurons within the central amygdala (CeA), bed nucleus of the stria terminalis (BNST), the paraventricular hypothalamic nucleus (PVN) and the cortex; no *Cre* expression in other CRH positive neurons within the brain. Deletion of the GABA(A)α1 receptor subunit in CRH specific neurons within the BNST, PVN and CeA enhances anxiety and impairs fear extinction. Deletion of the NMDA receptor 1 in CRH positive excitatory neurons within the CeA enhances fear memory acquisition and retention.	*(171)* *(172)* *(173)*
CRH-Cre (KN282)	**BAC transgenic:** insertion of the cDNA encoding *Cre* followed by a poly A signal directly at the START codon of the CRH gene in BAC RP24-239F10	Partial endogenous gene expression pattern; colocalization with CRH in the PVN. CRH neurons in the PVN are modulated by the stress-derived neurosteroid THDOC. Loss of Gabrd in CRH neurons of the PVN decreased stress-related behaviors.	*www.gensat.org* *(174)* *(175)*

Table 1: Summary of Cre-driver lines targeting the CRH/UCN system (continued)

Transgenic Line	Targeting Strategy	Expression/Phenotype	Reference
Crh-IRES-Cre	**Knock-in:** insertion of an *IRES-Cre* cassette followed by a poly A signal into the 3' UTR (after the translational termination site) of the CRH locus	Expression of *Cre* with high fidelity to endogenous CRH expression sites throughout the brain. Photoactivation of CRH terminals (projections from the CeA) in the LC causes increased tonic firing of LC neurons and mediates stress-induced anxiety. Oxytocin-dependent inhibition of CRH neurons in the PVN attenuates stress-induced HPA axis activation and promotes anxiolysis. CRH represents a marker of preoptic sleep neurons.	*(106)* *(176)* *(177)* *(178)*
Crh-IRES-Cre	**Knock-in:** insertion of an *IRES-Cre* cassette three base pairs after the STOP codon of the endogenous CRH gene	The endogenous CRH promoter controls *Cre* expression and reporter gene expression recapitulates CRH expression pattern. NPY Y1 receptor (Y1R) activation inhibits CRF neurons within the BNST to suppress binge alcohol drinking. Serotonin engages a CRH inhibitory microcircuit within the BNST via actions at 5-HT2C receptors and silences anxiolytic BNST outputs to the VTA. Inhibition of CRH neurons projecting from the BNST to the VTA attenuates binge-like drinking.	*(179)* *(180)* *(181)* *(74)*
CRH-creER^{T2}	**BAC transgenic:** insertion of an *IRES-CreER^{T2}* fusion gene directly at the ATG of the human CRH locus in BAC RP11-1006.F7; targeting into the upstream region of the Hprt locus	*Cre* expression is regulated by CRH promoter elements and *Cre* recombination is induced by tamoxifen; *Cre* expression only scattered and mostly absent in CRH positive brain nuclei and/or unspecific as revealed by reporter gene expression (own studies, data not published).	*www.informatics.jax.org MGI:5568222*
CRH-Cre (rat)	**BAC transgenic:** insertion of a ~2.7kb fragment containing a modified human beta-globin intron within the Cre coding sequence directly at the START codon of the CRH gene in BAC CH230-206D8	BAC transgenic CRH-*Cre* rat; *Cre* expression limited to CeL and dorsal BNST neurons; no *Cre* expression detectable in ventral BNST and PVN and other CRH positive brain nuclei.	*(182)*

Table 1: Summary of *Cre*-driver lines targeting the CRH/UCN system (continued)

Transgenic Line	Targeting Strategy	Expression/Phenotype	Reference
Ucn3-Cre (KF31)	**BAC transgenic:** insertion of the cDNA encoding *Cre* followed by a poly A signal directly at the START codon of the UCN3 gene in BAC RP23-332L13	*Cre* expression detectable in thalamic and hypothalamic nuclei and neurons in the caudoputamen and midbrain; weak and scattered expression detectable in the cerebral cortex, basal forebrain and olfactory bulb. Comparison of *tdTomato* expression with endogenous *Ucn3* mRNA expression confirmed high specificity of the transgenic line (~90% of UCN3 cells express the reporter protein) in the perifornical nucleus (PeF), BNST and MeA. Inhibition of the MeA UCN3-CRHR2 circuit increases pro-social behavior in mice.	*www.gensat.org (183)*
Ucn3-Cre (KF43)	**BAC transgenic:** insertion of the cDNA encoding *Cre* followed by a poly A signal directly at the START codon of the UCN3 gene in BAC RP23-332L13	*Cre* expression within the cerebellum, medulla, pons, midbrain, hypothalamus, thalamus, amygdala and striatum.	*www.gensat.org www.connectivity.brain-map.org*
Crfr2α-eGFPCre	**BAC transgenic:** insertion of an *eGFPCre-SV40pA* cassette directly at the START codon in the third exon of the *Crhr2*α gene in BAC RP23-78P13	Comparison of *eGFPCre* expression with endogenous *Crhr2* mRNA expression confirmed high specificity of the transgenic line (~87% of *Cre* positive cells contain *Crhr2* mRNA), but restricted to a subset of cells in the lateral septum. A subset of CRHR2 positive projecting neurons within the lateral septum enhance stress-induced anxiety related behavior in mice.	*(184)*
Crhr2-Cre (RT30-Cre)	**BAC transgenic:** insertion of the cDNA encoding *Cre,* followed by a poly A signal directly at the initiating ATG codon of the CRHR2 gene	Scattered signal within the hypothalamus; moderate to strong signal in the dorsal and ventral horn of the spinal cord.	*www.gensat.org*

Table 1: Summary of *Cre*-driver lines targeting the CRH/UCN system (continued)

Transgenic Line	Targeting Strategy	Expression/Phenotype	Reference
CRFR2-chy-Cre	**BAC transgenic:** insertion of a *mCherry-f2A-Cre* cassette directly at the initiating ATG codon in the third exon of the alpha-splice variant of the *Crfr2* gene	Detection of tdTomato reporter gene expression in the olfactory bulb, lateral septal nucleus, ventromedial hypothalamic nucleus, cortical nuclei of the amygdala, ventral hippocampus, raphe nuclei and posterior BNST. Activation of CRFR2 neurons in the posterior BNST decreases anxiety, attenuates corticosterone release after stress, ameliorates stress-induced anxiety and attenuates memory of the stressful event. Activation of CRHR2 in the medial amygdala increases preference for novel mice.	*(183)* *(185)*

Recently Arenkiel and colleagues generated a BAC transgenic CRHR1-*Cre* mouse line to virally overexpress a constitutively active CRHR1 fused to EGFP (*137*). The *Cre* recombinase expression pattern was validated via breeding to a *lacZ* reporter line (data not shown) and subsequent comparison with the endogenous CRHR1 expression sites. Beside this, further characterization has not been shown, an aspect that deserves particularly critical scrutiny in view of known problems associated with BAC transgenesis, such as random genome integration, variable copy number and lack of genomic regulatory elements (*186*). Almost concomitantly with the present thesis, a targeted knock-in strategy was used to generate a mouse line expressing *Cre* recombinase under the endogenous promoter of the CRHR1 (*62*). An *IRES-Cre-GFP* sequence was inserted into the 3'UTR to preserve a functional receptor. For validation of the *Cre* expression pattern *Cre*-positive males were bred to Ai14 reporter mice (*187*), most likely due to the fact that *GFP* expression levels are not sufficient for visualization of *Cre* expressing cells. CRHR1 expression levels and corticosterone levels in CRHR1-*Cre* mice are reported as unaltered when compared to wild-type mice. The authors used this *Cre*-driver line to dissect the local CRH circuitry within the central amygdala and postulate that CRH/CRHR1 signaling in the CeA is critical for fear learning at low threat levels (Table 2).

Table 2: Summary of *Cre*-driver lines targeting the CRH receptor type 1

Transgenic Line	Targeting Strategy	Validation	Reference
CRHR1-Cre	**BAC transgenic:** insertion of the cDNA encoding *Cre* followed by a poly A signal directly at the START codon of the CRHR1 gene in BAC RP23-4B21	Crossing to a Rosa-*lacZ* reporter line (Soriano, 1999); data not shown.	*(137)*
CRHR1-IRES-Cre	**Knock-in:** insertion of an *IRES-Cre* cassette into the 3'UTR of the endogenous CRHR1 locus	Crossing to the Ai14 reporter strain (Madisen et al., 2010).	*(62)*

The expression of *Cre* recombinase under the endogenous CRHR1 promoter opens up new avenues for more precise expression and circuit analyses, especially because of the lack of specific antibodies and the low expression levels in certain brain regions (*99*). The following areas of application are of particular interest: 1. Breeding to *Cre*-dependent reporter strains would increase the sensitivity for visualization and morphological characterization of CRHR1 expressing cells and would enable anterograde tracing of labeled axons (*187*). Furthermore, it would facilitate co-expression analysis, laser capture dissection, fluorescence activated cell sorting and electrophysiological measurements 2. *Cre*-dependent viral delivery of transsynaptic tracers for circuit mapping (*188*) 3. Optically activating or silencing CRHR1 expressing neurons via *Cre*-dependent activation of viral vectors encoding opsins (e.g., channelrhodopsin, halorhodopsin) (*189*) 4. Cell type-specific transcriptome and epigenome analyses via breeding to the RiboTag mouse line, or Sun1-tagged line, respectively (*190*). 5. Gain-and-loss-of function approaches through breeding of the CRHR1 *Cre*-driver line to strains possessing "floxed genes", or Cre-inducible expression cassettes, respectively.

2.5 Recombinase-mediated cassette exchange (RMCE)

In recent years many *Cre*-driver mouse lines have been generated either by individual laboratories or by large-scale programs such as the gene expression nervous system atlas (GENSAT) *Cre* project, the EU funded project EUCOMMTOOLS, the inducible *Cre* line project from the Institute Clinique de la Souris (ICS) and the NIH Neuroscience Blueprint *Cre* Driver Network program. The procedures applied to generate these driver lines comprise classic random transgenic insertion of small promotor-driven *Cre* cDNA or BAC based large insert random insertion and several knock-in approaches (*169*). The targeted knock-in into an endogenous locus bears less risk regarding “off target activity” compared to the caveats of classic transgenesis, such as insertional mutagenesis, copy number variations or integration site dependent position effects. Nevertheless, a careful characterization of the *Cre*-driver line, e.g., breeding to respective reporter strains is crucial, particularly with regard to transient activation of expression during embryogenesis or deletion in the male/female germline. The term knock-in refers to a genetic engineering method which is based on homologous recombination between a specifically designed targeting vector and a locus of interest. As a result, the *Cre* recombinase is placed under the control of the promoter and regulatory sequences of the target gene and therefore expressed in replacement of the target gene. In 1989 the first mutant mice obtained by homologous recombination in ES cells were reported (*169*). Since then the basic principles of replacement targeting vectors have not changed: a 5’ and 3’ homology arm flank a heterologous DNA sequence, usually including a positive selection marker such as the neomycin (neo) or hygromycin (hyg) resistance gene and/or a reporter cassette. By flanking the positive selection marker with *loxP* or *frt* sites it can be removed later from the target locus to prevent interference with expression of neighboring genes. Random insertion of the targeting vector can be circumvented by insertion of a negative selection marker (e.g., thymidine kinase gene, *HSV-tk or* diphtheria toxin A fragment, DTA) adjacent to the target homology. Random integration will result in the integration of the negative selection marker into the genome; HSV-thymidine kinase converts the non-toxic guanine analogue ganciclovir into a toxic metabolite that will subsequently kill the cell, whereas DTA has a direct cytotoxic effect. For gene replacement, the targeting vectors are routinely introduced in mouse ES cells, which have the unique ability to retain their pluripotency after *in vitro* culture. Thus, when ES cells are injected into a

preimplantation embryo they can contribute to all tissues of the embryo, including the germ line. Contribution to germ cell formation leads to transmission of the introduced genetic modification to offspring from the chimeric mice (*191*). Once the so-called "parental" ES cell line is established by homologous recombination, recombinase-mediated cassette exchange (RMCE) enables rapid exchange of sequences flanked by specific recombinase target sequences directly in these "parental" ES cells. One of the big advantages compared to classical knock-in strategies is the possibility to generate ES cells carrying a series of different mutations in a gene of interest, derived from only one parental ES cell clone. This subsequently enables efficient and timesaving generation of a series of mutant knock-in mice at the locus of interest. To date three bacteriophage- or yeast-derived site-specific recombinases (SSR) are predominantly used. They belong to either of two families, tyrosine recombinases (Tyr) like *Cre* (recombination target sequence *loxP*) or *Flp* (recombination target sequence *frt*) and serine recombinases (Ser) such as ϕC31 integrase (*phiC31*) (recombination target sequence *attP* and *attB*) (*192*). Both family members can mediate different types of recombination events (integration, excision and inversion) dependening on the orientation of the respective recombination target sequences. *Cre* and *Flp* act in a reversible manner as they cause two identical recombinant sites, which enable consecutive rounds of recombination. The site-specific recombinase *phiC31* is derived from a *Streptomyces* phage that catalyzes the integration of recombinant DNA containing *attB* (*a*ttachment site *B*acterium) sites into a genomic target locus harboring *attP* (*a*ttachment site *P*hage) sites. The completed *attP/attB* recombination event leads to hybrid *attL* and *attR* (*L*eft and *R*ight) sites that are not substrates for the integrase, thus the exchange is irreversible. Other advantages of the *phiC31* integrase is the non-necessity for synthetic/heterospecific att-sites and the fact that the mouse genome per se contains only a limited number of endogenous target sites (so called "pseudo *attP* sites"). The principle of RMCE using *phiC31* integrase is depicted in Figure 6. A simultaneous recombination event between two heterotypic *attP* and *attB* sites results in exchange of cassettes. The presence of an excisable selection marker on the incoming plasmid allows for positive selection of the desired event. Recombination at the 5'-recognition site (type I insertion) or at the 3'-recognition site (type II insertion), respectively is a two-step process: first, integration of the complete donor plasmid followed by an integrase mediated deletion event between the intact *attP* and *attB* sites, resulting in removal of

the original “parental” cassette and the plasmid backbone (*193*). *PhiC31* integrase mediated methods in mice have been used so far, among others, for transgenesis in mouse ES cells (*193-195*), for generation of transgenic mice via microinjection of recombinant DNA into zygotic pronuclei (*196*), for *in vivo* gene delivery (*197*) and for gene therapy of hemophilia in factor IX knockout mice (*198*). Of special significance for human stem cell research is the possibility of generating a variety of induced pluripotent stem cell (iPSC) lines expressing different transgenes of choice from one parental line and subsequent applications in gene therapy (*199*).

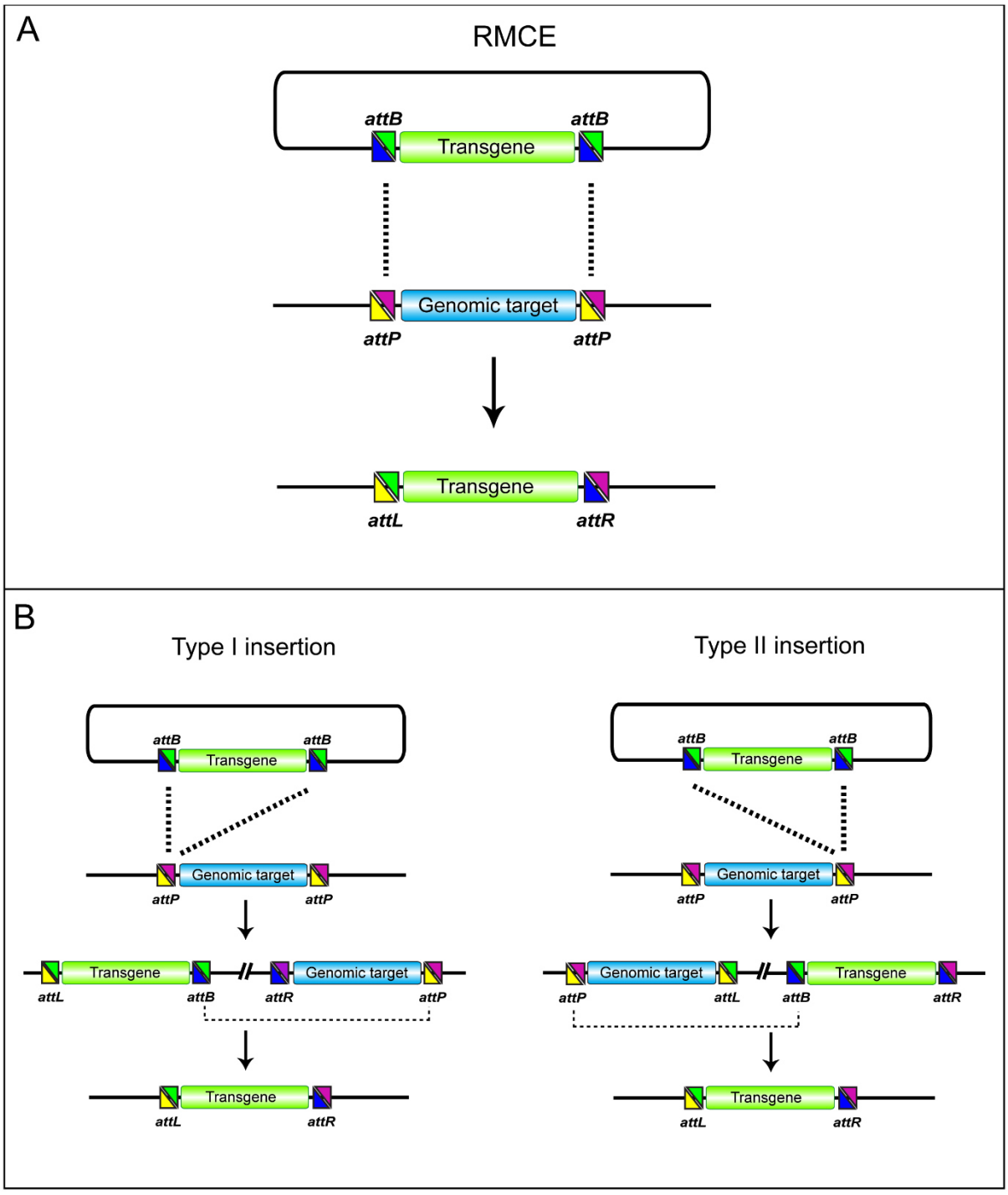

Figure 6: Schematic diagram illustrating different scenarios of the *phiC31* integrase-mediated cassette exchange strategy

(A) Cassette exchange via concurrent recombination between the two pairs of heterotypic recognition sites. (B) Type I and type II insertion at the 5'- or 3'- recognition site, respectively. In a second recombination step the original "parental" cassette and the plasmid backbone are removed through recombination of the intact *attP* and *attB* sites. Colored triangles represent the different *att* sites. For details, see text.

2.6 Beyond the *Cre/lox* system

Expanding the toolbox of SSRs to various members of the "CRH-family" would allow for a series of sophisticated experiments to further dissect and manipulate the complex neurocircuits and pathways underlying psychiatric disorders. *Flp* (also termed "Flippase" due to the ability of inverting/"flipping" a DNA segment in S.cerevisiae) is another site-specific DNA recombinase of the tyrosine recombinase family derived from the 2µm plasmid of the yeast *Saccharomyces cerevisiae*. Analogous to the *Cre/lox* system it recombines DNA at *frt* (*Flp* recombinase recognition target) sites without the need for cofactors. Although several modifications to the *Flp* coding sequence improved either the thermostability in mammalian cells ("enhanced", *Flpe*) or the recombination efficiency ("codon-optimized", *Flpo*), the *Flp/frt* system has never acquired equivalent significance to *Cre* and is most commonly used to remove *frt*-flanked ("flrted") selection cassettes from targeting constructs (*200*). Accordingly, only a limited number of *Flp*-driver lines have been established (see mouse genome informatics website, Jackson Laboratory; http://www.informatics.jax.org). New on the scene since 2004 is the phage D6 site-specific DNA recombinase *Dre*, a tyrosine recombinase closely related to *Cre* but with a distinct 32bp DNA recognition site (*rox*; region of crossover (x)) (*201*). With the development of a first *Dre*-deleter mouse strain (*202*) and more recently *Dre*-driver lines (*Nr4a2-SA-IRES-Dre; Pvalb-2A-Dre*) and double-dependent reporter lines (*Ai66*) (*203*) another set of efficient tools with high specificity extend the genomic toolbox for genome engineering (*204*).

The generation of inducible SSRs variants allows for temporal control of recombinase expression at any time, thereby circumventing the problem of "ectopic" expression - a result of transient recombinase activation during development and preventing potential toxic side effects of high levels of *Cre* activity (*205*). The most widespread approach to date is the *CreER^{T2}* recombinase, which is a *Cre* recombinase fused to

the mutated human estrogen receptor ligand binding domain (LBD) (G400V/M543A/L544A triple point mutation, rendering the LBD insensitive to endogenous estrogen binding). Thus the *CreER^{T2}* recombinase is only activated by the systemic or topic administration of Tamoxifen - a synthetic estrogen receptor ligand - which is metabolized in the liver to the active form 4-hydroxytamoxifen (4-OHT). In the absence of 4-OHT the *CreER-LBD* fusion protein forms a complex with heat shock protein 90 (hsp90) which prevents translocation from the cytoplasm to the nucleus. Binding of the active inducer 4-OHT leads to dissociation of the complex and translocation of *CreER-LBD* to the nucleus, where *Cre*-mediated recombination of target DNA can occur (*167, 206*). In the past, numerous *CreER^{T2}*-driver mouse lines have been generated in individual labs and by large-scale projects such as GENSAT, NIH Blueprint Cre Driver Network, EUCOMM and others (see mouse genome informatics (MGI) web portal for overview). The Institute Clinique de la Souris (ICS) has developed a specific *CreER^{T2}* database with standardized characterization of different inducible *Cre* mouse lines (http://www.ics-mci.fr/en/resources-and-technologies/creert2-zoo/). Recently Devine and colleagues generated the first inducible *DreER^{T2}* driver line for genetic fate mapping of cardiac progenitors (*207*). As an alternative to the *CreER-LBD* approach new alleles have been created via fusion of *Cre* with a modified E.coli dihydrofolate reductase (*DHFR*) protein. The common antibiotic trimethoprim (TMP), which is easy to administer and crosses the blood-brain barrier, constitutes the inducer that stabilizes the rapidly degraded *Cre/DHFR* fusion protein, which is then translocated to the nucleus and initiates DNA recombination. TMP-inducible *Cre* lines are an attractive alternative because they exclude the possibility of Tamoxifen binding to native estrogen receptors and provide faster temporal control (*208*).

Intersectional approaches where reporter gene expression depends on the simultaneous presence of two SSRs enable temporal and spatial refined labeling, identification and activation/inhibition of neuronal subsets within a larger defined cell population (e.g., primary classification according to promoter activity, location or connectivity). Intersectional alleles comprise two *STOP* cassettes disrupting double reporter genes; each of the reporter cassettes is flanked by recombinase specific recognition sites (e.g., *loxP* and *frt*). Thus, the “intersectional” population can be selectively marked or activated. Intersectional alleles could also be designed for “subtractive” labeling strategies in a way that a “floxed” transcriptional terminator

blocks the activity of the reporter and additionally the reporter cassette is flanked by *frt* sites. In this constellation, the expression of the reporter protein is “turned on” by *Cre* recombinase and “turned off” simultaneously in all cells/regions where the *Flippase* is active, which means that only *Cre* positive/*Flp* negative cells are labeled. Dedic and colleagues identified triple-positive GABAergic/Camk2a/CRH neurons in the BNST and CeA by combining this dual-recombinase intersectional method with immunohistochemistry. Breeding the *RC::FrePe* double reporter mouse line (*209*) to *Dlx5/6 –Flp* mice leads to the expression of *mCherry* reporter gene in GABAergic neurons and subsequent crossing to *Camk2a-CreER*^{T2} mice resulted in deletion of the l*oxP*-flanked *mCherry STOP* sequence and expression of *eGFP* reporter protein in double-positive GABAergic/Camk2a neurons. Combination with immunohistochemistry against CRH identified a specific CRH subpopulation within a fear-suppressing mesolimbic neurocircuit (*100*). A dual recombinase conditional allele (Ai80D mice, Jackson Laboratory, stock no # 025109) which enables expression of a mutant channelrhodopsin variant (CatCh) is also available, but functional testing if light-induced opsin activation effectively depolarize/activate neurons has not been published yet. Fenno and colleagues developed a more flexible viral approach-called “INTRsect” (INTronic Recombinase sites enabling combinatorial targeting), which circumvents transient developmental promoter activity triggering recombinase expression. They expand the DIO (double inverted open-reading-frame) expression system in a way to independently manipulate ORF fragments. Both *Flp* and *Cre* recombinases are necessary to produce a complete reading frame in sense orientation. Using components of this system, they targeted mesolimbic dopaminergic projection neurons within the VTA: a *Cre*-dependent *Flp* cassette was packaged into a retrograde herpes-simplex virus (HSV) and injected into the nucleus accumbens (NAc) of *TH-Cre* transgenic mice, while a *Flp* inducible targeting construct (AAV-fDIO-ChR2-eYFP) was injected into the VTA. Only VTA-NAc projecting dopaminergic neurons (*TH* positive) that both express the *Cre* and are transduced by HSV express *Flp* and activate ChR2-eYFP expression. With this approach it is possible to restrict expression of a reporter to cells which are defined by genetic identity and projection pattern (*210*).

As alternative to the simultaneous utilization of two different SSRs, the so called “split-*Cre* system”, has been demonstrated as a highly specific technique to generate intersectional *Cre*-drivers. The system is based on the spontaneous

complementation of two separately inactive *Cre* protein fragments (termed *NCre,* amino acids 15-59 and *CCre,* amino acids 60-343) in overlapping expression sites (*211*). Further development of this method increased the efficiency of split-Cre reconstitution, because it prevents dissociation of the two fragments. The “split-intein-split-Cre”-system is based on Cre-reconstitution through protein splicing. In short, a “split-intein” protein from the cyanobacterium *Synechocystis sp*. has the capability to splice the two halves of *Cre* recombinase (termed *Cre*-N-Intein-N and Intein-C-*Cre*-C) into one functional protein while excising itself. Targeting the *Cre*-N to a region/tissue specific promoter in combination with the *Cre*-C being expressed in a cell-type specific manner facilitates two-dimensional spatial and temporal (Split-*CreER*^{T2}-system) control of DNA recombination and therefore enables the precise genetic labeling of a distinct subpopulation (*212*-*215*).

An overview of existing *Cre*-driver mouse lines related to the CRH/CRHR system is listed in chapter 2.4 and was recently reviewed by Dedic et al., 2017. It becomes obvious that there are needs for further development of *Flp* and *Dre* driver lines within the “CRH-family” to use all the possibilities and benefits of above described intersectional and subtractive approaches. With the extremely successful advent of a genome editing technology known as CRISPR/Cas9 (*Clustered Regularly Interspaced Short Palindromic Repeats*), the rapid generation of numerous reporter/recombinase/transcriptional effector knock-ins is achievable. Recently Quadros and colleagues published a further development of the technology termed “*Easi-CRISPR*” (*Efficient additions with ssDNA inserts-CRISPR*), a one-step delivery of long single-stranded DNA donors in combination with pre-assembled crRNA + tracrRNA + Cas9 ribonucleoprotein (ctRNP) complexes directly into mouse zygotes. The robustness, efficiency and high flexibility of this method offers the possibility of high-throughput genome engineering applications in the future (*216*).

3 Aim of the thesis and individual development steps

The aim of this study was the generation of a novel *Cre* mouse line with constitutive *Cre* recombinase activity restricted to CRHR1 expressing cells.

Initially, a genetic *Cre* targeting vector was engineered and introduced via RMCE into a “pre-inserted docking site” in the genome of embryonic stem (ES) cells. The RMCE strategy relies on a multifunctional CRHR1 knock-in allele, which contains targeting sites for the *phiC31* integrase. The advantage of this knock-in approach into the endogenous locus of the CRHR1 gene is the fact, that the *Cre* expression pattern is more likely to reflect endogenous gene expression compared to classical transgenic approaches, because all regulatory elements of the targeted gene are present at their native position.

The resulting *CRHR1*^{tZCre} mouse line however revealed an alternative recombination event resulting in *Cre* expression in a subpopulation of CRHR1 expressing neurons. To get rid of a residual reporter cassette and the hygromycin selection cassette a consecutive round of breeding was performed. The *CRHR1*^{tZCre} mouse line was crossed with a line expressing the enhanced form of the site specific recombinase *Flp* (FLPeR, “flipper”) to generate the CRHR1 *Cre*-driver mouse line.

In the next step both recombinase driver lines, CRHR1^{tZCre} and CRHR1^{Cre} were thoroughly analyzed with regard to specificity and efficiency of *Cre* expression and *Cre*-mediated deletion.

This new *Cre* mouse line will allow a variety of sophisticated experiments that will contribute to a more precise circuit analysis of CRH/CRHR1 pathways in the brain. In this context, a *Cre*-dependent anterograde viral tracer was used for mapping forebrain CRHR1-specific output pathways. Furthermore, this *Cre*-driver line was used for ligand independent mesolimbic pathway activation by expression of a constitutively active version of CRHR1 in the VTA.

In the figure below the generation and characterization of this new *Cre*-driver line is summarized in a flow chart highlighting the critical parameters associated with production and validation of *Cre*-driver transgenic lines.

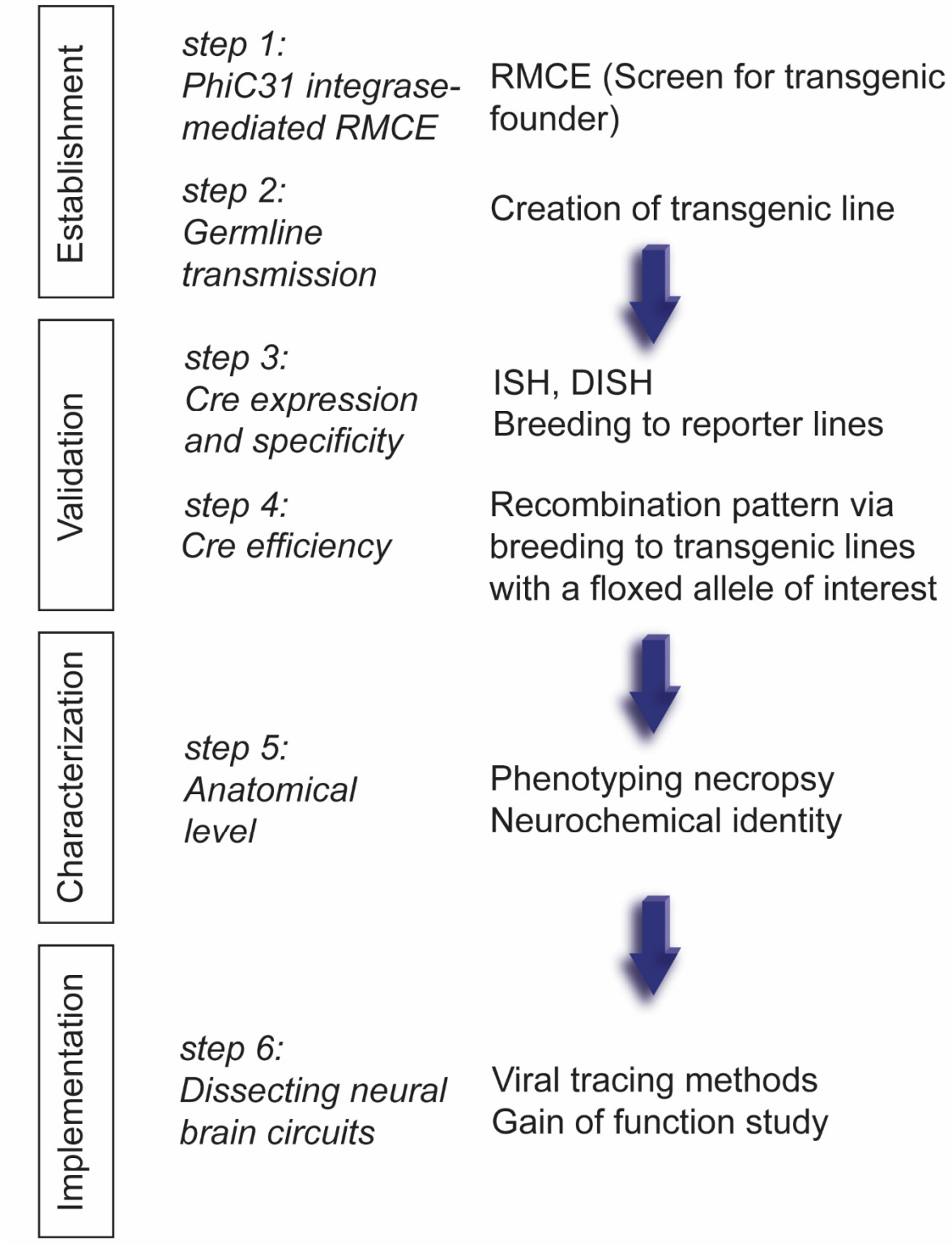
Establishment
step 1:
PhiC31 integrase-mediated RMCE
RMCE (Screen for transgenic founder)
step 2:
Germline transmission
Creation of transgenic line
Validation
step 3:
Cre expression and specificity
ISH, DISH
Breeding to reporter lines
step 4:
Cre efficiency
Recombination pattern via breeding to transgenic lines with a floxed allele of interest
Characterization
step 5:
Anatomical level
Phenotyping necropsy
Neurochemical identity
Implementation
step 6:
Dissecting neural brain circuits
Viral tracing methods
Gain of function study

4 Materials

4.1 Devices

Table 3: Listing of devices

Device	Manufacturer
AxioCam MRc5 color ccd camera	Zeiss, Göttingen, Germany
AxioCam MRm greyscale ccd camera	Zeiss, Göttingen, Germany
Axioplan 2 microscope	Zeiss, Göttingen, Germany
Balance LP1040	Sartorius,Göttingen, Germany
Biofuge Pico	Heraeus, Hanau, Germany
Bullet Blender Storm 24	Kisker, Steinfurt, Germany
Cell Culture Incubator	Heraeus, Hanau, Germany
Centrifuge J2-MC	Beckman Instruments, Krefeld, Germany
Centrifuge Heraeus® Pico®	Thermo Fisher Scientific, Waltham, USA
Concentrator 5301	Eppendorf, Hamburg, Germany
Confocal Microscope LSM 800	Zeiss, Göttingen, Germany
Cryostat HM560 M	Thermo Fisher Scientific, Waltham, USA
Cryostat CM3050S	Leica, Wetzlar, Germany
Developing automate	Kodak, Rochester, USA
DNA electrophoresis chambers	Peqlab, Erlangen, Germany
Electrophoresis power supply	Peqlab, Erlangen, Germany
Fluorescence Stereomicroscope M205FA	Leica, Wetzlar, Germany
Gel documentation	Vilber Lourmat, Eberhardzell, Germany
Glassware	Schott, Mainz, Germany
Laminar Air Flow Cabinet HB2488	Heraeus, Hanau, Germany
Light Source KL1500	Leica, Wetzlar, Germany
Magnetic stirrer	IKA, Staufen, Germany
Nanophotometer P330	Implen, München, Germany
Stereomicroscope MZ APO	Leica, Wetzlar, Germany
Orbital Mixer Unimax 2010	Heidolph, Nürnberg, Germany
PCR Cycler	Biorad, München, Germany
pH-Meter	Schott, Mainz, Germany
Picofuge	Stratagene, San Diego, USA
Pipettes	Gilson, Middleton, USAH
Pipettes	Eppendorf, Hamburg, Germany

Table 3: Listing of devices (continued)

Device	Manufacturer
Pipettes	Biohit, Helsinki, Finland
Polymax 1040	Heidolph, Nürnberg, Germany
Stereo Microscope	Leica, Wetzlar, Germany
Stereotactic frame	TSE systems, Moos, Germany
Stereotactic frame	Leica, Wetzlar, Germany
Thermomixer 5436	Eppendorf, Hamburg, Germany
UV-Stratalinker 2400	Stratagene, San Diego, USA
Vaporizer Key Fill Isoflurane Apollo	Northern Vaporizers, Kansas City, USA
Vibratom HM560	Thermo Fisher Scientific, Waltham, USA
Vortex MS1 Minishaker	IKA, Staufen, Germany
Waterbath 1002	GFL, Burgwedel, Germany

4.2 Cell Lines

Table 4: Listing of used cell lines

Cell Line	Origin
TBV2 (129S2) mouse ES cells	R. Kühn, Helmholtz Center Munich, Germany
EMFI (neomycin resistent fibroblasts)	S. Bourier; Helmholtz Center Munich, Germany
EMFI (hygromycin resistent fibroblasts)	S. Bourier; Helmholtz Center Munich, Germany
Primary neuronal cells	L.Tietze, MPI of Psychiatry, Munich, Germany

4.3 Antibodies

Table 5: Listing of used antibodies

Antibody	Supplier
Alexa Fluor 488 goat anti chicken	Invitrogen, #A11039, 1/1000
Alexa Fluor 488 goat anti rabbit	Invitrogen, #A11034, 1/1000
Alexa Fluor 594 goat anti chicken	Invitrogen, #A11042, 1/1000
Alexa Fluor 594 goat anti rabbit	Invitrogen, #A11037, 1/1000
Alexa Fluor 594 donkey α-goat	Invitrogen, #A11058, 1/1000
Anti-DIG alkaline phosphatase	Roche #11093274910
Anti-DIG(Fab) peroxidase	Roche #11207733910
Streptavidin alkaline phosphatase	Roche #11093266910

Table 5: Listing of used antibodies (continued)

Antibody	Supplier
Streptavidin horseradish peroxidase	Roche # 11089153001
Chicken anti-GFP	Abcam, #13970, 1/2000
Rabbit anti-Tyrosine hydroxylase	Pel Freez, # P40101-150 1/2000
Biotinylated donkey anti chicken	Jackson ImmunoResearch #48442

4.4 Mouse strains

Table 6: Listing of mouse strains used in this thesis

Mouse strain	Origin
Gt(ROSA)26Sor$^{tm9(CAG-tdTomato)Hze}$; ("Ai9")	Jackson Laboratory, stock no # 007905
Gt(ROSA)26Sor$^{tm5(CAG-Sun1/sfGFP)Nat}$	Jackson Laboratory, stock no # 021039
Gt(ROSA)26Sor$^{tm1(FLP1)Dym}$; ("Flipper")	Jackson Laboratory, stock no # 003946
Neurod6$^{tm1(cre)Kann}$; (NEX-CRE)	provided by Dr. Klaus-Armin Nave, MPI of Experimental Medicine, Goettingen, Germany
Crhr1$^{\Delta Egfp}$	MPI of Psychiatry, Munich, Germany

4.5 Viral Vectors

Table 7: Listing of viral vectors used in this thesis

Viral Vector	Origin
pAAV-Ef1a-DIO-*mCherry*	Addgene #50462
pAAV-Ef1a-DIO-Syn-eGFP	pAAV-Syn-eGFP provided by Dr. Valery Grinevich, DKFZ, Heidelberg, Germany; subcloned into "Flex" vector by Dr. Nina Dedic
EGFP ((CA)CRHR::EGFP)	provided by Dr. Arenkiel, Baylor College of Medicine, Houston. USA

4.6 Consumables

Table 8: Listing of consumables

Item	Company
1,5ml, 2ml reaction tubes	Sarstedt, Nürnbrecht, Germany
15ml Falcon tubes	Greiner, Frickenhausen, Germany
50ml Falcon tubes	Greiner, Frickenhausen, Germany

Table 8: Listing of consumables (continued)

Item	Company
Agarose	Invitrogen, Karlsruhe, Germany
Ampicillin	Sigma, Deisenhofen, Germany
BioMax MR film	Carestream Health, Stuttgart, Germany
DAB substrate kit (#SK-4100)	Biozol, Eching, Germany
Deoxynucleoside Triphosphate Set	Roche, Mannheim, Germany
DIG RNA Labeling Kit	Roche, Mannheim, Germany
DIG Wash and Block Buffer Set	Roche, Mannheim, Germany
DnaseI	Roche, Mannheim, Germany
DPX mounting medium	Merck, Darmstadt, Germany
Ethidiumbromide	Roth, Karlsruhe, Germany
Herculase Enhanced DNA Polymerase	Agilent Technologies, Santa Clara, USA
Hygromycin B	Calbiochem, Darmstadt, Germany
Isoflurane	Abbott, Chicago, USA
Kanamycin	Sigma, Deisenhofen, Germany
LB Agar	Becton Dickinson, New Jersey, USA
LB Medium	Becton Dickinson, New Jersey, USA
Nalgene™ freezing container	Thermo Fisher Scientific, Waltham, USA
Neon™ Transfection System	Invitrogen, Karlsruhe, Germany
NTB Emulsion	Carestream Health, Stuttgart, Germany
NTP mix (10mM)	Roche, Mannheim, Germany
Nunclon™ cell culture petri dishes	Thermo Fisher Scientific, Waltham, USA
Oligo(dT)$_{15}$ Primer	Roche, Mannheim, Germany
PCR tubes and plates	Sarstedt, Nürnbrecht, Germany
Petri Dishes	Greiner, Frickenhausen, Germany
Pipette tips	Sarstedt, Nürnbrecht, Germany
Protector RNase Inhibitor	Sigma, Deisenhofen, Germany
ProTaq mounting medium	Biozol, Eching, Germany
Qiagen Plasmid Mini Kit	Qiagen, Hilden, Germany
Qiagen Plasmid Plus Maxi Kit	Qiagen, Hilden, Germany
Qiaquick Gel Extraction Kit	Qiagen, Hilden, Germany
Qiaquick PCR Purification Kit	Qiagen, Hilden, Germany

Table 8: Listing of consumables (continued)

Item	Company
Restriction enzymes	New England BioLabs, New England, USA
RNeasy Plus Mini Kit	Qiagen, Hilden, Germany
Serological pipettes	Sarstedt, Nürnbrecht, Germany
Shrimp Alkaline Phosphatase	New England BioLabs, New England, USA
Sp6 RNA polymerase	Roche, Mannheim, Germany
Superscript II	Invitrogen, Karlsruhe, Germany
T3 RNA polymerase	Roche, Mannheim, Germany
T4 DNA Ligase (5U/µl)	Thermo Fisher Scientific, Waltham, USA
T7 RNA polymerase	Roche, Mannheim, Germany
ThermoPrime Taq DNA Polymerase	Thermo Fisher Scientific, Waltham, USA
TOPO®TA Cloning Kit	Thermo Fisher Scientific, Waltham, USA
Trizol	Invitrogen, Karlsruhe, Germany
TSA™ Biotin System	PerkinElmer, Waltham, USA
UTPαS (35S) 1250Ci/mmol	PerkinElmer, Waltham, USA
Vectashield® Mounting Medium	Biozol, Eching, Germany
Vector Red Alkaline Phosphatase Kit	Biozol, Eching, Germany
X-Gal	Thermo Fisher Scientific, Waltham, USA

4.7 Oligonucleotide Sequences

All oligonucleotides were ordered at Metabion AG (Planegg, Germany) and used as either PCR primers, genotyping primers, primers for generation of ISH probes or sequencing primers.

Table 9: Oligonucleotides

Oligonucleotide	Sequence
Crhr1_Intron2_long_MfeI_for.	caattggatctgtttcacaaactgcaga
Crhr1_Intron2_long_SpeI_rev.	actagttctcccgccggaaacgcc
Crhr1_Intron2_small_AgeI_for.	accggtctccttcaggtggagcct
Crhr1_Exon 3 all_rev.	ttgtggtgttgtagcggaca
Crhr1_Exon 3 all_for.	caatgcctccgtggacct
Crhr1wt_AscI_rev.	ggcgcgcctcacactgctgtggactgct
AscI *IRES*Cre fwd.	ggcgcgccgaattccgccccccccccc

Table 9: Oligonucleotides (continued)

Oligonucleotide	Sequence
Cre rev.-SwaI	ttaattaagatctagtggatccaga
Hygro_BstBI_for..	ttcgaaatgaaaaagcctgaactcacc
Hygro_BsrGI rev.	tgtacaaagcttctgatggaattagaacttg
cre fwd.	gatcgctgccaggatatacg
cre rev.	aatcgccatcttccagcag
Thy1-F1	tctgagtggcaaaggaccttagg
Thy1-R1	ccactggtgaggttgagg
hygro fwd.	cggtgagttcaggctttttc
Primer 2cre rev	cacccatggttagtcccagt
Flipase 1 fwd	gacctgcaggaaccaactgt
tau rev.	tctgcaggggagactctttc
neo fwd.	cgatcccatggtttagttcc
Primer 2 cre rev.	cacccatggttagtcccagt
P-PGK-fwd-2	cctaccggtggatgtggaat
P-Cre-downs-fwd-2	aataataaccgggcaggggg
Flipper-rev-1	gactagagcttgcggaaccc
P-T2A-rev-1	ccacgtcaccgcatgttaga

4.8 ISH probes

Table 10: mRNA probes

Target	Vector	Size	Accession number
CRHR1 (Exon 2-8)	pCRII-Topo	654bp	NM_007762 (nucleotides 265-918)
CRHR1 (Exon 8-12)	pCRII-Topo	396bp	NM_007762 (nucleotides 901-1296)
CRHR1-3'UTR	pCRII-Topo	702bp	NM_007762 (nucleotides 1728-2428)
lacZ	pCRII-Topo	649bp	X65335 (nucleotides 2649-3281)
Cre	pCRII-Topo	575bp	AB449974 (nucleotides 567-1062)
Tomato	pCRII-Topo	689bp	AY678269 (nucleotides 740-1428)
GFP	pCRII-Topo	724bp	U55762 (nucleotides 677-1396)
TH	pGEM	765bp	NM_009377 (nucleotides 23-788)
GAD65	pBluescript II KS	847bp	NM_008078 (nucleotides 753-1600)
GAD67	pBluescript II KS	956bp	NM_008077 (nucleotides 984-1940)

5 Methods

5.1 Polymerase chain reaction (PCR)

Standard PCR for further cloning was performed to amplify the required DNA sequences from a template DNA (genomic DNA, plasmid DNA or cDNA). The respective flanking sequences of the target DNA were used to design primer pairs with the aid of Primer3 (http://primer3.ut.ee); primers were purchased from Metabion AG (Planegg, Germany). For a standard 50µl PCR reaction the following reaction mixture was prepared on ice:

xµl template DNA (typically 100ng-1µg)
5µl 10x reaction buffer
3µl 25mM $MgCl_2$
1µl dNTPs (dATP, dGTP, dCTP, dTTP, 10mM each)
0.1µl forward primer (100mM)
0.1µl reverse primer (100mM)
0.5µl Taq DNA polymerase (5U/µl)
Water ad 50µl

The following standard PCR program was used:

Step 1	95°C/5’	initial DNA denaturation
Step 2	95°C/2’	DNA denaturation
Step 3	55°-65°C/30s	primer annealing (dependent on the primer melting temperature)
Step 4	72°C/30s	elongation time (estimated 1kb elongation/kb PCR product)
Step 5	got to step 2	29 cycles
Step 6	72°C/5’	final elongation
Step 7	12°C	hold

Analysis of the PCR products was made via gel electrophoresis (0.8%-2% agarose in 1x TAE, containing 0.01% ethidium bromide). Typically 1/10 of the PCR reaction volume was mixed with 6x Orange G loading dye and loaded on the gel (running conditions 160V constant/~1h/30’). For visualization, a UV transilluminator and gel documentation system was used (Quantum gel documentation system 1100 from Vilber Lourmat, Eberhardzell, Germany). For subcloning 1-4µl of fresh PCR product was ligated to pCRII Topo TA vector (Topo TA Cloning kit, Invitrogen, Karlsruhe, Germany) following the manufactures instructions. To control for mutations,

subcloned PCR products were sent for sequencing (Sequiserve, Vaterstetten. Germany). For PCR products longer than 1kb a Taq polymerase with proofreading capability was applied (Herculase Enhanced DNA Polymerase; Agilent, Santa Clara, USA) following the manufacturer's protocol.

5.2 Molecular Cloning Procedures

5.2.1 Topo TA cloning

Taq-amplified PCR products were cloned into the pCRII™ vector (TOPO TA Dual promoter cloning kit, Invitrogen, Karlsruhe, Germany), containing the T7 and sp6 promoters for efficient *in vitro* transcription in sense or antisense direction and M13 forward and reverse primer sites for sequencing. The ligation set up was as follows: 0.5-4µl fresh PCR product, 1µl salt solution, 1µl TOPO® vector, water to a total volume of 6µl. After incubation 5-30 minutes (depending on size of the PCR product) at room temperature, the reaction was placed on ice and up to 10µl were used for transformation in One Shot® competent *E.coli* (TOP10, Life Technologies™, Carlsbad, USA) according to the manufactures instructions. For blue-white selection of colonies, LB-agar plates containing X-Gal (40µg/ml) were used for plating different volumes of the cloning reaction.

5.2.2 Transformation of plasmid DNA into competent bacteria

For transformation of plasmids electrocompetent or chemically competent *E.coli* were used (TOP10, Life Technologies™, Carlsbad, USA), applying either the One Shot® chemical transformation or electroporation protocol provided by the manufacturer. After uptake of the plasmid DNA prewarmed SOC medium was added and bacteria were incubated for 1hour at 37°C on a horizontal shaker (225rpm). Subsequently 10-50µl from the transformation was spread on prewarmed selective LB plates, containing the appropriate selection marker (ampicillin 100µg/ml or kanamycin 50µg/ml) and incubated overnight at 37°C. The next day white or light blue colonies were picked and inoculated in 5-150ml selective LB medium and incubated overnight at 37°C on a horizontal shaker for subsequent DNA preparation (see next chapter).

5.2.3 Isolation of plasmid DNA

Preparation of plasmid DNA was performed either with the Qiagen Plasmid Mini Kit (5ml overnight bacterial culture) or Qiagen Plasmid Plus Maxi Kit (150ml culture volume). Bacteria from overnight cultures were pelleted by centrifugation, denatured by alkaline lysis, filtered through microspin columns, washed twice and finally eluted in 50µl nuclease free water. DNA, respectively RNA concentrations were measured by UV-spectrophotometry at 260nm (Nanophotometer, Implen, Munich, Germany); the concentration can be calculated according to Beer–Lambert law with the following equation: X µg/ml = OD260 x n x f, with f being the dilution factor and n the default factor (50µg/ml double stranded DNA; 33µg/ml single stranded DNA; 40µg/ml RNA).

5.2.4 Isolation of genomic DNA

For genotyping murine tail DNA was isolated according to a modified protocol adapted from Extract-N-Amp™ Tissue PCR Kit (Sigma-Aldrich, Taufkirchen, Germany): genomic DNA is extracted from tail clips of 2mm length that have been incubated in 100µl 50mM NaOH for 30 minutes at 95°C and neutralized with 30µl 1M Tris-HCL pH 7.0. An aliquot of the DNA extract (1-2µl) is then added directly to 25µl PCR mix. The following standard PCR program was used: 95°C/3min, 34cycles of 95°C/30sec, 57°C/30sec, 72°C/1min (per 1kb DNA), final elongation at 72°C/10 min and indefinite hold at 12°C.

To prepare genomic DNA from mouse liver mice were killed in an inhalation chamber with an overdose (>5%) of isoflurane; the organ was isolated and homogenized in liquid nitrogen using a precooled mortar and pestle. The resulting powder was resuspended (1ml buffer/100mg tissue homogenate) in NET-extraction buffer (2mM Tris pH 7.5, 25mM EDTA, 100mM NaCl). After addition of 1/10 volume 10% SDS and 1/10 volume Proteinase K (10mg/ml) the suspension was incubated overnight at 56°C. The next day DNA was purified by phenol-chloroform extraction and subsequent ethanol precipitation: addition of 1 volume Phenol/Chloroform/Isoamyl alcohol (25:24:1), centrifugation 10min/500rpm/4°C, removal of upper aqueous phase, addition of 1 volume Chloroform/Isoamyl alcohol (24:1), centrifugation 10min/500rpm/4°C and addition of 1/10 volume precipitation mix (3M NaAcetate, 2 volumes ice-cold 100% ethanol). The DNA precipitates at room temperature and can be “fished” with a glass Pasteur pipette. After a short rinse in 70% ethanol the DNA is air dried and resuspended in an appropriate amount of ddH_20.

5.2.5 Restriction digest

Restriction digest of plasmid DNA either for analytical or preparative purposes was carried out using restriction enzymes and recommended buffers from NEB (New England BioLabs, New England, USA). Usually 1µg-5µg of plasmid DNA was digested for one hour at 37°C with 10U/µg DNA of the restriction enzyme in corresponding buffers. For setting up double digest reactions the Double Digest Finder tool from NEB was used for selection of proper conditions; particular attention focused on star activity, methylation sensitivity and special incubation and storage temperatures of the enzymes.

5.2.6 Gel extraction

To extract and purify DNA fragments from agarose gels the Qiaquick Gel Extraction Kit from Qiagen (Hilden, Germany) was used according to the manufacturer's manual. DNA was eluted in 30µl nuclease free water (Ambion GmbH, Kaufungen, Germany). The concentration was determined by spectrophotometry and DNA integrity was assessed by gel electrophoresis.

5.2.7 Ligation of DNA fragments

For ligation of DNA fragments the T4 DNA Ligase (Thermo Fisher Scientific, Waltham, USA) was used which catalyzes the connection of fragments by generating a phosphodiester bond between the 5'- and 3'-ends. To this end 50ng of vector backbone was mixed with 3-10-fold molar excess of insert (depending whether fragments had sticky or blunt ends). H_2O, 2µl of T4 DNA ligase buffer and 10U of T4 DNA ligase were added to a final volume of 20µl and incubated overnight at 16°C. The next day an aliquot of the ligation mix was used without further purification for transformation in competent bacteria; storage is possible at -20°C. Whenever prevention of vector backbone religation was necessary, shrimp alkaline phosphatase from NEB (New England BioLabs, New England, USA) was used to dephosphorylate 5'-DNA termini according to the manufacturer's protocol.

5.3 RNA Techniques

5.3.1 RNA isolation

RNA was isolated from mouse brain using TRIzol™ (Invitrogen, Carlsbad, USA) together with the Bullet Blender® homogenizer from Next Advance (Kisker, Steinfurt, Germany). TRIzol is a ready to use mixture of phenol and guanidine isothyocyanate, which effectively dissolves RNA during homogenization. For tissue disruption one volume of beads together with two volumes of TRIzol (1ml/50-100mg tissue sample) were mixed in a safe-lock tube and homogenized for 3 minutes at speed 9. To permit complete dissociation of nucleoprotein complexes samples were incubated 5min at room temperature before adding chloroform (0.2ml/ml TRIzol Reagent). During centrifugation (12.000rcf/15min/4°C), the mixture separates and RNA remains in the upper aqueous phase, which is removed and transferred into a new tube. For precipitation of RNA 0.5ml 100% isopropanol/ml TRIzol was added and after centrifugation at 12.000g/10min/4°C, RNA forms a gel-like pellet at the bottom of the tube. After washing with 70% EtOH the RNA pellet was air dried, resuspended in RNase free water and stored at -80°C. RNA concentration was determined by UV-spectrophotometry at 260nm using the NanoPhotometer® (Implen GmbH, Munich, Germany); RNA integrity and RNA integrity number (RIN) were determined by analyzing the sample with the Agilent 2100 Bioanalyzer System (Agilent, Santa Clara, Germany).

5.3.2 Reverse transcription

To convert RNA in cDNA for subsequent PCRs, reverse transcription (RT) was performed using SuperScript II from Invitrogen (Carlsbad, USA) and oligo dT primers (Thermo Fisher Scientific, Waltham, USA). The standard approach comprised the following reagents: 3µg total RNA; 1µl DNase I (10U/µl), H_2O to a final volume of 10µl; to degrade genomic DNA this mixture was incubated first at 37°C/20min and afterwards DNase I was inactivated by heating up to 70°C for 15 minutes. Then 1µl oligo dT primer (500µg/ml), 4µl 5x first strand buffer, 2µl 0.1M DTT, 1µl dNTPs (10mM each), 1µl RNase Inhibitor (40U/µl) and finally 1µl of SuperScript II were added. After incubation at 42°C for 1 hour the reaction was stopped by elevating the temperature to 70°C for 15 minutes. To degrade template RNA 1µl RNase H was added and incubated at 37°C/20 min, followed by an incubation step at 70°C for 15 minutes to stop the reaction. In conjunction with every RNA sample, a “no RT” control

sample (no addition of SuperScript II) was prepared to check for genomic contaminations. For PCR reactions 1µl of RT reaction was used as template; cDNA was stored at -20°C.

5.4 Radioactive *in situ* hybridization (ISH)

For ISH cryostat sections of wild-type, transgenic or reporter mice were mounted side by side on Superfrost™ Plus slides (Thermo Fisher Scientific, Waltham, USA) to avoid technical variances and to secure precise comparison of hybridization signals. ISH was carried out as previously described (Refojo et al., 2011; Kühne et al., 2012). All relevant *in situ* probes had been amplified by PCR, subcloned into pCRII-TOPO® vector (Invitrogen, Carlsbad, USA) and sequence verified (Sequiserve, Vaterstetten, Germany). Specific riboprobes were generated by PCR using sp6, T3 or T7 primers to amplify templates for generation of sense and antisense ^{35}S-UTP (PerkinElmer, Waltham, USA) radioactive labeled cRNA probes by *in vitro* transcription:

2µl	PCR product
13µl	Rnase-free Water
3µl	10x transcription buffer
3µl	NTP mix (10mM each)
1µl	0.5M DTT
1µl	RNasin (RNase inhibitor, 40U/µl)
6µl	^{35}S-UTP (12.5mCi/mM)
1µl	sp6, T3 or T7 RNA polymerase (20U/µl)

Reaction was incubated at 37°C for 1 hour, then again 0.5µl of respective RNA polymerase was added and incubation continued for another 2 hours. To destroy the DNA template 2µl of RNase-free DNase I (Roche, Basel, Switzerland) was added for 15 minutes at 37°C and finally riboprobes were purified using the RNeasy Kit from Qiagen (Hilden, Germany) according to the manufacturer's instructions. Probes were eluted in 100µl Rnase-free water and concentration was determined using a scintillation counter (LS 6000, Beckman Coulter Biomedical GmbH, Munich, Germany). Sections were hybridized overnight with a riboprobe concentration of 7 x 10^6 cpm/µl at 57°C and washed as described below. Wherever cellular resolution was required, autoradiography was performed by dipping slides into Kodak NTB2 emulsion (Sigma, Deisenhofen, Germany). Slide development and cresyl violet counterstain was conducted 1-4 weeks after, depending on expression levels. For

long-term storage slides were embedded with DPX mounting medium (Merck, Darmstadt, Germany). The exact pretreatment and washing procedure is shown below.

Table 11: ISH Protocol

Pretreatment of slides			
Step	**Temperature**	**Time**	**Solution**
1.Fixation	on ice	10min	4%PFA/PBS/DEPC-H_2O
2.Washing	RT	2x 5min	1x PBS/DEPC-H_2O
3.Acetylation	RT	10min	0,1M Triethanolamine-HCL (TEA), pH 8.0; add freshly 600µl acetic anhydride/200ml TEA with rapidly stirring bar
4.Washing	RT	2x 5min	2x SSC/DEPC
5.Dehydration	RT	1min 1min 1min 1min 1min 1min	60% Ethanol/DEPC 70% Ethanol/DEPC 96% Ethanol/DEPC 100% Ethanol/DEPC $CHCl_3$ 100% Ethanol/DEPC
6.Drying	RT	~1hour	air dry in dust free area
Hybridization overnight in humidified chamber at 57-62°C			
7.Washing	RT	4x 5min	4x SSC
8.RNase A	37°C	20min	1x NTE + 500µl RNase A (20µg/ml)
9.Washing	RT	2x 5min	2x SSC/1mM DTT
10.Washing	RT	10min	1x SSC/1mM DTT
11.Washing	RT	10min	0.5x SSC/1mM DTT
12.Washing	64°C	2x 30min	0.1x SSC/1mM DTT
13.Washing	RT	2x 10min	0.1x SSC
14.Dehydration	RT	1min 1min 1min 1min 1min 1min	30% Ethanol/300mM NH_4OAc 50% Ethanol/300mM NH_4OAc 70% Ethanol/300mM NH_4OAc 95% Ethanol/300mM NH_4OAc 100% Ethanol/300mM NH_4OAc 100% Ethanol/300mM NH_4OAc
15.Drying	RT	~1hour	air dry in dust free area

Autoradiography: To visualize gene expression dried slides were exposed to high-resolution X-ray films (BioMax MR, Carestream Health, Stuttgart, Germany) for different time intervals, depending on expression levels (3-14 days).

Image Acquisition: Photographs were taken with digital cameras attached to a Zeiss Axioplan2 microscope (Zeiss, Göttingen, Germany) or a binocular stereomicroscope (Leica, Wetzlar, Germany). Images were digitalized using AxioVision Rel. 4.5 (Zeiss, Göttingen, Germany) and integrated into plates using Adobe Photoshop CS2 and Illustrator CS2 (Adobe, San Jose, USA). Only contrast, brightness and sharpness were adjusted to optimize signals.

5.5 Double *in situ* hybridization with DIG and ^{35}S labeled riboprobes

In order to colocalize two gene transcripts in the same tissue and to analyze the mRNA expression in specific cell populations, radioactive- and nonradioactive-labeled cRNA probes were combined to the so-called “double” *in situ* hybridization (DISH). The DIG-hybridization signal was detected by an enzymatic color reaction resulting in a somatic red precipitate that can be visualized by light field microscopy, whereas the radioactive riboprobe appeared as black silver grains after dipping slides into an autoradiographic emulsion (NTB2, Sigma, Deisenhofen, Germany). To this end, one probe is tagged with ^{35}S-UTP and the other with digoxigenin (DIG)-UTP, respectively. Antisense riboprobes were synthesized and labeled with ^{35}S-UTP or DIG-UTP by *in vitro* transcription from 200ng of PCR product as described in the chapter before. The efficiency of DIG labeling was determined by a dot blot assay. For hybridization 7 x 10^6 counts/slide of ^{35}S-cRNA was combined with ~200ng DIG-cRNA in an appropriate amount of hybridization mix (100µl/slide) and slides were incubated overnight at 57°-62°C in a humidified chamber. The exact pretreatment and washing procedure is shown below (adapted from Refojo et al., 2011).

Table 12: Double *in situ* hybridization protocol

Pretreatment of Slides for DISH			
Step	**Temperature**	**Time**	**Solution**
1.Fixation	on ice	15min	4%PFA/PBS/DEPC-H_2O
2.Washing	RT	2x 5min	1x PBS/DEPC-H_2O
3.Quenching	RT	15min	1% H_2O_2 in 100%MeOH
4.Washing	RT	2x 5min	1x PBS/DEPC-H_2O
5.Blocking	RT	8min	0.2M HCL/DEPC-H_2O
6.Washing	RT	2x 5min	1x PBS/DEPC-H_2O
7.Acetylation	RT	10min	0,1M Triethanolamine-HCL (TEA), pH 8.0; add freshly 600µl acetic anhydride/200ml TEA with rapidly stirring bar
8.Washing	RT	5min	1x PBS/DEPC-H2O
9.Dehydration	RT	1min 1min 1min 1min	60% Ethanol/DEPC-H_2O 70% Ethanol/DEPC-H_2O 96% Ethanol/DEPC-H_2O 100% Ethanol/DEPC-H_2O
10.Drying	RT	~1hour	air dry in dust free area
Hybridization overnight in humidified chamber at 57-62°C			
Washing and primary antibody			
1.Washing	42°C	20min	4x SSC/0.05% Tween® 20/1mM DTT
2.Washing	42°C	20min	2xSSC/50% Formamide/ 0.05% Tween® 20/1mM DTT
3.Washing	42°C	20min	1xSSC/50% Formamide/ 0.05% Tween® 20/1mM DTT
4.Washing	62°C	20min	0.1xSSC/0.05% Tween® 20/1mM DTT
5.RNase A	37°C	20min	1x NTE + 500µl RNAse A (20µg/ml)
6.Blocking	30°C	15min	15mM Iodoacetamide
7.Washing	30°C	3x 5min	1x NTE/0.05%Tween® 20
8.Blocking	30°C	60min	4%BSA/TNT
9.Washing	30°C	60min	TNT
10.Blocking	30°C	30min	NEN-TNB
11.1st ab	4°C	overnight	Anti-DIG(F_{ab})-POD in NEN-TNB
Incubation overnight/4°C/humidified chamber			

Table 12: Double *in situ* hybridization protocol (continued)

Washing, 2nd antibody and signal amplification			
Step	**Temperature**	**Time**	**Solution**
1.Washing	30°C	3x 5min	TNT
2.TSA	30°C	15min	TSA in 300µl DMSO 1/50 in amplification diluent
3.Washing	30°C	3x 5min	1x Roche wash buffer
4. 2nd ab	30°C	30min	Streptavidin-AP (1/400 in blocking buffer)
5.Washing	30°C	3x 5min	1x Roche wash buffer
6.Equilibration	RT	5min	100mMTris/HCL, pH8.2-8.5
7.Staining	RT	1-30min	Vector Red®
8.Stop	RT	10min	1xPBS
9.Fixation	RT	20min	2.5% Glutaraldehyde/PBS
10.Washing	RT	3x 5min	0.1x SSC
11.Dehydration	RT	30sec. 30sec. 30sec. 30sec.	30% Ethanol 50% Ethanol 70% Ethanol 96% Ethanol
12.Drying	RT	~1hour	air dry in dust free area

Data analysis: See chapter before (ISH) for dipping and slide development. Bright field images of Vector red- and silver grain developed DISH slides were captured with a Zeiss Axioplan microscope (Zeiss, Göttingen, Germany) using the 40x objective. For quantification of *Cre* co-expression with *Tomato* and *Crhr1*, respectively, cell counts were performed on three sections (thickness 20µm) per region (n=3 mice).

5.6 Histochemistry

5.6.1 Immunohistochemistry

Mice were euthanized in an inhalation chamber with an overdose (>5%) of isoflurane (Abbott, Chicago, USA) and the thorax was opened to dissect the heart. Transcardial perfusion was carried out with 4%PFA/PBS 1x for 5-7 minutes at a flow rate of 10ml/minute. After perfusion was completed, brains were removed and post fixed in

4%PFA/PBS 1x at 4°C (2-24hours). For long term storage brains were stored in 30%(w/v) saccharose/0.5% PFA/PBS 1x at 4°C until sectioning was performed. Depending on the antibody, various cutting protocols were established: either 30-50µm cryo- or 40µm vibratome- sections were prepared and stored in cryopreservation solution until further use. For immunofluorescent detections, the following standard protocol was used; blocking solution and antibody dilution were adapted for each antibody (according to manufacturer's recommendations).

Table 13: Immunohistochemistry protocol

Day 1			
Step	**Temperature**	**Time**	**Solution**
1.Washing	RT	overnight if slides were stored in cryoprotection solution	PBS 1x
2.Blocking	RT	1 hour	Blocking solution
3.1st antibody	4°C	overnight	1st antibody solution
Day 2			
Step	**Temperature**	**Time**	**Solution**
1.Washing	RT	3x 15min	PBS 1x
2.2nd antibody	RT	2hrs	2nd antibody solution
3.Washing	RT	3x 15min	PBS 1x
Mounting with anti-fading mounting medium (VectaShield® medium, Biozol, Eching, Germany)			

5.6.2 Hematoxylin and eosin staining

Hematoxylin and eosin (H&E) staining was performed on mounted cryosections according to the following protocol:

Table 14: H&E staining protocol

Step	Time	Solution
1.Hematoxylin staining	10-20min	Mayers Hämalaun
2.Differentiation	rinse	0.1% HCl
3.Development	20min	Tap water
4.Eosin-staining	10-15min	0.1% Eosin Y
5.Washing	rinse	$H_2O_{dest.}$
6.Differentiation	rinse	80% Ethanol

Table 14: H&E staining protocol (continued)

Step	Time	Solution
7.Dehydration	5min	Ethanol 70%
8.Dehydration	5min	Ethanol 96%
9.Dehydration	5min	Ethanol 100%
10.Incubation	5min	Xylol
11.Mounting		DPX

5.6.3 *LacZ*-staining

X-Gal staining was performed either on mounted or on free floating sections by incubating the sections or whole organs overnight at 37°C in *lacZ* staining solution according to the following protocol:

Table 15: *LacZ*-staining protocol

Day 1	
Fixation	intracardial perfusion using *lacZ*-Fix 30'' – 1min PBS 1x 5 – 7min *lacZ* Fix 30'' – 1min PBS 1x Brain transfer into 20% sucrose/PBS, containing 0.005M EGTA and 0.001M MgCl2; overnight/4°C
Day 2	
Cutting	freeze the brain rapidly on dry ice prepare 50µm thick cryosections transfer sections into PBS containing 0.005M EGTA and 0.001M MgCl2 (storage overnight possible)
Staining	immerse sections for 5min in *lacZ*-wash buffer immerse them in *lacZ*-stain at 37ºC (up to 12hrs) wash for 6x 10min in 0.1M PBS1x fix at least for 1h in 4% PFA/PBS (here storage possible)
Embedding	wash sections in PBS 1x (3x 10min) mount them on slides and embed them with aqueous mounting medium

5.7 Image acquisition

Bright-and dark field images ware taken with a color CCD camera (AxioCam MRc5, Zeiss, Göttingen, Germany) attached onto a Leica MZ APO stereomicroscope (Leica, Wetzlar, Germany) or the Axioplan 2 microscope from Zeiss. Fluorescence images were captured with either a CCD camera (AxioCam MRm attached to Axioplan2) and a X-cite fluorescence illuminator (EXFO Photonic Solutions), or with the M205FA fluorescence stereomicroscope from Leica, or with the LSM 780 confocal microscope from Zeiss, respectively. Pictures were digitalized using AxioVision Rel. 4.5 or LSM ZEN software from Zeiss and exported for further image processing with Adobe Photoshop CS2 or Illustrator CS2 (Adobe, San Jose, USA). Location relative to bregma was determined using *The Mouse Brain in Stereotaxic Coordinates* (Atlas from Franklin&Paxinos, 2008).

5.8 Endocrine Analyses

One week before experiments, animals were separated and single housed. To determine basal plasma hormone levels, mice were left undisturbed the night before the experiment. Blood sampling was performed in the morning (07:30-09:30 am) and afternoon (04:30-05:30 pm) by tail punctation within 45s of initial cage disturbance. For evaluation of stress-induced hormone elevations, blood was collected immediately after 10min of restraint stress, for which the animals were placed in a 50ml falcon tube with the bottom removed. Plasma corticosterone was measured using a commercially available RIA kit (ICN Biomedicals, Irvine, USA).

5.9 Statistical Analysis

In the figures results are presented as mean $\pm$ standard error of mean (SEM). Significant statistical results are indicated with stars *** $p<0.001$, ** $p<0.01$, * $p<0.05$. Data processing and statistics were performed with the commercially available GraphPad Prism5 software (GraphPad software Inc, La Jolla, USA). Pairwise group comparisons were evaluated with Student's T-Test or Mann-Whitney U-Test (for non–Gaussian distribution).

5.10 BLAST and Digital Vector Constructions

Sequiserve (Vaterstetten, Germany) or Eurofins (Ebersberg, Germany) carried out sequencing reactions. For sequence analysis the program BLAST (Basic Local Alignment Search Tool) was used to compare nucleotide sequences to the sequence databases of NCBI (https://blast.ncbi.nlm.nih.gov). Alignment of multiple sequences was done by using the algorithm published by Corpet et al, 1988. Sequence data were copied into the MultAlin web interface with default parameters (http://multalin.toulouse.inra.fr/multalin). The commercially available Vector NTI software package (Thermo Fisher Scientific, Waltham, USA) was used to generate DNA constructs *in silico*.

5.11 Cell Culture Techniques

5.11.1 Preparation of mouse embryonic feeder plates

Hygromycin resistant embryonic mouse fibroblast (EMFI) feeder cells were prepared by the staff of the transgenic mouse facility of the Institute of Developmental Genetics (IDG) at the Helmholtz Center Munich from E14 embryos of mouse line *C57BL/6 Y-TGN pgkneobpA 3-Emg* (obtained from Charles River). For preparation of feeder cell plates, one aliquot ($3x10^7$cells) was transferred from LN2 to ice and thawed quickly in a 37°C water bath until cells are in liquid. Cells were immediately transferred in a 15ml Falcon tube containing 9ml of feeder cell medium and centrifuged at 1400rpm for 5 minutes. The cell pellet was resuspended in 9ml medium and cells were seeded onto 3x 15cm petri-dishes containing 22ml feeder cell medium. Incubation conditions for cultivation of feeder cells or embryonic stem cells were 37°C/5% CO_2 constant. At ~70% confluency, feeder cells were splitted on the one hand to maintain untreated cells for expansion, on the other hand to mitotically inactivate them for seeding ES cells. For this, the medium was exchanged with culture medium containing 150µl mitomycin C (1mg/ml)/15ml feeder cell medium. Subsequently plates were incubated at 37°C/5% CO_2 for 2.5 hours, followed by trypsinization. After washing two times with phosphate buffered saline (PBS), 7,5ml trypsin/EDTA was added to each plate and incubated for 5 minutes at 37°C. To avoid cell damage equal amounts of feeder medium were added and the resulting cell suspension was pipetted gently up and down to avoid cell aggregates. After pelleting at 1200rpm for 5 minutes at room

temperature feeder cells were resuspended to a final concentration of $2x10^5$cells/ml and immediately plated at a density of $6x10^5$ cells/10cm diameter petri dish (EMFI feeder plates). Feeder plates were prepared at least one day in advance of seeding ES cells. Excess of feeder or ES cells was resuspended in freezing medium and transferred for one day to -80°C in an isopropanol freezing-container and then stored in liquid nitrogen.

5.11.2 Culture of embryonic stem cells (ES cells)

Before seeding ES cells an appropriate amount of EMFI feeder plates was prepared by exchanging the medium to ES cell medium at least 4h before use. A vial of frozen TBV2 mouse embryonic stem cells (gift from S. Bourier, Helmholtz Center Munich) was thawed quickly at 37°C and cells were washed once in ES cell medium. Cells were pelleted by centrifugation (1200rpm/5 minutes) and seeded onto 10cm feeder plates at about $2x10^6$ cells/plate. For DNA preparation cells were seeded on gelatin coated plates (0,1%) and incubated until ~100% confluency. Growth of cells and stage of confluency was checked daily and medium was exchanged every day for optimal growth.

5.11.3 Transfection of ES cells with donor DNA construct

Approximately two days before electroporation ES cells were splitted and seeded on feeder cells so that they are in the exponential growth phase at ~70% confluency at the day of transfection. For transfection, the Neon™ Transfection System (Thermo Fisher Scientific, Waltham, USA) was used according to the user manual: ES cells were harvested, washed in PBS and centrifuged at 1400rpm for 5 minutes. The cell pellet was resuspended in resuspension buffer R (included with the transfection kit) to a final density of $1x10^7$ cells/ml and 100µl of this cell suspension were transferred together with 25µg of the circular donor plasmid and 25µg of circular *phiC31* integrase expressing plasmid into the Neon™ pipette. Electroporation was performed according to the manufacture's protocol with the Neon™ pipette station (parameters: 1200V, 2 pulses with 20ms pulse width). Transfected cells were immediately seeded onto prepared feeder plates containing prewarmed ES medium and incubated at above-mentioned conditions. Medium was changed on a daily basis; three days after electroporation, selection with hygromycin (125U/ml) was initiated and drug resistant colonies were picked two weeks after and incubated in selection medium. Each clone was transferred to one well of a 96-well plate and cultured until ~80% confluency.

Medium was not changed before color change from red to pink to guarantee optimal growth conditions. Clones were passaged to produce three “master plates”: one 96-well plate grown on EMFI feeder plates for later expansion of positive clones for blastocyst injection; two 96-well plates with clone duplicates grown on gelatin plates for DNA isolation and screening by PCR.

5.11.4 DNA preparation for detection of positive clones via PCR

One 96-well gelatinized ES cell plate with duplicates of clones was removed from the -80°C freezer and thawed for 5 minutes at room temperature. To each well 50µl of ES cell lysis buffer with Proteinase K was added and the plate was incubated overnight at 50°C in a humidified chamber. The next day the plate was spun down for two minutes at 4000rpm and 100µl/well precipitation mix was added. Plates were shaken for at least 30 minutes or until “DNA spider web” structures could be detected by eye. After centrifugation (1400rpm/4minutes/RT), plates were gently inverted and blotted onto paper towels to adsorb excessive ethanol. Subsequently DNA was washed three times with 150µl/well 70% EtOH; blotting procedure was repeated and samples were dried at room temperature. For PCR 50µl/well sterile ddH_2O was added and the plate was incubated overnight at 4°C on a horizontal shaker. For each PCR reaction, 1.5µl of DNA suspension was added to the appropriate PCR master mix.

5.11.5 Expansion of targeted ES cell clones for blastocyst injection

After putative positive clones have been identified by PCR they are pulled from the 96-well master plate and expanded for microinjection. Therefore, the master plate - stored at -80°C in freezing medium – was thawed quickly in a water bath at 37°C. After centrifugation freezing medium was replaced by ES cell medium without antibiotics. Cells were transferred to freshly prepared 96-well EMFI feeder plates and subsequently expanded by repeated splitting onto 24-well plates, 6-well plates and 10cm EMFI feeder plates when ~70% confluency was reached. For storage, expanded clones from one 10cm plate were trypsinized, splitted into three vials containing ES cell freezing medium and stored in liquid nitrogen. Three days before microinjection the desired clone was thawed and plated onto one 6cm EMFI feeder plate. The day before injection the positive clone was seeded onto a gelatin coated 6cm petri dish. For blastocyst injection, the cells were trypsinized and resuspended in 1.5ml ES cell medium and stored on ice. Cells were handed over immediately to the

staff (Susanne Weidemann and Adrianne Tasdemir) of the transgenic mouse facility of the Institute of Developmental Genetics (IDG) at the Helmholtz Center Munich.

5.12 Animal experiments

All animal experiments were conducted in accordance with the guidelines for care and use of laboratory animals of the government of Upper Bavaria, Germany. The local government authorized the experiments (permission number 55.2-1-54-2532-142-2015).

5.12.1 Mouse housing

Animals were housed in standard Macrolon type II cages (350cm^2) or standard IVC cages (Mouse IVC Green Line, 501cm^2) with food (Altromin #1324) and tap water available ad libitum under controlled, constant conditions (light cycle 12:12 hours-beginning light phase at 8am; room temperature 20-22°C; air humidity 50-60%).

5.12.2 Stereotactic surgery - viral Injection

In-house made adeno-associated virus (AAV) serotype 1/2 was used to express the constitutively active *CRHR1-IRES-GFP* fusion protein (*(CA)CRHR::EGFP*) or the anterograde fluorescent protein *mCherry* in the VTA of *CRHR1^{Cre}* mice. The constitutively active *CRHR1::EGFP* fusion construct (*136*) was subcloned into a conditional flexed adeno-associated viral vector (*217*) and was kindly provided by Dr. Arenkiel (*137*). The plasmid pAAV-Ef1a-DIO-*mCherry* was purchased from Addgene (#50462, Addgene, Cambridge, USA).

Stereotactic surgeries were conducted by Anna Mederer, Dr. Rosa Eva Hüttl and Dr. Mira Jakovcevski at the MPI core unit “Behavior and Physiology” headed by Dr. Carsten Wotjak. Adult male mice (10-12 weeks old) were anesthetized with isoflurane and fixated in a stereotactic apparatus (TSE systems, Bad Homburg, Germany). 20 minutes before surgery analgesic treatment (Metamizol, 200mg/kg s.c.) was administered. Body temperature was held at constant 37.5°C by placing a heat pad underneath the animal (Harvard Homothermic Blanket Control, Hugo Sachs Electronics, March-Hugstetten, Germany). To avoid drying of the cornea, Bepanthen® eye ointment was administered at the beginning of the surgery. Under local anesthesia (0.5% Lidocain) a small hole was drilled into the skull and a

Hamilton® syringe containing the virus was positioned at the appropriate coordinates (coordinates from bregma: anterior/posterior -3,0mm, medial/lateral +/-0,6mm, dorsal/ventral -4,50mm. The virus (500nl) was injected using an automated microinjection pump (World Precision Instruments, Friedberg, Germany) at a rate of 100nl/min. Subsequently the skull was disinfected and the scalp sewn up; animals were kept warm and monitored until awakening. Postoperative analgesia (Meloxicam, 1mg/kg s.c.) was administered for three consecutive days. Four weeks after AAV delivery animals were single housed to habituate to behavioral test room conditions at least one week before testing. To analyze anxiety-like behavior in these mice a set of behavioral tests have been performed, arranged from least to most stressful: Open field (OF) test, Elevated plus maze (EPM) test and Dark-light box (DaLi) test (detailed description of test paradigms see next chapter). For anterograde tracing experiments the in-house made virus (AAV-EF1a-DIO-*mCherry*) was positioned at the following coordinates in mm from bregma: striatum (anterior/posterior 1.5mm, medial/lateral +/-1.5mm, dorsal/ventral -3.5mm); hippocampus (anterior/posterior -1.9mm, medial/lateral +/- 1.3mm, dorsal/ventral -2.0mm); PVN (anterior/posterior -0.82mm, medial/lateral +/- 0.05mm, dorsal/ventral -4.55mm); Rt (anterior/posterior -0.5mm, medial/lateral +/- 1.2mm, dorsal/ventral -4.2mm and -3.4mm); LC (anterior/posterior -5.4mm, medial/lateral +/- 0.85mm, dorsal/ventral -3.75mm); CeA (anterior/posterior -1.1mm, medial/lateral +/- 2.75mm, dorsal/ventral -4.55mm); PFC (anterior/posterior 2.2mm, medial/lateral +/- 0.30mm, dorsal/ventral -1.5mm); Thalamus (anterior/posterior -1.06mm, medial/lateral +/- 0.20mm, dorsal/ventral -3.4mm); PIR (anterior/posterior -1.54mm, medial/lateral +/- 2.3mm, dorsal/ventral -4.6mm).

5.12.3 Behavioral studies

To investigate the impact of the CRH/CRHR1 system on anxiety and depression-like behaviors a variety of well-established behavioral tests in mice are available. The main principle of the tests described below is an approach-avoidance conflict, meaning inhibition of their naturally exploratory drive of unknown environments by aversive test conditions like bright illumination or elevated space.

If not indicated otherwise all behavioral experiments were carried out in male mice (age 9-15 weeks); at least one week before testing mice were single housed and habituated to test room conditions. Behavioral tests were performed during light

phase (light phase adaption 1 hour) and ended at the latest 1pm, tissue collection included. Animal's behavior was tracked and analyzed with an automated video-tracking system (ANY maze, Stoelting Europe, Terenure, Ireland). All results were analyzed by the commercially available GraphPad Prism 5 software (GraphPad software Inc., La Jolla, CA) and presented as mean ± standard error of the mean (s.e.m.). Simple comparisons were evaluated with a two-tailed unpaired t-test. Statistical significance was defined as $p < 0.05$.

Open field exploration test: Originally designed to measure emotional behavior in rats this test was successfully adapted to mice and is often used as an initial screen for anxiety-related behavior in rodents as it characterizes novel environment exploration and locomotor activity. The test apparatus comprises an evenly illuminated (<15 lux) large square chamber (50 x 50 x 60cm (length x width x height) made of grey polyvinyl chloride (PVC). The open field arena was virtually divided into an outer and inner zone (15 x 15cm). At the beginning, each mouse was placed into the same corner of the arena and was allowed to freely explore the chamber for 15 minutes meanwhile the following parameters were scored: total distance traveled, number of inner zone entries and inner zone time. Naturally, mice prefer exploring the periphery of the arena (protected area; mice usually keep in contact with the walls). Mice spending significantly more time in the inner zone demonstrate anxiolytic-like behavior under basal conditions. The first five test minutes reflect general locomotor activity, which is reflected by total distance traveled.

Elevated plus-maze test (EPM): The elevated plus maze is designed to assess the competing tendency of mice to explore a novel arena versus avoidance of open, brightly lit areas. Mice can freely choose between enclosed, protected arms and open, unprotected arms, all elevated 37cm from the floor. Mice tend to avoid the open arms of the EPM, especially when they are brightly illuminated. The test apparatus consists of plus-shaped arms (30 x 5cm) extending from a central zone (5 x 5cm) with two arms being enclosed with 15cm high walls, all made of grey PVC. The open arms were illuminated with 20 lux and the closed arms with <15 lux. With this dim light levels the natural exploratory tendency is not inhibited. Each mouse was placed in the central arena facing the closed arm and was allowed to freely explore the maze for 5 minutes, meanwhile the parameters time spent in the open and closed arms, number of open arm entries and total distance traveled were recorded.

Dark-light box test (DaLi): The dark-light exploration test provides an additional instrument to investigate anxiety-like behavior. As with the EPM it is based on the inherent conflict between spontaneous exploratory behavior and risk avoidance reflected by inhibition of exploration. The test apparatus was a rectangular, grey PVC box and consists of a secure black compartment (15 x 18 x 27cm, length x width x height; illumination <5 lux), a tunnel of 5cm length and a larger aversive white compartment (48 x 28 x 27cm), illuminated with 700 lux. Initially, animals were placed into a corner of the dark box and were allowed to freely explore the chamber for 5 minutes. The following parameters were recorded: number of lit compartment entries, time spent in the lit compartment and total distance traveled. Naturally, mice prefer the dark, protected compartment and thus mice exhibiting anxiolytic behavior will have more transitions into the brightly illuminated open area. Results were interpreted with use of caution regarding general locomotor activity as recorded with the open field test.

6 Results

6.1 Generation of the “parental” CRHR1 allele

The RMCE strategy presented in the following section relies on the multifunctional CRHR1 allele, generated by Kühne et al., 2012 (see Figure 7).

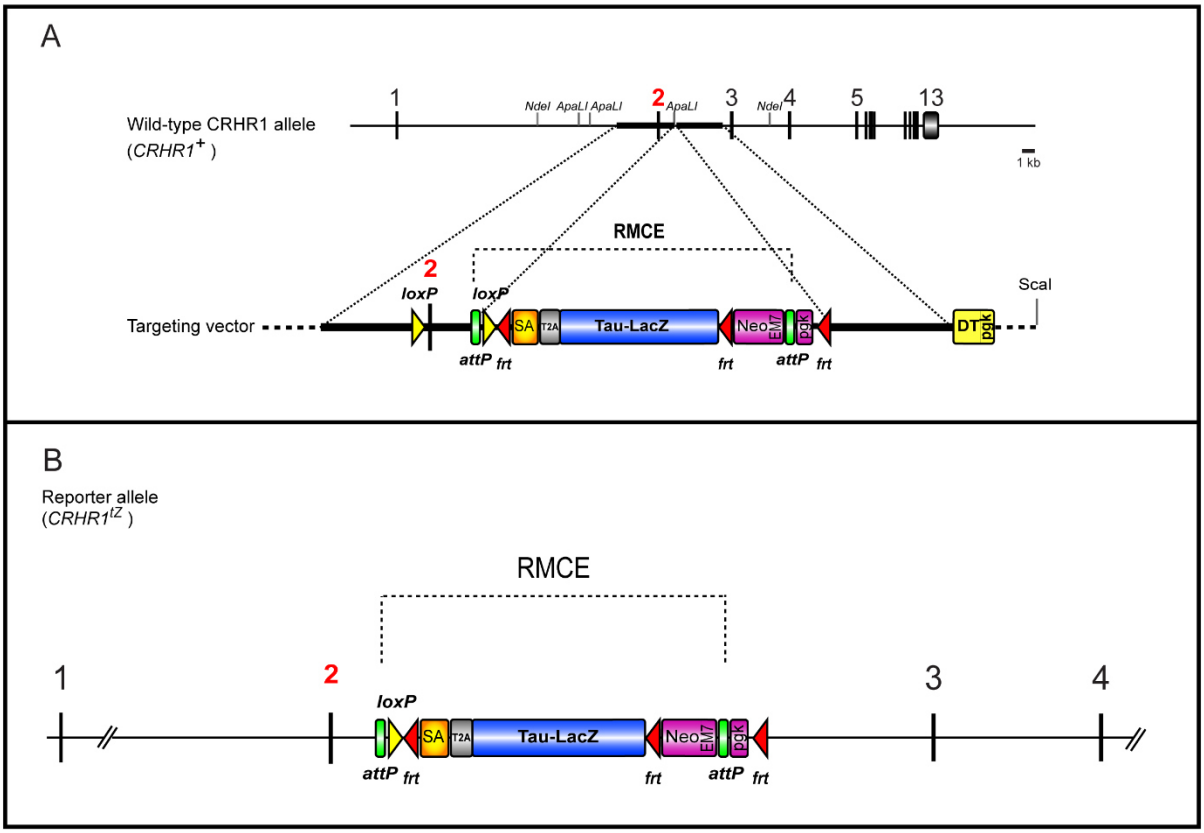

Figure 7: Generation of conditional CRHR1 knockout mice

Strategy for targeted manipulation of the CRHR1 locus; based on Kühne et al., 2012. (A) Schematic representation of the wild-type locus and targeting vector. (B) Recombined reporter allele (*CRHR1*^{tz}) following homologous recombination in ES cells. See text for more details.

This knock-in allele genetically labels CRHR1-expressing cells with a *tau-lacZ* (tZ) reporter gene. In addition to this, it also offers the possibility to conditionally restore or delete CRHR1 via *Flp* and *Cre* recombinase, respectively. Furthermore, it contains targeting sites for the *phiC31* integrase, allowing repetitive manipulation of the same “pre-inserted docking site” in the genome of ES cells via RMCE. This approach simplifies and accelerates the search for correct integration events in ES cells.

6.1.1 Generation of the targeting vector

The donor construct comprises the following components, which were flanked by *attB* sites, thereby enabling a recombination event with the heterotypic *attP* sites of the "docking" allele: a 4,6kb fragment encoding the 3' part of CRHR1 Intron 2 including the endogenous splice acceptor, the coding sequence of CRHR1 exon 3 -13 followed by insertion of an *IRES Cre* cassette at the 3'UTR and a reverse orientated *hygromycin* positive selection cassette, including a bovine growth hormone polyadenylation signal (pA). By insertion of the *IRES* site at the 3'UTR of the gene of interest the mRNA is translated into two independent proteins thus preserving expression of the wild-type CRHR1 and simultaneously expressing *Cre* recombinase under the control of the endogenous CRHR1 promoter (Figure 8).

In detail: The targeting vector was based on a universal shuttle vector (constructed by Webb and Deussing in our group) which contains two full length *attB* sites inserted between the *NotI* and *XhoI* site of a pBluescript II KS (+) vector. Additional restriction sites (*Mfe I, SpeI, AgeI, AscI, SwaI, AflIII, BsrGI, BstBI*) where inserted via annealed linker oligonucleotides into the multi cloning site to facilitate further cloning steps. In addition, the shuttle vector contains the 34bp minimal *frt* site sequence (5'-GAAGTTCCTATTCtctagaaaGtATAGGAACTTC-3') inserted between the SwaI and AflII site (Figure 8). Five independent rounds of PCRs were performed with the respective products being subcloned into the pCRII TOPO vector using the TOPO TA cloning kit and then sequenced. The first part of 3' intron 2 was generated by long range PCR of murine C57/BL/6J genomic DNA using primer pair *Crhr1_Intron2_long_MfeI_for and Crhr1_Intron2_long_SpeI_rev.* The second half of 3' Intron 2 (500bp length) and first part of Exon 3 (spanning the *SbfI* restriction site) was PCR amplified with the primer pair *Crhr1_Intron2_small_AgeI_for* and *Crhr1_Exon 3 all_rev.* The coding sequence of *Crhr1* exon 3 -13 was generated from a cDNA template of the full-length receptor subcloned in the pCRII Topo (Primers: Crhr1_Exon 3 all_for and Crhr1wt_AscI_rev). Origin for amplification of the *IRES Cre* cassette was genomic DNA isolated from a homozygous animal of the *(B6(Cg)-Crh$^{tm1(cre)Zjh}$/J* (*CRH-IRES-Cre*) mouse line, obtained from Jackson laboratories (stock number 012704) (primer pair: *AscI IRESCre fwd* and *Cre rev-SwaI)*. Finally the hygro pA cassette was generated via PCR amplification using primer pair *Hygro_BstBI_for* and *Hygro_BsrGI rev*. (template plasmid pBS_attB_hygro_attB, kindly provided by

Dr. Katharine Webb). Completion of the shuttle vector was achieved by preparative digests of the subcloned PCR products, gel extraction and purification, followed by several rounds of consecutive ligation steps (see Figure 8).

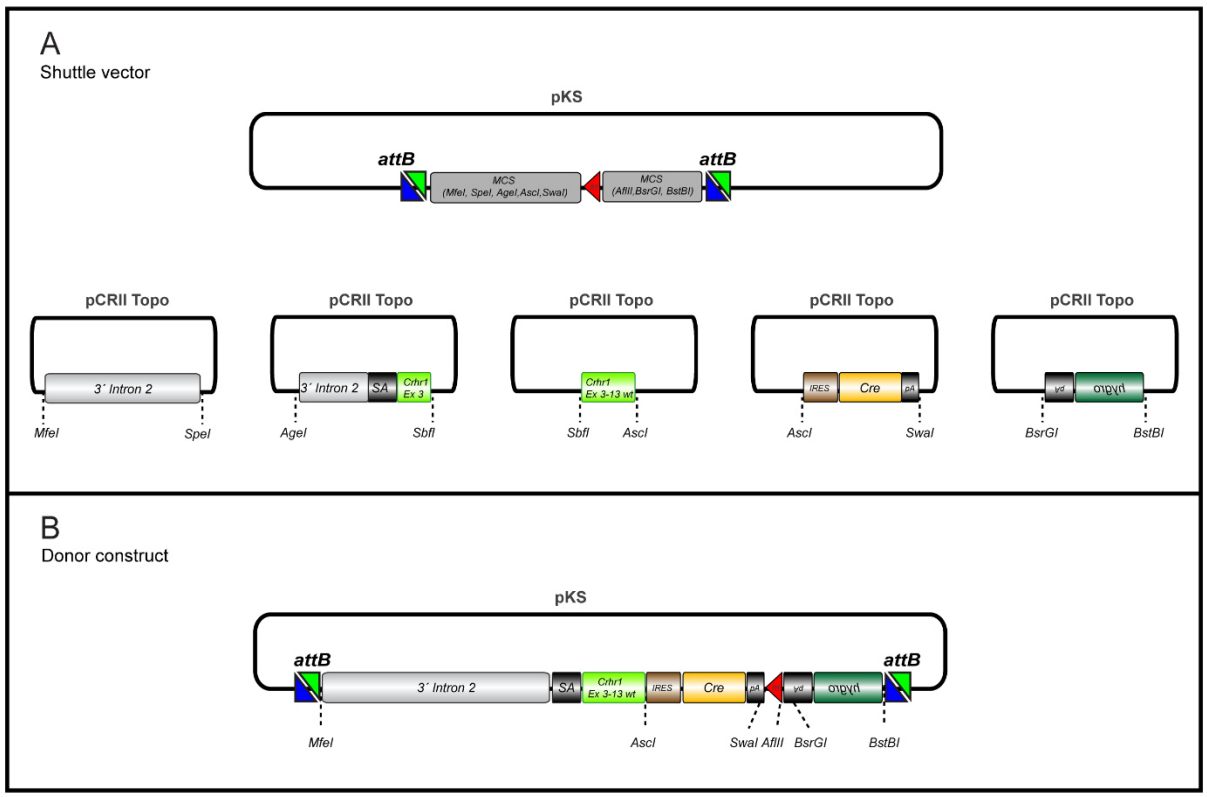

Figure 8: Cloning steps for completion of the donor vector

PCR and ligation strategy for the donor construct. (A) Schematic representation of the shuttle vector and five different PCR reactions with relevant restriction sites, subcloned into pCRII Topo®. (B) Recombined donor construct following successive ligation steps into the shuttle vector. For details, see text.

6.1.2 Generation of recombinant embryonic stem cells via RMCE

Site-specific bacteriophage *phiC31* integrase mediates irreversible recombination between the two heterotypic sites *attB* and *attP* and can therefore be used for efficient DNA integration. For this, the docking site/landing path was inserted into the CRHR1 locus by homologous recombination in mouse ES cells (*41*). Subsequently, the circular donor plasmid (containing the coding sequence of CRHR1 exon 3 -13 followed by insertion of an *IRES-Cre* cassette and a reverse orientated *hygro* positive selection cassette) – all flanked by *attB* sites - was introduced in these ES cells (Figure 9B). Simultaneously recombination between the two pairs of recognition sites results in cassette exchange and stable integration as the *phiC31* integrase is inert

on the product sites of the recombination event: *attL* and *attR* sites. To prevent self-excision of its own *loxP*-flanked coding sequence we made use of ES cells lacking the *loxP* site upstream of exon 2 for integrating the *Cre* donor cassette (Figure 7B, 9).

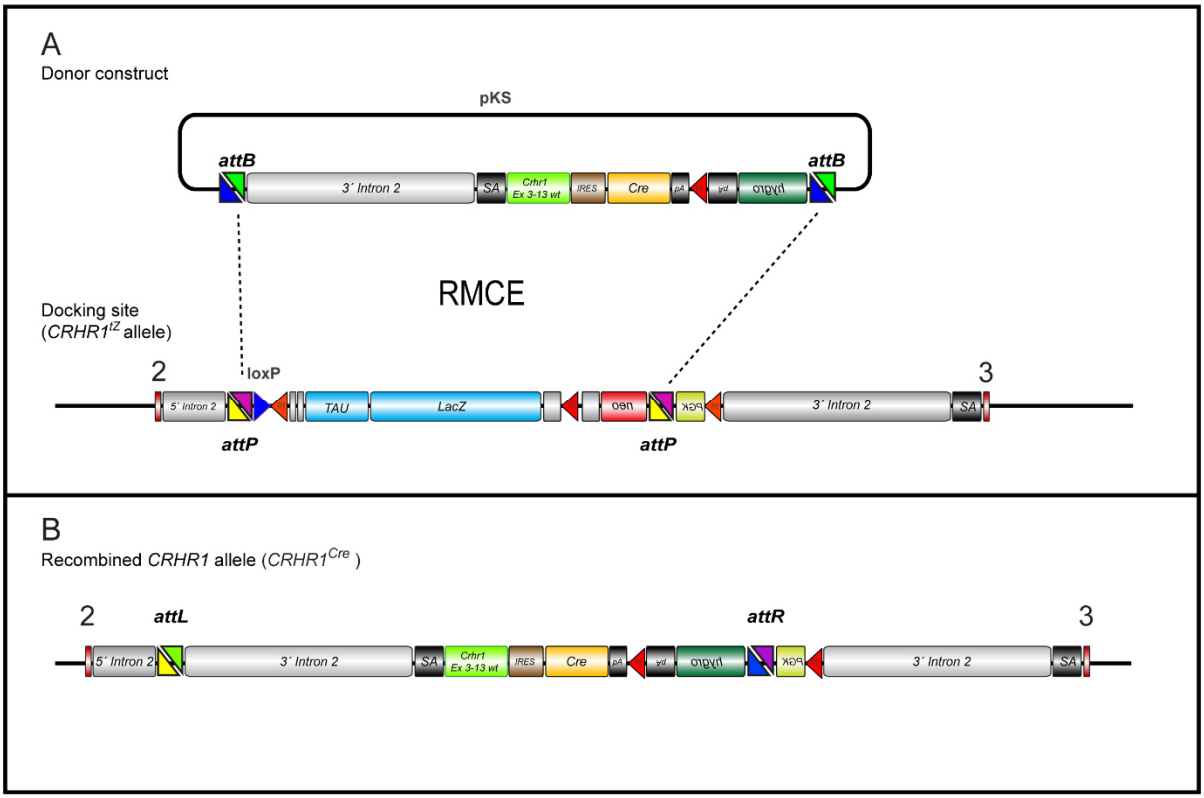

Figure 9: Strategy for *phiC31* integrase-mediated cassette exchange (RMCE)

Exchange strategy for replacing the target cassette within the CRHR1 locus by a compatible donor construct. (A) Schematic drawing of the incoming RMCE-donor cassette and the genomic "docking site". (B) Recombined CRHR1 allele (*CRHR1*^{Cre}) following *phiC31* integrase-mediated site-specific recombination simultaneously between the two pairs (attP and attB) of recognition sites from the "donor cassette" and the chromosomal "acceptor cassette" in embryonic stem cells. See text for more details.

Standard procedures for ES cell work were used (see Materials and Methods). To introduce the donor construct murine TBV2 ES cells (derived from strain 129S2), containing a single copy integrant of the docking site were electroporated via the Neon Transfection System from Invitrogen. ES cells were cultivated on mitotically inactivated feeder cells. For electroporation 1x 10^6 ES cells were used and electroporated simultaneously with 25µg of circular plasmid DNA of pBS_CRHR1-*IRES-Cre* and 25µg of pPGK*PhiC31*obpA (mammalian *phiC31* integrase expression vector, purchased from Addgene). Three days after electroporation positive selection was started with ES cell selection medium containing hygromycin B. On day 9 after electroporation ideal colonies with clearly defined borders were picked and further

cultivated under selection conditions for another week. Colonies were split at ~80% confluency; half of the culture was plated into a new 96 well plate dish and was cryopreserved at day 14 after picking. The duplicates of the colonies were seeded on gelatin coated plates for DNA extraction and subsequent screening for positive clones via polymerase chain reaction (PCR) (Figure 10).

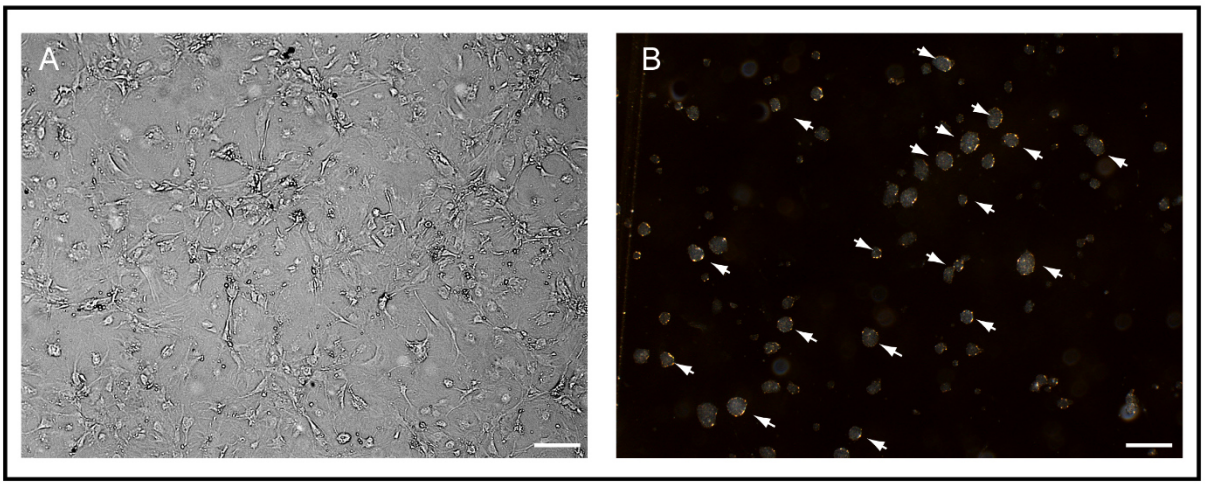

Figure 10: Appearance of EMFI feeder cells and ES cells

(A) Mitotically inactivated feeder cells for supporting ES cell growth. (B) Appearance of ES cells plated on a 96-well gelatin-coated plate for DNA extraction. Scale bars represent 100µm.

6.1.3 Screening of ES cell clones for construct integration

In order to identify ES cell clones with the desired recombination event, screening by PCR was performed. Genomic DNA as PCR template was isolated from remaining hygromycin resistant ES cell clones by precipitation (for details see Materials and Methods section). For this purpose several PCR primer pairs were designed (the PCR strategy is detailed in Figure 11) to examine two hypothesized scenarios namely (1) cassette exchange (illustrated in Figure 6) or (2) recombination at the *3' attP* site (type II insertion). It is important to note that the latter listed recombination event is theoretical followed by integrase-mediated deletion between the intact *attP* and *attB* sites, thereby also resulting in cassette exchange (Figure 11).

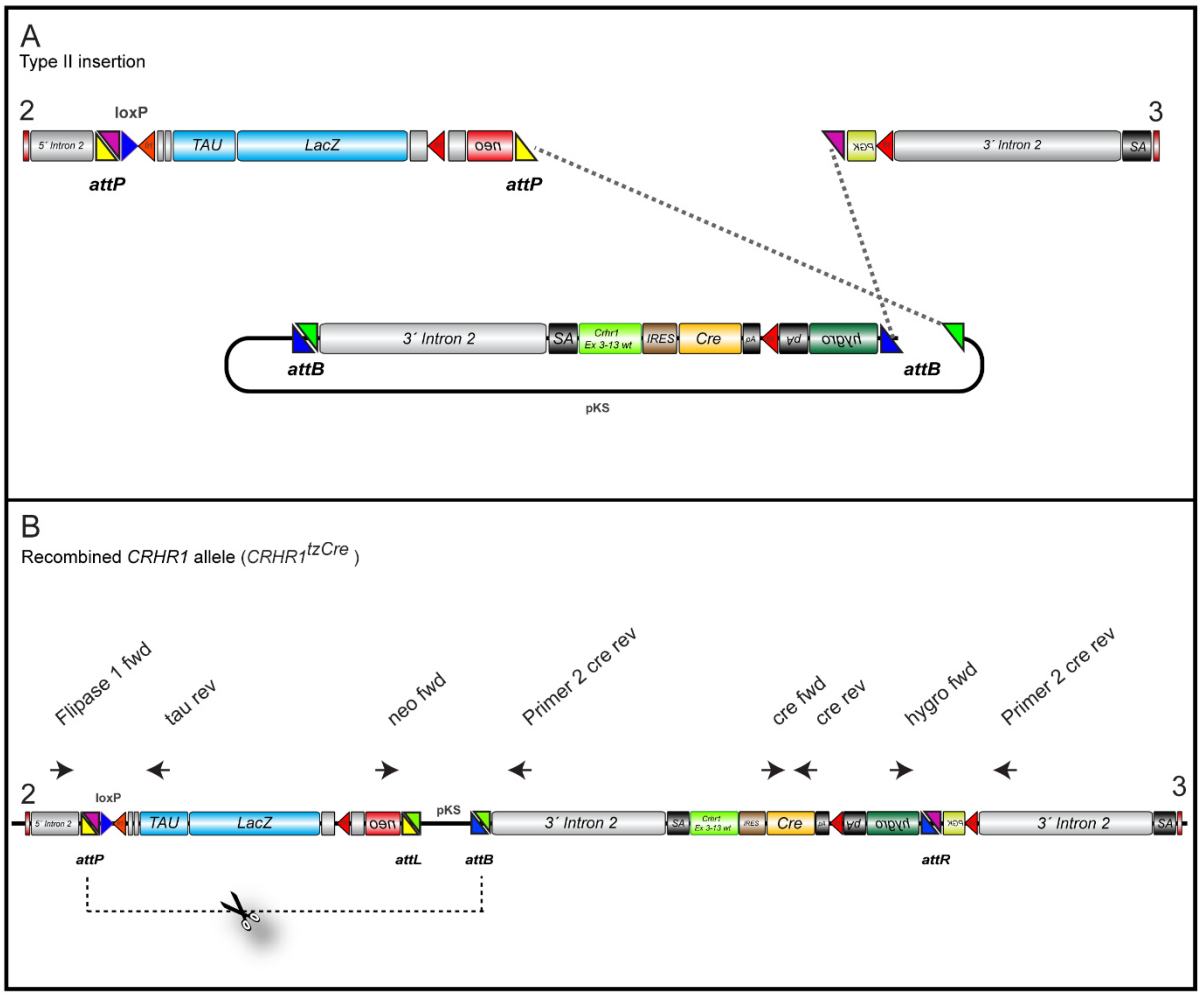

Figure 11: Transgene configuration after type II insertion

(A) Schematic representation of recombination at the 3' recognition site (type II insertion). (B) Type II insertion results in cassette exchange by an integrase-mediated deletion event between the intact *attP* and *attB* site. Primers for analyzing construct integration are indicated by arrows. For details, see text.

All positive clones produced a band of the expected size with primer pair cre fwd./cre rev. as well as primer pair hygro fwd./Primer 2cre rev.. Sequencing of the latter PCR product confirmed the existence of the expected *attR* site. Surprisingly all clones revealed a band with primer pair Flipase 1 fwd./tau rev. indicating that the *tau-lacZ-neo* cassette (*tz-neo* cassette) is still present. This can only occur as result of an "incomplete" type II insertion event without deletion of the sequence between the remaining *attP* and *attB* sites, most probably due to inefficient intramolecular recombination or insufficient/decreasing amount of *phiC31* integrase. After sequencing of the PCR products, the existence of the intact 5' *attP* site was proven. Additionally, all clones were screened for existence of vector backbone with primer pair neo fwd./Primer 2 cre rev. In 25% of all clones, the vector backbone was

detectable, whereas PCR results in 75% of all cases pointed towards a different recombination event. Thorough analysis of the sequencing results for the PCR product generated by primer pair neo fwd/Primer 2 cre rev revealed the existence of an *attL* site instead of pBluescript backbone sequence, hinting towards an alternative recombination event between the 3' docking *attP* site and the incoming donor *attB* sites (Figure 12).

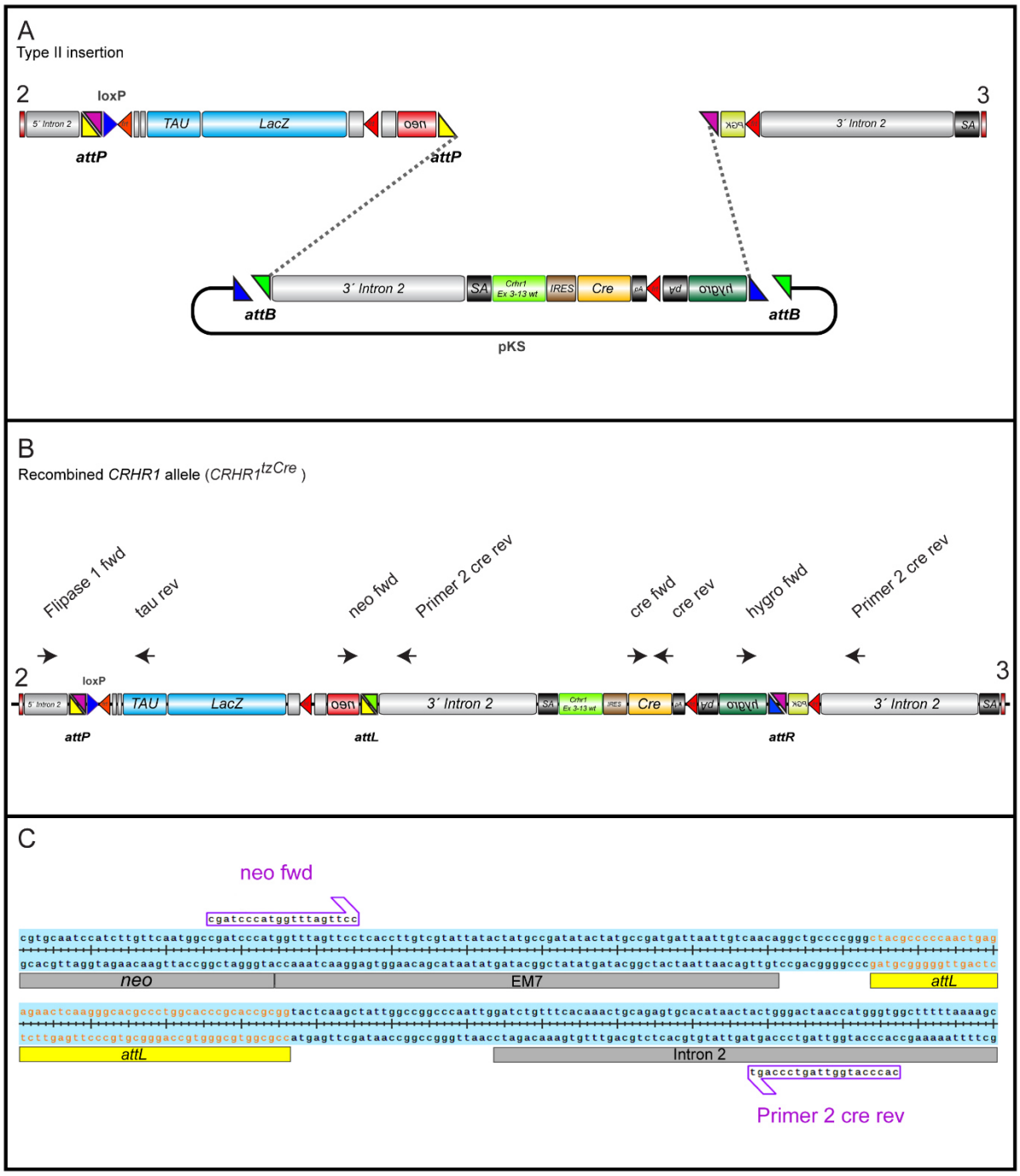

Figure 12: Resulting allele after RMCE at the 3' *attP* recognition site

Transgene configuration due to alternative recombination. (A) Schematic representation of recombination at the 3' *attP* recognition site (type II insertion). (B) Type II insertion with an alternative recombination event between the 3' docking *attP* site and the *attB* sites of the donor plasmid. Primers for analyzing construct integration are indicated by arrows. (C) The recombination between the 3' *attP* site and the donor *attB* sites was validated by sequencing. For details, see text.

6.2 Generation of the *CRHR1^{tZCre}* mouse line

6.2.1 Characterization of chimeras and germline transmission

All positive clones showing integration of *Cre* recombinase at the 3' docking site (Figure 11,12) were expanded and used for blastocyst injection, which were transferred into pseudo-pregnant foster females using standard procedures (injection and transfer was performed by the staff of the transgenic mouse facility of the Institute of Developmental Genetics (IDG) at the Helmholtz Center Munich). A number of chimeric mice were born of which three highly chimeric males (90% coat color chimerism) were mated to wild-type mice. One chimera exhibited germline transmission as revealed by coat color (pups with agouti fur) and genotyping of the heterozygous offspring; the resulting mouse line was named *CRHR1^{tZCre}* and demonstrates the successful RMCE-based manipulation of mouse ES cells (Table 3).

Table 16: Summary of the results from the blastocyst injection

Blastocyst donor strain	ES cell Clone (TBV2 origin)	transferred blastocysts	born pups	Chimera male	Chimera female	Coat color chimerism (%) male	Coat color chimerism (%) female
Balb-c	C12	?	?	1	1	5%	5%
Balb-c	A9	18	4	0	0	-	-
Balb-c	A9	18	3	3	0	3x 90%	-
Balb-c	B11	20	0	0	0	-	-
Balb-c	B11	20	0	0	0	-	

Table 16: Summary of the results from the blastocyst injection (continued)

Blastocyst donor strain	ES cell Clone (TBV2 origin)	transferred blastocysts	born pups	Chimera male	Chimera female	Coat color chimerism (%) male	Coat color chimerism (%) female
Balb-c	B11	18	2	0	0	-	-
Balb-c	B6	20	9	7	0	80%+70% +2x 40% +1x 30% +2x 20%	-
Balb-c	B6	20	7	2	2	2x60%	60%+30%
Balb-c	B9	20	5	0	0	-	-
Balb-c	B9	20	5	1	0	20%	-
Balb-c	B9	19	8	1	1	70%	10%
Balb-c	B9	20	4	0	0	-	-

6.2.2 Establishment of Genotyping

Genotyping was performed by a multiplex PCR assay using primers Flipase 1 fwd, Primer 2 cre rev and tau rev. Standard PCR conditions resulted in a 232bp wild-type product and a 623bp product indicating the presence of the *tZ-neo cassette*. The presence of *Cre* recombinase was proven using primers cre fwd, cre rev, Thy1-F1 and Thy1-F2, resulting in a *Cre*-specific PCR product of 574bp and a 372bp control product verifying addition of DNA template into the PCR master mix (Figure 13).

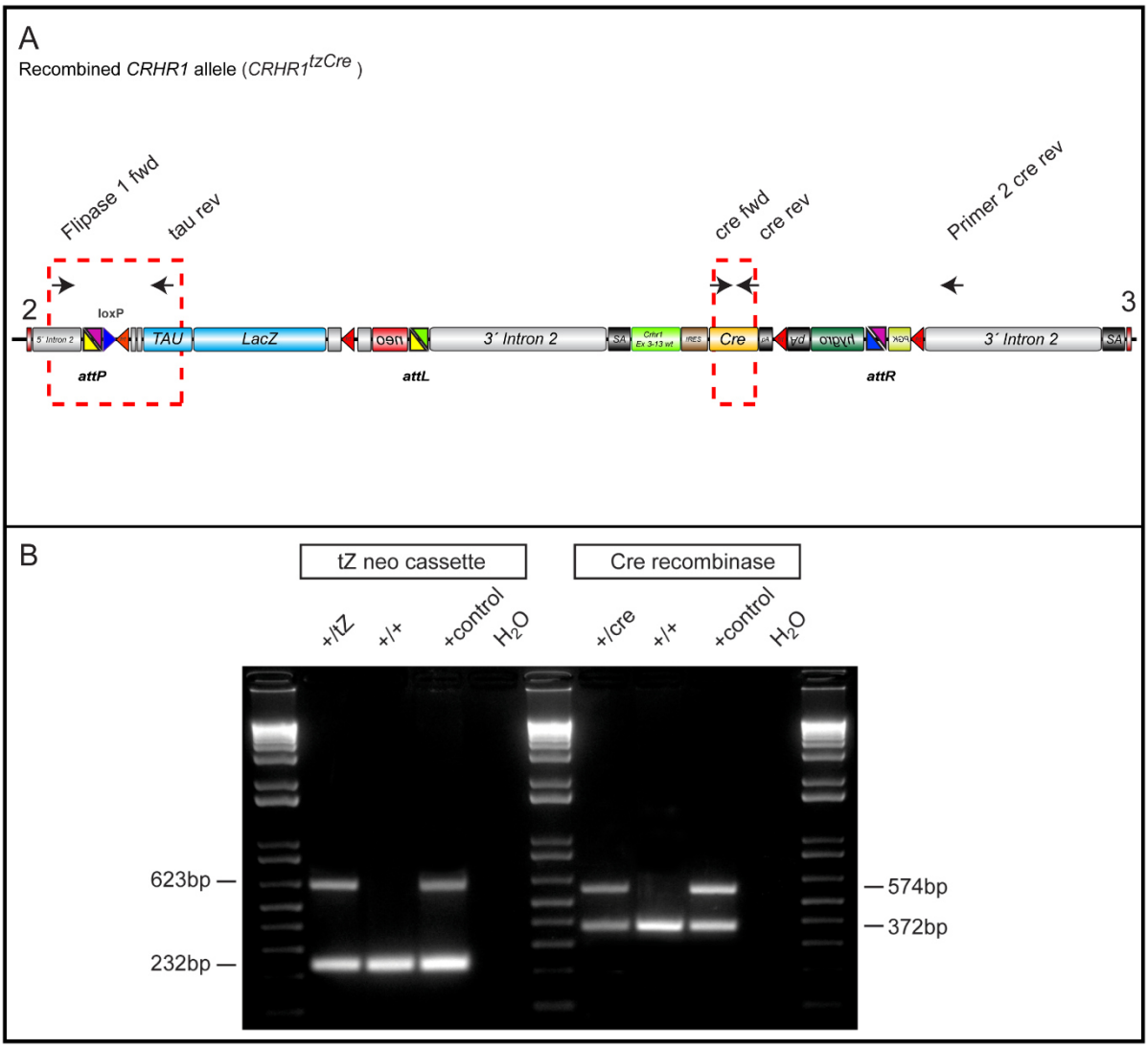

Figure 13: Genotyping of the *CRHR1*^{tZCre} mouse line

Genotyping of mice via PCR. (A) Schematic representation of the recombined CRHR1 allele; primers for detecting the *tZ-neo* cassette and the *Cre* recombinase are indicated by arrows. (B) Multiplex PCR displaying wild-type and heterozygous mice of the *CRHR1*^{tZCre} mouse line.

6.3 Characterization of the subpopulation-specific *CRHR1*^{tZCre} mouse line

By application of RMCE a “new” CRHR1 allele based on a multifunctional founder allele was generated. Due to an alternative recombination event, the *tau-lacZ* reporter cassette with its strong adenoviral splice acceptor is still present at the integration site. The splice acceptor from the intron 1/exon 2 boundary of the type II adenovirus has been shown to mediate efficient splicing into 3’ exons and is off sufficient strength to override endogenous splicing. Thus, alterations in splice site choice can result in alternative splicing patterns depicted in figure 14.

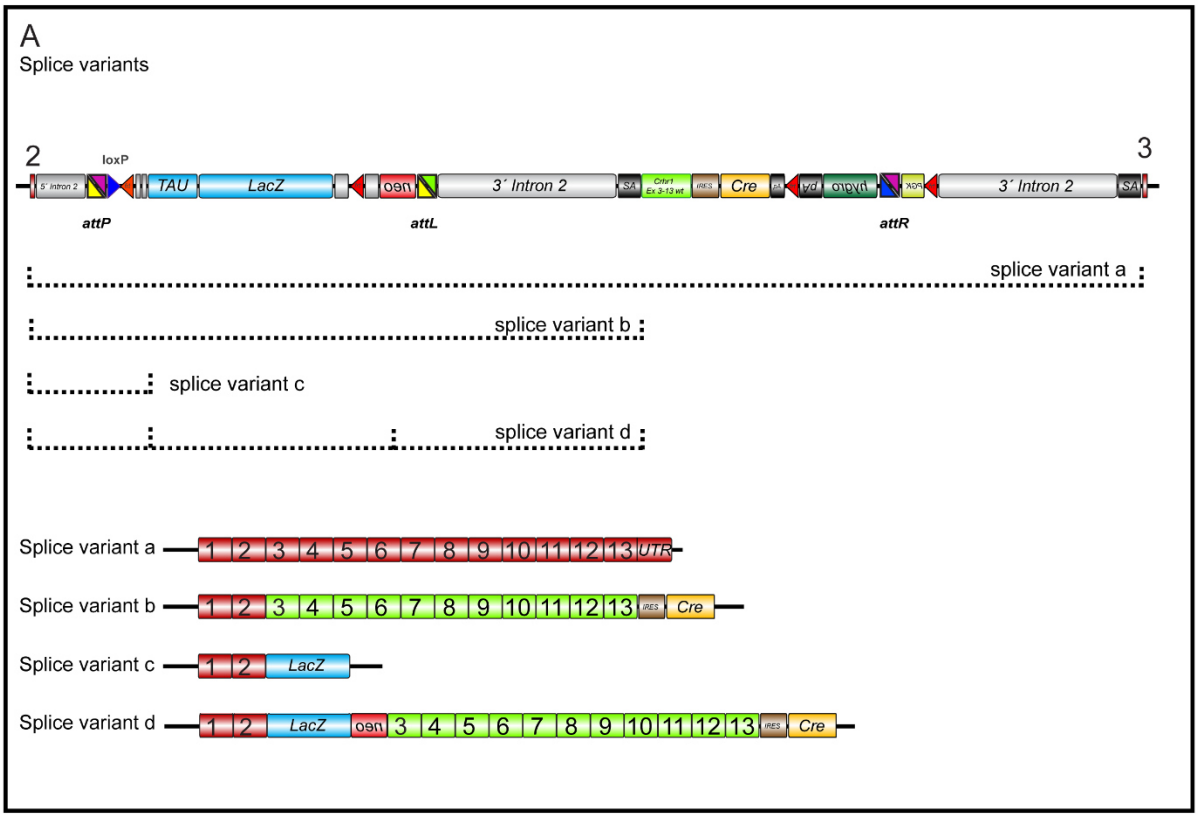

Figure 14: Result after *phiC31* Integrase-mediated cassette exchange using the single 3' *attP* docking site

(A) Schematic drawing of the recombination event at the 3'-recognition site. Recombined CRHR1 allele (*CRHR1*^{tZCre}) representing an insertion event rather than a cassette exchange. Alternative splicing events leads to different potential mature mRNA molecules that generate multiple functional proteins. Detailed description see text.

Utilization of the CRHR1 Intron 2 endogenous splice acceptor should result either in a wild-type *Crhr1* mRNA (splice variant a in Figure 14) or in a transcript variant encoding for CRHR1 exon 1 - 13 followed by insertion of an *IRES Cre* cassette at the 3'UTR (splice variant b in Figure 14). In the latter case, the *IRES Cre* cassette is part of a mature fusion transcript initiated from the endogenous CRHR1 promoter where the *IRES* sequence encodes an RNA motif that allows independent ribosome binding and initiation of translation of the *Cre* recombinase sequence 3' to the *IRES* site. Alternatively, CRHR1 exon 2 could be spliced to the synthetic splice acceptor site in a way that the N-terminal portion of CRHR1 is in-frame with the *tZ* reporter gene (splice variant c in Figure 14). The presence of the neomycin resistance coding sequence involves the possibility of other splice variants, because the neomycin gene has been shown to contain cryptic splice acceptor and donors sites (splice variant d in Figure 14) (*127, 218*).

6.3.1 Evaluation of CRHR1- and *Cre* expression by *in situ* hybridization

In situ hybridization was used to verify expression of the *lacZ* reporter, *Cre* recombinase and endogenous *Crhr1* mRNA, respectively (Figure 15). Examination of adult mouse brain sections from heterozygous *CRHR1*$^{+/tZCre}$ mice revealed expression of *Cre* in a subset of neurons. *Cre* positive neurons could be identified in the mitral and granular layer of the olfactory bulb (Mi, GrO), cortical layer II-IV (ctx), pontine nuclei (Pn) and granular layer of the cerebellum (gr). Other sites of strong receptor expression such as the hippocampus (CA1), amygdala, globus pallidus, reticular thalamic nucleus (Rt), VTA, red nucleus (RMC) and medial vestibular nucleus (MVE) were lacking *Cre* expression. A nearly identical epression pattern of the *lacZ* mRNA points towards alternative splicing events.

At this point, it is not entirely clear which particular splicing events occur. Further analyses such as reverse transcription polymerase chain reaction (RT-PCR) or rapid amplification of cDNA-ends (RACE-PCR) are necessary to decipher the splicing process. Single cell electrophysiological analysis of hippocampal CA1 neurons (Figure 18) revealed that these cells do not respond to an exogenous CRH stimulus (data not shown) – which would be equivalent to a knockout allele. This points towards aberrant splicing of neo sequences into the adjacent CRHR1 exon 3-13 coding sequence, however, the latter splice variant results in a non-functional receptor due to a shift in the reading frame. Furthermore intercross of heterozygous *CRHR1*$^{+/tZCre}$ mutant male and female mice did not result in homozygous offspring, most probably due to lung dysplasia induced by a corticosteron deficit, although this phenomenon has been described so far only for homozygous intercrosses where low levels of maternal corticoids result in insufficient neonatal lung maturation (*156*).

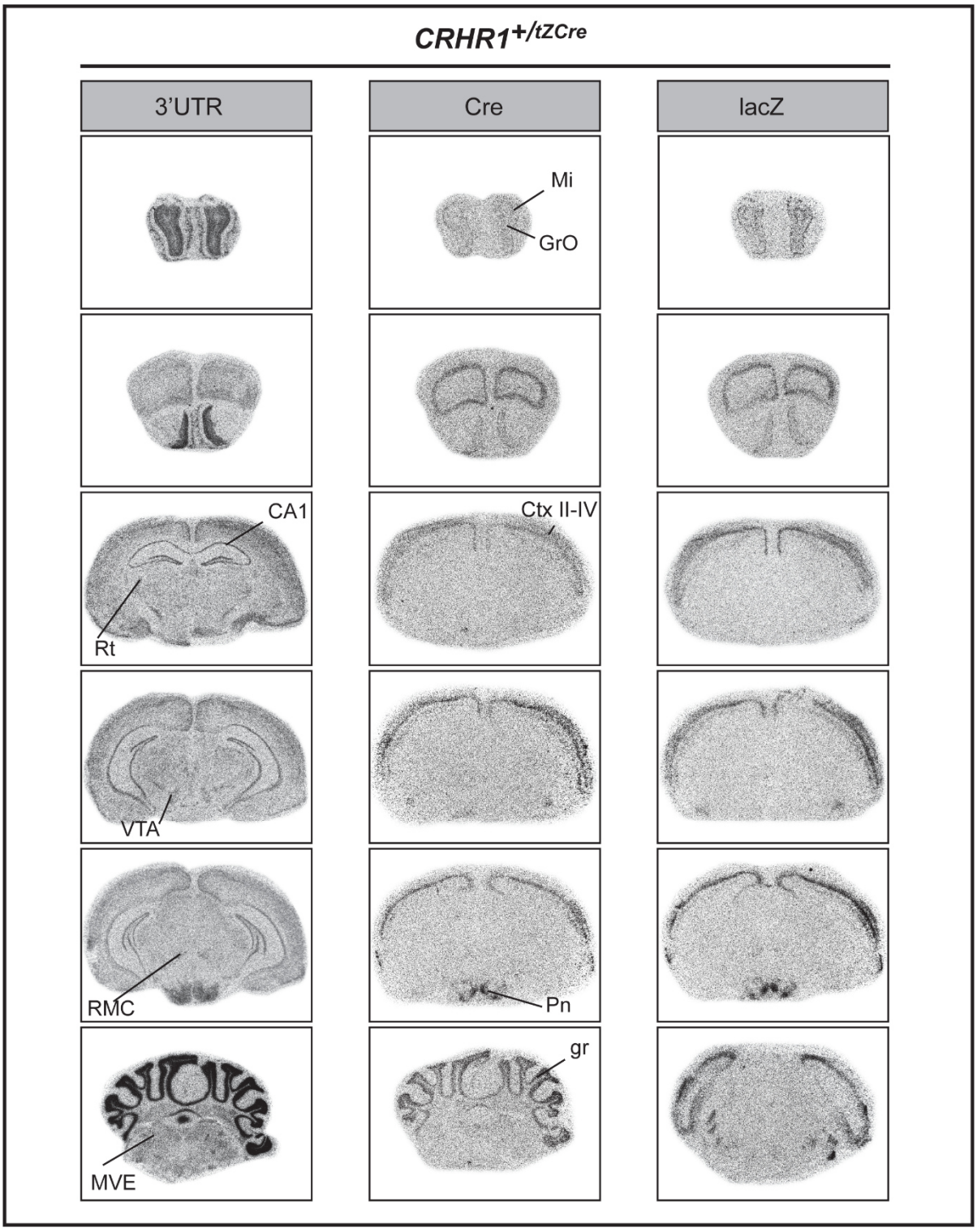

Figure 15: Analysis of *Cre* and *lacZ* expression in the adult heterozygous *CRHR1*$^{+/tZCre}$ mouse brain by *in situ* hybridization

An antisense riboprobe was hybridized to 20µm-thin cryosections. Representative bright field photomicrographs arranged from rostral to caudal showing *Cre* mRNA (middle) and *lacZ* mRNA (right) on coronal brain sections. ISH using a specific riboprobe detecting endogenous *Crhr1* mRNA from the heterozygous allele (left) reveals expression of the reporter cassette and *Cre* recombinase, respectively only in a subset of CRHR1 neurons. For abbreviations and details, see text.

6.3.2 Validation of *Cre* expression using a reporter line

To examine the spatial and temporal expression of *Cre* recombinase *CRHR1*$^{+/tZCre}$ mice were bred to the R26-CAG-tdTomato (Ai9) reporter line (*187*). The expression of the reporter gene *tdTomato* driven from the CAG promoter inserted into the *Rosa26* locus relies upon *Cre*-mediated removal of an upstream *loxP*-flanked stop cassette (Figure 16).

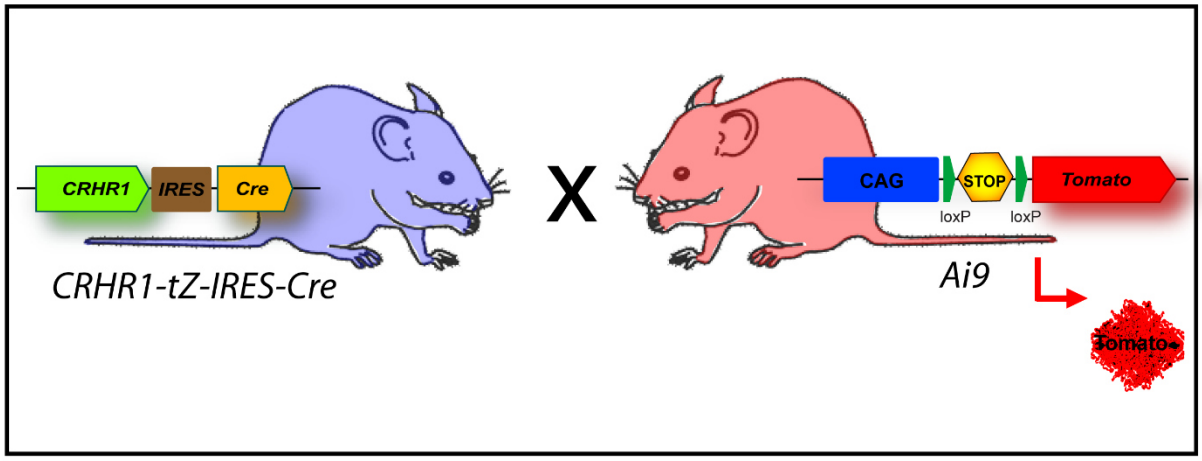

Figure 16: Validation of *Cre* recombinase expression of *CRHR1*$^{+/tZCre}$ mice

Expression of the fluorescent *tdTomato* reporter gene is blocked by an upstream stop signal. Expression of *Cre* driven from the CRHR1 promoter within the same cell results in recombination between the flanking *loxP* sites and deletion of the stop cassette, thus activating expression of the reporter gene under control of the ubiquitous CAG promoter.

The *Cre*-mediated recombination event and subsequent expression of the reporter gene will persist in all cells irrespective of whether or not they continue to express *Cre*. With this approach the cumulative expression history of the *Cre* recombinase can be made fully visible. Strong native *tdTomato* fluorescence allows direct visualization of neurons including their processes (dendrites and axons) and long-range axonal projections. A direct comparison of the reporter *tdTomato* at mRNA and protein level by ISH and native fluorescence, respectively, is displayed in Figure 17.

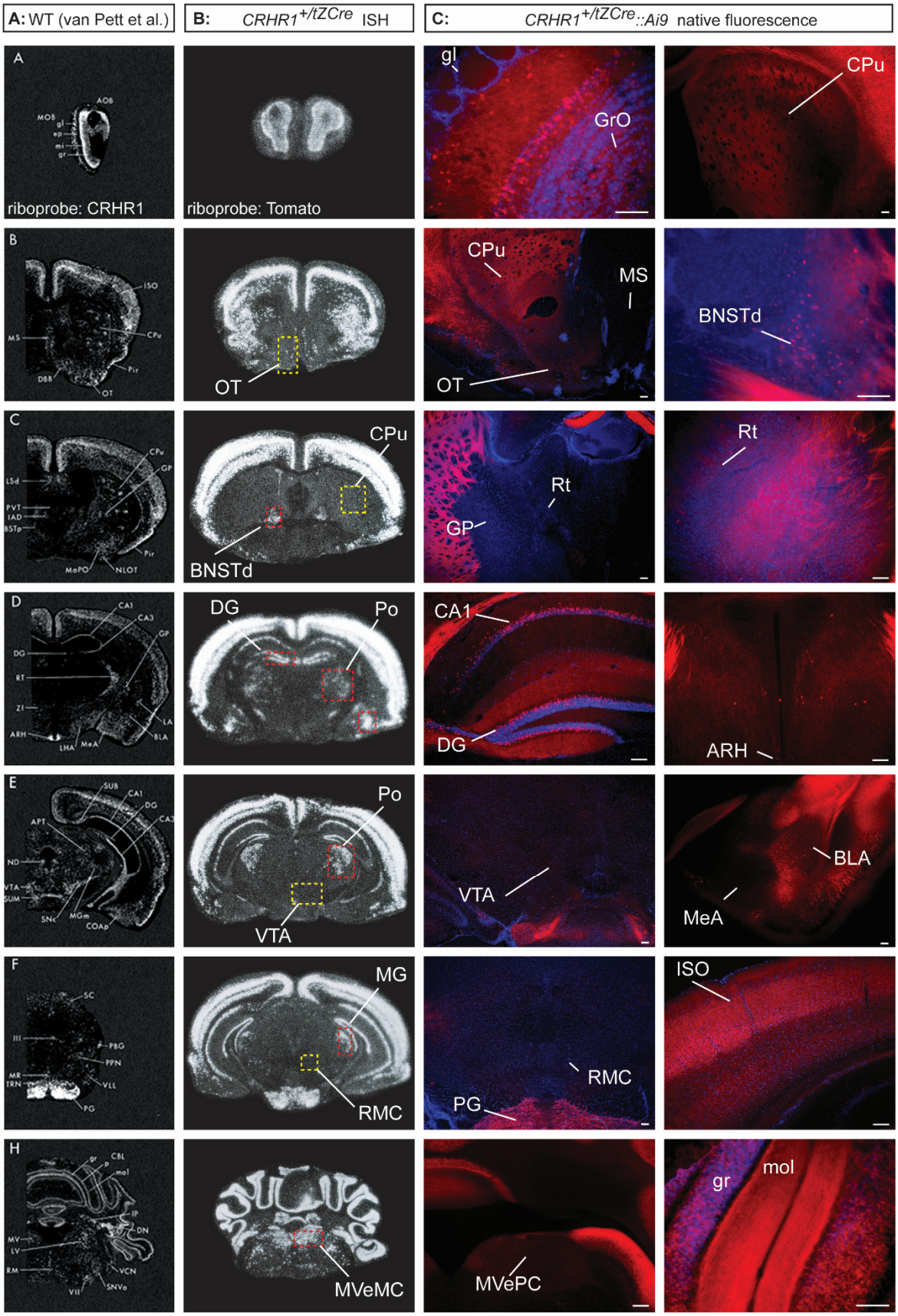
A: WT (van Pett et al.)
B: CRHR1+/tZCre ISH
C: CRHR1+/tZCre::Ai9 native fluorescence
riboprobe: CRHR1
riboprobe: Tomato
gl
GrO
CPu
MS
OT
BNSTd
Rt
GP
DG
Po
CA1
ARH
VTA
BLA
MeA
MG
RMC
PG
ISO
gr
mol
MVePC
MVeMC

Figure 17: Analysis of *tdTomato* reporter gene expression in the adult heterozygous *CRHR1$^{+/tZCre}$* mouse brain

Row (A) depicts dark-field photomicrographs arranged from rostral to caudal showing *Crhr1* mRNA expression in brain sections of wild-type mice (copyright 2000 Wiley and Sons; used with permission # 4257670565929 from van Pett, *Distribution of mRNAs encoding CRF receptores in brain and pituitary of rat and mouse*, Figure 1A-F, H). (B) Dark-field photomicrographs illustrating distribution of neurons expressing *tdTomato* mRNA. Areas framed in red, highlight brain nuclei with developmental or transient *Cre* recombinase expression resulting in a permanent "on state" of reporter gene expression. Nuclei with absent *Cre* mRNA expression during development and adulthood are surrounded by a yellow rectangle. (C) Coronal brain sections of adult mice depicting expression of the *tdTomato* reporter gene in a subpopulation of CRHR1 positive neurons. Regions of interest are highlighted. Abbreviations: arcuate nucleus (ARH), basolateral amygdaloid nucleus (BLA), bed nucleus of the stria terminalis dorsal (BNSTd), field CA1 of hippocampus (CA1), caudate putamen/striatum (CPu), dentate gyrus (DG), glomerular layer of the olfactory bulb (gl), globus pallidus (GP), granule cell layer of the olfactory bulb (GrO) or cerebellum (gr), isocortex (ISO), medial amygdaloid nucleus (MeA), medial geniculate complex (MG), medial septal nucleus (MS), medial vestibular nucleus magnocellular (MVeMC), medial vestibular nucleus parvicellular (MVePC), molecular layer cerebellum (mol), olfactory tubercle (OT), pontine grey (PG), posterior thalamic nuclei (Po), red nucleus magnocellular part (RMC), reticular thalamic nucleus (Rt), ventral tegmental area (VTA). Scale bars represent 100µm.

Early developmental or temporally restricted *Cre* expression could be detected in the bed nucleus of the stria terminalis (BNSTd), dentate gyrus (DG), posterior thalamic nuclei (Po), medial geniculate complex (MG) and medial magnocellular vestibular nucleus (MVeMC) (areas marked with red rectangles in Figure 17). It should be mentioned that this reporter line strategy for systematic characterization of CRHR1 promoter driven *Cre* recombination pattern is very sensitive to low levels of *Cre*, potentially leading to more recombined cells than expected from previous mRNA expression studies. In contrast, less recombination than expected when compared with endogenous CRHR1 expression in wild-type animals (Row A, Figure 17) was apparent in the granule cell layer and glomerular layer of the olfactory bulb (gl, gr), the olfactory tubercle (OT), the medial septum (MS), the hippocampus (CA1), the basolateral- and medial amygdala. Among subcortical structures *tdTomato* expression in the basal ganglia, namely the striatum (CPu), the globus pallidus (GP), and the VTA was absent or only sporadicly detectable. Furthermore, the reticular thalamic nucleus as well as the arcuate nucleus – two prominent sites of CRHR1 expression – are almost entirely lacking reporter gene expression. It remains unclear whether these absent recombinations in certain cell populations are due to alternative splicing and subsequent nonsense-mediated mRNA decay.

As illustrated in Figure 17, expression of *Cre* during adulthood is restricted to a subpopulation of CRHR1 positive neurons. However, the rather sparse labeling of CRHR1 expressing neurons provides substantive benefits for imaging axons and dendrites. CRHR1 is relatively widely expressed and expression of the reporter in all cells would complicate tracking of processes for morphological analyses. In addition, isolation of individual CRHR1 positive neurons for electrophysiological recordings or single cell expression profiling is considerably easier in this mouse line. For example, a single cell electrophysiological analysis in hippocampal CA1 region of *CRHR1*$^{+/tZ}$*Cre* mice revealed that the *tZCre* allele is a "knockout allele" as these cells, marked by *dtTomato* fluorescence, are not reactive to exogenous CRH administration (Figure 18; personal communication; experiment was conducted by Dr. Julien Dine at the electrophysiological core unit of the MPI for Psychiatry, Munich)

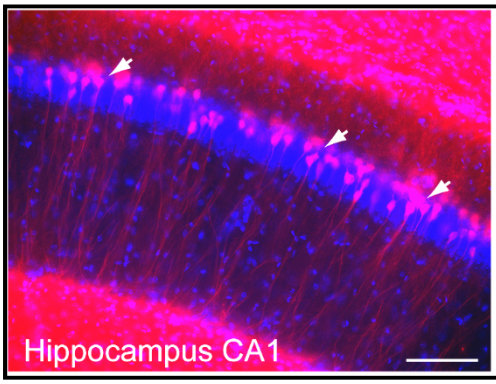

Figure 18: Analysis of sparse labeled neurons in hippocampal CA1 field

Single cells filled with *tdTomato* reporter protein can be simply identified by native fluorescence and targeted for patch clamp recordings. Scale bar represents 100µm.

6.4 Generation of the *CRHR1*^{Cre} mouse line

6.4.1 Removal of the *tZ-neo* reporter and *hygromycin* selection cassettes

For identification of targeted ES cell clones, the positive selection marker hygromycin was included within the targeting vector. As such markers can alter the splicing and regulation of the targeted locus, it was flanked with *frt* sites to enable its removal *in vivo* by crossing to a *Flp* recombinase deleter strain. Because of the alternative recombination event, the *tau-lacZ*-reporter cassette of the genomic docking locus is still present but due to residual flanking *frt* sites also accessible for *Flp* mediated recombination. For this, the *CRHR1*^{tZCre} mouse line was bred to the FlpeR ("flipper") mouse strain (obtained from the Jackson Laboratory; stock number 003946). The latter strain expresses a thermostable variant of *Flp* under control of the ubiquitous *Rosa26* promoter. Target gene recombination can be achieved from preimplantation

onwards and includes most tissue types and cells of the developing germ line. As different recombination events are likely, a PCR based screening strategy was designed to detect the desired recombination event in F1 progeny (Figure 19).

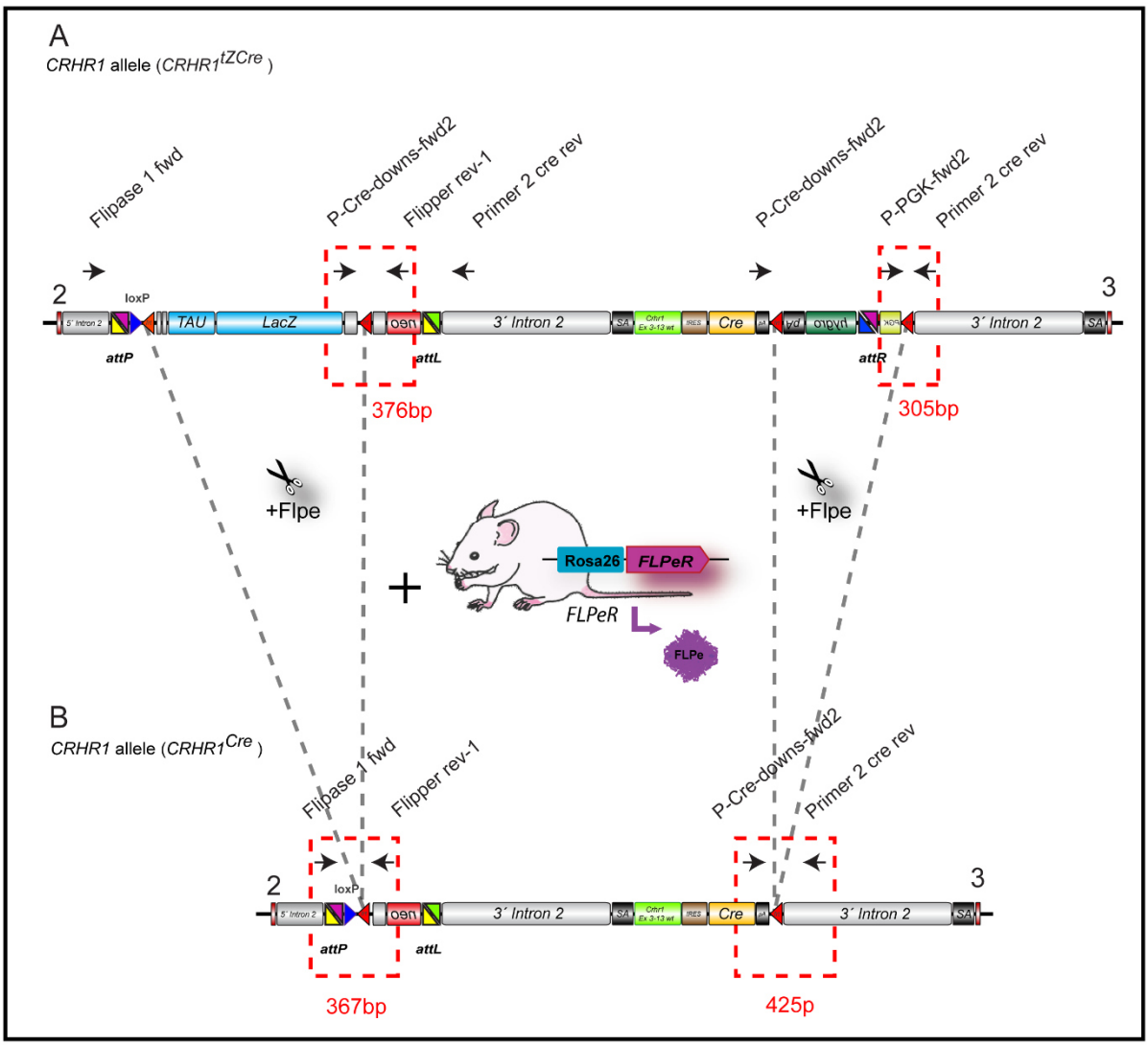

Figure 19: *Flpe*-mediated removal of the *tZ-neo* reporter and *hygromycin* selection cassettes

Using the FlpeR ("flipper") mouse strain to restore the targeted knock-in allele. (A) Overview of *Flpe*-mediated excision of the reporter (*tau-lacZ*) and selection (*hygro*) cassettes. Primers for detecting the *tZ-neo* cassette and the *Cre* recombinase are indicated by arrows. (B) Recombined CRHR1 allele (*CRHR1*^{Cre}) with *Cre* recombinase being expressed under control of the endogenous CRHR1 promoter. Red rectangles indicate the PCR strategy and primer combinations for detection of hetero- and homozygous offspring. For details, see text.

6.4.2 Establishment of Genotyping

PCR analyses to identify removal of the *hygro* selection cassette as well as the *tau-lacZ-reporter cassette* was performed by a multiplex PCR assay. A 305bp product indicates the presence of the hygromycin gene with primer pairs P-Cre-downs-fwd 2, P-PGK-fwd 2 and Primer 2 cre rev. A PCR product of 425bp displayed deletion of the selection cassette with *Cre* recombinase still present. Under standard PCR conditions primer pairs P-Cre-downs-fwd2. and Flipper rev-1. resulted in a 376bp PCR product, indicating the presence of the *tZ-neo cassette*. After recombination and removal of the reporter cassette the primer combination Flipase 1 fwd and Flipper rev-1 resulted in a smaller PCR product of 367bp. Primer pair Flipase 1 fwd and Primer 2 cre rev (232bp PCR product) indicate the presence of the wild-type allele. (Figure 20 left panel).

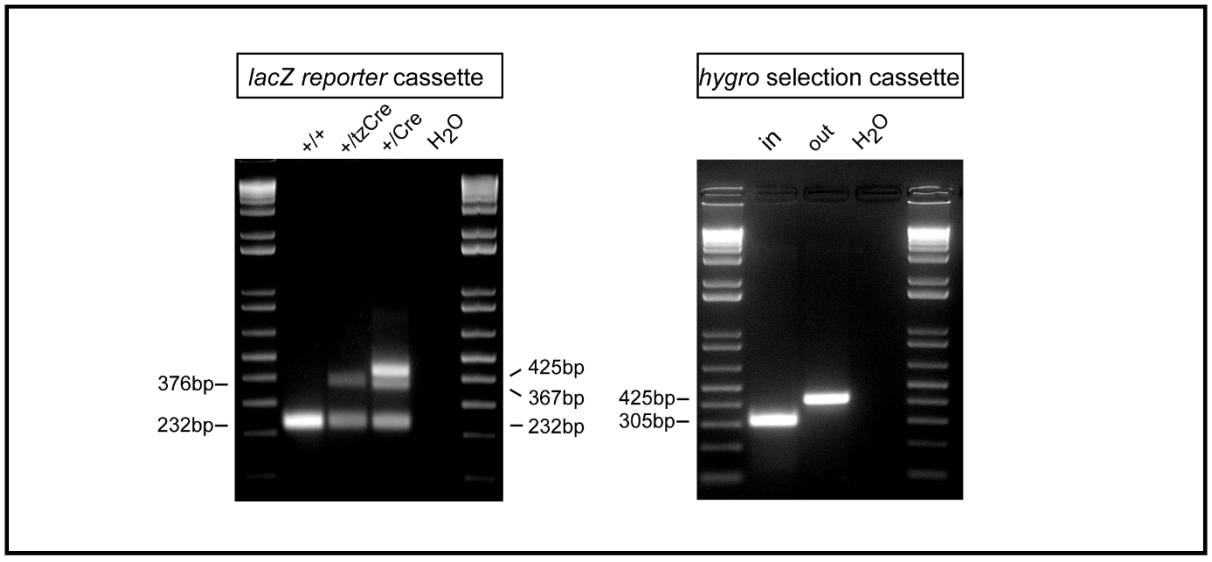

Figure 20: PCR analyses of *CRHR1^{tzCre}* x *FlpeR* offspring

Genotyping of F1 progeny from breeding heterozygous *CRHR1^{tZCre}* mice to *FLPeR* mice. Left panel: removal of the *tZ* reporter cassette is indicated by a 367bp PCR product. An additional 425bp product indicates simultaneously removal of the hygromycin cassette. Right panel: presence of the selection cassette is indicated by a 305bp product; after recombination and deletion standard PCR conditions resulted in a 425bp PCR product.

6.5 Characterization of *Cre* expression

6.5.1 Systematic characterization of *Cre* expression by *in situ* hybridization

To evaluate the utility of the *CRHR1*^{Cre} mouse line as a tool enabling genetic access to CRHR1-specific subpopulations of cells in the mouse brain, the *Cre* expression pattern was systematically analyzed by radioactive ISH (Figure 21). Direct comparison of *Cre* mRNA and *Crhr1* mRNA (riboprobe located in the 3' UTR of the receptor) on adjacent brain sections from heterozygous animals allows for direct comparison of the *Cre* recombination pattern with the endogenous CRHR1 expression. To summarize, expression of the *Cre* recombinase exactly recapitulates the spatial distribution of endogenous *Crhr1* mRNA and is in line with previously described expression patterns of the receptor (*29, 41*). Major sites of *Crhr1* mRNA expression include cortical layers II-VI, pyramidal cell layer of the hippocampus, granule and glomerular layer of the main and accessory olfactory bulbs, basolateral and medial amygdala, pontine nuclei and Purkinje and granule layers of the cerebellar cortex. As expected *Flp*-mediated removal of the reporter and hygromycin selection cassettes from the *CRHR1*^{tZCre} allele restored expression of *Cre* in central components of the basal ganglia, namely globus pallidus and caudoputamen as well as their major sources of input, the substantia nigra and VTA. Furthermore, *Cre* expression is now detectable in the red nucleus, reticular thalamic nucleus and in sensory structures like the vestibular nuclei, all of them lacking signal in the *CRHR1*^{tZCre} mouse line. Taken together, the knock-in approach inserts the *Cre* transgene cassette directly into the endogenous locus of CRHR1 thereby ensuring that the *Cre* driver line mirrors the expression pattern of the receptor and by the use of an *IRES* site the expression of the wild-type receptor is preserved.

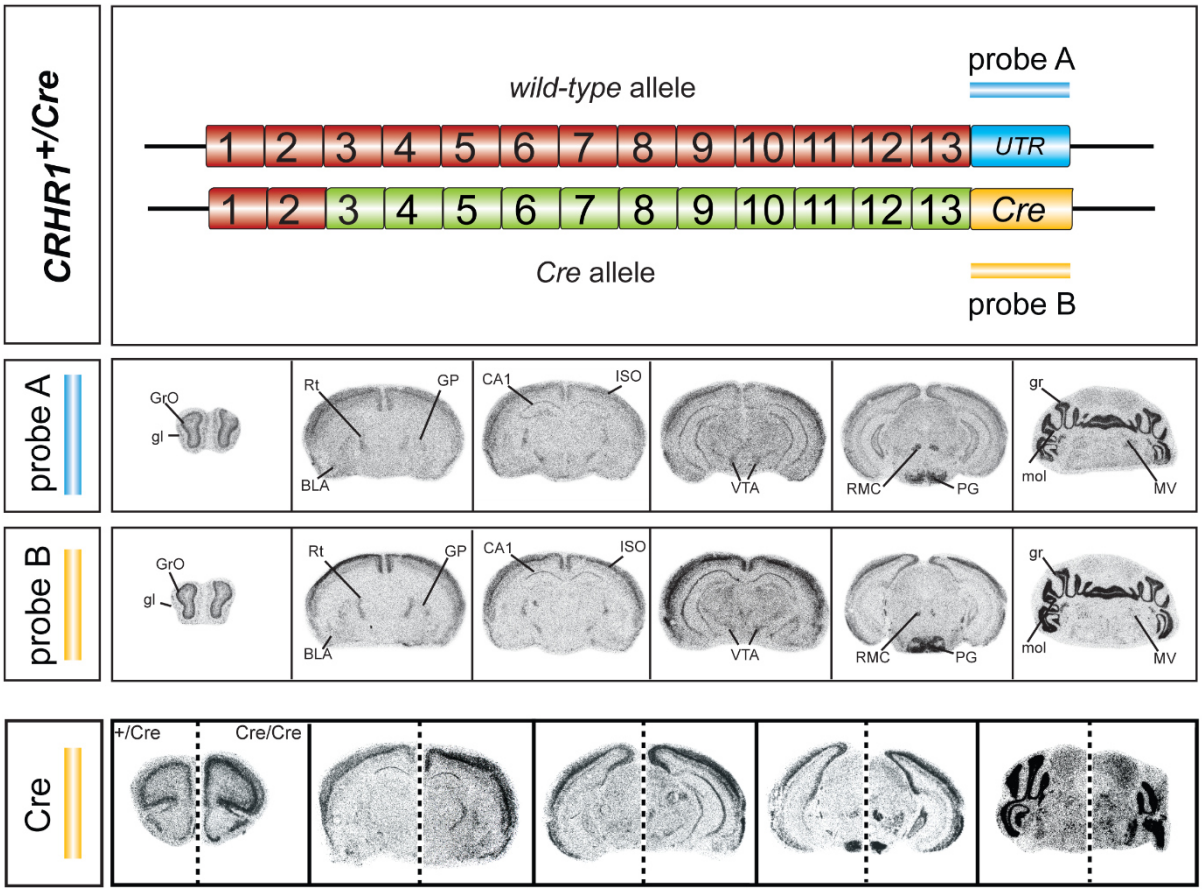

Figure 21: *Cre* expression fully recapitulates *Crhr1* mRNA expression in the brain

The anticipated transcripts produced from the indicated allele and the localization of the respective *in situ* probes A (*3' UTR*) and B (*Cre*) are schematically depicted on the top. Representative bright field photomicrographs showing *Crhr1* mRNA (probe A) and *Cre* mRNA (probe B) on adjacent coronal brain sections arranged from rostral (left) to caudal (right). Bottom row: the level of *Cre* mRNA expression is gene dosage-dependent as demonstrated by the stronger *in situ* hybridization signals detected in homozygous *CRHR1*$^{Cre/Cre}$ (right side) versus heterozygous *CRHR1*$^{+/Cre}$ (left side) animals. Abbreviations: basolateral amygdaloid nucleus (BLA), field CA1 of hippocampus (CA1), glomerular layer of the olfactory bulb (gl), globus pallidus (GP), granule cell layer of the olfactory bulb (GrO) or cerebellum (gr), isocortex (ISO), medial vestibular nucleus (MV), molecular layer cerebellum (mol), pontine grey (PG), red nucleus magnocellular part (RMC), reticular thalamic nucleus (Rt), ventral tegmental area (VTA).

Based on a thorough ISH analysis of homozygous transgenic mice (*CRHR1*$^{Cre/Cre}$) versus wild-type littermates (*CRHR1*$^{+/+}$) we could confirm that normally spliced *CRHR1* mRNA is produced and that no aberrantly spliced sequences are co-expressed from the knock-in *Cre* allele. A schematic representation of the wild-type and transgenic allele and the localization of the respective *in situ* probes are shown in Figure 22. Homozygous mutants of both sexes are viable and fertile and the transgenic *Cre* allele does not affect embryonic or neonatal survival. The level of *Cre* mRNA expression is gene dosage-dependent as demonstrated by the stronger *in situ*

hybridization signals detected in *CRHR1*$^{Cre/Cre}$ versus *CRHR1*$^{+/Cre}$ animals (Figure 21).

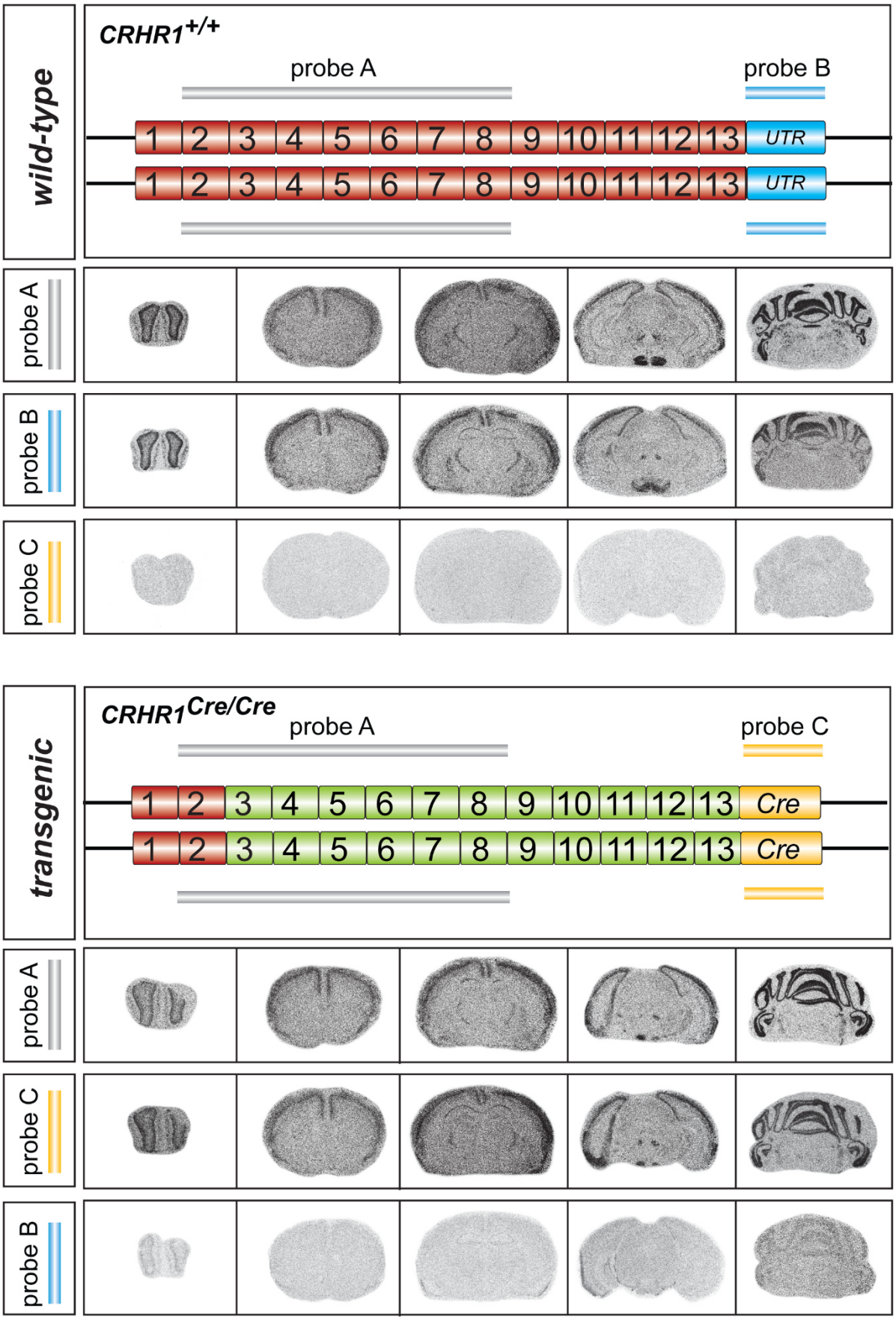

Figure 22: Validation of the *Cre* mRNA expression in wild-type mice and homozygous CRHR1 *Cre*-driver mice

A schematic representation of the wild-type and transgenic knock-in allele and localization of respective *in situ* probes are shown at the top of the chart. Endogenous *Crhr1* mRNA expression and *Cre* mRNA expression was demonstrated by *in situ* hybridization using specific riboprobes (probe B and C, respectively). Depicted are representative bright field photomicrographs of coronal brain sections from rostral to caudal taken from autoradiographs. The absence of *in situ* hybridization signals using probe B and C as specific negative controls on the corresponding sections confirmed the correct splicing and reconstitution of the CRHR1 in the *CRHR1*$^{Cre/Cre}$ transgenic mouse line.

6.5.2 Evaluation of *Cre* specificity by double *in situ* hybridization

In order to further validate the specificity of *Cre* expression on the cellular level we performed double *in situ* hybridization on brain sections from adult heterozygous animals to verify that the *Cre* recombines exclusively in endogenously CRHR1 expressing neurons. The double ISH approach has been chosen in preference to the double immunohistochemistry technique due to the lack of specific CRHR1 antibodies. Because of the relatively weak CRHR1 promoter we expect a rather low expression level of the endogenous CRHR1 and the *IRES*-dependent downstream *Cre*. Therefore, we analyzed the *Cre*-dependent *tdTomato* reporter gene expression. Upon *Cre* recombinase-mediated removal of the transcriptional STOP cassette from the *R26CAG::loxP-STOP-loxP-tdTomato* (Ai9) allele, *tdTomato*-reporter expression is driven by a CAG promoter and continuously detected in all neurons that have expressed CRHR1 at any given time point within their lineage. Quantification of double positive cells revealed that most *tdTomato*-expressing neurons co-expressed CRHR1 and vice versa, the majority of CRHR1-positive neurons also expressed *tdTomato* (Figure 23). This outcome displays the full potential and utility of the new *Cre* driver line for providing access to CRHR1-specific neurons. It is important to mention that the *tdTomato* expression pattern reflects the cumulative/developmental expression history of *Cre* and amplifies expression levels. Thus, *tdTomato*-positive neurons that lack CRHR1 expression could represent cells that expressed CRHR1 during the course of development, but ceased to do so in adulthood. The presence of CRHR1-positive, but *tdTomato*-negative cells, could be explained by lack of activity of the CAG promoter (that drives tdTomato expression) in those particular cells. Care must also be taken in interpreting negative colorimetric ISH results (“cold ISH”) as very low levels of mRNA may not be detectable even with the high sensitive TSA biotin plus system used here.

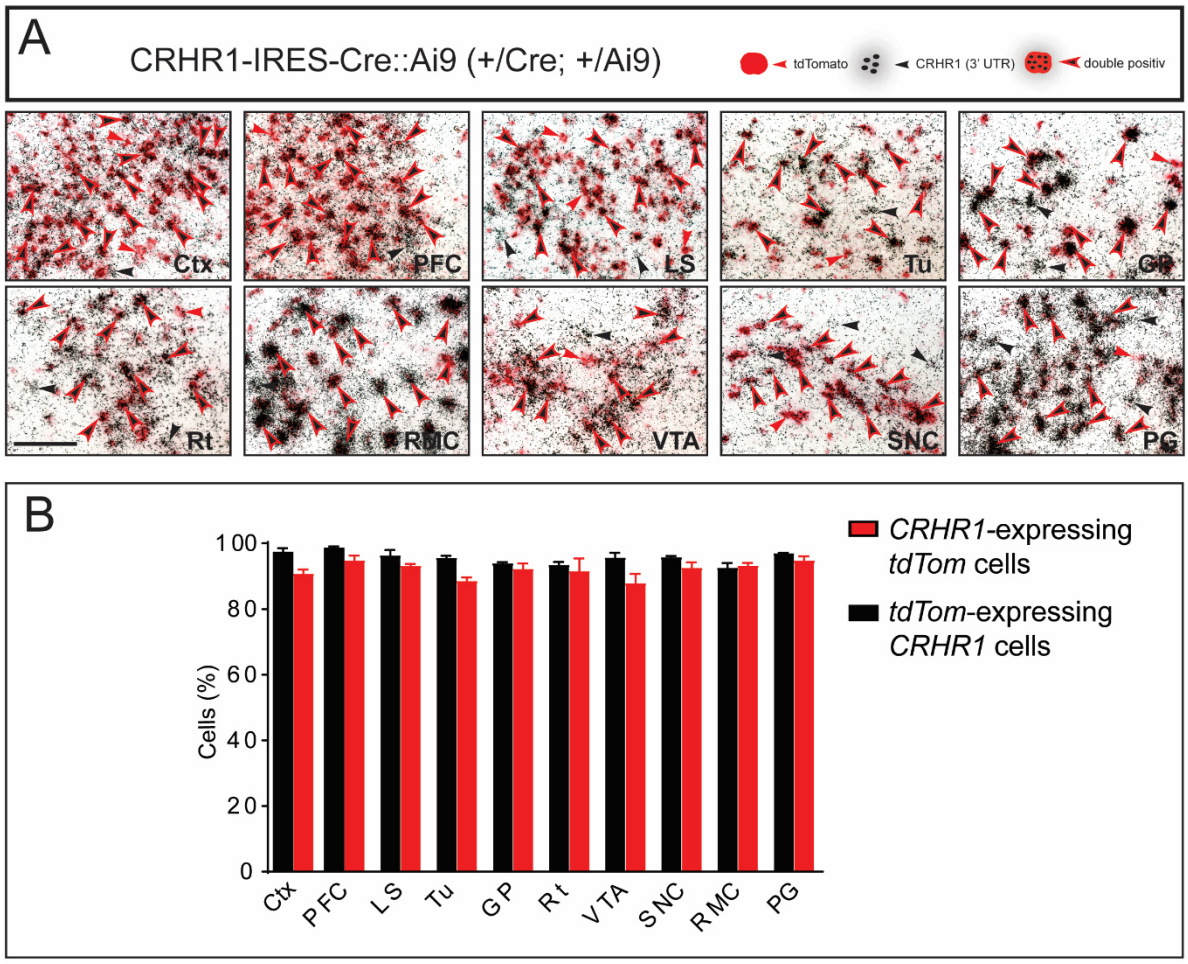

Figure 23: Validation of *Cre* expression/recombination specificity in CRHR1^{Cre} mice

Bright field photomicrographs of coronal brain sections obtained from heterozygous *CRHR1*$^{+/Cre}$ mice bred to *Ai9* reporter mice (*CRHR1*^{Cre}*::Ai9*) depicting high specificity of *Cre* recombinase expression. (A) The upper row depicts double ISH of endogenous *Crhr1* mRNA (black silver grains) and CRHR1-*IRES*-*Cre*-driven *tdTomato* (red staining). Black arrowheads indicate cells expressing only *Crhr1* mRNA, red arrowheads depict cells expressing only *tdTomato* mRNA, respectively. Red-framed, black arrowheads indicate *Crhr1*-positive neurons coexpressing *tdTomato*. (B) Quantification of double positive cells in different brain regions of interest; n = 3 mice, 3 sections/mouse. Most *tdTomato*-expressing neurons co-expressed *Crhr1*, and likewise the majority of *Crhr1*-positive neurons also expressed *tdTomato*. Scale bar represents 100µm; all pictures were taken with the same objective (40x). For details, see text.

6.5.3 Visualization of *Cre* expression via breeding to reporter lines

Expression analysis of *Cre* itself via radioactive *in situ* hybridization (see Figure 21-23) is a good indicator of adult *Cre* expression patterns, but care must be taken as very low levels of mRNA may not be detectable by this method. To circumvent this limitation, the *CRHR1*^{Cre} mouse line was crossed with two different *Cre*-inducible reporter lines that express a fluorescent reporter gene upon *Cre*-mediated recombination of l*oxP* sites flanking a STOP cassette. Every *Cre*-mediated recombination event will lead to persistent reporter gene expression regardless whether the cells continue to express *Cre* (Figure 24). As predicted, there is a discrepancy between *Cre* mRNA expression (Figure 21, probe B) and *Tomato* mRNA expression (Figure 25 top panel) in the adult mouse brain. The two most likely cause of the “ectopic” *tdTomato* expression is a transient expression in neurons during development or so far undetected expression of low receptor levels due to a relatively weak endogenous promoter. The latter possibility could be verified by injection of *Cre*-dependent reporter viruses in respective target regions of adult mice, thereby excluding developmental *Cre*-mediated recombination events (see chapter 6.5.4). A detailed analysis of expression with regard to temporal and spatial specificity using a double ISH approach is provided in chapter 6.5.2. The following section first outlines expression of the two reporter genes *tdTomato* and *sfGFP*, respectively.

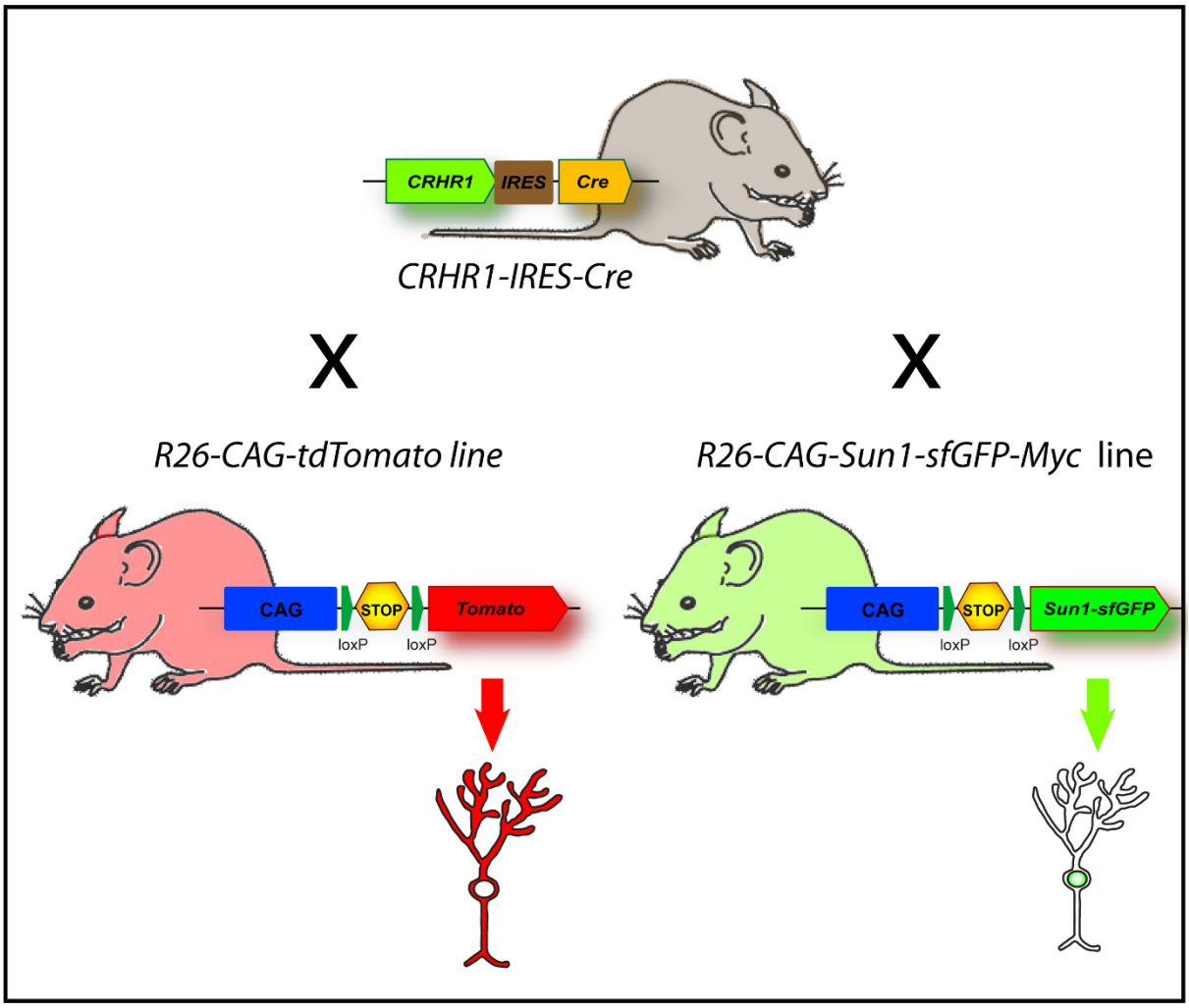

Figure 24: Schematic diagram illustrating the *R26* Tomato and R26 *Sun1-sfGFP* knock-in reporter constructs

A *loxP* flanked STOP cassette prevents transcription of the downstream reporter proteins. *Cre*-mediated excision of the STOP cassette activates expression of *tdTomato* and the nuclear membrane fusion protein *Sun1-sfGFP*, respectively, in CRHR1 positive neurons (for details, see text).

In the R26-CAG-tdTomato (Ai9) *Cre*-responder line, the fluorescent marker protein *tdTomato* is expressed under the strong and ubiquitous CAG promoter inserted within the *Rosa26* locus (Madisen et al., 2010*). Cre*-mediated removal of an upstream floxed STOP cassette activates expression of the reporter protein. The fluorescent reporter is a tandem fusion protein of two *Tomato* copies leading to an exceptional brightness and excellent photostability. Strong native *tdTomato* fluorescence distributes uniformly throughout the targeted cell and allows direct visualization of fine neuronal structures like dendritic spines and axons. Therefore, it is possible to trace long-range axonal projections.

Systematic analysis of CRHR1 distribution in the mouse brain was impeded by the lack of CRHR1-subtype specific antibodies (*99*) and therefore relies mainly on *in situ* hybridization based studies (*29*) and transgenic reporter mice (*41, 219*), the latter expressing the reporter gene *GFP* or *tau-lacZ,* respectively, under the relatively weak endogenous CRHR1 promoter. Even though both reporter lines almost entirely mimic the CRHR1 mRNA expression they reached their limits with respect to sensitivity in major stress-related central autonomic cell groups such as the central amygdala, LC and hypothalamic paraventricular nucleus. Moreover, expression of *GFP* is restricted to the soma and proximal dendrites and detection of the *tau-lacZ* reporter is not possible in live tissues or cells. In contrast, breeding of the *CRHR1^{Cre}* mouse line to *Cre* inducible reporter lines comprising a strong and ubiquitous promoter will provide a definite picture of CRHR1 expressing cells and their projections. CRHR1 promoter driven expression of *Cre* and *tdTomato*, respectively, is detectable throughout the brain, including the mitral and granule cell layer of the olfactory bulb, cortical layers II-VI, hippocampus, caudate putamen, bed nucleus of the stria terminalis, basolateral amygdala and granule layer of the cerebellum. In line with previous reports, reporter gene expression is also visible in the retina and hair follicles (*41*). In accordance with scattered CRHR1 mRNA signals in the hypothalamic paraventricular nucleus (*29*) only a few *tdTomato* labeled cells were detectable substantiating a rather weak expression of the receptor under basal conditions (Figure 25).

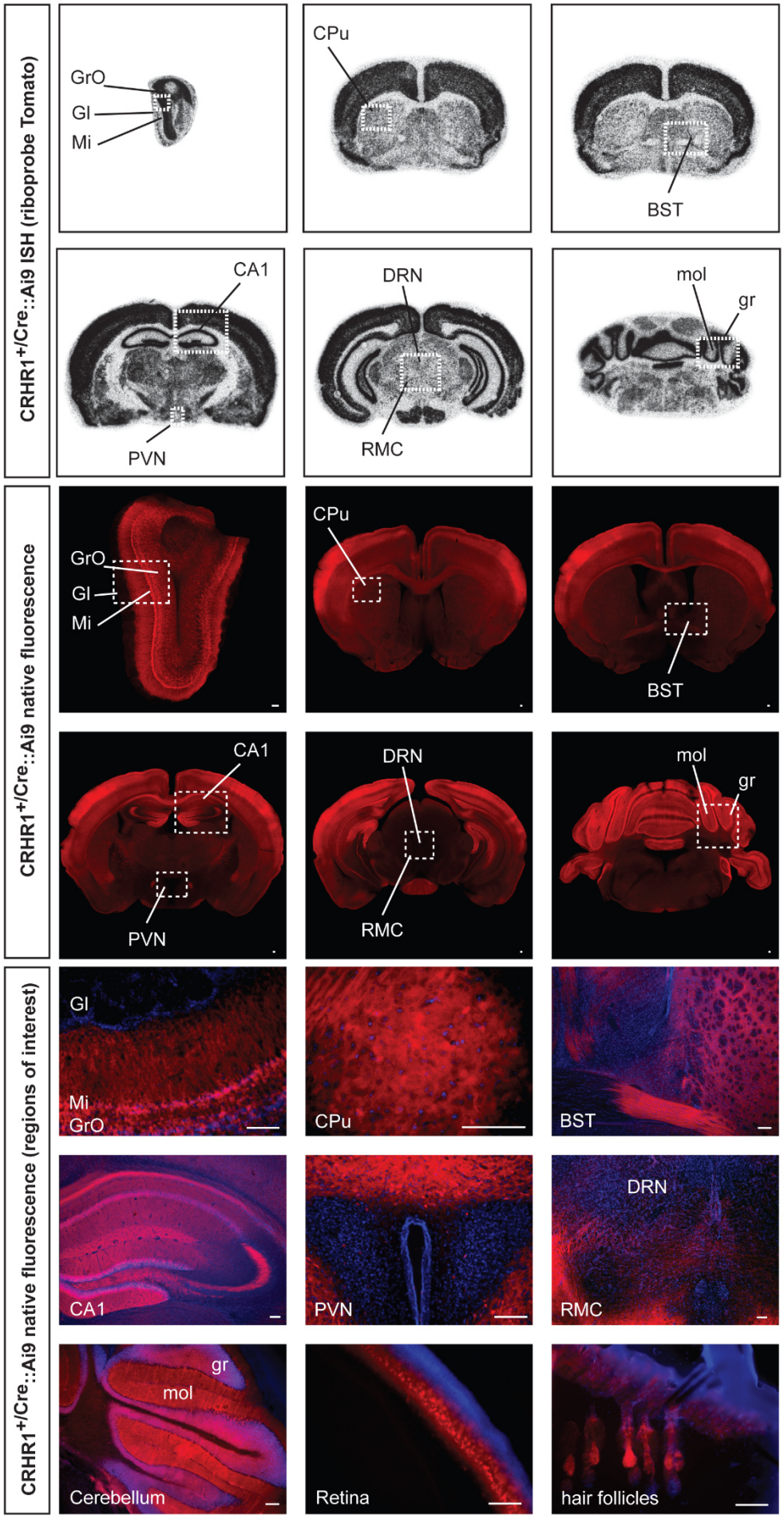
CRHR1+/Cre::Ai9 ISH (riboprobe Tomato)
GrO
Gl
Mi
CPu
BST
CA1
PVN
DRN
RMC
mol
gr
CRHR1+/Cre::Ai9 native fluorescence
GrO
Gl
Mi
CPu
BST
CA1
PVN
DRN
RMC
mol
gr
CRHR1+/Cre::Ai9 native fluorescence (regions of interest)
Gl
Mi
GrO
CPu
BST
CA1
PVN
DRN
RMC
gr
mol
Cerebellum
Retina
hair follicles

Figure 25: CRHR1 *Cre*-driven reporter expression reproduces endogenous CRHR1 expression pattern during adulthood and additionally labels developmental sites and/or sites of very low levels of CRHR1 expression

Top panel depicts *tdTomato* mRNA expression in sections of *CRHR1-Cre* mice crossed with *Ai9* reporter mice (*R26::loxP-STOP-loxP-tdTomato*). Middle panel depicts an overview of *tdTomato* reporter protein expression in coronal sections of adult mouse brain. A dense set of fluorescent cells and neuronal processes is visible. Regions of interest are highlighted with dashed rectangles and displayed at higher magnification in the bottom panel. Abbreviations: bed nucleus of the stria terminalis BST), field CA1 of hippocampus (CA1), caudate putamen/striatum (CPu), glomerular layer of the olfactory bulb (gl), granule cell layer of the olfactory bulb (GrO) or cerebellum (gr), molecular layer cerebellum (mol), red nucleus magnocellular part (RMC), paraventricular nucleus of the hypothalamus (PVN). Scale bars = 100µm.

Due to the fact that CRHR1 is widely expressed throughout the brain and that *tdTomato* evenly distributes throughout cells, a dense net of labeled neurites prevented tracing of distinct neurocircuits and detection of single labeled neurons in prominent sites of *Crhr1* mRNA expression such as globus pallidus, reticular thalamic nucleus, VTA, red nucleus as well as other sites of rather low expression of *Crhr1* mRNA. For tracing specific CRHR1 dependent neurocircuits a more specific approach via injection of *Cre*-dependent viruses in distinct target regions is preferable especially since several “FLEXed” adeno-associated viruses are commercially available. Here, expression of *tdTomato* depends on *Cre*-mediated inversion of the *loxP* flanked reporter cassette (so called “double-floxed inverse open reading frame”, DIO-AAVs). In combination with specific promoters, it is thereby possible to dissect region-specific or neurotransmitter type-specific CRHR1 connectivities.

To evaluate the full potential of the CRHR1 *Cre*-driver line we examined *tdTomato* reporter gene expression in peripheral organs of double transgenic CRHR1^{Cre}::Ai9 tdTomato mice. Consistent with previous results (*29, 41, 219*), expression of the reporter gene was detectable in pancreatic islet cells, in the spinal cord and dorsal root ganglia, in the optic part of the retina (inner nuclear and ganglion cell layer), in the root sheath and ring sinus of hair follicles, in the anterior and intermediate lobe of the pituitary gland as well as in a narrow band across the cortex of the adrenal gland, the latter indicating the superiority of cumulative *tdTomato* expression to *GFP* and *tau-lacZ* reporter gene expression (Figure 26 A-F). In line with expression studies in humans and rats (*220*) *tdTomato* fluorescence signal was detectable in proximal and distal convoluted tubes as well as collecting tubes within the cortex of the kidney

(Figure 26 G). Furthermore, by way of immunohistochemistry and mRNA expression studies, CRHR1 presence was shown in gastrointestinal tissues, thymus, spleen and ovary of rats (*221*). Up to now, corresponding studies in mice are lacking. The use of double transgenic CRHR1^{Cre}::Ai9 tdTomato mice offers the possibility to detect cumulative expression of the receptor with highest sensitivity. With this approach CRHR1 expression was proven in the mucosa (villi) of the small intestine (Figure 26 H), in filiform papilla of the tongue (Figure 26 I) and in lymphatic tissues including thymus, spleen and liver (Figure 26 J-L). There is experimental evidence that CRH modulates the immune and inflammatory responses and by means of RT-PCR mRNA expression of CRHR1 was shown in thymic and splenic cell populations, namely lymphocytes and macrophages (*221, 222*). The expression of CRHR1 was also depicted in Kupffer cells (KCs), macrophages that mediate the hepatic immune response (Figure 26 L), which is in line with reports of CRH receptor expression in human and rat liver tissue (*223*). Furthermore, the presence of CRH and its receptor type 1 is clearly demonstrated within rat ovaries. Detection of mRNA encoding CRHR1 revealed expression in stroma cells and the theca layer surrounding the ovulatory follicles (*224*). In cryosections from CRHR1^{Cre}::Ai9 tdTomato mice native *tdTomato* fluorescence was also visible in ovarian stroma cells, but was absent in granulosa cells of primordial and maturing follicles and lutein cells of corpora lutea (Figure 26 M). A peripheral organ, which has recently been reported to express CRHR1, is the fetal lung (*225, 226*). Expression of *tdTomato* in cryosections from adult CRHR1^{Cre}::Ai9 tdTomato mice was restricted to few cells within the respiratory epithelium (Figure 26 N). Taken together, this *Cre*-driver line significantly facilitates the neuroanatomical analysis of CRHR1 expression and opens up new avenues to address extrapituitary actions of the neurohormones CRH and UCN.

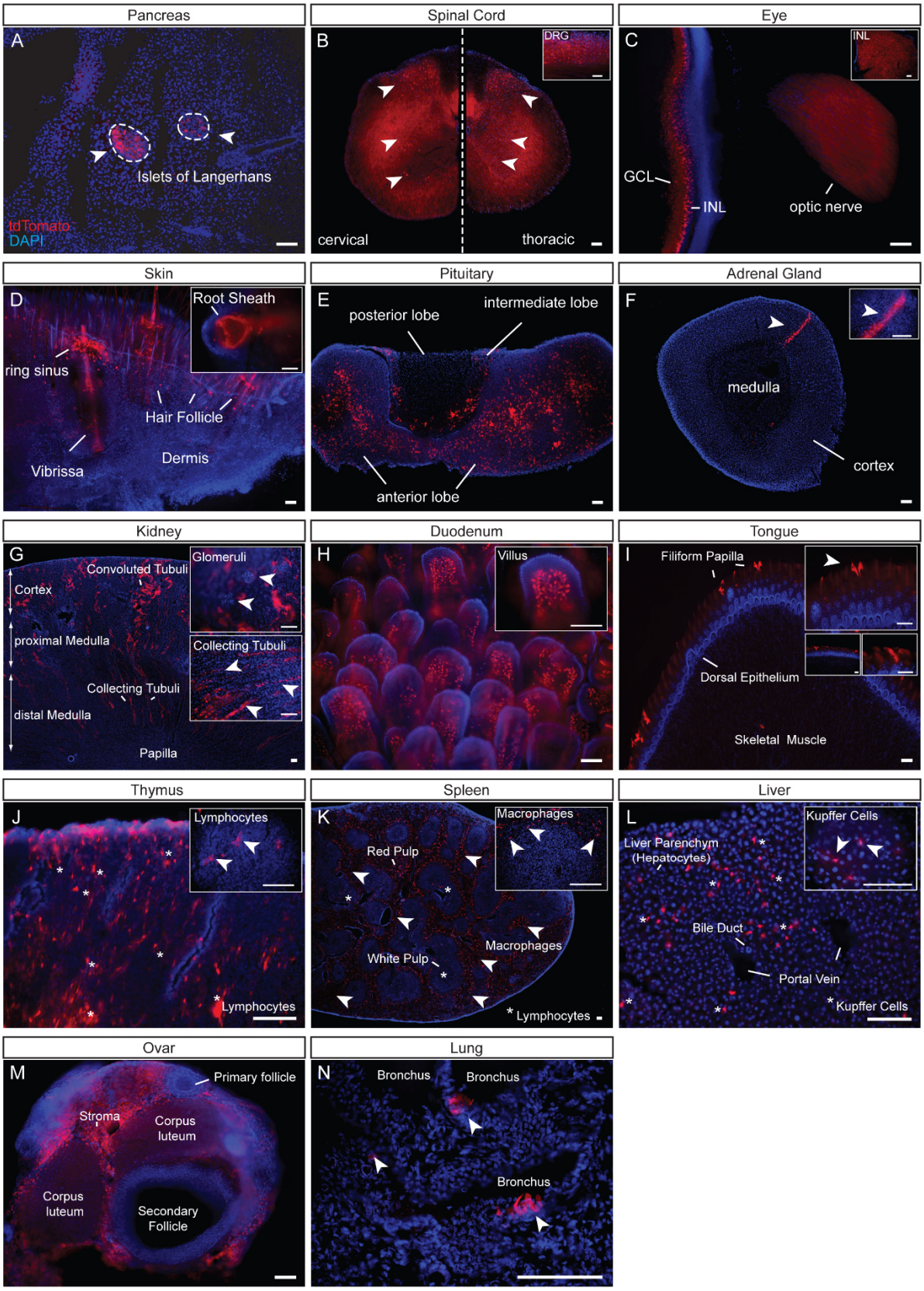

Figure 26: Characterization of *Cre* activity in peripheral organs of the CRHR1^{Cre}::Ai9 tdTomato mouse line

(A-N) *Cre*-mediated expression of *tdTomato* in organs dissected from double transgenic CRHR1^{Cre}::Ai9 tdTomato mice. For details, see text. Scale bars =100µm.

To analyze *Cre*- dependent expression pattern with maximum resolution we made use of a second reporter line (Gt(ROSA)26Sort$^{m5(CAG-Sun1/sfGFP)Nat}$; Jackson Laboratory stock number 021039), where two copies of superfolder *GFP* are tagged to the C-terminus of mouse SUN1, a nuclear membrane protein (*227*). The targeting vector containing a CAG promoter and an upstream *loxP*-flanked STOP cassette was inserted into the *Rosa26* locus. CRHR1-dependent expression of *Cre* recombinase leads to removal of the STOP cassette and expression of the SUN1-sfGFP fusion protein at the inner nuclear membrane in CRHR1 expressing cells. In direct and indirect immunofluorescence microscopy CRHR1 expressing cells display a nuclear rim-like fluorescence pattern. Therefore, labeled neurons can easily be detected in above mentioned brain areas, where a dense network of labeled neurites prevented detection of single labeled neurons, such as globus pallidus (GP), reticular thalamic nucleus (RT), VTA and red nucleus (RMC) (Figure 27). Thorough analysis of *sfGFP*-reporter gene expression revealed that expression of *Cre* was essentially similar to the spatial distribution of endogenous CRHR1 mRNA (*29*), as well as to the recently published *GFP*- (*219*) and *tZ*-reporter mouse lines (*41*). As already described in detail above, also here developmental expression of *Cre* recombinase leads to a permanent expression of *sfGFP* fusion protein. This is the reason why *Cre* expression analysis itself represents the better indicator of adult expression patterns, whereas expression of the reporter protein under the strong CAG promoter facilitates detection of neurons with low levels of CRHR1 expression (Figure 27).

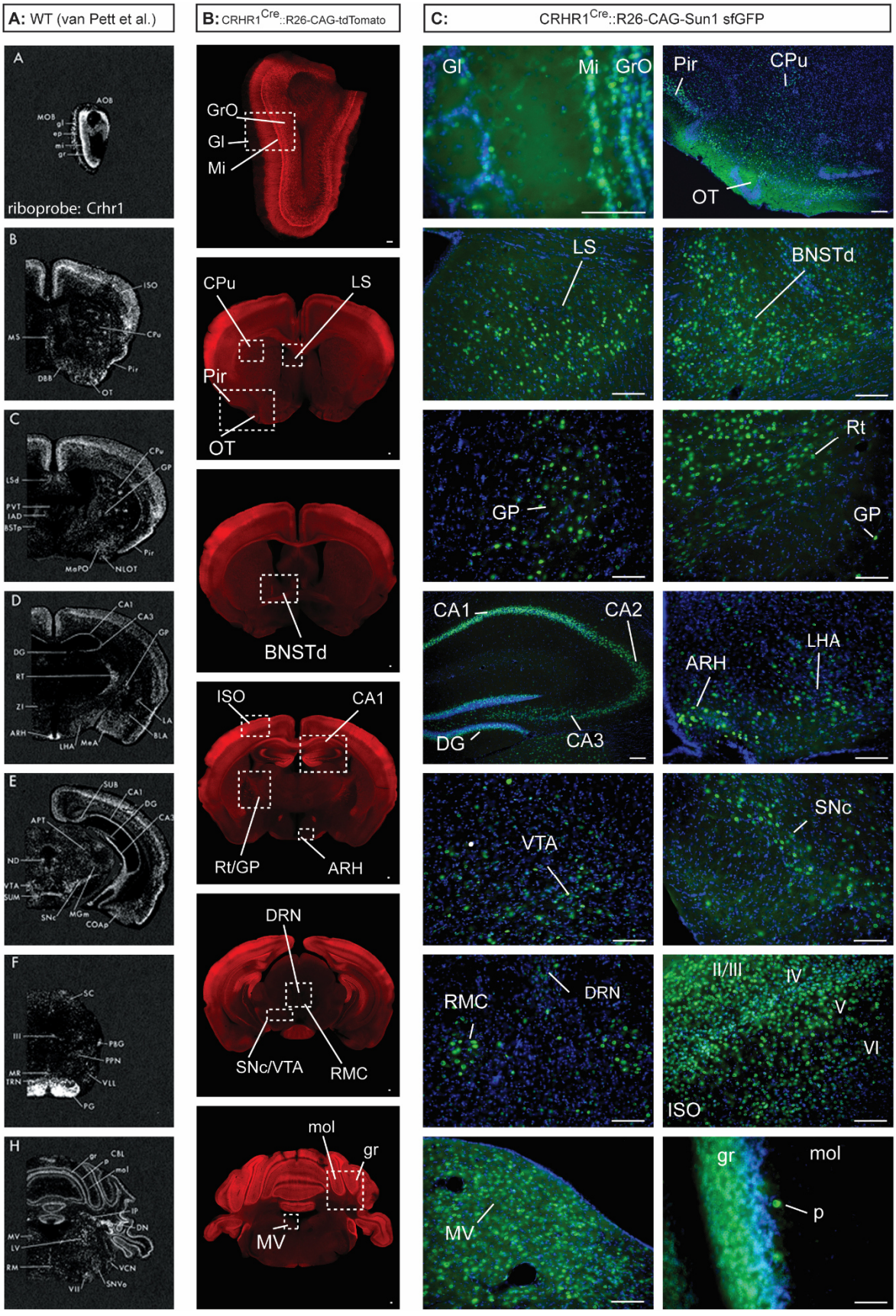
A: WT (van Pett et al.)
B: CRHR1Cre::R26-CAG-tdTomato
C: CRHR1Cre::R26-CAG-Sun1 sfGFP
riboprobe: Crhr1
GrO
Gl
Mi
CPu
LS
Pir
OT
BNSTd
ISO
CA1
Rt/GP
ARH
DRN
SNc/VTA
RMC
mol
gr
MV
Gl
Mi
GrO
Pir
CPu
OT
LS
BNSTd
GP
Rt
GP
CA1
CA2
DG
CA3
ARH
LHA
VTA
SNc
RMC
DRN
ISO
II/III
IV
V
VI
MV
gr
mol
p

Figure 27: Expression of *Cre* dependent *tdTomato* and *sfGFP* reporter protein in *CRHR1^{Cre}::Ai9 tdTomato* and *CRHR1^{Cre}::Sun1 sfGFP* mice

(A) Localization of *Crhr1* mRNA in the mouse brain; source of photomicrographs: (*29*). (B) Overview of *tdTomato* reporter protein expression in coronal sections of adult mouse brain arranged from rostral to caudal. Regions of interest, where a dense set of labeled neurites prevent single cell resolution, are highlighted with dashed rectangles and displayed at higher resolution with a second reporter in the right panel. (C) Expression of *GFP* at the inner nuclear membrane enables single cell resolution of CRHR1 expression in neurons. For details, see text. Abbreviations: arcuate hypothalamic nucleus (ARH), bed nucleus of the stria terminalis dorsal division (BNSTd), field CA1, CA2 and CA3 of hippocampus (CA1, CA2, CA3), caudate putamen/striatum (CPu), dentate gyrus (DG), dorsal raphe nucleus (DRN), glomerular layer of the olfactory bulb (Gl), globus pallidus (GP), granule cell layer of the olfactory bulb (GrO) or cerebellum (gr), isocortex layers (ISO), lateral hypothalamic area (LHA), lateral septal nucleus (LS), mitral cell layer of the olfactory bulb (Mi), medial vestibular nucleus (MV), molecular layer cerebellum (mol), olfactory tubercle (OT), piriform cortex (Pir), Purkinje cell (p), substantia nigra compact part (SNc), reticular thalamic nucleus (RT), red nucleus magnocellular part (RMC), ventral tegmental area (VTA). Scale bars = 100µm.

6.5.4 Mismatches between the localization of CRH and CRHR1 in stress-responsive brain nuclei

Crh mRNA expression studies have demonstrated a broad distribution of CRH throughout the brain including stress-related limbic forebrain structures and autonomic cell groups. This suggests that this peptide not only acts as secretagogue within the HPA axis but also exhibits neuromodulatory properties, thereby controlling stress-related emotional behavior (such as anxiety and arousal) and autonomic responses (*108*). A whole series of different studies have shown a positive correlation between CRHR1 expression sites and brain nuclei that are activated in response to stress, central (intracerebroventricular) or local administration of CRH and/or antagonists (*31, 151, 219, 228*). Conversely, within the central autonomic cell group the endocrine, autonomic and/or behavioral responsiveness to a wide variety of stressors contrasts with expression of the CRHR1. Except for the lateral parabrachial nucleus which shows strong receptor expression, several approaches via transgenic reporter lines failed to provide a uniform/convincing picture of basal CRHR1 expression in the CeA, PVN, LC and solitary tract nucleus (*41, 99, 219*). The data on distribution of CRHR1 mRNA expression in activated brain regions responsible for integrating stress-related behavioral and autonomic responses are summarized in Table 17.

Table 17: Expression of CRHR1 mRNA in stress-related sites of CRH impact

Anatomical region	CRHR1 mRNA expression (*29*)	Adaptive response (*31*)
Limbic system		
Hippocampus	++	increased anxiety-like behavior, enhancement of context- and tone-dependent fear acquisition
Bed nucleus of stria terminalis (BNST)	++	increased startle amplitude, increased anxiety-like behavior, feeding inhibition, increase in depressive-like behavior, reduced social interaction
Basal ganglia		
Nucleus accumbens (NAc)	+	changes in appetitive behavior
Ventral tegmental area	++	modulation of dopaminergic neurotransmission
Central autonomic system		
Central amygdalar nucleus (CeA)	lateral division – medial division +	changes in locomotor activity, increased anxiety-like behavior
Paraventricular hypothalamic nucleus (PVN)	+	HPA-axis activation, increase in grooming behavior, changes in locomotion, decreased food intake, increased social avoidance
Lateral parabrachial nucleus (PB)	+++	autonomic/sympathomimetic response (fluid homeostasis)
Locus coeruleus	-	increased arousal/agitation, learning and memory facilitation, increased anxiety-like behavior
Solitary tract nucleus (NTS)	-	autonomic/sympathomimetic response (cardiovascular)

Expression of *Cre*-dependent *sfGFP* reporter protein in *CRHR1^{Cre}::Sun1 sfGFP* mice provides another level of detection sensitivity not only with regards to expression patterns during development but also enables persuasive qualitative and quantitative coexpression studies with neurotransmitter identity markers. By means of electron microscopic studies, *in vitro* electrophysiological studies and treatment with a selective CRHR1 antagonist, a direct stress- or CRH-induced activation of locus

coeruleus neurons mediated via CRHR1 has been demonstrated even though *in situ* hybridization studies failed to detect *Crhr1* mRNA in these neurons (*36*). A recent study using a highly sensitive knock-in reporter allele (*41*) and a BAC transgenic reporter mouse line (*219*) could not provide convincing data about receptor expression within this noradrenergic cell group. Taking a different approach using a CRHR1-*Cre*-dependent reporter line and thereby circumventing low reporter expression due to a relatively weak endogenous CRHR1 promoter confirmed limited CRHR1 expressing neurons in the LC (Figure 28). Additionally we could confirm scattered expression of the receptor in the nucleus of the solitary tract, which is in line with previous *in situ* hybridization studies (*29*) (Figure 28). There is also an on-going controversial debate about expression of CRHR1 in the PVN. We could not verify immunohistochemical data from recent studies which describe numerous stained CRHR1 positive neurons using either BAC-transgenic *GFP* reporter mice (*219*) or an antibody against CRHR1 (*229*). In accordance with published *in situ* data using a riboprobe against the endogenous CRHR1 mRNA (*29*), we see only a sparse number of CRHR1 positive neurons within the PVN under basal conditions (Figure 28). As several groups have described inducible expression of the receptor in the PVN of brain sections derived from stressed rats we investigated reporter gene expression with a riboprobe against *GFP* mRNA (using the *BAC-GFP* transgenic reporter mouse line RP23-4B21, described by Justice et al., 2008). In contrast to the induced expression seen in rat, we could not detect an increase in hybridization signals for *GFP* mRNA on brain sections from mice 120 minutes after restrained stress (unpublished data). The central amygdalar nucleus represents another central autonomic structure to be considered as main stress-related site of CRH action where conflicting data exist about cellular CRHR1 expression. Our data revealed only a small number *sfGFP* labeled neurons in the central amygdala (Figure 28). Further experiments (namely co-staining with somatostatin - a marker for the lateral division of the CeA) are necessary to exactly localize the CRHR1 neurons within the different parts of the CeA.

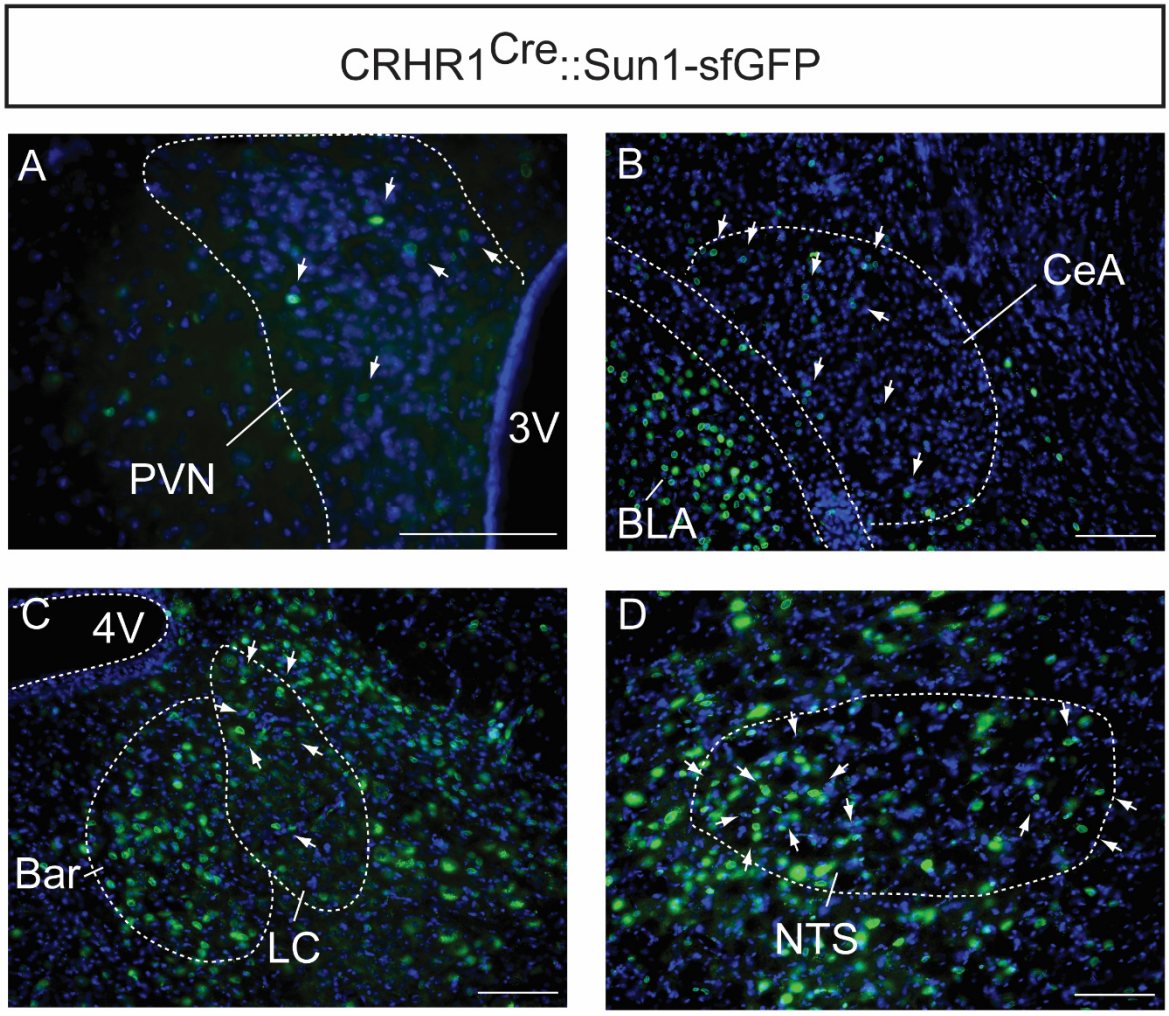

Figure 28: CRHR1 *Cre*-dependent expression of *sfGFP* in neurons of the central autonomic cell group

High magnification images of CRHR1 expressing neurons in main structures of stress responsive central autonomic cell groups. For details, see text. Abbreviations: third ventricle (3V), fourth ventricle (4V), basolateral amygdaloid nucleus (BLA), Barringtons's nucleus (Bar), central amygdaloid nucleus (CeA), locus coeruleus (LC), nucleus of the solitary tract (NTS), paraventricular nucleus of the hypothalamus (PVN). Scale bars represent 100µm.

As mentioned above *Cre*-induced expression of s*fGFP* produces a cumulative picture of all cells that have ever expressed CRHR1 during development and adulthood. One approach to circumvent this shortcoming is the use of *Cre*-dependent recombinant adeno-associated viruses (rAAV vectors) to drive temporally and spatially restricted expression of a fluorescent reporter protein. To evaluate the current expression of CRHR1 in the CeA, PVN and LC of adult mice we performed local injections of a *Cre*- inducible virus (AAV-EF1α-Dio-*mCherry*; purchased from Addgene) into the CRHR1 *Cre*-driver line. Stereotactic injection of AAV-EF1α-Dio-*mCherry* into the region of interest will transduce all neurons surrounding the injection site (n=2 mice

per region). Upon *Cre*-mediated recombination in CRHR1 expressing neurons the reporter gene sequence is inverted and translated. The fluorescent protein *mCherry* fills cell somata and processes of these neurons and thereby allows visualization of CRHR1 expression, approximately two weeks after virus injection (Figure 29). To demonstrate the discrepancy between cumulative and current expression analysis we injected AAV-EF1α-Dio-*mCherry* into the mediodorsal thalamic nucleus where van Pett et al., 2000 described absence of Crhr1 mRNA. In contrast to numerous *sfGFP* labeled cell nuclei throughout the central, lateral and medial mediodorsal thalamic nuclear groups, we could not detect a respective counterpart in these regions in adult mice. In addition, the small number of *sfGFP* labeled neurons within the PVN and LC resulted most likely from a transient expression of *Cre* recombinase during development as no reporter gene expression was seen after injection of rAAVs. The precise neuronal identity and functional significance of these transiently CRHR1 expressing cells remains to be elucidated. Consistent with mRNA studies only a few scattered labeled cells were visible within the CeA of adult mice. At this point, it should be noted, however, that we could not fully exclude false negative results due to low viral transduction efficacy (*230, 231*).

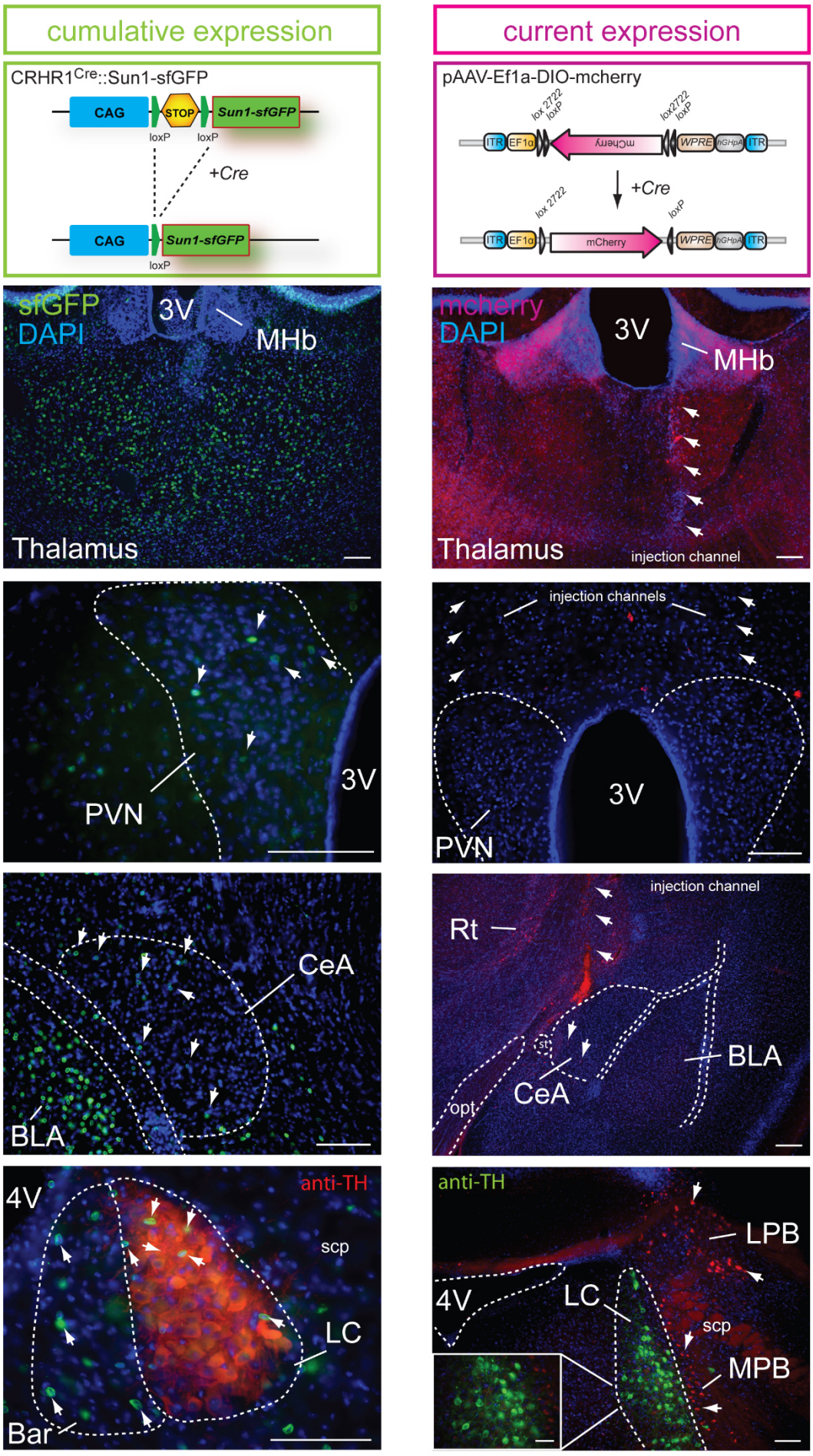
cumulative expression
current expression
CRHR1Cre::Sun1-sfGFP
CAG
STOP
Sun1-sfGFP
loxP
loxP
+Cre
CAG
Sun1-sfGFP
loxP
pAAV-Ef1a-DIO-mcherry
lox 2722
loxP
lox2722
loxP
ITR
EF1α
mCherry
WPRE
hGHpA
ITR
+Cre
lox 2722
loxP
ITR
EF1α
mCherry
WPRE
hGHpA
ITR
sfGFP
DAPI
3V
MHb
Thalamus
mcherry
DAPI
3V
MHb
Thalamus
injection channel
PVN
3V
injection channels
3V
PVN
CeA
BLA
injection channel
Rt
st
BLA
CeA
opt
4V
anti-TH
scp
LC
Bar
anti-TH
LPB
4V
LC
scp
MPB

Figure 29: **Comparison between cumulative and current reporter gene expression after CRHR1 *Cre*- mediated recombination**

Left panel: coronal mouse brain sections from *CRHR1^{Cre}::Sun1-sfGFP* mice depicting cumulative *sfGFP* expression during development. Right panel: respective counterpart images showing *Cre*-dependent *mCherry* expression in *CRHR1^{Cre}* mice after local injection of AAV-EF1α-Dio-*mCherry* into the thalamus, PVN, CeA and LC of adult mice. For a clearer distinction of the locus coeruleus an immunohistochemical staining against the noradrenergic marker tyrosine hydroxylase (anti-TH) was performed. For details, see text. Abbreviations: third ventricle (3V), fourth ventricle (4V), basolateral amygdaloid nucleus (BLA), Barrington's nucleus (Bar), central amygdaloid nucleus (CeA), lateral parabrachial nucleus (LBP), locus coeruleus (LC), medial parabrachial nucleus (MBP), paraventricular nucleus of the hypothalamus (PVN), reticular thalamic nucleus (Rt), superior cerebellar peduncle (scp). Scale bars represents 100µm.

6.5.5 Efficiency of *Cre*-mediated deletion: Breeding to the *CRHR1$^{N\text{-}Egfp}$* mouse line

The *CRHR1^{Cre}* mouse line was created using a targeted knock-in approach and thorough evaluation of the *Cre* expression pattern by means of radioactive ISH and *Cre*-dependent reporter lines verified its specificity. Efficiency of *Cre/loxP* recombination has already been validated with the reporter gene studies, but differences in *Cre/loxP* excision efficiency can be locus dependent. Therefore, differences in recombination patterns between the reporter gene and a floxed target gene - due to different genomic locations - cannot be excluded. To this end, the *CRHR1^{Cre}* line was crossed with the *CRHR1$^{N\text{-}Egfp}$* mouse line (*99*), where *GFP* is introduced into the CRHR1 polypeptide directly behind the signal peptide cleavage site. Simultaneously the *EGFP* bearing exon 2 is flanked with *loxP* sites, which allows for conditional CRHR1 inactivation via *Cre*-mediated recombination. To investigate excision efficiency of the CRHR1 *Cre*-driver line at the endogenous CRHR1 gene locus, radioactive ISH was used to detect *GFP* mRNA in adult mouse brain sections. The *Cre* recombinase and *GFP* reporter protein are both expressed under the control of the endogenous CRHR1 promoter. Therefore, complete absence of *GFP* transcripts in all sites of CRHR1 expression is expected. Indeed, there was no detectable *GFP* signal in the cortex, CA1, granular and molecular layer of the cerebellum - all sites with high CRHR1 transcript levels. By contrast, *GFP* expression was still present - albeit at greatly reduced rate – in other prominent sites of CRHR1 expression, such as RT, GP, VTA, RMC, PG and MV (Figure 30). This is surprising since the *Cre* expression pattern in these brain regions is consistent with the specific expression pattern of the endogenous CRHR1 (compare Figure 21). Interestingly,

reproducibility of the deletion pattern does not vary between littermates (data not shown), but a slightly higher *Cre* activity was detectable when it was inherited from the maternal allele (Figure 30 weaker ISH signal within the VTA, RMC and MV). Thus, monitoring recombination at the target locus is mandatory and has to be taken into consideration in functional analyses, to ensure the correct interpretation of resulting phenotypes. Possible factors that affect the efficiency of recombination, such as chromatin structure at the locus of interest, state of DNA methylation or cell type-dependent recombination variances are discussed in chapter 7.2

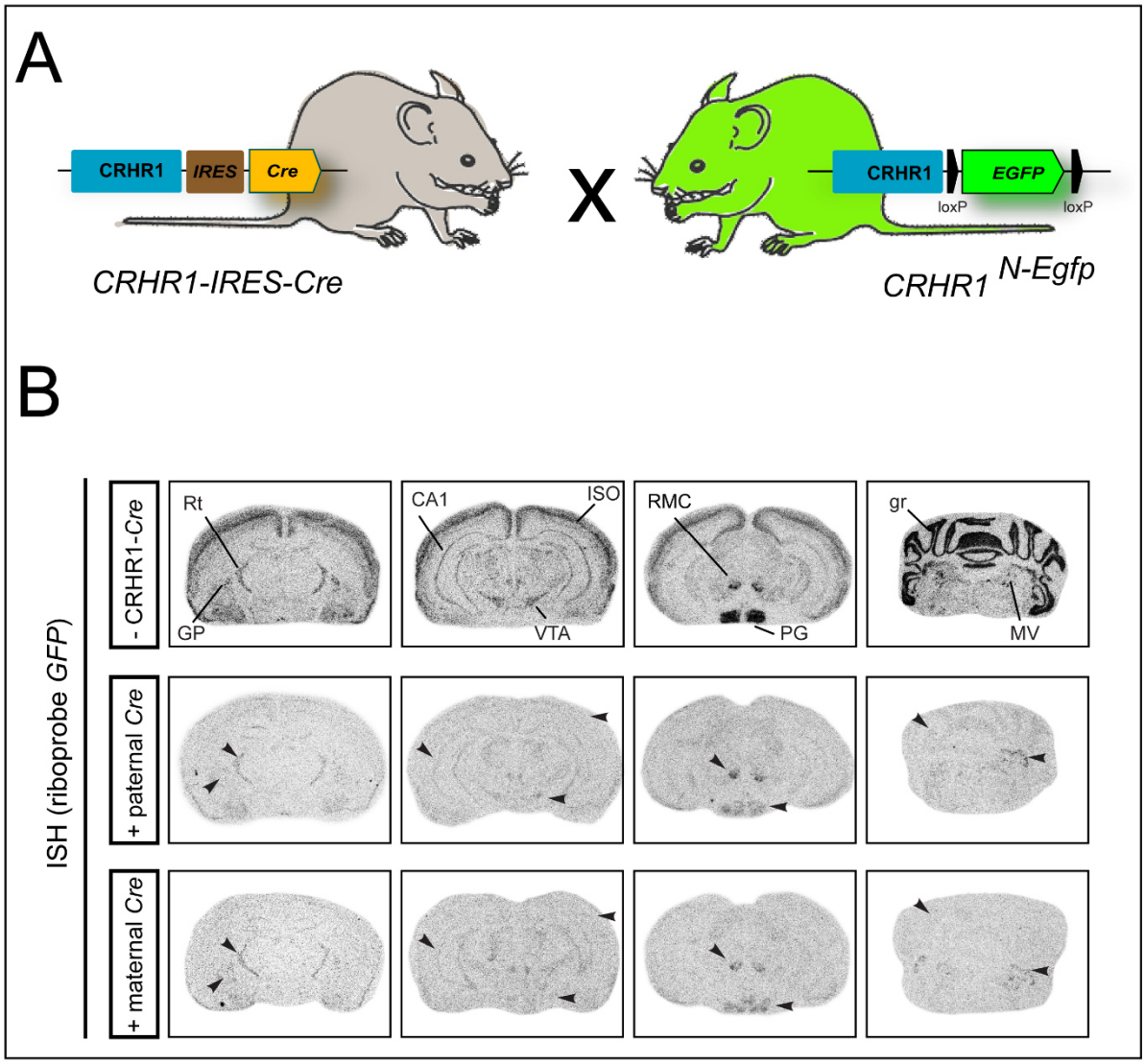

Figure 30: Efficiency of Cre-mediated deletion

Expression analysis of *GFP* mRNA transcripts in CRHR1$^{+/cre}$::CRHR1$^{+/N\text{-}Egfp}$ mice. (A) Breeding strategy for *Cre*-mediated excision of loxP flanked ("floxed") *EGFP* tagged CRHR1 exon 2. (B) Representative photomicrographs of coronal brain sections depicting *Cre* recombinase efficiency by using a *GFP*-specific riboprobe. Absence of *GFP* signals indicates maximal efficiency of the CRHR1 *Cre*-driver mouse line. Abbreviations: field CA1 of hippocampus (CA1), globus pallidus (GP), granule cell layer of the cerebellum (gr), isocortex

(ISO), medial vestibular nucleus (MV), pontine grey (PG), red nucleus magnocellular part (RMC), reticular thalamic nucleus (Rt), ventral tegmental area (VTA). Regions of interest are highlighted with black arrowheads For details see text.

6.5.6 *Cre* expression in the male germline

The use of *Cre*-positive males for breeding to females of the Ai9 reporter strain resulted in germline deletion of the *loxP* flanked STOP cassette and strong expression of the reporter throughout the body in bitransgenic F2 offspring. Previous studies based on microarray and ISH data demonstrate expression of CRHR1 in fetal mouse Leydig cells where it plays an important role in fetal steroidogenesis (*232*). Moreover expression of *Crhr1* mRNA was detected by RT-PCR in spermatocytes and spermatogonia, but not in mature spermatozoa (*233*). To localize the expression of CRHR1 in mouse testis we analyzed *sfGFP* expression in cryosections from adult *CRHR1^{Cre}::Sun1-sfGFP* mice. To better visualize the cell-specific distribution we performed immunohistochemistry using a chicken anti-*GFP* antibody in combination with Hematoxylin and eosin (H&E) staining. Fluorescent- and immunolocalization of *sfGFP* was detectable in all previously reported germline cells. Furthermore, we could reveal the expression of the reporter protein in spermatids and epithelial cells of the epididymis, the latter has been described in rats so far (*234*) (Figure 31). The expression of *Cre* in male sperm cells must be taken into account in any experiment designed to study autonomic gene function, since breeding setups with heterozyous *Cre*-positive males to obtain recombined floxed alleles can lead to unwanted ubiquitous deletion of the target allele and misinterpretation of phenotypes. So far, there is no indication for *Cre* expression in the female germline; therefore, we use *Cre*-positive females for maintaining the CRHR1-*Cre* alongside floxed alleles.

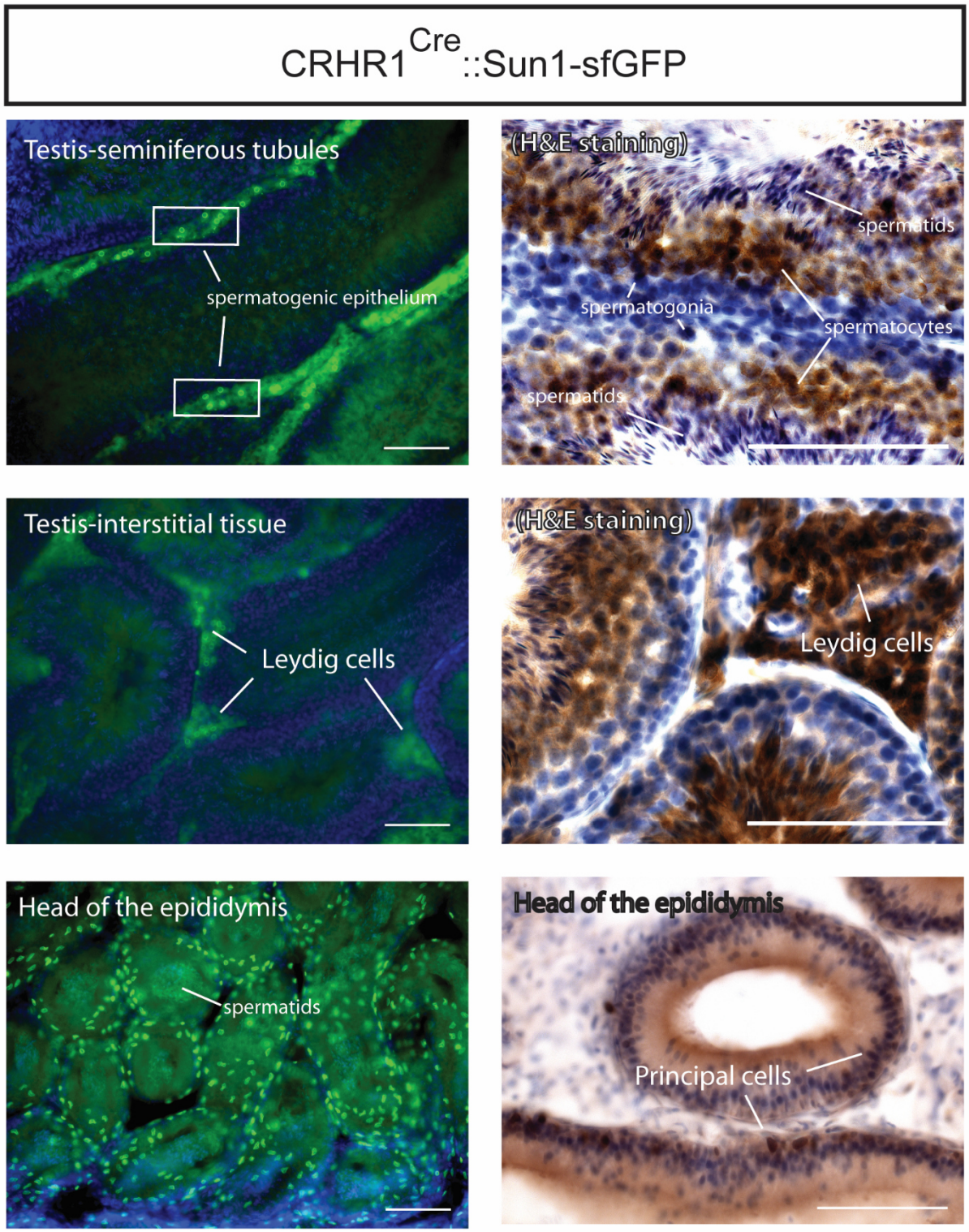

Figure 31: *Cre* expression in the male germline

Fluorescent (left panel) and immunohistochemical (right panel) detection of CRHR1 in mouse testis and epididymis. Immunoreactive sites were visualized brown with diaminobenzidin (DAB) after incubation with horseradish (HRP) conjugated chicken anti-*GFP* secondary antibody. Expression of CRHR1 was confirmed in Leydig cells, spermatogonia and spermatocytes. Additionally, reporter protein expression revealed existence of the receptor in spermatids. Scale bar represent 100µm.

6.6 Hypothalamic-pituitary-adrenal axis activity in *CRHR1*^{Cre} mice is normal

CRHR1 is highly expressed in anterior pituitary corticotrophs and essential for HPA-axis function via activating ACTH release upon CRH stimulation. ACTH, in turn, stimulates the synthesis and release of glucocorticoids (corticosterone in rodents) from the zona fasciculata of the adrenal cortex. To determine whether the function of the HPA axis is impaired in the CRHR1 *Cre*-driver line, although *Cre* was inserted downstream of an internal ribosomal entry (*IRES*) site in the 3'UTR of the endogenous receptor, wild-type control mice (CRHR1$^{+/+}$) and respective homozygous *CRHR1*$^{Cre/Cre}$ mice were subjected to a short physical restraint stress. Plasma corticosterone levels where measured in blood samples collected under basal conditions and after a 10-min restraint period. In *CRHR1*$^{Cre/Cre}$ mice the CRHR1 function and concomitant HPA axis activity was indistinguishable from wild-type control mice as demonstrated by plasma corticosterone levels which did not differ significantly from the parallel tested control littermates (Figure 32). Thus, in addition to its expression, functionality of CRHR1 activity is not compromised in CRHR1 *Cre*-driver mice.

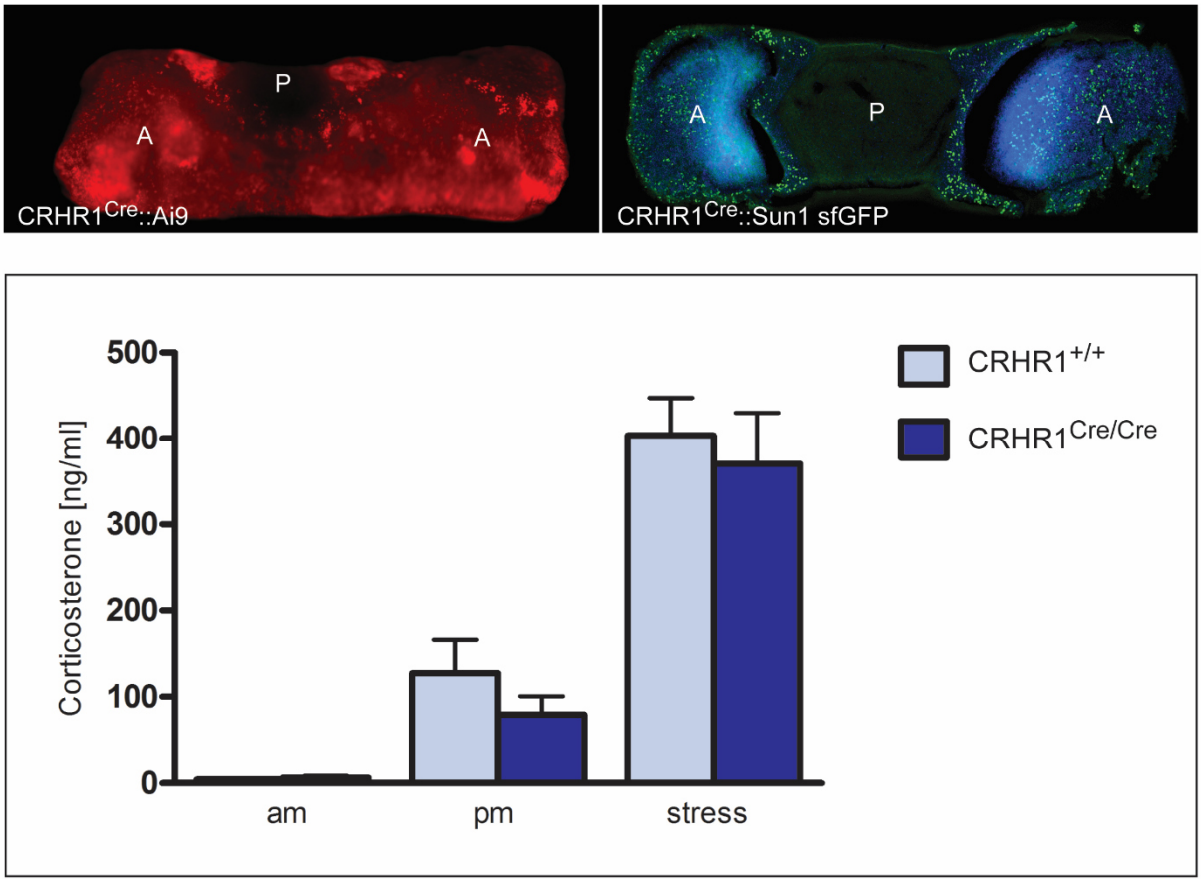

Figure 32: Demonstration of full functional capacity of the HPA axis

Top row depicts expression of CRHR1-promoter driven *Cre*-mediated expression of *tdTomato* (left) and *sfGFP* (right) reporter protein in pituitary glands from *CRHR1^{Cre}::Ai9 and CRHR1^{Cre}::Sun1 sfGFP* mice, respectively. *Cre* expression is predominantly detectable in the anterior lobe of the pituitary. Abbreviations: anterior lobe (A), posterior lobe (P). Bottom: plasma corticosterone levels of *CRHR1$^{Cre/Cre}$* mice did not differ significantly from wild-type mice under all tested conditions (Unpaired t-test: am $t_{(12)} = 0.86$, $p = 0.41$; n = 6 Crhr1$^{+/+}$, 8 Crhr1$^{Cre/Cre}$ / pm $t_{(11)} = 0.41$, $p = 0.69$; n = 5 Crhr1$^{+/+}$, 8 Crhr1$^{Cre/Cre}$ / stress $t_{(12)} = 0.42$, $p = 0.68$; n = 6 Crhr1$^{+/+}$, 8 Crhr1$^{Cre/Cre}$; mean ± s.e.m).

6.7 Cell type-specific sparse labeling for the analysis of neuronal morphology using *Flp*-mediated recombination

Characterizing the structure of the brain at single-neuron resolution (so called “Connectomics”) has become a fast growing research field in neuroanatomy during the past few years. Recent advancement in imaging (two photon tomography, micro-optical sectioning tomography, MOST) and labeling techniques such as mGRASP, iDISCO and Clarity (for review see (*235*)), has opened up new avenues towards understanding neural circuits and brain function.

Cellular resolution of neurons requires identification of the soma, dendrites, axon and corresponding synapses and is extremely challenging in densly packed brain structures. In the past, different methods were developed and applied for visualization of individual neuronal morphology, such as the historic but highly effective Golgi silver impregnation method and Nissl staining method. Moreover, intracellular injection of tracers such as fluorescent dyes or transsynaptic neural tracers, as well as transfection with viral vectors enable expression of fluorescent proteins in a subpopulation of cells. Transgenic labeling techniques represent an alternative approach where expression of reporter proteins, restricted to a given cell type, is achieved via the *Cre/lox* system (*187, 236*). Unraveling the CRHR1-specific connectome via breeding to such a *Cre*-responder line (Ai9 for example) is challenging, because the broad expression of CRHR1 in neurons does not allow for morphological analyses at high resolution (compare Figure 17, 25). Therefore, we used a sparse labeling approach to limit the labeled population to a subset of neurons. To achieve sparse cell-type specific labeling we bred the two *Cre*-driver mouse lines *CRHR1^{Cre}* and *CRHR1^{tZCre}* to the FlpeR (“flipper”) mouse strain (obtained from the Jackson Laboratory; stock number 003946), which results in *Flp*-mediated deletion of the *frt*-flanked *Cre* cassette (compare Figure 19). As a result,

excision of the *loxP*-flanked STOP cassette in Ai9 reporter mice and subsequent expression of the *tdTomato* reporter gene is prevented. As “Flipper”-mice – which express the recombinase under the ubiquitous *Rosa26* promoter - display a partial recombination pattern (*237*) an “overall” reduction of ~20% CRHR1-expressing neurons allows for single cell analysis as demonstrated for CA1 neurons in the hippocampus (Figure 33). This is especially evident in progeny from *CRHR1^{tZCre}::FlpeR* mice, as this *Cre*-driver line per se exhibits subset expression of the receptor (see chapter 6.3 for details). In addition, it should be noted that *Flp*-mediated recombination in the *CRHR1^{tZcre}* line allows for selective reconstitution of CRHR1 expression.

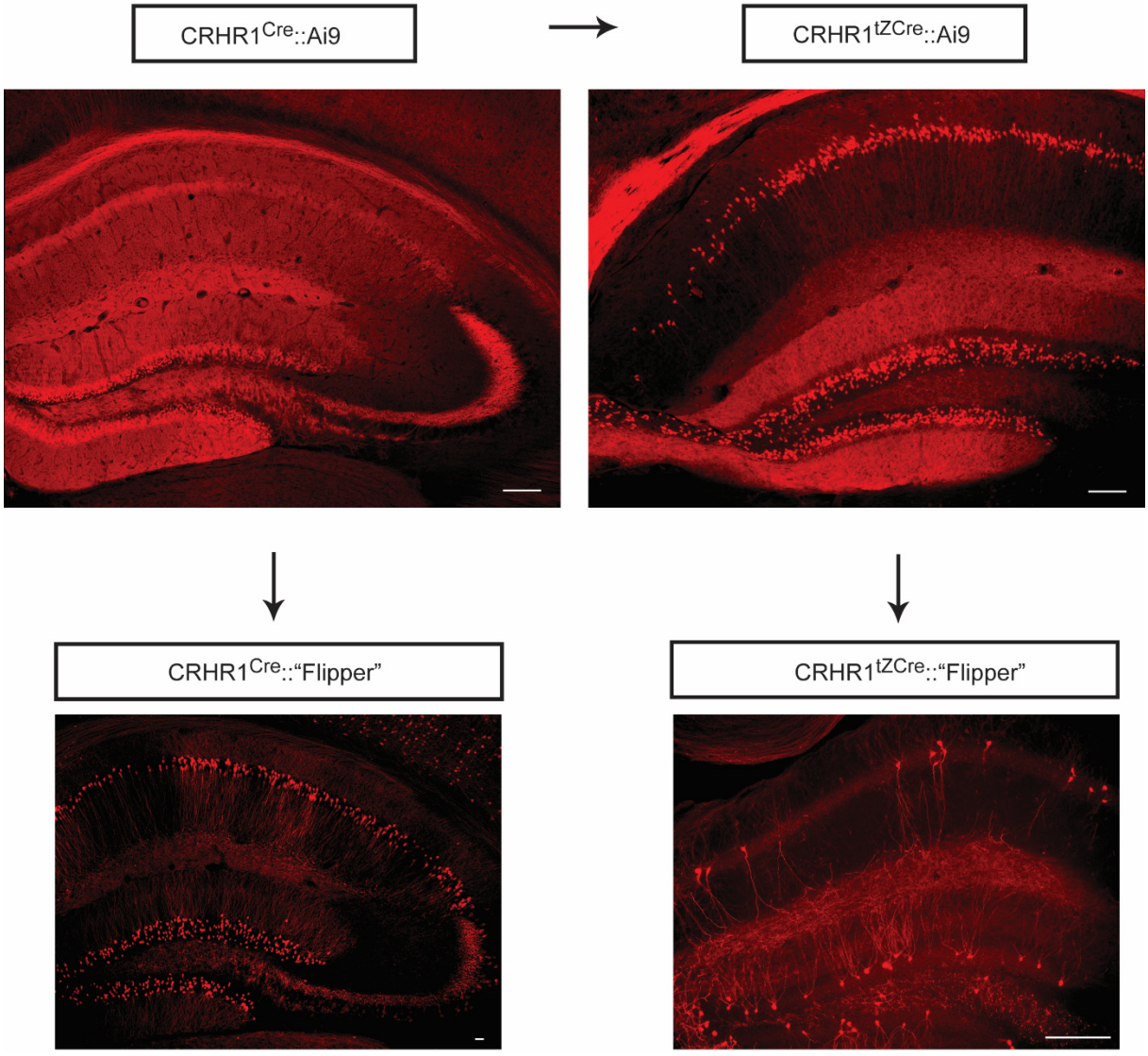

Figure 33: Sparse labeling of pyramidal CRHR1 neurons in the hippocampal CA1 field

Top row depicts subset labeling in the *CRHR1^{tZCre}*-driver line (right) compared to the full labeling in the *CRHR1^{Cre}*-driver line (left). Bottom row shows *Flpe*-mediated quantitative reduction of *Cre* and associated *tdTomato* expression in CRHR1-specific neurons. Scale bars represent 100µm.

6.8 The driver line: a valuable tool for circuit-level analysis of the brain

6.8.1 Insights into forebrain neural circuits using viral tracing methods

Dissecting neural brain circuits involved in mood disorders is hampered by the diversity of brain regions and circuits that are dysregulated. Especially CRHR1-specific pathway analysis via transgenic reporter lines is impeded by the widespread expression that limits the possibility to track individual connectivities (see chapter 6.5.3). Recent advances in "genetic neuroanatomy" allow for labeling and manipulation of genetically defined neuronal types *in vivo*. Local injection of *Cre*-dependent (FLEx) viruses into *Cre*-driver lines enables temporally and spatially restricted reporter transgene expression in specific subsets of neurons and offers the possibility of pathway-specific analysis and functional control of neuronal activity. (*188, 235, 238*). AAVs expressing fluorescent proteins for visualization of axonal projections between distinct brain areas are widely used due their stable expression, ease of production and low toxicity. In addition, they are available from various academic or commercial sources (e.g., Penn Vector Core, Pennsylvania). The combination with immunohistochemistry or *in situ* hybridization allows for further characterization of the infected cell type and of cell types in the projection target region. For injection into the CRHR1 *Cre*-driver line we used the serotype AAV1/2 with a strong pan-neuronal promoter (Elongation Factor 1 alpha (EF1α) promoter) to drive expression of *mCherry* fluorescent protein. Heterotypic *lox* sites (*loxP* and *lox2272*) are placed in reverse orientation around the inverted reporter cassette. Upon *Cre*-mediated recombination between these sites the reporter gene sequence is inverted and translated (see Figure 29, right panel). The fluorescent protein *mCherry* is a red monomer which matures rapidly, is highly photostable and produces strong somatic and anterograde axonal labeling.

We used the combination of the CRHR1 *Cre*-driver mouse line in conjunction with this "*CRE*-ON" rAAV based approach to dissect forebrain- and midbrain-specific neurotransmitter circuits that are expressing CRHR1 and are involved in mood-related behaviors. Recent studies using region- and neurotransmitter-specific conditional CRHR1 knockout mice and neurochemical mapping tools revealed that deletion of the receptor in forebrain glutamatergic circuits reduces anxiety and that CRH-induced activation of CRHR1 amplifies excitatory neurotransmission within the trisynaptic hippocampal circuit (*8, 9*). Moreover it has been shown that the

CRH/CRHR1 system mediates medial prefrontal cortex (mPFC) impairments, such as temporal order memory and cognitive flexibility (*239*). In contrast to the anxiolytic effect of limbic CRHR1 in conditional knockout mice, downregulation of the receptor in GABAergic neurons of the globus pallidus (GP) exhibits anxiogenic properties of CRHR1 within the basal ganglia neurocircuit (*162*). To decipher respective glutamatergic and GABAergic CRHR1-specific connectivities within above mentioned forebrain structures we injected AAV-EF1α-DIO-*mCherry* into the prefrontal cortex, hippocampus, globus pallidus/reticular thalamic nucleus and caudoputamen of heterozygous *CRHR1*$^{+/Cre}$ mice. *Cre*-mediated reporter gene expression allows for visualization of *mCherry* labeled axonal projections in putative target regions (see Figure 34, 35).

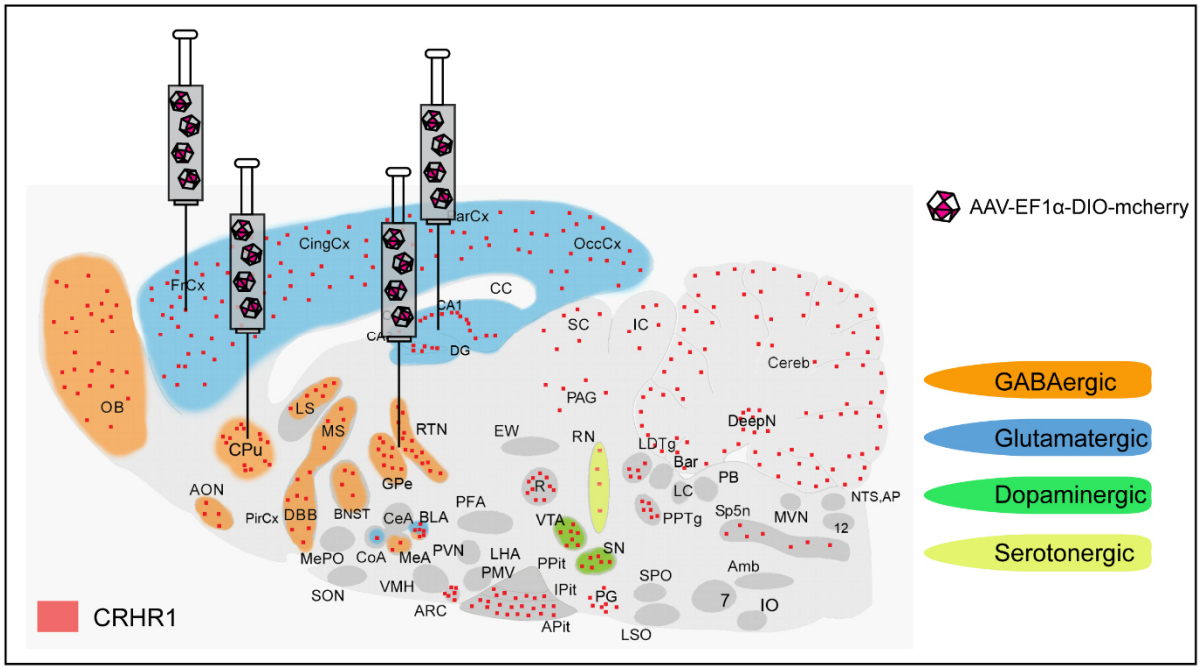

Figure 34: Injection of AAV vector into distinct forebrain structures of the adult mouse brain

Schematic drawing illustrating the position of AAV-EF1α-DIO-*mCherry* injection into forebrain nuclei expressing CRHR1 in neurotransmitter-specific cell types. Red rectangles depict CRHR1 distribution in glutamatergic, GABAergic, dopaminergic and serotonergic neurons. Relevant abbreviations: caudate putamen (CPu); frontal cortex (FrCx); hippocampal formation (CA1, CA2, DG); globus pallidus externus (GPe); reticular thalamic nucleus (RTN). Modified with permission from Dr. Jan Deussing.

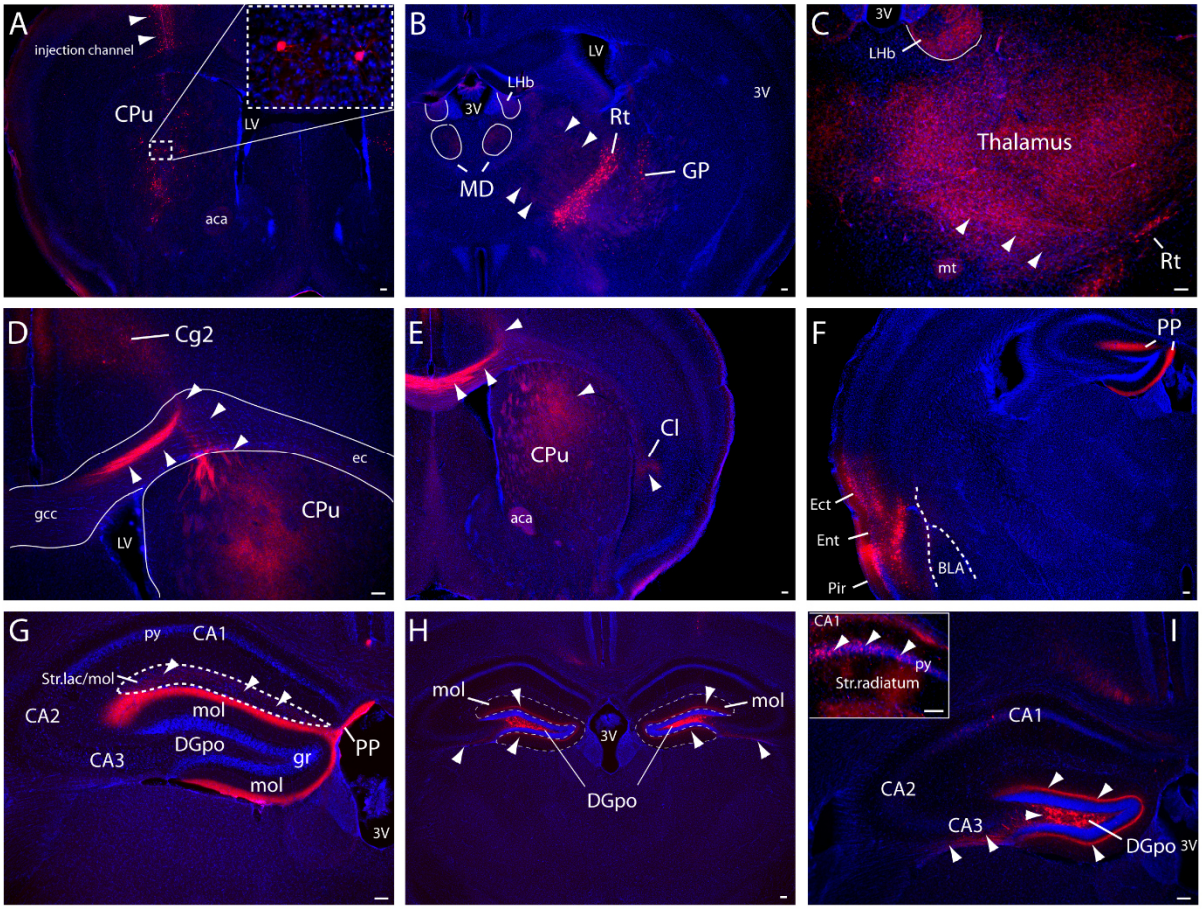

Figure 35: CRHR1 *Cre*-driver line allows for cell-specific anterograde tracing

AAV-EF1α-DIO-*mCherry* was injected into the caudoputamen (A), globus pallidus/reticular thalamic nucleus (B), prefrontal cortex (D), entorhinal cortex (F) and polymorph layer of the dentate gyrus (H). Representative coronal sections showing the somatic labeling and axon projections of infected CRHR1 neurons are depicted in panels C,E,G,I. Scale bar=100µm. Abbreviations: 3rd ventricle (3V), anterior commissure (aca), basolateral amydala (BLA), field CA1, CA2 and CA3 of hippocampus (CA1, CA2, CA3), cingulate cortex area 2 (Cg2), claustrum (Cl), caudate putamen/striatum (CPu), polymorph layer of the dentate gyrus (DGPo), external capsule (ec), genu of corpus callosum (gcc), granule cell layer of the dentate gyrus (gr), ectorhinal cortex (Ect), entorhinal cortex (Ent), globus pallidus (GP), lateral habenula (LHb), lateral ventricle (LV), mediodorsal thalamic nucleus (MD), molecular layer of the dentate gyrus (mol), mamillothalamic tract (mt), perforant path (PP), piriform cortex (Pir), pyramidal cell layer (py), reticular thalamic nucleus (Rt). For details, see text.

Two weeks after striatal virus injection (Figure 35A) prominent *mCherry* staining of cell soma and proximal neurites could be detected throughout the caudoputamen. As no axonal labeling was visible in main striatal output target sites such as substantia nigra pars reticulata (SNR) or globus pallidus we therefore speculate that CRHR1 expressing neurons within the striatum represent locally projecting GABAergic interneurons which constitute about 5-10% of all striatal neurons and coexpress different subclasses of dopamine receptors (D1-D5). Recent work suggests an

important role of these interneurons in regulating the two main output pathways in response to a global dopamine signal (*240, 241*).

Injections of AAV-EF1α-DIO-*mCherry* into the reticular thalamic nucleus (Rt) (Figure 35 B) led to anterograde labeling of fibers in the following ipsilateral thalamic nuclei: ventrolateral (VL), ventromedial (VM), posterior (Po), posterolateral (VPL), posteromedial (VPM), submedial (Sub), central medial (CM), mediodorsal (MD), and lateral habenula (LHb) (Figure 35 C). Somatic labeling of CRHR1 was detectable throughout the reticular thalamic nucleus and the described projection sites are in line with data sets from the adult mouse connectivity atlas (*242*). The Rt of the mouse is a shell-shaped diencephalic GABAergic nucleus that lies at the thalamus-internal capsule interface and plays a key role in integrating sensory information between the thalamus and cortex as it receives input from passing corticothalamic and thalamocortical axons. Inhibitory afferents from the Rt project exclusively to various thalamic nuclei, thereby controlling thalamic transmission to the cortex (*243*). Up to now, a CRHR1-specific role within the Rt in relation to stress-related disorders has not been described. Due to virus spread *Cre* recombination and subsequent *mCherry* expression was also detectable in neurons of the globus pallidus (external segment, GPe). This so called “intrinsic nucleus” is part of the indirect basal ganglia pathway and contains sparsely distributed GABAergic neurons that are tonically active and project to the internal segment (GPi) and to the subthalamic nucleus thereby increasing the inhibitory output of the basal ganglia (*244*). Thorough analysis of these target regions failed in providing evidence for CRHR1 specific synaptic input as we could not detect axonal projections in these target regions. By contrast, scattered labeled axons could be tracked within the striatum. Anterograde and retrograde tracing studies in rat revealed a pallidostriatal projection that terminates within the striatum on proximal dendrites of medium spiny neurons (*245*). Although further experiments are necessary to prove this circuit in mice, we speculate on a pallidofugal projection pathway where CRHR1 positive cells in the GPe project back to striatal direct/indirect pathway neurons. In recent years, the original view of the basal ganglia as relay station coordinating proper execution of movements has been expanded with other roles, such as control of behavior and emotions. In this line there is experimental evidence that genetic downregulation and pharmacological blocking of CRHR1 in GABAergic neurons of the GPe results in an increased

anxiety-like behavior, a phenotype that could result from CRHR1 modulated enkephalin release in reciprocal striatopallidal projection neurons (*162*).

There is accumulating evidence that abnormalities in frontal-subcortical circuits (FSC) play a role in the pathophysiology of neuropsychiatric disorders (*246*). In highly simplified terms the FSC system consist of two main pathways (direct and indirect FSC pathway), where information flows from several cortical areas through the basal ganglia, then on to the thalamus and finally back to the cortex. Under “normal” conditions a balanced dynamic between glutamatergic (excitatory) and GABAergic (inhibitory) information flow in both pathways leads to either a stimulating (direct pathway) or depressing (indirect pathway) outflow to the cortex. This provides the anatomical basis for emotional, motor and cognitive processing. AAV-EF1α-DIO-*mCherry* injection into the prefrontal cortex (namely cingulate cortex, area 1 and 2, prelimbic cortex, infralimbic cortex) (Figure 35 D) revealed that within this FSC loop, glutamatergic CRHR1 expressing neurons project to the ipsilateral caudoputamen (Cpu), the basal ganglia input nucleus, as revealed by strong anterograde axonal labeling. Furthermore we could detect labeled commissural fibers within the corpus callosum (cc) that pass to the contralateral hemisphere and corticostriatal fibers that run within the external capsule and terminate in the claustrum (CL) (Figure 35 E). Taken together these data suggest an important role of the CRH/CRHR1 system within the corticostriatal pathway and basal ganglia circuits in motor control, cognition and emotion (see figure 36 summarizing the anterograde tracing results within above described neurocircuits).

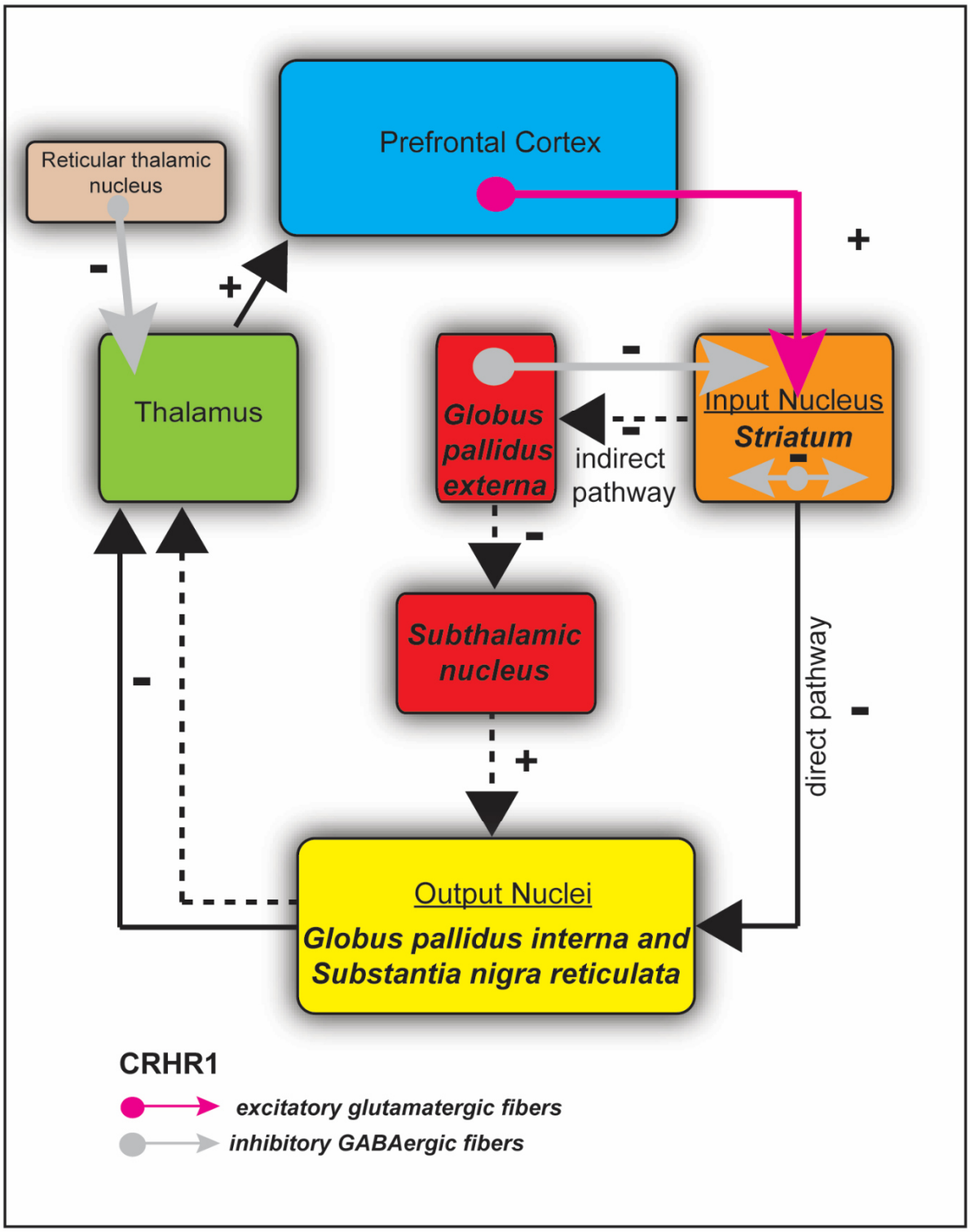

Figure 36: Schematic representation of basal ganglia-thalamocortical circuitry

Black arrows indicate direct pathway projections and black dotted arrows indicate indirect pathway projections. Colored red and grey arrows show CRHR1-specific excitatory (+) and inhibitory (-) connectivities: glutamatergic cortical CRHR1-specific neurons project to the caudoputamen; within the striatum CRHR1 is expressed in locally projection GABAergic interneurons. CRHR1 inhibitory neurons in the external segment of the globus pallidus project back to the striatum (pallidofugal pathway). Reticular CRHR1 GABAergic neurons project ipsilateral to the thalamus. For details, see text.

Based on our previous work (*41*), we used the AAV based tracing approach to further dissect the hippocampal CRHR1 circuits. To address this, we injected AAV-EF1α-DIO-*mCherry* into the lateral and medial area of the entorhinal cortex (the main hippocampal entry point for sensory information) of *CRHR1^{Cre}* mice (Figure 35 F). We thereby confirmed the participation of CRHR1-expressing neurons in the perforant path (PP) - the major cortical afferent projection path to the hippocampus. The CRHR1-specific projections from the entorhinal cortex (EC) to the ipsilateral dentate gyrus (DG) originate from cortical glutamatergic CRHR1 neurons in layer II and terminate in the outer one-third of the molecular layer of the dentate gyrus. Further, CRHR1 positive neurons in layer III of the EC terminate in the stratum lacunosum-moleculare of CA1 (so called temporoammonic path) (Figure 35 G). The lack of corresponding contralateral projections as well as CA3 projections from the EC is in line with a study using the anterograde transported tracer biotinylated dextran amine (BDA) and the retrograde tracer fast blue to investigate the cortico-hippocampal connections in adult mice (*247*). Previous studies based on voltage-sensitive dye imaging (VSDI) revealed that CRH – via activation of CRHR1 - specifically amplifies neuronal excitation in the hippocampal formation (trisynaptic EC-DG-CA3-CA1 network) (*42, 99*). Subcortical inputs to DG granule cells arise - amongst others - from ipsi- and contralateral neurons in the polymorphic layer (so-called mossy cells) of the DG, which innervate the inner third of the molecular layer. As CRHR1 is expressed in the hilar region of the dentate gyrus we injected AAV-EF1α-DIO-*mCherry* into the polymorphic layer of the DG (Figure 35 H) and in fact could detect intense somatic staining in this layer as well as intensive fiber labeling in the adjacent molecular layer of the dentate gyrus (Figure 35 H,I). We therefore postulate that CRHR1 is expressed in glutamatergic mossy cells within the polymorph layer of the dentate gyrus that synapse on the dendrites of granule cells (excitatory associational/commissural projections). It should be noted that we couldn't exclude CRHR1 expression in the other neuron types of the polymorphic region, such as HICAP (hilar commissural-associational pathway related cells) or HIPP (hilar perforant path-associated cells). A schematic summary of CRHR1-specific projections within the hippocampal formation is depicted below.

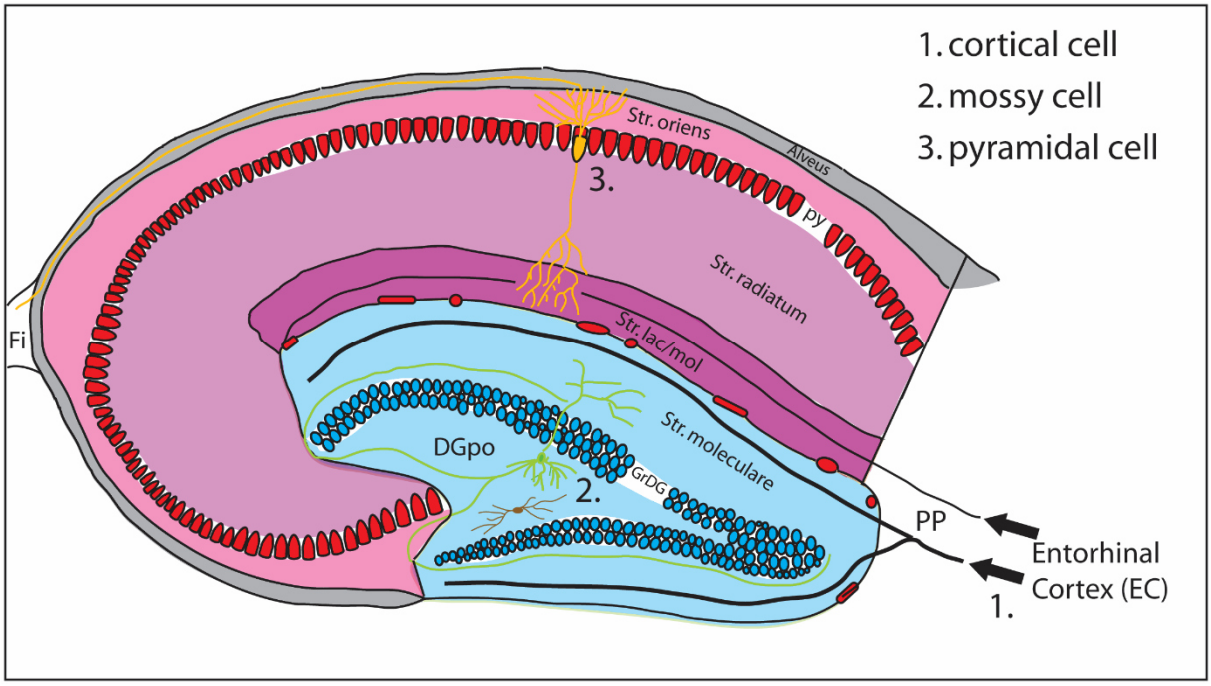

Figure 37: CRHR1 expression in specific neuronal cell types of the hippocampal formation

Schematic representation of CRHR1 neuronal connectivities: CRHR1- cortical cells within the entorhinal cortex layer II/III project to the molecular layer of the dentate gyrus and to the stratum lacunosum moleculare of hippocampal CA1 field. Hilar mossy cells expressing CRHR1 synapse on dentate granule cells within the adjacent molecular layer. Axonal projections from CA1 pyramidal neurons positive for CRHR1 are detectable in the alveus passing on towards the fimbria (Fi)/fornix.

6.8.2 Viral vector-based dissection of CRHR1-specific projections within the midbrain dopaminergic system

We applied AAV mediated *mCherry* expression in *CRHR1*^{Cre} mice after injection in the VTA to identify CRHR1-specific afferent dopaminergic fibers within the brain's reward circuitry. An increasing number of studies suggest that dysregulation in the brain's reward system may be involved in mediating stress-related mood disorders, including anxiety and depression (*95*). Recent studies point towards a specific subpopulation of dopaminergic neurons within the VTA that are activated by stressful and aversive stimuli (*82*). Identification of this stress responsive population and targeting the projection sites will provide valuable insights into how stress can promote psychiatric disorders associated with the mesocorticolimbic dopamine system.

Along this line, it has been shown that CRHR1 is expressed in dopaminergic neurons of the VTA and SNC and that CRH released by stress increases the activity in VTA neurons via CRHR1 signaling, resulting in dopamine release in the prefrontal cortex (PFC). Deletion of the receptor in midbrain dopaminergic neurons increases anxiety-like behavior in mice and leads to decreased extracellular dopamine levels in the PFC. (*85, 99*). We used the CRHR1 *Cre*-driver line to specifically target the CRHR1-positive cells in the VTA/SNc and to identify their putative postsynaptic target sites (Figure 38). Two weeks after bilateral stereotactic injection of AAV-EF1α-Dio-*mCherry* into the VTA, infected cells showing strong somatic staining were detectable in the following anterior and posterior VTA subdivisions (according to the atlas of Franklin and Paxinos, 2008): VTA, SNC, parabrachial pigmented nucleus, parainterfascicular nucleus (PIF) and paranigral nucleus (PN) (Figure 39 G-I). Earlier studies, using conventional anterograde and retrograde tracing methods, indicate three anatomically and functionally distinctive pathways: the mesostriatal, mesolimbic and mesocortical pathway (*248*). Although this simplified classification is still valid today, latest findings revealed a high degree of diversity among midbrain dopaminergic neurons ranging from neuroanatomical heterogeneity, electrophysiological properties, behavioral functions, wiring diversity to diverse neurotransmitter content (*91, 249-251*). In the present study, axonal projections originating from CRHR1-expressing neurons in the ventral mesencephalic dopaminergic complex, run within the medial forebrain bundle (mfb) and project to the striatum (Cpu) via the nigrostriatal bundle (ns). In addition, labeled projections were detectable within the cingulate cortex (cg) (mesocortical pathway), the nucleus accumbens core (AcbC) and shell (AcbSh) as well as the ventral pallidum, the latter afferents being part of the so called mesolimbic pathway (Figure 39 A-F). Furthermore, descending projections to the brainstem are clearly visible within the medial longitudinal fasciculus (mlf). This path possibly reflects the parallel diencephalon-spinal dopaminergic pathway, which modulates spinal locomotor circuits, as was described in a recent publication where dopaminergic neurons within the diencephalic A_{10}/A_{11} group were identified after retrograde tracing with FluoroGold (FG) injections into the dorsal column of the mouse spinal cord (*252, 253*) (see figure 39 J-L).

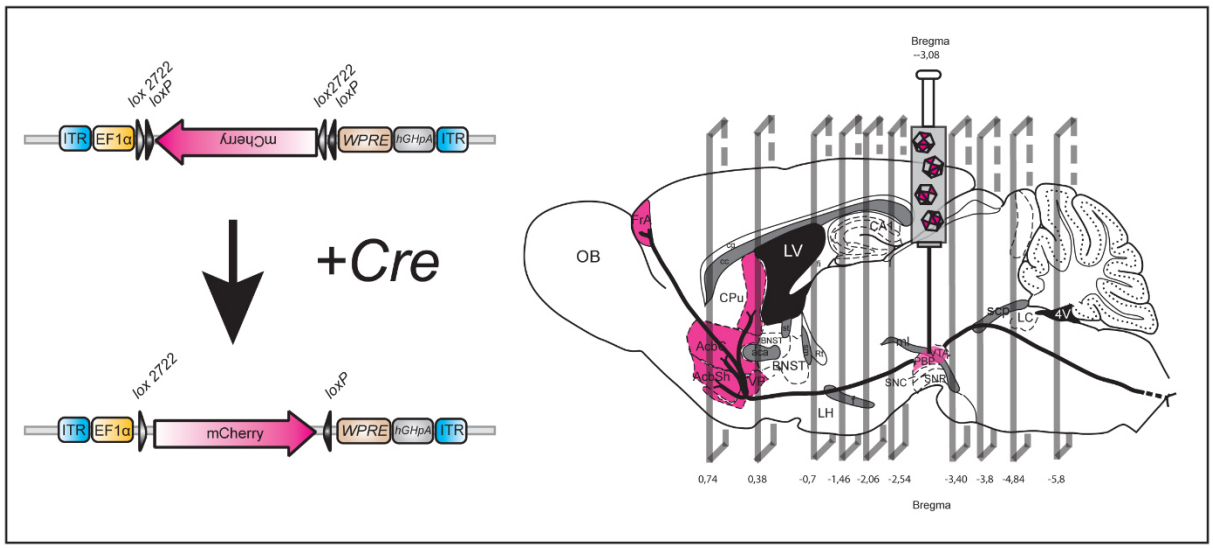

Figure 38: Dissection of CRHR1-specific projections within the midbrain dopaminergic system

Schematic drawings providing a general overview of the viral vector (left) and injection of the AAV-*mCherry* vector into the VTA of *CRHR1*^{Cre} mice (right). Injection site and afferent projections are highlighted in red color. For details, see text. Abbreviations: fourth ventricle (4V), anterior commissure anterior part (aca), nucleus accumbens core (AcbC), nucleus accumbens shell (AcbSh), bed nucleus of the stria terminalis (BNST), field CA1 of hippocampus (CA1), corpus callosum (cc), cingulate cortex (cg), caudate putamen (CPu), fornix (f), frontal association cortex (FrA), locus coeruleus (LC), lateral hypothalamic area (LH), lateral ventricle (LV), medial lemniscus (ml), olfactory bulb (OB), parabrachial pigmented nucleus (PBP), reticular thalamic nucleus (Rt), superior cerebellar peduncle (scp), stria medullaris (sm), substantia nigra, pars compacta (SNC), substantia nigra, pars reticularis (SNR), stria terminals (st), ventral tegmental area (VTA), ventral pallidum (VP).

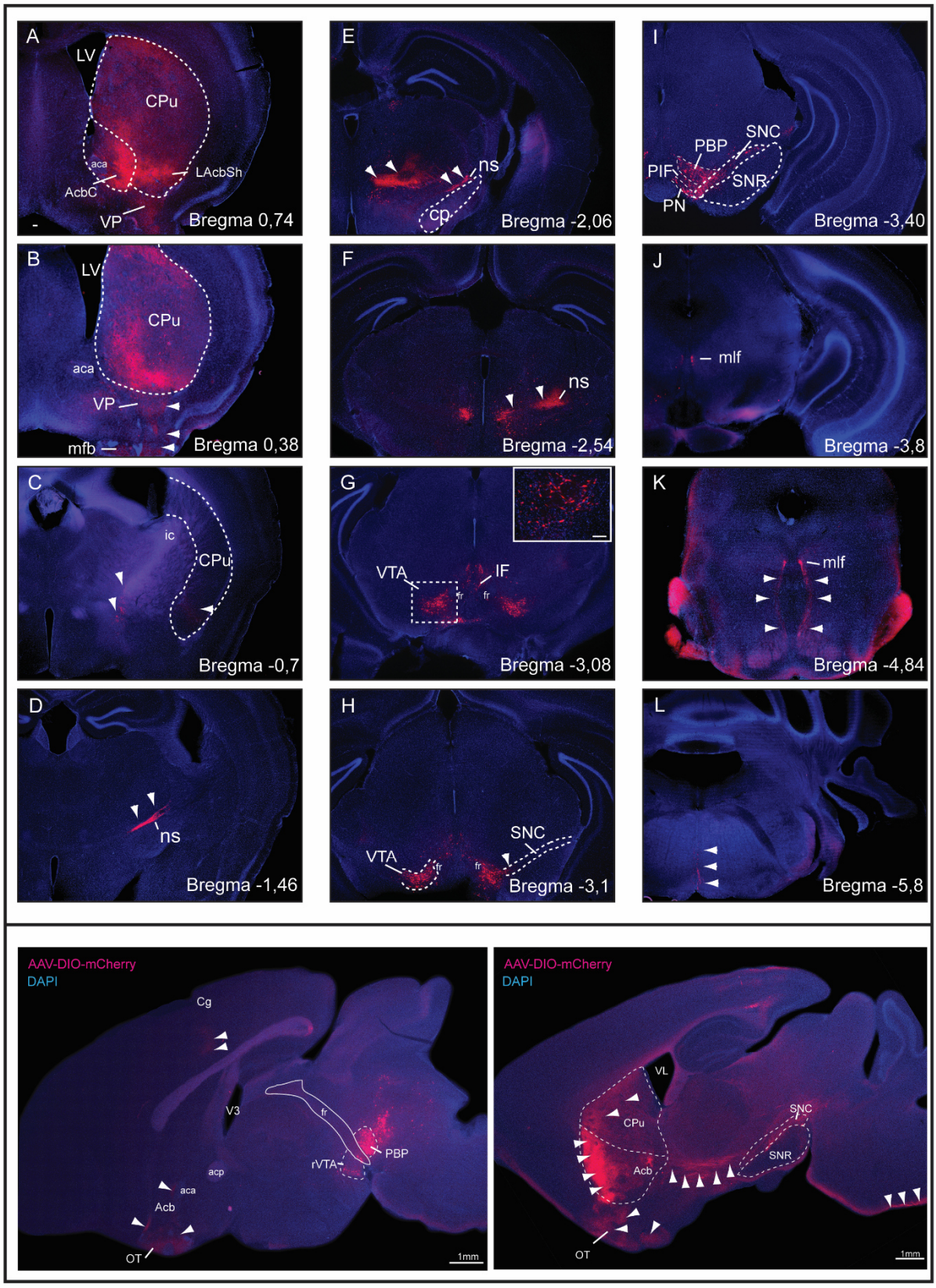

Figure 39: Afferent projections from CRHR1 expressing neurons in the ventral mesencephalic dopaminergic complex

(Top) Rostro-caudal coronal sections showing anterograde projections originating from CRHR1-expressing neurons in the ventral tegmental area. Inset in G shows transfected neurons expressing *mCherry* upon *Cre*-mediated recombination Scale bars = 100µm. (Bottom) Sagittal vibratome sections from a *CRHR1*^{Cre} mouse brain showing long range

mesocorticolimbic projections (highlighted with white arrowheads). Note the transfected cell bodies within the rostral VTA (rVTA), parabrachial pigmented nucleus (PBP) and substania nigra pars compacta (SNC) For details, see text. Abbreviations: nucleus accumbens shell (AcbSh), cingulate cortex (cg), caudate putamen (CPu), cerebral peduncle (cp), fasciculus retroflexus (fr), internal capsule (ic), interfascicular nucleus (IF), lateral ventricle (LV), medium forebrain bundle (mfb), medial longitudinal fasciculus (mlf), nigrostriatal bundle (ns), parabrachial pigmented nucleus (PBP), parainterfascicular nucleus (PIF), paranigral nucleus (PN), substantia nigra, pars compacta (SNC), substantia nigra, pars reticularis (SNR), ventral tegmental area (VTA), ventral pallidum (VP).

In order to corroborate the distal projecting sites originating from CRHR1-specific neurons within the mesocorticolimbic circuit we used AAV-EF1α-Dio-Synaptophysin-*eGFP* for anterograde labeling of presynaptic terminals. Synaptophysin (Syp) is a synaptic vesicle glycoprotein, abundantly expressed in almost all neurons in the brain and a fusion with the green fluorescent protein *GFP* is commonly used to mark active presynaptic terminals (synapses) (*254*). This AAV vector is driven by the ubiquitous EF1α promoter and the double-floxed inverse open reading frame ("DIO") arrangement ensures *Cre* dependent inversion of the coding sequence and subsequent expression of the transgene (Figure 40 A). Two weeks after bilateral injection of AAV-EF1α-Dio-Synaptophysin-*eGFP* into the VTA of *CRHR1^{Cre}* mice a few labeled neuronal cell bodies were visible at the injection site, whereby the predominant labeling pattern was largely punctate, reflecting local synaptic connections within the VTA and SNC (Figure 40 B,C). Interestingly also somatic and dendritic ("pearl of string" like) localization of Syp-*eGFP* puncta at the injection site was observed (Figure 40C). This probably reflects the soma as the site of massive protein synthesis and redistribution of Syp between the dendritic and axonal compartment, a fact which has also been reported by Li et al., 2010. A recent study revealed various VTA projection neuron phenotypes (distinct axonal arborization pattern) and four different types of forebrain-projecting neurons (distinct projection targets: mesocorticolimbic, mesocortical, mesolimbic and mesostriatal neurons) (*250*). Thorough analysis of forebrain structures in coronal brain sections of *CRHR1^{Cre}* mice demonstrates numerous Syp-*eGFP* puncta within the nucleus accumbens core division (Figure 40 D), the dorsal caudoputamen and cingulate cortical territories, which is in line with our previous findings using the fluorescent anterograde axonal tracer *mCherry* (see above) (Figure 40 E). Additional experiments are necessary to unravel the exact localization, neurotransmitter identity and axonal arborization pattern of individual CRHR1-specific neurons.

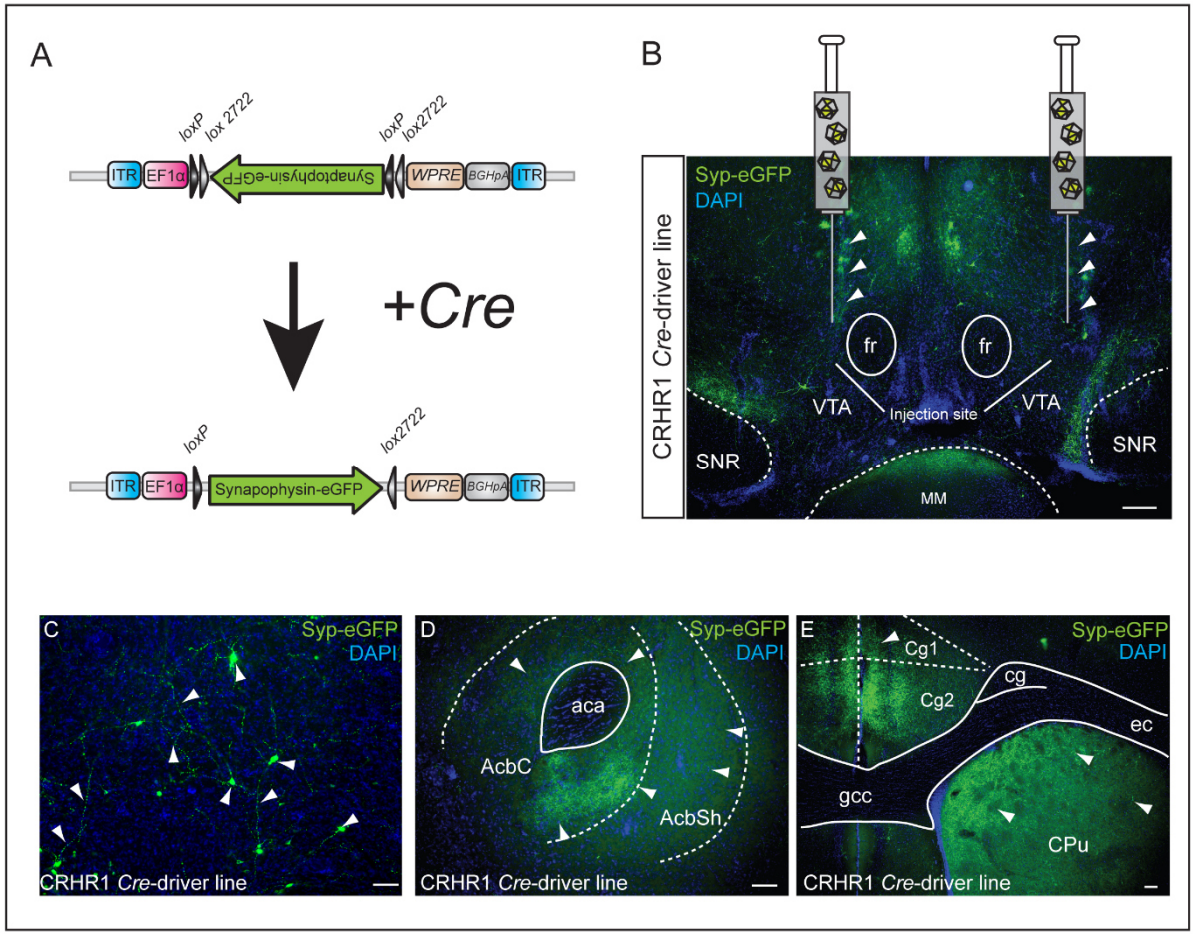

Figure 40: Strategy for presynaptic genetic labeling of individual CRHR1 expressing neurons in the VTA with a fluorescent marker

(A) Schematic drawing of the *Cre*-dependent AAV-Flex vector for Synaptophysin-*eGFP* expression. (B). Coronal mouse brain section showing the injection site of AAV-EF1α-Dio-Synaptophysin-*eGFP* into the VTA of *CRHR1*^{Cre} mice; arrowheads depict bilateral injection channels. (C) Synaptophysin-*eGFP* distribution pattern in transduced neurons of the VTA. The Syp-*eGFP* labeled presynaptic termini are located on dendritic and axonal processes like pearls on a necklace. (D) Strong Syp-*eGFP* puncta are detectable in mesolimbic projection sites including the nucleus accumbens core and shell. Representative coronal mouse brain section, counterstained with DAPI (E) Distribution of Syp-*eGFP* labeled terminals in the prefrontal cortex (Cg1, Cg2) and caudoputamen (Cpu) of *CRHR1*^{Cre} mice. Abbreviations: anterior commissure anterior part (aca), accumbens nucleus core (AcbC), accumbens nucleus shell (AcbSh), cingulate cortex area 1,2 (Cg1, Cg2), caudate putamen (CPu), external capsule (ec), fasciculus retroflexus (fr), genu of the corpus callosum (gcc), medial mammillary nucleus (MM), substantia nigra pars reticularis (SNR), ventral tegmental area (VTA). Scale bar represents 100µm.

6.8.3 Gain-of-function-circuit analysis: *Cre*-dependent activation of a constitutively active version of CRHR1 in the VTA

Genetic dissection of neuronal circuits provides a unique tool to elucidate distinct pathways involved in neuropsychiatric disorders. One widely used approach is the use of *Cre*-driver lines as they provide access to a genetically defined cell population. Injection of *Cre*-inducible recombinant viruses into the *CRHR1*^{Cre} mouse line allows for spatial and temporal control of reporter gene expression, including fluorescent proteins, transneuronal tracers, calcium indicators, optogenetic molecules or chemogenetic manipulators, specifically in CRHR1 expressing neurons. This is of special importance for the analysis of the CRH/CRHR1 system at the circuit level since it was shown that that CRHR1 regulates anxiety-related behavior in a bidirectional manner (*99*). CRHR1 in forebrain glutamatergic circuits enhances anxiety whereas CRHR1 in midbrain dopaminergic neurons mediates anxiolytic effects, respectively. Recent studies using a conditional CRH knockout mouse model revealed a new population of CRH expressing neurons in the BNST and central amygdala that innervate the VTA and mediate anxiolytic and fear suppressing behavior (*100*). To test whether CRH release in the VTA produces anxiolytic behavior several gain-of-function experiments are conceivable: (1) direct injection of CRH into the VTA (2) injection of a *Cre* inducible virus into the extended amygdala of a CRH *Cre*-driver mouse line to express light-activated channelrhodopsin-2 and subsequent stimulation of the respective CRH dependent BNST/CeA-VTA neurocircuit (3) overexpression of CRH in the VTA by injection of an inducible viral vector (4) ligand independent pathway activation by expression of a constitutively active version of CRHR1 in the VTA.

For the latter we generated a conditional flexed adeno-associated-virus that carries a constitutively active version of CRHR1 fused to *eGFP* in an inverted orientation (*136*) (AAV serotype 1/2; the plasmid was a kind gift from Dr. Arenkiel, Baylor College of Medicine, Houston; virus production at the MPI virus core unit by Maria Holzapfel). Upon *Cre*-mediated recombination, the *loxP*-flanked receptor is switched to the functional orientation resulting in constitutive/ligand-independent activity of CRHR1. For conditional gain-of-function studies with spatiotemporal– and cell-type specificity we target the VTA of *CRHR1*$^{+/Cre}$-driver mice by bilateral injection of the conditional AAV-flex-(CA) CRHR1::*GFP* virus (Figure 41 A-D). To confirm enhanced signaling

exclusively in CRHR1-specific neurons we performed double ISHs against *GFP*- and endogenous *Crhr1* mRNA and could demonstrate that virtually all transduced cells coexpress the endogenous CRHR1 (Figure 41 E).

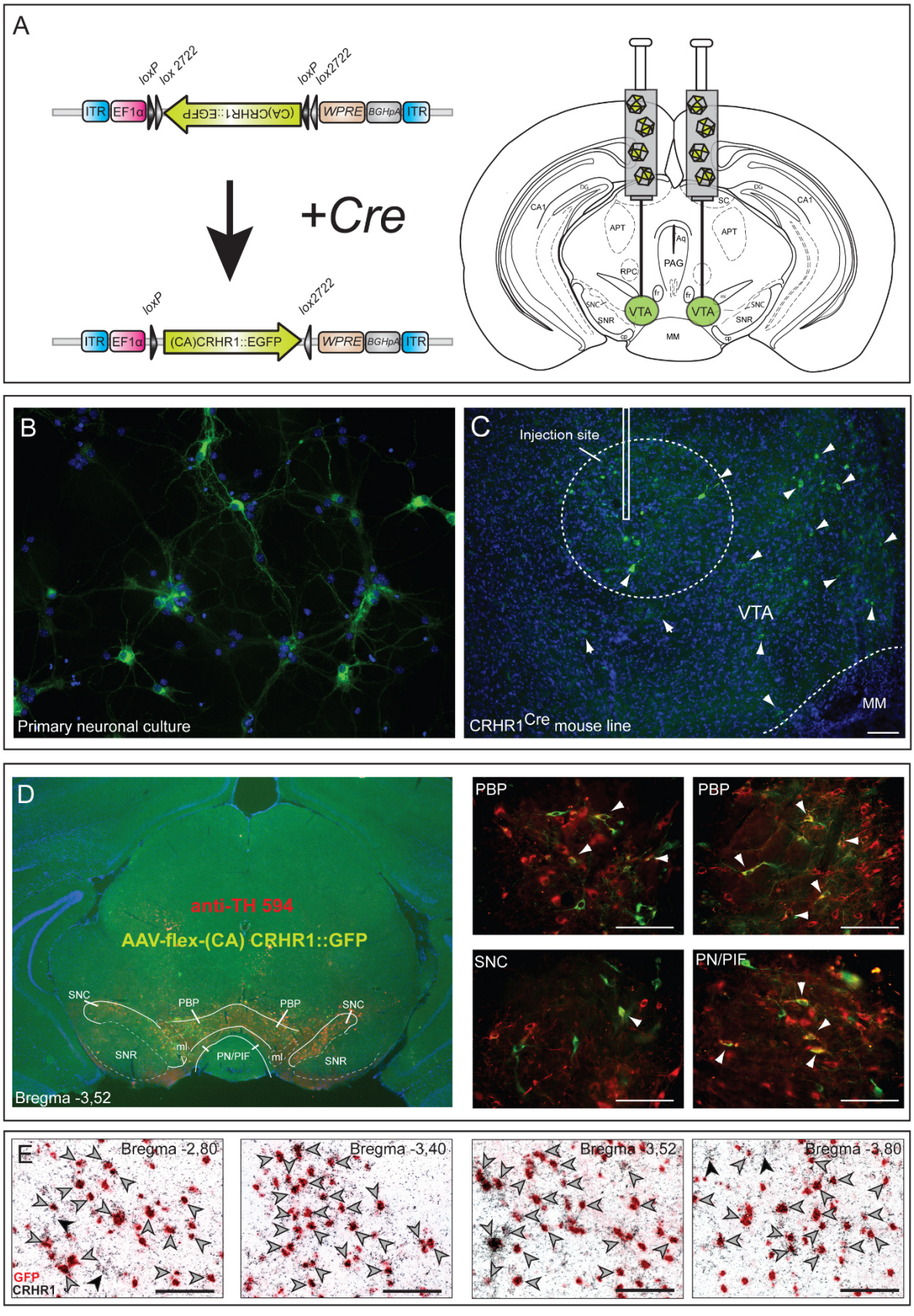

Figure 41: Expression of a constitutively active version of CRHR1 in the VTA

(A) Schematic drawing of the experimental scheme: the VTA of adult *CRHR1*$^{+/Cre}$ mice was targeted by bilateral injection of the conditional AAV-flex-(CA)CRHR1::GFP. (B) *In vitro* validation of AAV-flex-(CA)CRHR1::GFP in primary neuronal cell culture. Visualization of the constitutive active CRHR1 in the membrane of *Cre* expressing primary cortical neurons. (C) Infusion of AAV-flex-(CA)CRHR1::GFP results in expression of the active CRHR1 in *Cre*-expressing cells of the VTA. Representative image of the target region in *CRHR1*$^{+/Cre}$ mice. Arrowheads point to *Cre*-positive cells expressing the *GFP* tagged active CRHR1. (D) Sections depicting coexpression of *(CA)CRHR1-GFP* with the dopaminergic marker tyrosine hydroxylase (TH) in distinct subregions of the ventral tegmental area. Arrowheads point to (CA)CRHR1-*GFP/TH*-double positive neurons. (E) Sections from the anterior and posterior VTA depicting double ISH against *GFP* (red soma) and endogenous *CRHR1* (black silver grains) mRNA confirmed high specificity of constitutive receptor activity; virtually all transduced cells co-express the endogenous CRHR1 (grey arrowheads); black arrowheads indicate untransfected CRHR1 positive cells. Abbreviations: parabrachial pigmented nucleus (PBP), parainterfascicular nucleus (PIF), paranigral nucleus (PN), substantia nigra pars compacta (SNC), ventral tegmental area (VTA). Scale bars =100µm.

To verify whether activation of CRHR1 in the VTA is mediating the anxiolytic effect of CRH a general behavioral screen was conducted to investigate general locomotion and anxiety, namely open field test (OF), elevated plus maze test (EPM) and Dark-Light-Box test (DaLi). In all tests the behavior of control mice (injection of control virus AAV-DIO-*mCherry*; Ctrl) was compared to mice injected with AAV-flex-(CA)CRHR1 ((CA)CRHR1). First the OF test was conducted to assess novel environment exploration and general locomotor activity. Compared to the control mice the group with the activated CRHR1 showed increased general locomotion and novel environment exploration ($p<0.05$), whereas anxiety-related parameters of the OF, including time and number of inner zone entries were not significantly altered in *CRHR1-Cre::(CA)CRHR1* mice (Figure 42, upper panel). In the EPM *CRHR1-Cre::(CA)CRHR1* mice displayed reduced anxiety-related behavior compared to control mice, which is depicted by increased open-arm time ($p<0.05$) and entries. Importantly, no difference in distance traveled was detected (Figure 42, middle panel). In addition, a decrease in anxiety-related behavior was also detected in the DaLi test, as revealed by increased lit zone time ($p<0.05$) and entries (Figure 42, lower panel). Taken together, the results obtained so far strengthen the working hypothesis that enhanced CRHR1 signaling in the VTA promotes decreased anxiety (*100*).

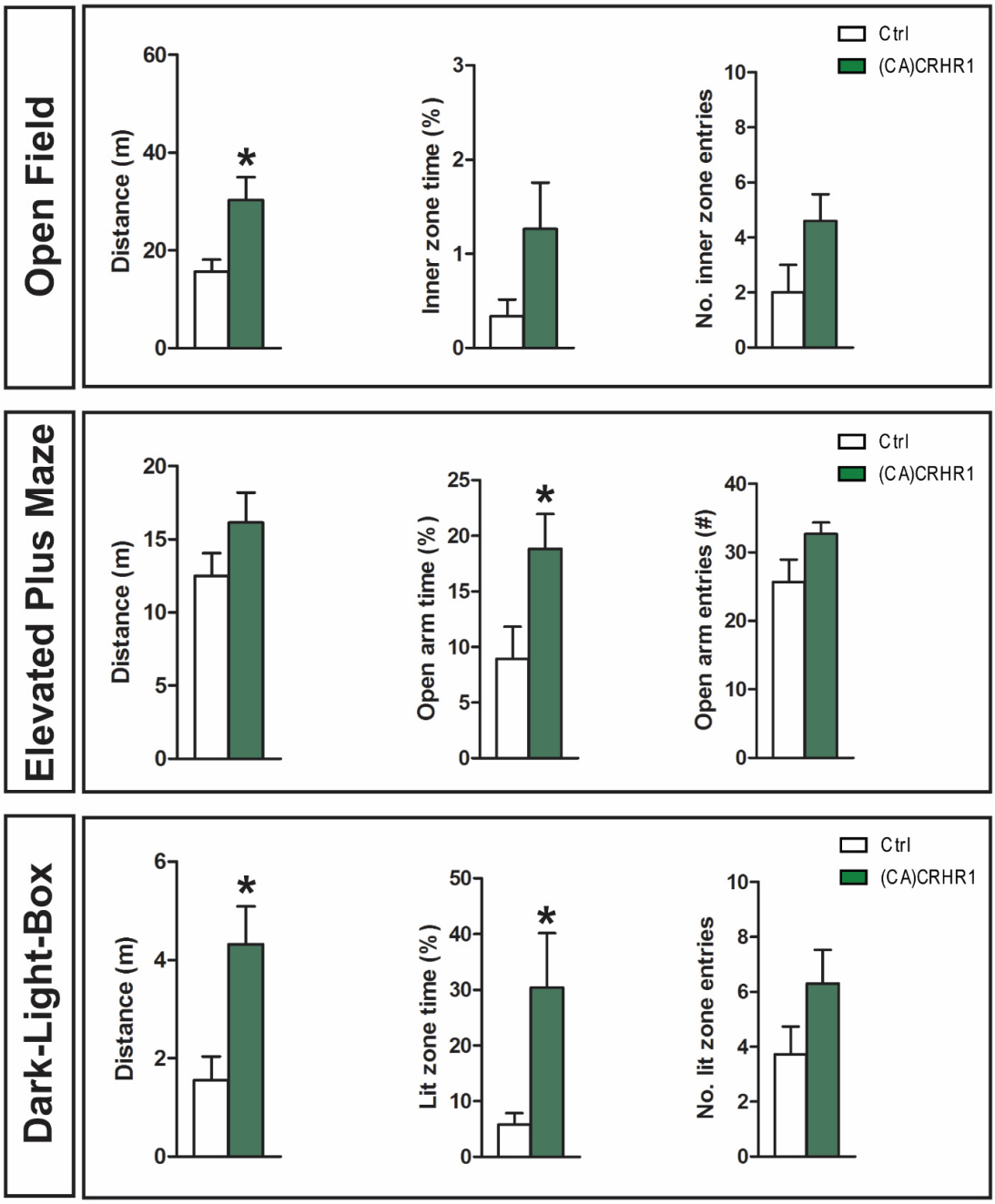

Figure 42: Activation of CRHR1 in the ventral tegmental area resulted in an anxiolytic phenotype

Viral-mediated expression of a constitutively active (CA)CRHR1-EGFP fusion construct in VTA neurons of *CRHR1^{Cre}* mice. *CRHR1^{Cre}* mice expressing (CA)CRHR1-EGFP in the VTA exhibit decreased anxiety in the elevated plus maze test: open arm time ($t_{(15)}$ = 2.2, *p = 0.043; unpaired t-test, n = 7 Ctrl, 10 (CA)CRHR1); open arm entries ($t_{(15)}$ = 1,43, p = 0.17/ unpaired t-test n = 7 Ctrl, 10 (CA)CRHR1); distance traveled ($t_{(15)}$ = 1.3, p = 0.21/ unpaired t-test n = 7 Ctrl, 10 (CA)CRHR1) and dark-light box test (lit zone time: U = 14, *p = 0.043; lit zone entries: U = 20, p = 0.1 / Mann Whitney U test, n = 7 Ctrl, 10 (CA)CRHR1); distance traveled ($t_{(15)}$ = 2.72, *p = 0,016/ unpaired t-test n = 8 Ctrl, 10 (CA)CRHR1). Open field test: distance traveled ($t_{(15)}$ = 2.45, *p = 0.027); inner zone time (%) ($t_{(15)}$ = 1.5, p = 0.15); inner zone entries ($t_{(15)}$ = 1.8, p = 0.09); n = 8 Ctrl, 10 (CA)CRHR1. Student's t test or Mann-Whitney U-test in case of non-Gaussian distribution was used to analyze statistical differences using GraphPad prism 5 (GraphPad Software). All data values are presented as means ±SEM. Statistical significance was set at p<0.05 (*), p<0.01 (**), p<0.001(***).

6.8.4 In depth characterization of constitutively active CRHR1 expressing neurons in the ventral mesencephalon

Accumulating studies indicate that dysregulated stress neurocircuits are linked to the development of mood disorders such as anxiety and depression. There is experimental evidence that on the one hand different brain regions (including different neurotransmitter systems) are “activated” by different classes of “stressors” (*255, 256*) and on the other hand that within a distinct circuit/region bidirectional changes in response to stress exist (*101, 257*). Another degree of complexity comes from the release of so called “stress mediators” resulting in specific downstream molecular changes. These mediators can be classified in neurotransmitters (e.g., noradrenaline, dopamine, serotonin), neuropeptides (e.g., CRH family members) and steroid hormones (e.g., corticosterone in rodents). Research during the last years revealed that they act in an overlapping spatial and temporal manner (*5*). The neuropeptide CRH for example not only coordinates the neuroendocrine response to stress by activation of the HPA axis, which leads to release of glucocorticoids from the adrenal glands, but also acts as a neuromodulator thereby regulating synaptic transmission within the central and peripheral nervous system (*108*). Therefore, CRH and its main receptor CRHR1 are subjects of ongoing research regarding their role in modulating the action of neurotransmitters by changing the electrophysiological properties of a given synapse (via facilitating or depressing the primary membrane potential induced by a neurotransmitter). In addition, the CRH/CRHR1 system seems to be involved in neurotransmitter receptor modifications such as phosphorylation and internalization, or impact the number of expressed receptors. Up to now CRH interactions with all main neurotransmitter systems within stress-responsive neurocircuits in the brain have been reported, namely monoamines, glutamate, GABA, serotonin and acetylcholine (*8*). Behavioral studies using conditional knockout technology revealed a bidirectional role for CRHR1 in emotionality, depending on co-expression in glutamatergic (anxiogenic phenotype) versus dopaminergic (anxiolytic) neurons (*99*).

Therefore, we analyzed the neurochemical identity of the constitutively active CRHR1 expressing neurons in the ventral mesencephalon that are mediating the anxiolytic behavioral phenotype. Neurochemical characterization was achieved through the combination of CRHR1 *Cre*-dependent expression of *EGFP* in combination with

immunohistochemistry against tyrosine hydroxylase (anti-TH), a highly reliable molecular marker for dopaminergic neurons in the VTA. In addition, the double *in situ* hybridization technique was applied for simultaneous detection of *(CA)CRHR1-EGFP* and of neurotransmitter identity markers, namely tyrosine hydroxylase (TH) and glutamic acid decarboxylase 65/67 (Gad65/67, marker for GABAergic neurons) on the mRNA level (Figure 43).

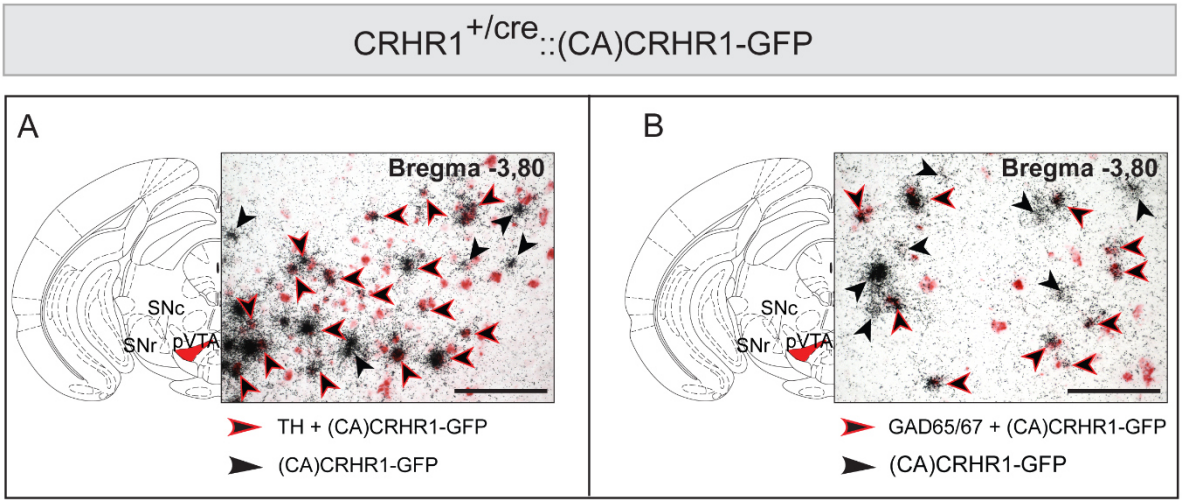

Figure 43: CRHR1 is expressed in dopaminergic and GABAergic neurons of the VTA

Representative bright field photomicrographs of coronal brain sections from *(CA)CRHR1-EGFP:: CRHR1$^{+/Cre}$* mice showing double *in situ* hybridization of *GFP* mRNA (silver grains) together with (A) tyrosine hydroxylase (TH, red staining) and (B) glutamic acid decarboxylase 65/67 (Gad65/67, red staining). Black arrowheads indicate cells only expressing *(CA)CRHR1-EGFP* (silver grains). Red framed black arrowheads indicate cells coexpressing *GFP* and *TH* (left) or *GAD65/67* (right). Scale bars = 100µm.

In line with previous results from Refojo et.al., (2011), we demonstrate that the constitutively active CRHR1 is predominantly expressed in dopaminergic cells within the VTA. Moreover, co-expression of *GFP* and *GAD65/67* revealed expression of the active CRHR1 in a subset of GABAergic neurons. There is growing awareness that midbrain neurons within the VTA include not only dopaminergic (65%), but also GABAergic (33%) and glutamatergic (2-3%) neurons, and various combinations of co-releasing neurons, which reflect the functional diversity associated with the VTA (*84, 258*). GABAergic neurons in the VTA have been shown to form local inhibitory pathways on dopaminergic neurons, but also comprise long-range mesocorticolimbic projection neurons (*89*). In a recent study from Stuber and colleagues it was shown that colocalization between *TH* mRNA and *GAD67* mRNA ranges from 16,7% in the anterior medial VTA to 0,38% in the posterior lateral VTA (*259*). As viral injections of

the constitutively active form of the CRHR1 mainly targeted the posterior VTA (see Figure 44) we speculate on a mixed population of both functional GABA/DA co-expressing neurons and those exclusively expressing GABA as a genetic marker. In this respect, it is important to note that genetic disruption of CRHR1 in midbrain dopaminergic neurons (generated by breeding CRHR1$^{flox/flox}$ with *DAT-cre/ER^{T2}* mice; see Refojo et al., 2011) mediated the anxiolytic effect of CRHR1. Therefore, it is most likely that the behavioral phenotype results from activation of the receptor in a specific subpopulation of VTA projection neurons that co-express CRHR1/DA/GABA and target the prefrontal cortex, thereby modulating dopamine release. Further experiments will be needed to dissect the heterogeneity at the cellular level. Single-cell RT-PCR can be used, e.g., for detailed molecular characterization of VTA CRHR1 neurons and specifically to quantify the amount of *GFP* positive neurons that coexpress GAD65/67 and DA, as well as to evaluate the gene expression profile of neurons that solely express the active receptor in GABAergic neurons.

In addition, the expression pattern was recapitulated on protein level by applying double immunohistochemistry using antibodies against the dopaminergic marker *TH* and GFP in *CRHR1$^{+/Cre}$::(CA)CRHR1-EGFP* mice. We could demonstrate that ~65% of GFP positive neurons co-express TH, which is in line with previous analyses on mRNA level. Various studies provide strong evidence for a functional antero-posterior heterogeneity of the VTA (*91*). We therefore analyzed the distribution of GFP positive neurons along the antero-posterior axis of the VTA. Most prominent GFP staining was detectable in the posterior part of the VTA (from bregma -3,4 to -3,8), including the parabrachial pigmented and paranigral subnuclei (Figure 44). Lammel and colleagues identified a unique subpopulation of dopaminergic neurons in the mouse VTA that project to the prelimbic and infralimbic cortices and mainly originate in the medial posterior VTA (*260*). These neurons are unique in a way that they do not express functional somatodendritic dopamine D2 autoreceptors and fire at higher frequencies in a sustained fashion. They conclude that this unique subpopulation with a low dopamine reuptake capacity could mediate behaviorally relevant and sustained DA release *in vivo*. Our anterograde studies point towards a population of CRHR1 expressing neurons in the VTA that project monosynaptically to the prefrontal cortex. Further studies are necessary to answer the question whether this dopaminergic CRHR1 positive neurons within the pVTA, that coexpress GABA are part of this unique mesocortical pathway, that mediates anxiolytic behavior by

modulating dopamine release. Questions that need to be addressed in the future include the neurochemical profile and projection patterns of the various functional CRHR1 subpopulations in the VTA as well as their anatomical distribution, electrophysiological properties and input sources.

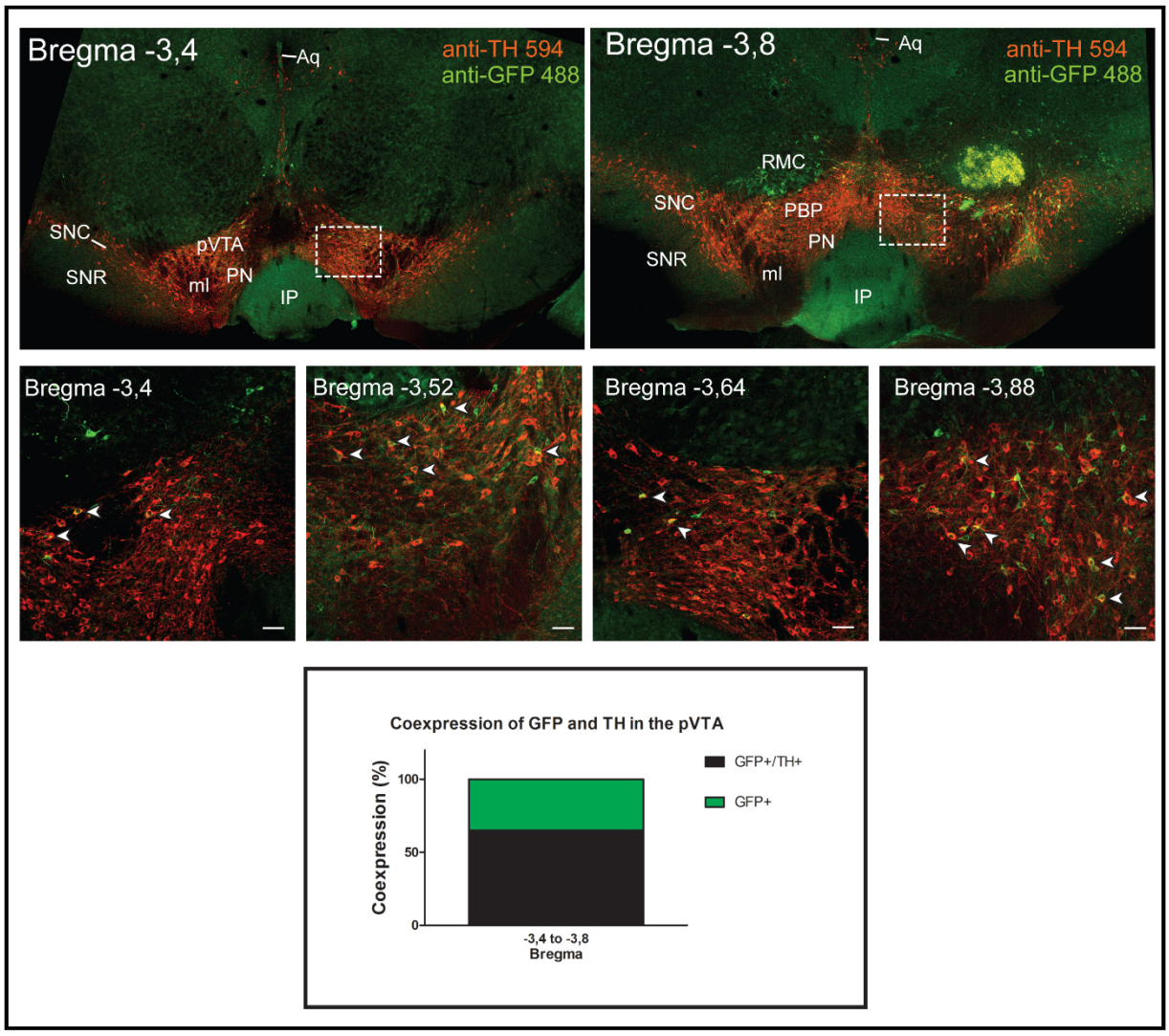

Figure 44: Expression of the constitutive active CRHR1 in the VTA and colocalization with dopaminergic neurons.

Representative confocal images from the posterior part of the VTA (bregma -3.4mm to -3.8mm) showing spread of the conditional AAV-flex-(CA)CRHR1::GFP virus injection. *TH* immunohistochemistry indicates dopaminergic neurons (labeled in red) and *GFP* immunohistochemistry was used to intensify the weak membrane restricted *GFP* signal (green neurons). Representative images of VTA sections corresponding to the transduced area were analyzed in *CRHR1$^{+/Cre}$::(CA)CRHR1-GFP* animals. *TH+/GFP+* neurons are indicated by white arrowheads. Bottom: Colocalization percentage of *TH+/GFP+* neurons within the VTA. Sections from *CRHR1$^{+/Cre}$::(CA)CRHR1-GFP* animals (n=3/genotype) were quantified within bregma -3,40mm to bregma -3,88mm (3 sections per animal). Percentage of *GFP*-expressing neurons that were also TH positive (64,9 ± 4,2%). Abbreviations: parabrachial pigmented nucleus (PBP), paranigral nucleus (PN), substantia nigra pars compacta (SNC), substantia nigra pars reticularis (SNR), ventral tegmental area, posterior (pVTA). Scale bars = 50µm.

7 Discussion

Overview

During the past decades, numerous well-established studies have shown that CRH and CRHR1 play a central role in coordinating the endocrine, autonomic and behavioral responses to stress. Unraveling of stress-related neurocircuits has been of great interest, because dysregulated stress circuits have been linked to the development of many neuropsychiatric disorders, such as depression and anxiety disorders. One of the prerequisites to functionally dissect the complex CRH/CRHR1 system is the specific targeting of CRHR1-expressing cells and to unravel their connectivities and synaptic partners. Therefore, the aim of this study was the generation of mice with *Cre* expression in all CRHR1-expressing cells. This CRHR1 *Cre*-driver line allows reliable experimental access to CRHR1-specific cells and sets the stage for systematic and comprehensive analyses of CRHR1-dependent neurocircuits. To this end, we used a knock-in approach - based on *phiC31* integrase mediated cassette exchange (RMCE) - to place an *IRES-Cre* cassette under the control of the CRHR1 promoter. The *IRES-Cre* cassette was inserted right after the stop codon within exon 13 of the CRHR1, thus preserving the endogenous CRHR1 coding region.

In the first part of the discussion, the rationale for the establishment of a CRHR1 *Cre*-driver line and the RMCE based strategy are discussed. Due to an alternative recombination event, *Cre* expression was limited to a subpopulation of CRHR1 expressing cells (*CRHR1*^{tZCre} mouse line). The possible reasons for this incomplete recombination are then discussed, with a special emphasis on the strategy applied for removal of the residual reporter cassette as well as the possible applications for the *CRHR1*^{tZCre} mouse line.

In the second part the potentials and limitations of *Cre*-driver lines, with special focus on the *CRHR1*^{Cre} mouse line, are discussed. Subsequently, the central and peripheral expression pattern of the *Cre* recombinase and *Cre*–activated reporter genes as well as the results from anterograde tracing studies are evaluated.

Furthermore, cell-type specific activation of the CRHR1 within the VTA resulted in an anxiolytic phenotype. The potentially underlying neurocircuits and CRHR1 functions are highlighted in the fourth part.

Finally, future applications of the CRHR1 *Cre*-driver line are outlined.

7.1 Methodological considerations

7.1.1 The rationale for establishing *Cre*-driver lines

Since the discovery of basic principles in gene targeting in the 1980s, advances in the sophisticated manipulation of the mouse genome have evolved. After completing the mouse genome sequence in 2005, the International Knockout Mouse Consortium (IKMC) and the International Gene Trap Consortium (IGTC) started a large-scale effort to systematically generate a comprehensive, publicly accessible, collection of conditional knockout mouse lines/mutagenized embryonic stem cells (ES cells) for almost all known and predicted genes (~20.000 genes) in the mouse genome (*169*). In most cases, an essential sequence, or more specifically, critical exons are flanked by short 34bp recognition sites (*loxP* sites). Deleting these so-called “floxed” alleles is achieved through crossing with mouse lines expressing the *Cre* recombinase that efficiently mediates recombination between *loxP* sites. Thus, exploitation of conditional genetically engineered mutant (GEMM) mouse lines depends on *Cre* transgenic mice that are validated for efficient and specific *Cre* expression and *Cre*–mediated recombination. Moreover, recent technological advances, such as *Cre*-dependent viral tracing tools or optogenetics (*Cre*-dependent expression of light-sensitive ion channels) and most recently, *Cre*-dependent DREADD (Designer Receptors Exclusively Activated by Designer Drugs) have brought about the need for new sharp tools for the genetic access to, and manipulation of specific cell types and neuronal circuits (*261*). Inserting the *Cre* coding cassette either at the translational start codon or immediately after the stop codon of an endogenous gene defines unique cell identity. An additional refinement is the inclusion of temporal control of the recombinase activity. Ligand-inducible *Cre* recombinases exclude the possibility of embryonic lethal phenotypes or compensatory mechanisms and limit the access to adult phenotypes. For this, a mutated ligand-binding domain (LBD) of the estrogen receptor (ER) is fused to the site-specific recombinase. In this arrangement the mutated ER can be activated only by synthetic ligands (e.g., tamoxifen), but is insensitive to natural estrogens. After tamoxifen binding, the *Cre-ER* fusion protein is translocated into the nucleus and can recombine “floxed” DNA substrates.

In the meantime, a substantial number of *Cre*-driver lines and other site-specific recombinase driver lines (e.g., *Flp*- or *Dre*-driver) have been generated and made publicly available through, e.g., the NIH Neuroscience Blueprint *Cre* Driver network

or the International Mouse Phenotyping Consortium (IMPC). Nevertheless, at the beginning of the study, no specific knock-in CRHR1 *Cre*-driver mouse line with *Cre* expression fully recapitulating the endogenous CRHR1 expressing pattern was available. Existing genetic tools, including conventional and conditional mouse mutants targeting CRH/CRHR1 system components have contributed significantly to the understanding of HPA axis regulation and neuronal circuitries involved in controlling autonomic and behavioral adaptations to stress (*9, 168*). The implementation of a CRHR1-specific *Cre*-driver line provides another level of cell-specific targeting and manipulation of stress-related neurocircuitries activated by CRH.

7.1.2 Driving *Cre* expression under control of the CRHR1 promoter

As stated above, the aim of the thesis was the development of a *Cre*-driver mouse line with expression of the recombinase restricted to a particular cell type as defined by the CRHR1 promoter. In the past, two main genetic targeting strategies have been used to target specific cell types in mice, bacterial artificial chromosome (BAC) transgenesis and knock-in strategies. BAC-based transgenesis replaced "conventional/classical" transgenesis due to its superiority with respect to reduced influence of position effects through the size of the transgenic construct, which protects against the influence of the chromosomal environment. Furthermore, the BAC vector backbone facilitates the integration of all necessary regulatory elements, such as enhancers or silencers, to confer reliable gene expression. However, two BAC transgenic mouse lines (based on BAC RP24-239F10 and BAC RP23-4B21), expressing *GFP* under the control of the CRHR1 promoter clearly highlighted the disadvantages of this strategy: for one thing, subset and/or ectopic gene expression and otherwise, low levels of reporter gene expression driven by the endogenous – transcriptionally weak - CRHR1 promoter (*41*). The latter is, however, less of an impact as even low levels of *Cre* expression will lead over time to an irreversible accumulation of DNA recombination events. Based on the identical mouse BAC (RP23-4B21) which Justice and colleagues used to generate a CRHR1-GFP reporter mouse line (*219*), Garcia et al. created a CRHR1-Cre transgenic mouse line for targeting granule cells in the olfactory bulb. For this, a cDNA encoding the *Cre* recombinase followed by a poly-adenylation signal was inserted right after the ATG

start codon of the CRHR1. The *Cre* expression pattern was evaluated after crossing to a *Rosa26 lacZ* reporter line and appeared almost identical compared to the endogenous CRHR1 expression pattern. However, there remain some doubts as supplementary figure S5 depicts a discrepancy between *GFP* and *Cre*-mediated *tdTomato* expression in the olfactory bulb of triple transgenic *CRHR1-EGFP::CRHR1-Cre::Rosa-LSL-tdTom* mice. *GFP* positive/*tdTomato* negative cells suggest that one or both of these BAC transgenic lines does not fully recapitulate endogenous CRHR1 expression (*137*). It must be critically mentioned that true ubiquitous promoters do not exist and the above mentioned and commonly used *Rosa26-LacZ* reporter strain is known to express marginal in specific cell types of the brain (*262*). Moreover, the level of *Rosa26* locus activation decreases postnatally. Hence, one needs to be aware that comprehensive evaluation of *Cre* expression studies must be complemented by additional data sets, such as ISH or DFISH to detect *Cre* mRNA on the cellular level (*165*).

During completion of this thesis Sanford et al. published the generation of an additional CRHR1 *Cre*-driver line (*CRHR1^{IRESCreGFP}*) to dissect CRHR1 signaling in the CeA (*62*). A knock-in strategy was used to place an *IRES-CreGFP* cassette under the control of the endogenous CRHR1 promoter. The targeting construct contains two PCR amplified homology arms flanking the *IRES-CreGFP* sequence, two negative selection marker (pgkDTA and HSV-TK) and one *frt*-flanked positive selection gene (*neo* cassette). To prevent disturbance of endogenous CRHR1 gene expression, the *IRES-CreGFP* cassette was targeted after the stop codon into the 3'UTR of the CRHR1 gene. For the RMCE based strategy described in this thesis, the incoming vector was also designed in a way to preserve expression and function of the endogenous receptor. The *IRES-Cre* cassette was inserted downstream of the coding sequence of CRHR1 exon 3 -13 right after the stop codon. In both cases a bicistronic transcript (mRNA) is made, encoding both genes, the endogenous CRHR1 and the *Cre* recombinase, that are then translated into two separate proteins, resulting in expression of the transgenes without disrupting the endogenous gene. This is of particular significance because CRHR1 insufficiency causes a marked decrease in the corticosterone producing zona fasciculata region of the adrenal glands. Consequently, CRHR1 mutant mice have very low plasma corticosterone levels and, as a result, a virtually 100% neonatal mortality of the progeny from CRHR1 null mutant intercrosses. Neonatal lung maturation is

depending on sufficient maternal corticosteroid concentrations and that is why offspring from homozygous CRHR1 mutant females displays a marked lung dysplasia and develop a severe neonatal respiratory distress syndrome (*156*). In both *Cre*-driver lines, corticosterone levels at baseline or following restraint stress are not altered as shown by a radioimmunoassay.

Bicistronic targeting vectors in which the first gene (here CRHR1) is translated in a cap-dependent manner and the second one (here *Cre* recombinase or the *CreGFP* variant, respectively) in an *IRES*-dependent manner have been widely used in transgenic animals to link two genes transcribed from a single promoter. Sanford and colleagues used this approach to drive *Cre* recombinase from the endogenous CRHR1 promoter and, at the same time, to monitor *Cre* expression via expression of the fluorescent *GFP* protein. *In vitro* and *in vivo* studies revealed that *IRES*-dependent translation of a second open-reading frame (ORF) is significantly less efficient compared to the first ORF (*263*). Studies in our group and analysis of a CRHR1-GFP reporter mouse line (*219*) have demonstrated that *GFP* expression driven by the endogenous CRHR1 locus is very weak, and reliably detectable only following immunohistochemistry (*41*). We speculate, therefore, that native *GFP* fluorescence in the *CRHR1*^{IRESCreGFP} mouse line from Sanford and colleagues is not strong enough to monitor *Cre* expression and that therefore only recombinase expression is evaluated – similar to the approach in this thesis - via a *Cre*-dependent reporter mouse line or a *Cre*-dependent AAV construct (see chapter 7.3.1 for discussion of central *Cre*-recombinase functionality).

7.1.3 Recombinase-mediated cassette exchange (RMCE): repeated genetic modification of the CRHR1 locus by targeted integration

In the past two decades, numerous *Cre*-driver mouse lines have been generated by employing a variety of sophisticated approaches, ranging from “traditional” random transgenic insertion of *Cre* cDNA driven by a short promoter to gene-targeting based Cre “knock-ins” into a defined endogenous gene driver locus (*168, 169*). Classical strategies, that rely on homologous recombination in embryonic stem cells to insert targeting cassettes into pre-defined suitable endogenous loci are labor intensive, expensive and time-consuming, mostly due to very low targeting frequencies (<1%) (*264*). For this reason, repeated genetic manipulation of the same locus via RMCE

evolved as a powerful tool for re-engineering mouse conditional alleles that harbor appropriate targeting sites, such as *attP* sites for the *phiC31* integrase. In addition, dual RMCE is a highly efficient and universal tool, developed for restructuring the large number of available conditional alleles that harbor *loxP* and *FRT* sites (*265*). To date, three genetic mouse models targeting the CRHR1 locus in a conditional fashion have been developed in our research group (*41, 99, 158*). The previously generated multifunctional allele comprises the possibility to label CRHR1-expressing cells with a *tau-lacZ* reporter gene and to conditionally restore or delete CRHR1 function (*41*). Furthermore, it is suited for subsequent modifications via RMCE as the allele contains targeting sites for the serine integrase *phiC31*. The comprehensive pre-characterization of the genomic locus so far has confirmed that the landing path in intron 2 offers the possibility for stable and reliable expression of other exogenous cassettes at physiological expression levels in a CRHR1-specific spatio-temporal manner. This largely “predictable outcome” at a pre-determined locus facilitates the future utilization of complementary techniques, such as trans-neuronal tracers, optogenetic and DREADD-based chemogenetic tools and site-specific recombinase variants - just to name a few.

Nevertheless, at this point it must be noted that most recently genome editing tools, based on the bacterial CRISPR/Cas9 system (clustered regularly interspaced short palindromic repeats/CRISPR-associated protein), have been developed to facilitate site-specific genomic modifications, thereby opening up new avenues for neuroscientists to decipher complex neuronal circuits and their role in stress-related disorders (*266*). The CRISPR/Cas9 reagents (consisting of Cas9 nuclease and a single guide RNA) can be transferred directly into the mouse zygote and result in DNA cleavage at any genomic locus of interest. The highly conserved DNA repair machinery restores the DNA double-strand break either by non-homologous end joining, or via homology-directed recombination (HDR), thereby enabling introduction of specific mutations or homologous exogenous DNA donor templates. Compared to traditional gene targeting and RMCE (using HDR in mouse embryonic stem cells), it is now possible to derive genetically modified founder mice within 2 months because there is no waiting time for cloning of the targeting vector, transduction and selection of embryonic stem cells, blastocyst injection and generation of chimeras. Moreover, embryos from any mouse strain can be manipulated, and also multiple gene targeting within one zygote is possible. This avoids the necessity for genetic backcrossing and

crossbreeding to generate double and triple mutant mice. In addition, elimination of "genetic background effects", due to residues of 129 ES cell-derived genetic material, prevents data misinterpretation especially in the field of behavioral genetics (*267*). A future challenge will be the improvement of the efficiency (mainly introduction of complex and large cDNAs) and specificity of the system in order to minimize off-target effects (*268*). Recently, the CRISPR/Cas9 system was used to generate a bicistronic knock-in *Cre*-driver line for gene manipulation specifically in pancreatic insulin-synthesizing β cells (*269*). The combination of a CRHR1 *Cre*-driver mouse line and local injection of *Cre*-inducible Cas9 and sgRNA expressing adeno-associated viruses provide enormous combinatorial power to decipher *in vivo*, how a specific cell type influences behavior and neurocircuit function, especially stress-related complex neuronal networks (*266, 270*).

7.1.4 Partial RMCE – The *CRHR1*^{tZCre}-driver line

As described in chapter 6.2 and 6.3 of this thesis, *phiC31* mediated RMCE was used to generate a novel CRHR1 *Cre*-driver mouse line. Surprisingly, the analysis of the first offspring demonstrated that *Cre* and a reporter gene expression was limited to a subset of CRHR1-specific cells. Possible reasons for the exceptional recombination event will be discussed in the following section. Large serine recombinases, such as *phiC31*, include a three-nucleotide recombination site, which determines directionality. In intramolecular direct orientation *phiC31* integrase excises the DNA interval, whereas a head-to tail orientation inverts the flanked DNA. Another characteristic of serine-integrases is the ability to recombine intermolecular, between different DNA molecules, whether or not they are supercoiled or linear (*271*). Thereby, the serine integrase mode of action is based on a DNA double-strand break and exchange of strands by a rotational mechanism. The cleaved DNA "half-sites" are covalently attached to the integrase subunit and the whole complex then "flips" through a horizontal 180° rotation. The cleaved DNA ends are rejoined in this rotated configuration, resulting in *attL* and *attR* sites. In the absence of a phage encoded recombination directionality factor (RDF) – not present in mammalian cells - the integration reaction is unidirectional, because the *attL* and *attR* sites form auto-inhibited complexes preventing intramolecular *attL* x *attR* recombination (*272*).

In 2003, Belteki and colleagues published the first successful *phiC31* integrase mediated site-specific cassette exchange and germline transmission in mouse ES cells (*193*). In line with our data the analysis of reaction products pointed towards inefficient intramolecular recombination. Type I and type II insertion events (see Figure 6) could result in hygromycin resistant colonies without subsequent deletion of the sequence (including plasmid backbone sequence) between the attB and attP sites. Incomplete type II insertion with residual vector backbone occurred in 25% of our colonies, similar to the results seen in the study from Belteki et al., where complete cassette exchange occurred only in approximately one-third of the cases. One possible explanation for the intramolecular integrase inefficiency might be the inability to rotate the chromatin template before recombination (*273*). In addition, recombination efficiency is strongly cell type specific and depending on the intramolecular distance between recognition sites (*271*). Increased distance between the recombination target sites (>400bp), as well as a too short distance (<120bp) lead to a decrease in recombination frequencies (*274*). Another factor, which affects recombination, is the level of active recombinases. Lack of recombinases decreases the probability of recombination, meaning an excess of enzymes over binding sites is required for higher efficiency (*275*). Therefore, the sole use of a *phiC31*-encoding plasmid could be responsible for the inefficient intramolecular recombination due to delay in translation and decreasing amount of the integrase. Recently, Schilit and colleagues demonstrated that the efficiency in pronuclear injection-based targeted transgenesis is considerably improved by use of mRNA injection instead of plasmid DNA encoding the recombinase or integrase (*276*). Unfortunately, none of our ES cells with incomplete type II insertions resulted in chimeras in which the ES cells contributed to germ cells and were passed to the offspring. For this, we had abandoned the plan to complete the recombination by breeding offspring to the R26*phiC31*o driver mouse line (Jackson Laboratory mouse strain # 007670), to obtain mice that have the targeted *attP-lacZneo-attB* sequence deleted and replaced with a single *att L* site.

In the majority of ES cells that where integrated into the germline, PCR results pointed towards a different recombination event. In these cases, *phiC31* integrase catalyzed a typical integration reaction instead of a cassette exchange reaction. For this reason, the *tau-lacZ* reporter cassette with its strong adenovirus splice acceptor and the *neo* selection cassette are still present at the integration site. In this

configuration CRHR1 exon 2 could be spliced to the synthetic splice acceptor site in a way that the N-terminal portion of CRHR1 is in-frame with the *tZ* reporter gene. *In situ* hybridization, l*acZ* staining and reporter gene expression revealed concurrent translation of two functional proteins, namely *Cre* recombinase and β-galactosidase, respectively, in a subset of CRHR1 specific cells. It is known, that the *neo* cassette contains cryptic splice sites, possibly causing aberrant splicing of CRHR1 transcripts in a way that the mutant transcript contains sequences from the noncoding *neo* strand. The effect of neo on the expression level could be very diverse, ranging from promoter interference, disrupting of normal splicing patterns, premature transcript termination, reduction or complete inactivation of targeted gene expression (*218*). Nonsense-mediated mRNA decay (NMD) eliminates aberrant mRNAs, harboring premature STOP codons in a cell-type-specific and developmental regulated manner (*277*). We speculate, therefore, that aberrant splicing of neo sequences into the adjacent CRHR1 exon 3-13 coding sequence generates mRNAs harboring premature termination codons, resulting in a cell-specific NMD, thereby explaining the partial absence of *lacZ* and *Cre* mRNA/protein in the *CRHR1^{tzCre}* mouse line.

7.1.5 Generation of the *CRHR1^{Cre}*-driver line via Flpe recombination

As outlined in the previous chapter, the presence of the positive selection marker *neo* can have unintended consequences on the targeted gene and on adjacent genes. The same is true for the second positive selection marker hygromycin, which was included in the RMCE donor construct. Generally, the selection cassettes are flanked with recognition sequences (*loxP* or *frt*) for site-specific recombinases (*Cre* or *Flp*), so that they can be removed either by transient transfection of the targeted ES clones or by breeding the transgenic mouse line with *Cre*- or *Flp*-deleter strains. In the *CRHR1^{tzCre}* mouse line the transgene configuration after RMCE is as follows: the *tau-lacZ*-reporter cassette of the genomic docking locus is still present but due to residual flanking *frt* sites accessible for *Flp* mediated recombination as well as the positive selection marker hygromycin, which was included within the targeting vector and flanked with *frt* sites, to enable its removal *in vivo* by crossing to a *Flp*-deleter strain. The efficiency of intramolecular recombination between two *frt* sites depends on the distance between them and was observed highest at a distance of 200bp. The deletion of large *frt*-flanked segments is less efficient, as recombinase efficiency

decreases the further apart *frt* sites are (*278*). We therefore assumed that *Flp* mediated recombination occurs with a higher probability between the *frt* sites flanking the *lacZ* reporter and *hygro* selection cassette, thereby preserving the coding sequence of CRHR1 exon 3 -13 followed by the *IRES-Cre* cassette.

To date, two *Flp*-deleter strains with generalized expression of the thermostable variant of *Flp* (*Flpe*) have proven as versatile tools for *in vivo* genetic engineering in a variety of tissues, including cells of the developing germ line. The largest application is the generation of selection marker-free conditional alleles to avoid interference of the selection gene. The transgenic strain *hACTB::FLPe* published by Rodriguez et al., expresses a *FLP1* recombinase gene under the direction of the human *ACTB* promoter and mediates recombination in F1 progeny as early as embryonic day 10.5 with highest efficiency (*279*). When breeding to the *CRHR1*^{tZCre} mouse line, all F1 progeny exhibited complete recombination, including deletion of the *frt*-flanked coding sequence of CRHR1 exon 3 -13 and the *IRES-Cre* cassette. As we could not detect any different recombination pattern or mosaicism, we assumed that recombination takes place between the outermost flanking *frt* sites (see Figure 19). For this, the *CRHR1*^{tZCre} mouse line was bred to the FlpeR ("flipper") mouse strain, which expresses *Flpe* under control of the ubiquitous *Rosa26* promoter. This line has been reported as somewhat less efficient, as complete recombination was observed in approximately 50% of double transgenic F1 progeny (*237*). Screening of the F1 generation for the desired recombination event (hygro selection cassette- and reporter cassette free allele) and subsequent breeding resulted in establishment of the *CRHR1*^{Cre} line. Although residual promoterless neo sequences are still present in intron 2, comprehensive ISH expression analyses provide no indications for aberrant splicing events, nor reduction of CRHR1 gene expression.

7.2 Potentials and limitations of *Cre*-driver lines

Over the past two decades, a number of large-scale projects and individual laboratories have invested great effort in developing a comprehensive toolbox of *Cre*-driver lines for functional and connectional studies in specific cell types and/or different regions of the brain and periphery. The full potential and utility of these various *Cre* lines depends on a systematic characterization of transgene expression

patterns and *Cre*-mediated recombination, to ensure that the *Cre*-defined cells represent the same population that endogenously expresses the gene of interest. Several studies that characterized *Cre*-recombination patterns in the brain and peripheral tissues, indicate a high variability with some *Cre* lines very faithfully recapitulating endogenous gene expression patterns, and others showing ectopic (both temporal and spatial) and/or subset expression. Moreover, variation among floxed alleles regarding efficiency of *Cre*-mediated recombination, unexpected germ line deletion or toxic effects of *Cre*, represent possible pitfalls and should be considered when interpreting experimental data (*165, 187, 280-285*). The key considerations associated with the *CRHR1*^{tZCre}*/CRHR1*^{Cre}-driver lines will be discussed in greater details in the following.

7.2.1 Specificity and efficiency of *Cre*-mediated recombination

For comprehensive validation of new *Cre*-driver lines, it is necessary to analyze *Cre* expression on mRNA level but also to evaluate *Cre* activity by reporter gene studies and as well by analysis of recombination pattern in mice harboring a floxed allele. The ability of a floxed target gene to be recombined may vary depending on the cell type- and/or development-specific chromatin structure/DNA methylation state at the gene locus of interest and should therefore be evaluated individually for each floxed allele, even when the *Cre*-driver is well characterized in the literature. In addition, the distance between l*oxP* sites and chromosomal location can affect the recombination efficiency (*203*). To ensure the correct interpretation of the behavioral phenotype in mice that express a constitutive active version of the CRHR1 in the VTA, we performed double ISH with riboprobes targeting the endogenous CRHR1 and the "flexed" constitutive active version of the receptor (expression only after *Cre*-mediated recombination of the *loxP* flanked inverted expression cassette). Virtually all cells that expressed the activated form *co-expressed* the wild-type receptor and thereby confirmed the high specificity of the driver line at least in this particular brain region.

In addition, specificity and efficiency of *Cre* activity was validated in a mouse line, harboring a floxed EGFP-CRHR1 allele (*Crhr1*$^{N\text{-}Egfp}$ knock-in line, described by Refojo et at., 2011). Complete absence of GFP transcripts in distinct brain regions of double transgenic mice demonstrated that Cre activity is highly specific and efficient. On the other hand, residual *GFP* signals in the RT, GP, VTA, RMC, PG and MV point towards nonuniformity in *Cre* activity. Moreover, *Cre* activity might also depend on

the parent-of-origin (see following chapter). Although DISH experiments proved the high specificity of *Cre* expression in these brain regions, it is likely that a subpopulation of neurons express insufficient levels of Cre protein for recombination to occur efficiently. At the moment, it is only possible to speculate about possible reasons for this phenomenon. Gregg and colleagues reported allele-specific expression effects due to epigenetic regulatory factors (*286*). These effects can lead to either complete silencing of an allele or to biases in which higher expression levels arise form one allele versus the other, e.g., maternal versus paternal. In addition, allele-specific different expression of isoforms/transcripts could be possible mechanisms for this so-called “non-canonical” imprinting effects. For example, for the genes Grb10, Igf2, Ube3a, Dlk1, it has been shown, that imprinting occurs in a cell type-specific manner (*287, 288*). Furthermore, non-canonical imprinting at the cellular level could lead to a bias, such that each cell express slightly more of one parental allele (*289*). We therefore speculate on reduced levels of *Cre*-recombinase due to non-canonical imprinting of the “*Cre*-allele” in a subpopulation of cells expressing the CRHR1.

7.2.2 Parent-of-origin effects

Cre activity can vary depending on maternal or paternal inheritance of the *Cre* transgene (*283, 290*). Therefore, we analyzed this issue in progeny from *CRHR1*$^{+/cre}$ *x CRHR1*$^{+/N\text{-}Egfp}$ breeding pairs via ISH to detect *GFP* mRNA in brains from double heterozygous mice. Interestingly, we found slightly weaker/subset recombination pattern (loss of *GFP* signal) when the CRHR1 *Cre* allele was inherited paternally, although the *Cre* expression pattern is consistent with the brain specific expression pattern of the endogenous CRHR1 (Figure 21). In a recent study Perez and colleagues investigated genomic imprinting (a chromatin modification in the parental germ lines, leading to variable expression of the maternally- or the paternally inherited allele) in the mouse brain and identified ~200 imprinted genes with many of them parentally biased, meaning that either the maternal or paternal allele is expressed at a higher level, rather then completely silenced (*291*). Bonthius and colleagues termed this “noncanoncial genomic imprinting” and demonstrated tissue- and cell-type specificity. Moreover, they revealed an enrichment of noncanonical imprinted genes in the brain (both autosomal and X-linked) and provided examples for allele-specific expression of genes in distinct subpopulation of neurons (*292*). In contrast, “canonical imprinting” leads to complete silencing of one gene copy. Both

effects – canonical and noncanonical – are associated with allele-specific chromatin modifications (*293*). As low levels of *Cre* activity can lead to differential recombination efficiencies, we therefore speculate on noncanonical imprinting of the paternal *Cre* allele in offspring from male *CRHR1*$^{+/cre}$ *x* female *CRHR1*$^{+/N\text{-}Egfp}$ matings and consequently only partial deletion of the floxed CRHR1-GFP allele. Furthermore, intercross of heterozygous *CRHR1*$^{+/tZCre}$ mutant male and female mice did not result in homozygous offspring, most probably due to perinatal/neonatal lethality due to lung dysplasia. This phenomenon has been described so far only for homozygous intercrosses where low levels of maternal corticoids result in insufficient neonatal lung maturation (*156*). As stated in chapter 6.3.1 electrophysiological analysis revealed that the *tZCre*-allele is a knockout allele, most probably due to an aberrant splicing of neo sequences into the adjacent CRHR1 exon 3-13 coding sequence, resulting in a non-functional receptor in consequence of a reading frame shift. Cell-specific monoallelic expression of the mutated/knockout allele in pituitary corticotrophs could be a possible cause for insufficient levels of maternal corticoids. In contrast, distinct CRHR1-specific brain regions were completely devoid of *lacZ* and *Cre* mRNA expression (Figure 15). Whether this originates from canonical genetic imprinting of the *tZCre*-allele or due to faster nonsense-mediated mRNA decay remains elusive at this stage of our knowledge.

7.2.3 *Cre* toxicity

Depending on its concentration, the *Cre* protein can be toxic for mammalian cells (*170*). Expression levels from heterozygous *CRHR1*$^{+/Cre}$ transgenic animals are sufficient for complete recombination of floxed alleles as demonstrated in offspring from *CRHR1*$^{+/cre}$ *x CRHR1*$^{+/N\text{-}Egfp}$ breedings (Figure 30). The absence of *GFP* mRNA in distinct brain regions clearly demonstrates the high efficiency and specificity of this driver line and it is not necessary to use animals homozygous for the *Cre* allele. Moreover, the *CRHR1*^{Cre} line was maintained as homozygotes. It is worth mentioning that the homozygous *Cre*-breeding colony showed no abnormalities that point to affected cell physiology, decreased viability and fertility, or recombination of cryptic *loxP* sites in the genome as reported in other *Cre* transgenic strains (*294*). As high levels of *Cre* expression can cause a phenotype induced by the *Cre*-driver alone (*280, 285*), we subjected homozygous *CRHR1*$^{Cre/Cre}$ mice to a standard functional test and measured basal and stress-induced corticosterone levels. Functionality of CRHR1 activity was not impaired as corticosterone levels were comparable to those

in wild-type mice (*CRHR1*$^{+/+}$). Moreover, we used *CRHR1*$^{+/cre}$ mice (injected with an AAV-Ef1a::DIO-*mCherry* control virus) with identical genetic background as control group in our behavioral studies instead of wild-type mice. Former studies have demonstrated that reporter gene expression driven from the endogenous CRHR1 locus is rather weak (*41*) and therefore we assume that the intracellular accumulation of *Cre* protein remains below a potential toxic level.

7.2.4 *Cre*-mediated germline deletion

A *Cre*-dependent reporter line revealed expression of *Cre* protein in the male germline, or more exactly, CRHR1 promoter-driven expression of *Cre* was detectable in spermatids and their progenitor cells. For this reason, recombination of *loxP*-flanked alleles can occur in the germ cells of *Cre*-positive males, with the consequence of generalized deletion of targeted alleles in the progeny. Therefore, the usage of *Cre*-positive males for brain-specific targeting of conditional alleles, and/or usage in behavioral/metabolic phenotyping experiments is restricted to the F1 generation of double-transgenic animals. In general, specific attention has to be paid in the PCR design for genotyping, to detect the deleted allele, e.g., in tail lysates from offspring of male and also female CRHR1-Cre mice. The latter will resolve potential problems with post-meiotic persistence of *Cre* protein in oocytes which could cause recombination of a floxed target allele in the zygote, even when the oocyte itself does not carry the *Cre* allele. This would lead to inheritance of the recombined allele in all tissues of the progeny. Reporter gene expression in *CRHR1*$^{+/Cre}$*::Ai9* double transgenic mice was restricted to ovarian stroma cells and did not show any evidence for *Cre* expression in in the female germline. For this, we used *Cre*-positive females for maintaining the CRHR1-*Cre* alongside floxed alleles.

7.2.5 Caveats associated with *Cre*-reporters

Universal *Cre*-reporter lines are designated for *Cre*-dependent expression of transgenic marker genes, such as *lacZ* or fluorescent markers like *GFP*, *YFP* or *tdTomato*. The most commonly used locus for *Cre*-responders is the *Rosa26* locus in combination with an inserted strong and ubiquitous promoter, e.g., the CAG promoter, to drive expression of the reporter gene cassette after *Cre*-mediated removal of a floxed stop cassette (*187*). Scientists should be aware that not all of them show ubiquitous and/or equal expression levels or recombination efficiencies. At low level of *Cre* activity, the *R26-CAG-tdTomato* responder line faithfully identifies

cells that underwent recombination in contrast to the *R26-eYFP* mouse line, which revealed lower recombination sensitivity. Moreover, *R26-eYFP* and *R26-CAG-eGFP* displayed different recombination sensitivities although they comprise identical floxed stop cassettes, most probably due to a different methylation status of sequence variances downstream of the *loxP* sites or different nucleasomal structures that affect accessibility of the recombinase target sequences (*295*). We made use of two fluorescent reporter lines to evaluate spatiotemporal CRHR1 promoter-driven *Cre* expression, the above mentioned R26-CAG-tdTomato (Ai9) line and in addition, the R26-CAG-SUN1-sfGFP reporter line. In both cases the reporter gene (tdTomato and SUN1-sfGFP fusion protein, respectively) are expressed under the control of the strong and ubiquitous CAG promoter, inserted within the Rosa 26 locus. We could not detect differences in recombination efficiencies nor sensitivities between the two lines, although the strong *tdTomato* native fluorescence outperforms the *sfGFP* fluorescence strength, which constituted a major advantage in detection of neurons with low levels of CRHR1 expression, respectively *Cre* recombinase expression.

Finally, it must be pointed out that it is essential for every user of *Cre*-driver lines to be aware of the outlined potential caveats - even when relying on lines that have been “adopted” as common tools. Therefore it is a prerequisite to complement published data with own unbiased and additional evaluation studies, to get an extensive impression of *Cre* recombinase accuracy (*169*).

7.3 Characterization of *Cre*-recombinase functionality

7.3.1 Central CRHR1-IRES-*Cre* expression

The bicistronic knock-in strategy for generation of the CRHR1 *Cre*-driver line was chosen because it enables endogenous gene-dependent *Cre* activity without losing one copy of the targeted CRHR1. The internal ribosomal entry site (*IRES*) has been frequently used for bicistronic gene expression although no equimolar expression of downstream cistrons in a cell-type specific manner has been reported (*296*). The use of a viral 2A peptide for multicistronic expression in transgenic mice has emerged as an attractive alternative to the *IRES* site. The 2A peptide mediates the co-translational cleavage of polypeptides and lead to more reliable expression of multiple cistrons at equimolar levels (*297*). However, after cleavage, the short 2A peptide remains fused to the upstream protein and can potentially interfere with

protein performance (*298*). In addition, a prolin relic of the 2A self-cleaving process is attached to the N-terminus of the second protein (*299*). In a recent study Bender and colleagues characterized the C-terminal PDZ binding motif of CRHR1 and revealed protein-protein interactions with multiple members of the membrane-associated guanylate kinase (MAGUK) family, which directly affects receptor function (*125*). To avoid that residues of the 2A peptide at the C-terminus potentially ablate this interaction and interfere with receptor function we used the *IRES* sequence for expressing the *Cre* recombinase under control of the CRHR1 promoter. Several approaches were applied to evaluate functionality of the receptor and the *Cre* recombinase, respectively. First, comprehensive ISH studies were conducted to verify expression of *Cre* recombinase (Figures 21). Using a riboprobe complementary to the 3'UTR of the wild-type allele in comparison to a riboprobe specific for the *Cre*, *CRHR1*$^{+/Cre}$ mice showed identical expression patterns of *Cre* compared to wild-type mice. Second, plasma corticosterone levels of *Crhr1*$^{Cre/Cre}$ mice under basal conditions and after acute stress were indistinguishable from wild-type animals, confirming the full functionality of the CRHR1. In contrast, distinct CRHR1-specific brain regions were completely lacking *Cre* mRNA expression in CRHR1$^{+/tZCre}$ animals (Figure 15). Possible mechanisms for this subset expression could be nonsense-mediated mRNA decay of an aberrantly spliced *tZCre*-allele, promoter inactivation due to residual neo sequences or cell type-specific canonical genetic imprinting of the *tZCre*-allele. Therefore the CRHR1$^{+/tZCre}$ driver line represents a genetic tool for sparse cell type-specific neuronal labeling, useful for the analysis of neuronal morphology, as demonstrated by crossing to the *tdTomato* reporter line (*300, 301*). Moreover, this line represents a unique tool for expression and visualization of fluorescent proteins that localize to subcellular structures, e.g., synapses, in CRHR1-specific neurons (*302*).

Crossing of *CRHR1*$^{+/cre}$ mice with the *R26-CAG-tdTomato (Ai9)* and *R26-CAG-Sun1-sfGFP Cre*-responder lines was used to validate the functionality of *Cre* recombinase on protein level and to visualize neurons with low levels of *Cre* expression that might not be reliably detectable on mRNA level. In line with recently published data from a different CRHR1 *Cre* knock-in allele (*62*), *tdTomato* reporter gene expression revealed that the distribution of labeled cells was fundamentally similar to previously described *Crhr1* mRNA expression (*29, 303*). It has to be noted, however, that in both driver lines a dense set of labeled neurites prevented evalution of single labeled

neurons in prominent sites of *Crhr1* mRNA expression such as globus pallidus, reticular thalamic nucleus, ventral tegmental area and red nucleus as well as in other sites of rather low expression of *Crhr1* mRNA. Therefore, we made use of a second reporter line, *R26-CAG-Sun1-sfGFP,* which facilitates single cell resolution. Overall, the results suggest that expression of *Cre* was essentially similar to the spatial distribution of endogenous *Crhr1* mRNA. In certain brain regions, however, the recombination pattern deviates from that of the endogenous CRHR1 expression in the adult mouse brain. These deviations most likely result from the fact that reporter gene expression reflect the cumulative expression history of the CRHR1 gene. CRHR1 expression was detectable in ED 10-11 embryo heads of mice by means of RT-PCR (*304*). To evaluate the specificity of our *Cre* line we performed double ISH with riboprobes complementary to *tdTomato* and to the endogenous CRHR1 (riboprobe located in the 3' UTR of the receptor). Quantification of double positive cells revealed that the majority of CRHR1-positive neurons also expressed *tdTomato,* which proved the high specificity on the one side and demonstrated that *tdTomato* expression reflects the cumulative/developmental expression history, rather than ectopic *Cre* recombinase activity

Sanford and colleagues used their CRHR1 knock-in *Cre*-driver to genetically label CRHR1 neurons in the central amygdala and stated that CRHR1 signaling in the CeA is critical for discriminative fear. They used a slightly different reporter line (Ai14^{tdTomato}) to reveal CRHR1 expression and reported that CRHR1 neurons are "*broadly localized within the central, lateral and medial CeA, partially overlapping with somatostatin neurons it the caudal CeA$_L$*" (*62*). We could not reproduce this "broad" reporter gene expression in sections obtained from crossing our driver line to the *R26-CAG-Sun1-sfGFP Cre*-responder line, where we could detect only a small number of *sfGFP* labeled neurons in the central amygdala. Moreover, with local injections of a *Cre*-inducible virus (AAV-EF1α-Dio-*mCherry*) into the CeA of our CRHR1 *Cre*-driver, we analyzed current expression of the receptor in the adult brain, and could detect only very few labeled CRHR1 cells in the CeA. Although we cannot exclude a higher recombination sensitivity of the Ai14^{tdTomato} reporter line, nor false negative results due to inefficient viral transduction, we think that some control experiments, such as viral-mediated knockout of the receptor in the central amygdala, would be necessary to strengthen their conclusions.

In line with previous data, where we used a knock-in approach to visualize CRHR1 expression via a β-galactosidase reporter, we assume that the small number of *sfGFP* labeled neurons within the PVN and LC also resulted most likely from a transient expression of *Cre* recombinase during development, as no current reporter gene expression was seen after injection of AAV-EF1α-Dio-*mCherry* into the adult mouse brain. This is in conflict with electrophysiological studies and electron microscopic studies in rats that reported a direct CRH/CRHR1 interaction within the LC (*36*). Although the distribution of *Crhr1* mRNA in mouse and rat brain was found to be quite similar (*29*), the relative strength of receptor expression displayed differences, e.g., in cortical layer 6, in the RTN and striatum. It is therefore possible that low receptor, and consequently low *Cre* expression is not sufficient to recombine the reporter alleles and remove transcriptional stop cassettes to initiate transcription of reporter genes. Another possible explanation could be an interaction of CRH with postsynaptically localized receptors on dendritic processes within the LC, that originate from neurons located in neighbored structures, such as the medial and parabrachial nuclei, where strong expression of *mCherry* labeled somata was visible after viral injection of AAV-EF1α-Dio-*mCherry* in the adult mouse brain (Figure 29). Another brain structure with inconsistencies with respect to *Crhr1* mRNA expression is the PVN. Stress inducible expression of *Crhr1* mRNA in the paraventricular nuclei has been described so far only in the rat (*29*) and could not be reproduced in mice (own studies, data not shown). Recently Ramot and colleagues described a distinct population of hypothalamic CRHR1 positive neurons that play a role in modulating HPA axis activity and are “recruited” specifically in chronic stress conditions (*305*). Overestimation of CRHR1 expressing neurons in the used transgenic BAC-GFP reporter mice (*219*) and/or low and inefficient levels of *Cre* recombinase under basal conditions could be an explanation for the discrepancies of our expression studies with functional evidences.

7.3.2 Peripheral CRHR1-IRES-*Cre* expression

The most complete analysis of CRHR1 expression is based on detection of mRNA and has focused on central expression in brain and pituitary, particular in mice and rats (*29, 70, 306*). An immunocytochemical study using an antibody against the C-terminus of the receptor focused on CRHR1 protein detection in the mouse brain and

the results are for the most part in line with published data on *Crhr1* mRNA expression (*229*). Apparent discrepancies, e.g., in the cerebellar granular cell layer, the PVN and LC were attributed to protein transport away from the synthesis locus in the soma or long half-life of the CRHR1 protein. On a critical note, the evaluation of antibody specificity has not been proven on brain sections of complete CRHR1 knockout mice. This is of special relevance since own studies in our group revealed the lack of reliable antibodies against CRHR1, especially at low physiological expression levels (*99*). To date, two CRHR1-reporter mouse lines have been generated that provide the possibility to visualize endogenous CRHR1 expression and additionally enable visualization of CRHR1 connectivities of CRHR1-expressing neurons (*41, 219*). *Tau-LacZ* reporter gene activity revealed novel aspects and sites of CRHR1 expression in mouse spinal cord, eye and skin, where expression of the receptor was based so far on immunohistochemistry, ISH and RT-PCR (*41*). The generation of an appropriate CRHR1-*Cre* mouse line in combination with a *Cre*-inducible reporter line for genetic labeling of CRHR1 expressing cells opens up new opportunities for spatiotemporal detection of CRHR1 expression in the periphery, particularly in sites with low endogenous expression levels. Expression of the *tdTomato* reporter gene in double transgenic CRHR1^{Cre}::Ai9 mice recapitulated CRHR1 expression obtained with the *tau-lacZ* reporter line in mouse pancreas, spinal cord, eye, skin, pituitary gland and adrenal gland (Figure 26). Expression of the receptor in the adrenal gland was restricted to a “stripe” of labeled cells within the adrenal cortex (Figure 26F). At the moment we can only speculate on the origin of these cells and the labeling pattern. Detection of CRHR1 in mouse adrenal gland was so far only detectable on mRNA level via ISH and RT-PCR and was shown to be most prominent in the zona fasciculata of mouse adult adrenals, whereas expression in adrenals from adult rat was detected via immunohistochemistry in the medulla and throughout the cortex (*307, 308*). Discrepancies between *Crhr1* mRNA expression and reporter gene expression in mouse adrenals require further experiments and cannot be clarified at the moment. Interestingly, development of the murine adrenal gland includes fetal cortical progenitor cells, located peripherally that give rise to radial adrenocortical cell lineage stripes from E14.5 on (*309*). Therefore, we speculate on transient CRHR1 promoter activity and *Cre* activity, respectively, in fetal steroidogenic progenitor cells and cell lineage specific reporter gene expression.

So far, expression of *Crhr1* mRNA in the kidney was described only in studies from humans and rats. Up to now, corresponding studies in mice are lacking and therefore *tdTomato* fluorescence signal in proximal and distal convoluted tubes as well as collecting tubes within the cortex of the kidney (Figure 26G) provides a first indication for potential direct CRH/CRHR1 interactions in context of stress and pathophysiology of chronic kidney disease (*310*).

Over the past years, a growing body of evidence confirms a prominent role for CRH in immunomodulation. CRH and/or CRHRs have been detected in major cellular components of the immune system: autoradiographic studies in mouse spleen revealed CRH receptor expression primarily on resident splenic macrophages (*311, 312*) and on human monocyte-macrophages and T-helper lymphocytes (*313*). Expression of the CRHR1 was described in granulocytes, lymphocytes, macrophages and perivascular mast cells within inflamed human and rat tissues (*314, 315*). The use of double transgenic CRHR1^{Cre}::Ai9 mice has demonstrated expression of the receptor in lymphatic tissues including thymus and spleen, and was also detected in Kupffer cells (KCs), macrophages that mediate the hepatic immune response (Figure 26J-L). Furthermore, strong expression of the reporter gene was evident in lingual filiform papilla. As immune cells (dendritic cells, macrophages and T-lymphocytes) are present in the human lingual mucosa (*316*) and T-lymphocytes were also detectable in mouse lingual epithelium (*317*) we assume that CRHR1 is expressed on T-lymphocytes within mouse lingual epithelial cells. In addition, tdTomato labeled cells were visible in lung epithelial cells (Figure 26N), most probably T-lymphocytes that are found in the epithelium and lamina propria of the bronchi (*318*). Moreover, CRHR1 expression is visible in the mucosa (villi) of the small intestine (Figure 26H), but additional experiments are necessary to determine the distinct cell-type and and localization of the receptor. Immunohistochemistry studies in combination with RT-PCR showed, that the receptor is *co-expressed* with CD163, a marker for resident macrophages, in human colonic biopsies (*319*). Porcher and colleagues evaluated expression of CRHR1 and CRHR2 in rat small intestine (duodenum and ileum) via immunohistochemistry. Both receptors were detected, amongst other structures like submucosal ganglia, in mucosal cells. Application of a CRHR1 antagonist blocked activation of duodenal motility (*320*). The number of macrophages co-stained for CRHR1 was significantly elevated in patients

with ulcerative colitis and indicate a role of CRHR1 signaling in modulating intestinal immune-inflammatory processes (*319*).

Finally, there is experimental evidence that CRH/CRHR1 modulate the immune/inflammatory response in a bidirectional manner: centrally released CRH stimulates glucocorticoid and catecholamine release, exerting anti-inflammatory effects and in contrast, peripherally secreted CRH is stimulating pro-inflammatory functions, such as proliferation of lymphocytes, expression of IL-2R antigen on T cells and stimulation of interleukin 1 and 2 production in an autocrine or paracrine manner (*221*). On the other hand, it has been shown that, e.g., proinflammatory interleukins play an important role in depression (*321*). Thus, the bi-directional relationship between the brain and immune system involves the perspective that CRH/CRHR1 antagonists with a central anti-inflammatory mechanism of action, represent a new generation of antidepressants (*322*) and also conversely, CRHR1 antagonists open new therapeutic options in the treatment of allergic conditions or lower gastro-intestinal inflammatory diseases such as inflammatory bowel syndrome and ulcerative colitis, that have been associated to CRH (*323*). As mentioned above the new *Cre*-driver line enables genetic access to CRHR1 expressing cells in the periphery and facilitates further anatomical and functional studies in peripheral organ systems, especially in the context of stress-related pathophysiology.

7.3.3 AAV-mediated identification of neural circuits

Over the past decade, the development of viral vector-based genetic tools that allow for cell-type specific anterograde and retrograde tracing and for manipulation of specific neuronal cell types and circuits, have changed the scientific landscape significantly and offer enormous potential for modern neuroscience to decipher the intersection between genes and neural circuits (*188*). The use of viral vectors as tools for optogenetics, chemogenetics, cell type-specific manipulation of gene expression and expression of fluorescent calcium sensors has proven especially useful in studying the function and manipulation of the CRH system and CRH/CRHR1-specific neurocircuits, respectively (*9*). Recent findings suggest that region- and cell type-dependent CRHR1 signaling within neural networks plays a key role in mediating anxiety and stress-related psychopathologies and have lead to a

rethink with regard to the classical view of CRH-mediated activation being “all-aversive”/anxiogenic. Whereas forebrain glutamatergic CRH/CRHR1-modulated circuits increase anxiety, dopaminergic mesocorticolimbic pathways evoke a positive emotional/anxiolytic state (*99*). Other examples of bi-directional CRH/CRHR1 signaling include the nucleus accumbens, where activation of CRHR1 can induce opposing emotional states depending on discrete stress levels (*101*). Many of the studies that were applied to analyze brain region-specific roles of CRHR1 were based on conditional mutagenesis, pharmacological interventions, electrophysiological measurements and viral manipulations. Viral mediated tracing studies using a CRHR1 *Cre*-driver line provide spatio-temporal genetic access to CRHR1-specific neurons and their involvement in CRH circuits that mediate anxiety- and stress- related behaviors.

For example, AAV based tracing proved the participation of CRHR1-expressing neurons in the hippocampal trisynaptic circuit, in particular in the perforant path and hilar mossy cells. CRH/CRHR1 signaling amplifies neuronal excitation in the hippocampal formation (trisynaptic EC-DG-CA3-CA1 network) and is involved in stress-mediated modulation of learning and memory processes in a dose-dependent manner (*8*). Latest data based on viral-genetic tracing, electrophysiological recordings and photostimulation, support a modulatory role of hilar mossy cells on the activity of dentate granule cells (“granule cell association” hypothesis) and an important role in integrating excitatory input from the CA3 region to granule cells (*324*). Degeneration of hilar mossy cells resulted in acute granule cell hyperexcitability, thereby supporting the “dormant basket cell” hypothesis (net inhibitory effect of mossy cells on granule cells). Moreover, acute mossy cell neurodegeneration led to increased anxiety behavior and impaired contextual discrimination (*325*). The CRHR1 *Cre*-driver mouse line enables specific genetic targeting of CRHR1 expressing hilar mossy cells. The combination with new emerging techniques, such as *in vivo* two photon Ca^{2+} imaging, or optogenetic manipulation in combination with voltage sensitive dye imaging (*326, 327*), can help to decipher the role of CRHR1 in modulating DG-CA3 network activity. Moreover, it is possible to analyze the role of CRHR1 positive hilar mossy cells in hippocampus-associated learning and memory behaviors, post-traumatic epileptic seizures and stress-related effects on hippocampal morphology and function.

Conditional mutagenesis, namely CRHR1 knockout in dopaminergic neurons of the VTA, revealed an anxiolytic role for the receptor in this brain region and reduced the release of dopamine in the prefrontal cortex (*99*). Our comprehensive analysis of viral-based tracing strongly suggest the presence of axonal terminals in mesostriatal, mesolimbic and mesocortical projection sites that originate form monosynaptically projecting CRHR1-expressing neurons within the VTA. This probably indicates a widespread collateralization of these mesocorticolimbic projection neurons and a potential role of a CRHR1-specific subset of VTA neurons in modulating dopaminergic signaling simultaneously in cortical and limbic target sites. Additional experiments that unravel the exact localization, neurotransmitter co-expression and axonal arborization pattern of individual CRHR1-specific neurons are necessary to decipher the specific subset of CRHR1-positive dopaminergic neurons and their postsynaptic targets, that mediate anxiolysis. One option would be the use of a modified fluorescent marker (*palGFP*), as the fusion of *GFP* with a palmitoylation site (*palGFP*) was shown to enable visualization of infected neurons in a Golgi stain-like manner (*328-330*). Moreover, a dual-recombinase intersectional strategy, *Cre*- and *Flp*- dependent (*cDIO*, *fDIO)*, to turn on doubly controlled reporter alleles or opsins would allow for spatiotemporal manipulation of a specific neuronal subset within this highly complex and heterogeneous brain region. Fenno and colleagues combined "*fDIO"* and "*cDIO"* with projection-targeting strategies to target dopaminergic cells of the VTA that project to the nucleus accumbens (*210*). Based on this approach it would be conceivable to inject retrograde LTHSV-lox-STOP-lox-mCherry-*IRES*-Flp into putative mesocorticolimbic target sites of *CRHR1^{Cre}* mice. Only VTA neurons that are transduced by LT-HSV and express *Cre* (CRHR1 specific) will express *Flp* and can therefore activate ,e.g., viral transduced fDIO-Chr2-eYFP constructs within the VTA for subsequent optogenetic manipulations.

Finally, our anterograde tracing studies suggest an important role of CRH/CRHR1 signaling within corticostriatal and basal ganglia neurocircuits (Figure 36). There is growing evidence that aberrant functional connectivities within the striatum and associated cortico-basal ganglia circuits are associated with the neuropathology of mood disorders (*246, 331, 332*). In general, information originating from the cerebral cortex is transmitted first to the basal ganglia, then on to the thalamus and finally back to numerous cortical areas where the input information is processed in cognitive, emotional, sensory and motor domains. Information flow can either be

direct/net effect excitatory (cortex ► caudoputamen ► globus pallidus internal segment/substantia nigra pars reticulata ► thalamus ► cortex), or indirect/net effect inhibitory (cortex ► caudoputamen ► globus pallidus externa ► subthalamic nucleus ► globus pallidus internal segment/substantia nigra pars reticulata ► thalamus ► cortex). In healthy subjects, a dynamically balanced neural tone in both pathways allow for appropriate behavioral execution and termination. CRHR1 is expressed in main structures of these circuits: in glutamatergic cortical neurons, GABAergic striatal neurons, in GABAergic neurons within the globus pallidus externa and in GABAergic neurons of the reticular thalamic nucleus, the latter playing a key role in integrating sensory information between the thalamus and cortex. Functional MRI and connectivity analyses lead to the conclusion that primary pathology of unipolar depression exists within subcortical components and/or altered connectivity with cortical regions. Additional studies hypothesized that decreased excitatory drive to the orbitofrontal cortex, as net consequence of reduced striatal GABAergic output underlies the etiology of bipolar disorders (*246, 332*). Up to now, there is no clear evidence for an exclusive region-specific role of CRHR1 within components of corticostriatal and basal ganglia neurocircuits in stress-related psychopathologies. CRH/CRHR1 signaling exhibits anxiolytic-like effects in the frontal cortex of rats (*333*). In mice, stress impairs mPFC-mediated cognition through CRH/CRHR1 interaction (*239*). Genetic downregulation and pharmacological blocking of CRHR1 in GABAergic neurons of the GPe results in an increased anxiety-like behavior (*162*). Recent work suggests an important role of striatal GABAergic interneurons in regulating the two main output pathways in response to a global dopamine signal (*240, 241*). CRHR1^{tZ}-reporter mice revealed that CRHR1 neurons in the striatal patch compartment are positive for the D1 dopamine receptor (*41*). Viral based tracing results in CRHR1^{Cre} mice demonstrated the locally projecting nature of these neurons. Taken together, we speculate on an important role of CRHR1, expressed on GABAergic/D1 positive interneurons in the striatum (input nucleus of the basal ganglia circuitry), with regard to regulation of GABAergic medium spiny neurons. The precise function of interneuronal and reciprocal striatopallidal inhibition in the striatum needs to be further evaluated. Moving forward, the CRHR1 *Cre*-driver will enable to study and manipulate the basal ganglia on a cell-specific circuit level, which is a prerequisite to better understand how cell types interact in modulation of emotional behavior.

7.4 Viral - mediated upregulation of CRHR1 in the VTA results in an anxiolytic phenotype

For a long time the research focus has been on hippocampal and frontal cortical circuits for their role in mood disorders and antidepressant treatment, whereas the mesocortibolimbic dopamine circuits were often associated with the rewarding effects of food, sex and drugs of abuse. Over time the VTA-associated reward and addiction circuits have gained attention from the scientific community with regard to their involvement in the etiology and treatment of depression (*102*). Based on defined genetic tools previous studies in our group revealed an anxiolytic role for a subpopulation of dopaminergic neurons expressing CRHR1 in the VTA (*99*). To test the hypothesis that enhanced CRH/CRHR1 signaling in the VTA modulates stress-related emotional behavior we used the *CRHR1*^{Cre} mouse line to express a constitutively active version of CRHR1 fused to EGFP, AAV-DIO-CA(CRHR1)-EGFP, specifically in CRHR1-expressing VTA neurons. CA(CRHR1) mice exhibited decreased anxiety-related behavior in the DaLi- and EPM test compared to controls (Figure 42). Collectively, our results confirmed an anxiety-suppressing CRH/CRHR1 mesocortical circuit that acts by positively regulating dopamine release. So far, studies have mainly focused on stress-related/CRH-induced region-specific effects in the context of modulation of drug-dependent behaviors (for review see (*8*)). In summary, the various surveys led to the conclusion, that the effects of CRH on dopamine release seem to be pathway-specific and that a specific subpopulation of VTA CRHR1 expressing neurons mediates anxiety-related behavior. With the use of a CRHR1-EGFP knock-in reporter line (*Crhr1*$^{\Delta EGFP}$) in combination with a neurotransmitter-specific CRHR1 conditional knock-out mouse line (*Crhr1*$^{Da\text{-}CKO}$) we could show that the majority of CRHR1 neurons in the VTA represent dopaminergic neurons and, moreover, a *tau-lacZ* CRHR1 reporter line indicated strong CRHR1 innervation of the dorsal and ventral striatum originating from dopamine transporter (DAT) positive neurons (*41*). The use of the CRHR1 *Cre*-driver line in combination with a viral-based anterograde tracing technique allows for cell-type specific monosynaptic anterograde tracing and revealed mesostriatal, mesolimbic and mesocortical projection sites.

To further characterize the specific-subpopulation of CRHR1 neurons within the VTA that mediates the anxiolytic behavioral phenotype in the gain-of-function experiment, we performed neurochemical characterization in *CRHR1*$^{CA(CRHR1)}$ mice on protein and

mRNA level through double immunohistochemistry and DISH with antibodies/riboprobes specific for *GFP* and *TH* or *Gad65/67*, respectively. DISH revealed a co-expression of CRHR1 with *TH* and *Gad65/67*, however, it must be noted that this approach does not reveal CRHR1 neurons that co-express both neurotransmitter markers. Recently Kim and colleagues revealed that dopamine neurons can synthesize GABA through an alternative synthesis pathway via aldehyde dehydrogenase 1a1 (not utilizing the conventional GABA synthesizing enzymes *GAD65/67*). GABA is then "co-packaged" with dopamine into vesicles, indicating the possibility of co-release at the same side/from the same synaptic vesicle (*334*). Another study reported co-release of GABA/dopamine in mesolimbic afferents, whereby GABA release relies on GABA uptake from the extracellular domain and is not synthesized *de novo* by these cells as they lack *GAD65/67* expression (*335*). Our DISH results indicate the presence of *GAD65/67* mRNA in neurons expressing the CRHR1 in the pVTA. Whether this is a distinct solely GABAergic CRHR1 positive subpopulation, or a subtype of dopaminergic neurons that synthesize GABA via *GAD65/67* is not clear at the moment. A triple IHC against GFP/GAD/TH is necessary to quantify the respective populations of dopaminergic neurons.

Quantification on protein level demonstrated co-expression of TH in ~65% of neurons positive for CRHR1. The latter result is not consistent to the deletion pattern analyzed in "floxed" CRHR1 mice, that were crossed with *Dat-cre/ER*^{T2}, to selectively disrupt CRHR1 in midbrain dopaminergic neurons. Semi-quantitative analyses of neurotransmitter-specific deletion patterns provided no clear evidence for a deletion in GABAergic CRHR1 neurons, but most likely such subtle changes in a small subset of neurons within a brain region that exhibits high anatomical, molecular and functional complexity, are not detectable by means of mRNA detection. It is of note that a *Cre*-line driven by the promoter for DAT also targets TH/GABA co-releasing neurons. Thus, the anxiogenic behavioral phenotype is most likely dependent on the co-release of both neurotransmitters.

In single-cell axon tracing analysis four subtypes of forebrain-projecting dopaminergic VTA neurons were identified: "mesocorticolimibic" (target areas neocortex, basal forebrain); "mesocortical" (target area neocortex), "mesolimbic" (target areas basal forebrain, nucleus accumbens and striatum), "mesostriatal" (target area striatum). In addition, there is evidence for segregated mesocortical and mesolimbic output

systems as well as a distinct mesocorticolimbic output system. The latter comprise VTA neurons that simultaneously innervate cortical and limbic brain structures and arise mostly from the PBP (*250*). Furthermore, there is behavioral evidence for functional differences between the anterior and posterior VTA subdivisions (*91, 257*). In addition, studies that have used measurement of calcium dynamics in dopaminergic axon terminals within the mPFC or nucleus accumbens, have demonstrated that dopaminergic terminals in the NAc exhibit increased activity to a rewarding stimulus, whereas dopaminergic terminals in the mPFC showed increased calcium dynamics/activity in response to an aversive stimulus, which adds another level of complexity.

Taken together, the combination of information about the anatomical distribution (CA(CRHR1) neurons mainly in pVTA subdivisions), neurotransmitter content (65% GFP/CRHR1 neurons that are positive for TH; potential co-expression of GAD65/67), projecting patterns (target regions dorsal and ventral striatum, PFC) and behavioral anxiolytic phenotype, defines a subset of dopaminergic CRHR1 neurons within the VTA that modulates emotional behavior. At the moment we can only speculate on a mesocorticolimbic subcircuit that simultaneously targets the mPFC and the basal forebrain (NAc, Cpu) and by this represents an integrative hub for processing of aversive stimuli.

Future experiments are needed to determine which afferent VTA pathways activate this specific subcircuit that acts anxiolytic by modulating dopamine release in the prefrontal cortex. The VTA neurons receive direct input from diverse excitatory, inhibitory, and modulatory afferents and exhibit specific input-output relationships (*84*). Amongst them, the BNST and amygdala play a central role in modulating anxiety and recent results provide evidence for an anxiolytic GABAergic BNST ► VTA circuit (*336*). Moreover, the neurochemical identity of BNST neurons is correlated to functional differences and the identification of the respective anxiolytic neuronal subtype has to be addressed in the future (*68, 337*). In this line, we recently identified a subset of CRH expressing GABAergic long-range projection neurons that acts anxiolytic by modulating dopamine release in the prefrontal cortex (*100*).

The CRHR1 *Cre*-driver will allow a number of sophisticated experiments, which combine cell-type specific optogenetic/pharmacogenetic manipulations in a projection-specific manner, to dissect the cellular and anatomic heterogeneity, as

well as to further parse out the molecular and cellular characteristics of CRHR1 neurons within the VTA, that mediate stress-related behavior (*338*). This will help to delineate specific dopaminergic subcircuits that are altered in stress-related mood disorders, as well as other neuropsychiatric disorders (e.g., Parkinson's disease, schizophrenia, substance abuse disorder), and opens up new avenues for the developing of novel therapeutic interventions.

7.5 Outlook

The generation of this novel CRHR1 allele specifically enables expression of *Cre* recombinase under the control of the endogenous CRHR1 promoter, thereby representing an essential tool for dissecting the CRH/CRHR1 system at the circuit level. It represents the next stage of a detailed analysis beyond brain region-dependent effects of CRHR1 activation. Numerous studies in recent years have demonstrated that CRH/CRHR1 circuits modulate emotional behavior in a bidirectional manner. Unraveling the precise subcircuits, as well as subcellular location and specific-downstream targets of CRHR1 and determination of neurochemical identities from neuronal CRHR1 subpopulations are challenges of the future. The combination of the CRHR1 *Cre*-driver line with latest techniques for anatomic tracing, neural manipulation and cell-type specific transcriptome characterization will help to address these open questions. The following paragraphs will give a brief overview of possible approaches:

AAVs have become indispensable tools for functional dissection of neurocircuits. Anterograde or retrograde viral-mediated gene transfer can be used to deliver *Cre*-dependent light-activated channels (optogenetics), designer receptors (DREADDS) and genetically encoded calcium indicators (GECIs) for specific manipulation and imaging of neural activity *in vivo*. In addition, AAVs can deliver genome-editing tools (CRISPR) for acute manipulation of gene expression. Additionally, the CRISPR technique would allow for rapid generation of mice expressing various recombinase variants, such as *CreER*^{T2}, *split-Cre*, *Flp* or *Dre* under control of the CRHR1 promoter. This would expand the genomic toolbox and allow for multiple intersectional approaches, e.g., with available CRH-*IRES*-*Cre* lines or other *Cre*- and *Flp*-drivers.

New technologies for cell type-specific labeling of synapses *in vivo* allow for illumination of afferent synaptic partners. The GFP/CFP reconstitution across synaptic partners (GRASP/CRASP) technique can be used to detect the location of synapses. It is based on two complementary split-GFP/CFP fragments, that are *per se* non-fluorescent. When two neurons, each expressing one of the fragments, are closely opposed across a synaptic cleft, fluorescent GFP/CFP is reconstituted in that location and indicates the size, number and subcellular positions of synapses. By this, one can think of building up a CRH/CRHR1-specific "synaptogram", thus revealing stress-related neurocircuits, by combination of *Cre and Flp* recombinase–dependent viral vectors that allow for *Cre/Flp*-specific expression of pre- and post-mGRASP components.

The RiboTag method allows isolation of mRNA from a specific cell population in complex tissue, including the brain. The RiboTag mouse has a targeted mutation of the ribosomal protein L22 locus. This line is compatible with any *Cre*-driver line and *Cre*- induced recombination results in a HA epitope-tagged ribosomal protein and allows for subsequent immunoprecipitation of ribosomes bound to mRNA from CRHR1-specific cell types. Moreover, AAV vectors containing a *Cre*-dependent expression cassette for the tagged ribosomal protein Rpl22 (AAV1-EF1α-Rpl22-HA) can be used for targeting very specific brain nuclei. By replacing the EF1α promoter with neurotransmitter-specific promoters, it would be possible to target dopaminergic neurons within such heterogeneous nuclei as the VTA. By this it can be used ,e.g., for monitoring CRHR1 dependent pharmacological- or stress- regulated transcriptome changes or molecular profiling of regional differences in CRHR1-specific gene expression.

For cell type-specific epigenomic studies, the *Cre*-driver line can be crossed to the R26-CAG-LSL-Sun1-sfGFP knock-in mouse line and used for "INTACT" (isolation of nuclei tagged in specific cell types, see chapter 6.5.3). In brief, CRHR1-dependent expression of *Cre* recombinase leads to removal of a transcriptional STOP cassette and expression of the SUN1-sfGFP fusion protein at the inner nuclear membrane in CRHR1 expressing cells. Nuclei form these cells could then be purified and used for cell type-specific measurement of the gene expression and chromatin profiles. To summarize, both methods facilitate analysis of cell type-specific molecular adaptations underlying CRHR1-mediated signaling and can also be used to explore

cell type-specific transcriptomics and epigenomics after acute or chronic stress or in diverse mouse models of neuropsychiatric disorders.

To summarize, the CRH/CRHR1 system modulates physiological and behavioral adaptation to a variety of stimuli in a brain region-, circuit- and cell type-specific manner. The established CRHR1 *Cre*-driver line will help to decipher dynamic stress-related changes under physiological and maladaptive conditions. This is a prerequisite for the development of new/more effective medical treatments of mood-related disorders.

8 Summary

Background: The corticotropin-releasing hormone (CRH) and its type 1 receptor (CRHR1) play a central role in coordinating the endocrine, autonomic and behavioral responses to stress. A prerequisite to functionally dissect the complexity of the CRH/CRHR1 system is to unravel the identity of CRHR1 expressing neurons and their connectivities. Along these lines, transgenic fluorescent protein (*GFP*) reporter mouse lines based on bacterial artificial chromosomes (BACs) have been developed for CRH, CRHR1 and CRHR2 (*105, 219, 339*). However, even BAC-based transgenesis can suffer from partial lack of regulatory sequences required for correct temporal and spatial expression or from secondary positional effects caused by enhancers/repressors near to the site of transgene integration. To overcome the potential limitations a knock-in mouse line, expressing *GFP* under the control of the endogenous CRHR1 promoter was generated (*99*). Unfortunately, the sensitivity of *eGFP* is relatively limited in particular when it comes to detection of endogenous expression levels. Another widely used reporter is *lacZ* encoding for β-galactosidase which has proven as a highly sensitive histochemical marker which can be easily visualized by X-gal staining and readily detects low levels of endogenous gene expression. The possibility to visualize CRHR1 expressing neurons and their connectivities in the *lacZ*-CRHR1 reporter line constituted an important next step to functionally dissect the complexity of the CRH/CRHR1 system (*41*). Newly advanced technologies in neural tracing, neural manipulation and cell-type specific transcriptome analysis are mostly dependent on *Cre*- and/or *Flp*-mediated recombination and therefore required expansion of the genetic toolbox related to the "CRH-family". The aim of this thesis was the generation and characterization of a novel CRHR1 allele, that enables the specific expression of *Cre* recombinase under the control of the endogenous CRHR1 promoter. It represents the next higher level to assess and decipher the CRH/CRHR1 system at the circuit level and comprises the possibility for the cell type-specific genetic manipulation of stress-related neural circuits.

Results: A *Cre* targeting vector was engineered and applied via recombinase mediated cassette exchange (RMCE) to generate a novel *Cre* knock-in mouse line with constitutive *Cre* recombinase activity restricted to CRHR1-expressing cells. The first offspring (*CRHR1^{tZCre}* mouse line) revealed an alternative recombination event,

which resulted in *Cre* activity in a subpopulation of CRHR1 expressing neurons only due to a *tau-lacZ* reporter cassette, which remained at the targeting site. In parallel, the reporter and the hygromycin selection cassette were removed by breeding to a mouse line expressing the enhanced variant of the site-specific recombinase *Flp*. As the first step in characterizing the novel *Cre*-driver lines, *CRHR1^{tzCre}* and *CRHR1^{Cre}*, respectively, expression of the endogenous CRHR1 transcript was compared to that of *Cre* and the *Cre*-dependent reporter *tdTomato*. In situ hybridization revealed a subset expression in the *CRHR1^{tzCre}* mouse line, whereas expression in the *CRHR1^{Cre}* line exhibited highest specificity for CRHR1 expressing cells. Moreover, the high efficiency of *Cre*-mediated recombination was revealed by absence of CRHR1 transcripts on brain sections from a mouse line harboring a targeted ("floxed") CRHR1 allele. In a second step, the central and peripheral *Cre* activity was assessed in *CRHR1^{Cre}* mice bred to two different reporter lines, expressing the fluorescent proteins *tdTomato* and *sfGFP*, respectively. In these dual transgenic mice, the pattern of reporter gene expression matched that of CRHR1 in the brain and periphery and additionally revealed sites of developmentally restricted expression of *Cre.* In addition, *tdTomato* expression was detectable in peripheral organs which had not been described in the mouse so far, including the kidney and most probably immune cells of the duodenum, tongue, thymus, spleen, liver and lung. Adeno-associated viral vectors (AAVs) were applied to test for current *Cre* expression and only very limited or absent expression of CRHR1 was detectable in the CeA, the LC and the PVN, a result which is in contrast to other studies in mouse and rat and topic of an ongoing discussion in the field. Viral-mediated tracing analyses were performed to dissect limbic forebrain neurocircuits. Anterograde tracing of CRHR1 neurons revealed axonal projections within the corticostriatal pathway and within basal ganglia circuits. Moreover, CRHR1 is expressed in glutamatergic mossy cells within the polymorph layer of the dentate gyrus that synapse on the dendrites of granule cells. In order to address the role of CRHR1 in mesencephalic neurons in the context of emotional behavior, viral vector based tracing studies and a gain-of-function experiment were conducted using a constitutively active version of the CRHR1, which was *Cre*-dependently expressed in the VTA. Strong expression of the *mCherry* reporter gene in the striatum, nucleus accumbens and prefrontal cortex, suggests the presence of axonal terminals in mesostriatal, mesolimbic and mesocortical projection sites that originate from

monosynaptically projecting dopaminergic and/or GABAergic CRHR1-expressing neurons within the VTA. Finally, anxiety-related behavior was evaluated in the open-field test, elevated plus maze test and in the dark-light box and the obtained results allowed us to conclude that CRHR1-signaling in a subpopulation of mesocorticolimbic projection neurons within the VTA mediates an anxiolytic phenotype. This result complements observations from conditional inactivation of CRHR1 in midbrain dopaminergic neurons.

Conclusion: This new *Cre* mouse line represent a valuable complement to the existing genetic tool box addressing “CRH-family” members and enables a variety of sophisticated experiments with lately advanced technologies, which will contribute to a more precise analysis of CRH/CRHR1 pathways on the functional and circuit level in the brain and periphery.

9 Zusammenfassung

Generierung einer CRHR1-spezifischen *Cre* Mauslinie zur Analyse von CRH/CRHR1-regulierten neuronalen Schaltkreisen

Hintergrund: Das Corticotropin-Releasing-Hormon (CRH) und sein Typ 1 Rezeptor (CRHR1) spielen eine zentrale Rolle bei der Koordinierung der endokrinen, autonomen und verhaltensbezogenen Reaktionen auf Stress. Eine Voraussetzung um die Komplexität des CRH/CRHR1-Systems funktionell zu analysieren besteht darin, die Identität von CRHR1 exprimierenden Neuronen und deren neuronale Verschaltungen zu entschlüsseln. Deshalb wurden in der Vergangenheit mit Hilfe von künstlichen Bakterienchromosomen (BACs) GFP-Reporterlinien für CRH, CRHR1 und CRHR2 entwickelt. Bei der BAC-basierten Technologie zur Erzeugung einer transgenen Mauslinie kann es durch das Fehlen von regulatorischen Sequenzen oder durch Positionseffekte in der Nähe des Integrationsortes zur unspezifischen Expression des Fluoreszenzproteins kommen. Deshalb wurde eine weitere *GFP*-Reporterlinie generiert, in der durch homologe Rekombination ein *GFP*-CRHR1 Fusionsprotein unter der Kontrolle des endogenen Promoters exprimiert wird. Bedingt durch die Schwäche der nativen *GFP*-Fluoreszenz können Neurone mit niedriger CRHR1 Expression nur sehr schwer detektiert werden. Um dies zu umgehen, wurde eine weitere Mauslinie generiert, in der das Enzym Beta-Galactosidase – ein hochempfindlicher histochemischer Marker – unter der Kontrolle des endogenen CRHR1 Promotors exprimiert wird. Die Möglichkeit, CRHR1-exprimierende Neurone und deren Schaltkreise sichtbar zu machen, ist ein wichtiger nächster Schritt, um die Komplexität des CRH/CRHR1-Systems zu entschlüsseln. Im Laufe der letzten Jahre wurden viele neue Technologien für die Neuroanatomie, die Manipulation neuronaler Schaltkreise und die Transkriptom-Analyse entwickelt, die meistens auf dem *Cre/loxP* bzw. *Flp/frt* Rekombinations-System beruhen und daher eine Erweiterung der „genetischen Werkzeugkiste“ für Mitglieder der „CRH-Familie“ erforderlich machten. Das Ziel dieser Arbeit war die Generierung und Charakterisierung eines neuen CRHR1 Allels, dass die Expression der *Cre*-Rekombinase unter der Kontrolle des endogenen CRHR1 Promotors ermöglicht. Es stellt die nächsthöhere Ebene dar, um neuronale CRH/CRHR1 Netzwerke

anatomisch und funktional zu entschlüsseln und beinhaltet die Möglichkeit der spezifischen Manipulation stressbezogener neuronaler Schaltkreise.

Ergebnisse: Ein entsprechender *Cre* Vektor wurde konstruiert und mittels Rekombinase abhängigem Kassettenaustausch (RMCE) in das Genom integriert, um dadurch eine neue knock-in Mauslinie zu erzeugen, in der die *Cre* Rekombinase Aktivität auf CRHR1 exprimierende Zellen beschränkt ist. Durch ein alternatives Rekombinationsereignis zeigen die Nachkommen der ersten Mauslinie (*CRHR1^{tZCre}*) nur in einem Teil der CRHR1 exprimierenden Neurone *Cre* Aktivität. Dies ist auf eine noch vorhandene *tau-lacZ* Reporterkassette an der Integrationsstelle zurückzuführen. Die Reporterkassette und parallel die Hygromycin Selektionskassette wurde durch Einkreuzen einer *Flp*-exprimierenden Mauslinie entfernt. Zuerst wurde in beiden Cre Linien - *CRHR1^{tZCre}* und *CRHR1^{Cre}* - die Expression des endogenen CRHR1-Transkripts mit der Expression von *Cre* und einem *Cre*-abhängigen Reporterprotein (*tdTomato*) auf der RNA Ebene (ISH) verglichen. Die Auswertung der ISH Daten zeigte eine sehr hohe Spezifität der *CRHR1^{Cre}* Linie an, wohingegen *Cre* in der *CRHR1^{tZCre}* Linie nur in einem Teil der CRHR1 positiven Zellen exprimiert wird. Darüber hinaus bewies die *CRHR1^{Cre}* Linie eine sehr hohe Effizienz in der Rekombination eines „gefloxten“ CRHR1 Allels, da auf Gehirnschnitten keine CRHR1 mRNA Transkripte nachweisbar waren. Im nächsten Schritt wurde die Rekombinase-Aktivität im Gehirn und in der Peripherie untersucht, indem die *CRHR1^{Cre}* Linie mit zwei Reporterlinien gekreuzt wurde, in der die fluoreszierenden Reporterproteine *tdTomato* und *sfGFP* nach *Cre*-abhängiger Entfernung einer Stopp-Kassette exprimiert werden. Das Muster der Reportergenexpression stimmt mit dem vom CRHR1 in adulten Mäusen überein und dokumentiert zusätzlich auch eine transiente Expression von *Cre* während der Entwicklung. Darüber hinaus war das *tdTomato* auch in peripheren Organen sichtbar, die bisher so noch nicht in der Maus beschrieben waren, nämlich in der Niere und sehr wahrscheinlich in Immunzellen die im Epithel vom Dünndarm, Zunge und Lunge lokalisiert sind, sowie in Makrophagen und Lymphozyten von Thymus, Milz und Leber. Adeno-assoziierte virale Vektoren (AAVs) wurden verwendet, um die Expression von *Cre* im Gehirn von adulten Tieren zu untersuchen. Es wurde nur eine sehr begrenzte bzw. keine Expression von CRHR1 in der CeA, dem LC und im PVN nachgewiesen. Dies ist ein Ergebnis das im Widerspruch zu anderen Studien in Maus und Ratte steht und Gegenstand einer anhaltenden und kontroversen

Diskussion auf diesem Gebiet ist. Weiterhin wurden anterograde Projektionen von CRHR1 Neuronen untersucht, um neuronale Schaltkreise im limbischen System des Vorderhirns zu entschlüsseln. Die Auswertung legt nahe, dass CRHR1 Axone aus dem präfrontalen Cortex ins Striatum projizieren und Synapsen innerhalb der Basalganglienschleife aufweisen. Darüber hinaus wird CRHR1 innerhalb des Hippocampus in glutamatergen Mooszellen exprimiert; diese Mooszellen sind in der polymorphen Schicht des Gyrus dentatus lokalisiert und projizieren auf Dendriten der Körnerzellschicht des Gyrus dentatus. Um die Rolle von CRHR1 Neuronen im Mittelhirn im Zusammenhang mit emotionalem Verhalten zu untersuchen, wurden einerseits anterograde Projektionsgebiete von CRHR1 Neuronen aus der VTA ermittelt und zum anderen ein konstitutiv aktiver CRHR1 in Abhängigkeit der *Cre* Rekombinase exprimiert, was gleichbedeutend mit einer Liganden-unabhängigen Rezeptoraktivierung ist. Die Expression des *mCherry* Reportergens im Striatum, Nucleus accumbens und präfrontalen Cortex deutet auf das Vorhandensein von synaptischen Verschaltungen in mesostriatalen, mesolimbischen und mesokortikalen Projektionsgebieten hin, die von einer dopaminergen und/oder GABAergen Subpopulation CRHR1 exprimierender Neurone innerhalb der VTA stammen. Zum Schluss wurde angstbezogenes Verhalten dieser Tiere in einer Reihe von standardisierten Verhaltenstest untersucht. Die Ergebnisse lassen den Schluss zu, dass spezifische CRHR1-kontrollierte Schaltkreise zwischen der VTA und dem präfrontalem Cortex, bzw. limbischen System für die Äußerung positiver emotionaler Reaktionen verantwortlich sind. Dieses Ergebnis steht im Einklang mit Versuchen in denen der CRHR1 in dopaminergen Neuronen des Mittelhirns inaktiviert wurde.

Schlussfolgerung: Diese neue Mauslinie, die die *Cre* Rekombinase spezifisch in CRHR1 Neuronen exprimiert, stellt eine wertvolle Ergänzung der bereits existierenden „genetischen Werkzeuge“ für Mitglieder der CRH-Familie dar und bietet die Möglichkeit, unter Zuhilfenahme von neuesten Technologien, die CRH/CRHR1-Schaltkreise im zentralen und peripheren Nervensystem mit einer bisher nicht möglichen Genauigkeit anatomisch und funktional zu untersuchen.

10 References

1. S. J. Cooper, From Claude Bernard to Walter Cannon. Emergence of the concept of homeostasis. *Appetite* **51**, 419-427 (2008).
2. H. SELYE, Stress and disease. *Science* **122**, 625-631 (1955).
3. B. S. McEwen, Protection and damage from acute and chronic stress: allostasis and allostatic overload and relevance to the pathophysiology of psychiatric disorders. *Ann N Y Acad Sci* **1032**, 1-7 (2004).
4. B. S. McEwen, Physiology and neurobiology of stress and adaptation: central role of the brain. *Physiol Rev* **87**, 873-904 (2007).
5. M. Joëls, T. Z. Baram, The neuro-symphony of stress. *Nat Rev Neurosci* **10**, 459-466 (2009).
6. W. Vale, J. Spiess, C. Rivier, J. Rivier, Characterization of a 41-residue ovine hypothalamic peptide that stimulates secretion of corticotropin and beta-endorphin. *Science* **213**, 1394-1397 (1981).
7. S. W. Jeon, Y.-K. Kim, Molecular Neurobiology and Promising New Treatment in Depression. *International Journal of Molecular Sciences* **17**, 381 (2016).
8. M. J. A. G. Henckens, J. M. Deussing, A. Chen, Region-specific roles of the corticotropin-releasing factor-urocortin system in stress. *Nat Rev Neurosci* **17**, 636-651 (2016).
9. N. Dedic, A. Chen, J. M. Deussing, The CRF family of neuropeptides and their receptors - mediators of the central stress response. *Curr Mol Pharmacol*, (2017).
10. P. Y. Collins *et al.*, Grand challenges in global mental health. *Nature* **475**, 27-30 (2011).
11. C. B. Nemeroff *et al.*, Elevated concentrations of CSF corticotropin-releasing factor-like immunoreactivity in depressed patients. *Science* **226**, 1342-1344 (1984).
12. C. B. Nemeroff, M. J. Owens, G. Bissette, A. C. Andorn, M. Stanley, Reduced corticotropin releasing factor binding sites in the frontal cortex of suicide victims. *Arch Gen Psychiatry* **45**, 577-579 (1988).

13. F. Holsboer, U. Von Bardeleben, A. Gerken, G. K. Stalla, O. A. Müller, Blunted corticotropin and normal cortisol response to human corticotropin-releasing factor in depression. *N Engl J Med* **311**, 1127 (1984).
14. F. Holsboer, M. Ising, Central CRH system in depression and anxiety--evidence from clinical studies with CRH1 receptor antagonists. *Eur J Pharmacol* **583**, 350-357 (2008).
15. E. B. Binder, C. B. Nemeroff, The CRF system, stress, depression and anxiety-insights from human genetic studies. *Mol Psychiatry* **15**, 574-588 (2010).
16. E. R. de Kloet, M. Joëls, F. Holsboer, Stress and the brain: from adaptation to disease. *Nat Rev Neurosci* **6**, 463-475 (2005).
17. H. Selye, A syndrome produced by diverse nocuous agents. 1936. *J Neuropsychiatry Clin Neurosci* **10**, 230-231 (1998).
18. S. Ramamoorthy, J. A. Cidlowski, Corticosteroids: Mechanisms of Action in Health and Disease. *Rheum Dis Clin North Am* **42**, 15-31 (2016).
19. A. Munck, P. M. Guyre, N. J. Holbrook, Physiological functions of glucocorticoids in stress and their relation to pharmacological actions. *Endocr Rev* **5**, 25-44 (1984).
20. R. M. Sapolsky, Stress hormones: good and bad. *Neurobiol Dis* **7**, 540-542 (2000).
21. S. M. Smith, W. W. Vale, The role of the hypothalamic-pituitary-adrenal axis in neuroendocrine responses to stress. *Dialogues Clin Neurosci* **8**, 383-395 (2006).
22. J. M. Reul, E. R. de Kloet, Two receptor systems for corticosterone in rat brain: microdistribution and differential occupation. *Endocrinology* **117**, 2505-2511 (1985).
23. P. E. Sawchenko, Evidence for a local site of action for glucocorticoids in inhibiting CRF and vasopressin expression in the paraventricular nucleus. *Brain Res* **403**, 213-223 (1987).
24. L. Jacobson, R. Sapolsky, The role of the hippocampus in feedback regulation of the hypothalamic-pituitary-adrenocortical axis. *Endocr Rev* **12**, 118-134 (1991).
25. M. E. Keller-Wood, M. F. Dallman, Corticosteroid inhibition of ACTH secretion. *Endocr Rev* **5**, 1-24 (1984).

26. F. Holsboer, The corticosteroid receptor hypothesis of depression. *Neuropsychopharmacology* **23**, 477-501 (2000).
27. L. Stojanovich, D. Marisavljevich, Stress as a trigger of autoimmune disease. *Autoimmun Rev* **7**, 209-213 (2008).
28. C. E. Keegan *et al.*, Expression of corticotropin-releasing hormone transgenes in neurons of adult and developing mice. *Mol Cell Neurosci* **5**, 505-514 (1994).
29. K. Van Pett *et al.*, Distribution of mRNAs encoding CRF receptors in brain and pituitary of rat and mouse. *J Comp Neurol* **428**, 191-212 (2000).
30. B. A. S. Reyes, D. A. Bangasser, R. J. Valentino, E. J. Van Bockstaele, Using high resolution imaging to determine trafficking of corticotropin-releasing factor receptors in noradrenergic neurons of the rat locus coeruleus. *Life sciences* **112**, 2-9 (2014).
31. Y. Sztainberg, A. Chen, in *Handbook of Neuroendocrinology,* D. W. Pfaff, J. E. Levine, Eds. (Academic Press, San Diego, 2012), pp. 355-375.
32. A. F. Mello, M. F. Mello, L. L. Carpenter, L. H. Price, Update on stress and depression: the role of the hypothalamic-pituitary-adrenal (HPA) axis. *Rev Bras Psiquiatr* **25**, 231-238 (2003).
33. D. F. Swaab, A. M. Bao, P. J. Lucassen, The stress system in the human brain in depression and neurodegeneration. *Ageing Res Rev* **4**, 141-194 (2005).
34. R. P. Waters *et al.*, Evidence for the role of corticotropin-releasing factor in major depressive disorder. *Neuroscience and biobehavioral reviews* **58**, 63-78 (2015).
35. P. W. Gold, The organization of the stress system and its dysregulation in depressive illness. *Mol Psychiatry* **20**, 32-47 (2015).
36. R. J. Valentino, E. Van Bockstaele, Convergent regulation of locus coeruleus activity as an adaptive response to stress. *European journal of pharmacology* **583**, 194-203 (2008).
37. G. Aston-Jones, C. A. Meijas-Aponte, B. Waterhouse, in *Encyclopedia of Neuroscience*. (Academic Press, Oxford, 2009), pp. 1237-1248.
38. T. J. Shors, Stressful Experience and Learning Across the Lifespan. *Annual Review of Psychology* **57**, 55-85 (2006).

39. E. J. Kim, B. Pellman, J. J. Kim, Stress effects on the hippocampus: a critical review. *Learning & Memory* **22**, 411-416 (2015).
40. Y. Chen *et al.*, HIPPOCAMPAL CORTICOTROPIN RELEASING HORMONE: PRE- AND POSTSYNAPTIC LOCATION AND RELEASE BY STRESS. *Neuroscience* **126**, 533-540 (2004).
41. C. Kühne *et al.*, Visualizing corticotropin-releasing hormone receptor type 1 expression and neuronal connectivities in the mouse using a novel multifunctional allele. *J Comp Neurol* **520**, 3150-3180 (2012).
42. G. von Wolff *et al.*, Voltage-sensitive dye imaging demonstrates an enhancing effect of corticotropin-releasing hormone on neuronal activity propagation through the hippocampal formation. *Journal of Psychiatric Research* **45**, 256-261 (2011).
43. S. Kratzer *et al.*, Activation of CRH receptor type 1 expressed on glutamatergic neurons increases excitability of CA1 pyramidal neurons by the modulation of voltage-gated ion channels. *Frontiers in Cellular Neuroscience* **7**, 91 (2013).
44. A. Medina *et al.*, Glucocorticoid and Mineralocorticoid Receptor Expression in the Human Hippocampus in Major Depressive Disorder. *Journal of psychiatric research* **47**, 307-314 (2013).
45. L. Givalois, S. Arancibia, L. Tapia-Arancibia, Concomitant changes in CRH mRNA levels in rat hippocampus and hypothalamus following immobilization stress. *Molecular Brain Research* **75**, 166-171 (2000).
46. Y. Chen, C. M. Dubé, C. J. Rice, T. Z. Baram, Rapid Loss of Dendritic Spines after Stress Involves Derangement of Spine Dynamics by Corticotropin-Releasing Hormone. *The Journal of neuroscience : the official journal of the Society for Neuroscience* **28**, 2903-2911 (2008).
47. Y. Chen, A. L. Andres, M. Frotscher, T. Z. Baram, Tuning synaptic transmission in the hippocampus by stress: the CRH system. *Frontiers in Cellular Neuroscience* **6**, 13 (2012).
48. K. J. Kovacs, CRH: the link between hormonal-, metabolic- and behavioral responses to stress. *J Chem Neuroanat* **54**, 25-33 (2013).
49. M. Segal, G. Richter-Levin, N. Maggio, Stress-induced dynamic routing of hippocampal connectivity: a hypothesis. *Hippocampus* **20**, 1332-1338 (2010).

50. G. MacQueen, T. Frodl, The hippocampus in major depression: evidence for the convergence of the bench and bedside in psychiatric research? *Mol Psychiatry* **16**, 252-264 (2011).
51. D.-J. Saaltink, E. Vreugdenhil, Stress, glucocorticoid receptors, and adult neurogenesis: a balance between excitation and inhibition? *Cellular and Molecular Life Sciences* **71**, 2499-2515 (2014).
52. Y. Koutmani *et al.*, Corticotropin-releasing hormone exerts direct effects on neuronal progenitor cells: implications for neuroprotection. *Mol Psychiatry* **18**, 300-307 (2013).
53. Y. Koutmani, K. P. Karalis, Neural stem cells respond to stress hormones: distinguishing beneficial from detrimental stress. *Frontiers in Physiology* **6**, 77 (2015).
54. D. L. Walker, M. Davis, Double dissociation between the involvement of the bed nucleus of the stria terminalis and the central nucleus of the amygdala in startle increases produced by conditioned versus unconditioned fear. *J Neurosci* **17**, 9375-9383 (1997).
55. G. F. Alheid, Extended amygdala and basal forebrain. *Ann N Y Acad Sci* **985**, 185-205 (2003).
56. M. Davis, Are different parts of the extended amygdala involved in fear versus anxiety? *Biol Psychiatry* **44**, 1239-1247 (1998).
57. A. J. Shackman, A. S. Fox, Contributions of the Central Extended Amygdala to Fear and Anxiety. *J Neurosci* **36**, 8050-8063 (2016).
58. T. Steimer, The biology of fear- and anxiety-related behaviors. *Dialogues in Clinical Neuroscience* **4**, 231-249 (2002).
59. D. L. Walker, D. J. Toufexis, M. Davis, Role of the bed nucleus of the stria terminalis versus the amygdala in fear, stress, and anxiety. *Eur J Pharmacol* **463**, 199-216 (2003).
60. M. Davis, D. L. Walker, L. Miles, C. Grillon, Phasic vs sustained fear in rats and humans: role of the extended amygdala in fear vs anxiety. *Neuropsychopharmacology* **35**, 105-135 (2010).
61. M. W. Pitts, C. Todorovic, T. Blank, L. K. Takahashi, The Central Nucleus of the Amygdala and Corticotropin-Releasing Factor: Insights into Contextual Fear Memory. *The Journal of neuroscience : the official journal of the Society for Neuroscience* **29**, 7379-7388 (2009).

62. C. A. Sanford *et al.*, A Central Amygdala CRF Circuit Facilitates Learning about Weak Threats. *Neuron*, (2016).
63. L. Regev, M. Tsoory, S. Gil, A. Chen, Site-specific genetic manipulation of amygdala corticotropin-releasing factor reveals its imperative role in mediating behavioral response to challenge. *Biol Psychiatry* **71**, 317-326 (2012).
64. E. Keen-Rhinehart *et al.*, Continuous expression of corticotropin-releasing factor in the central nucleus of the amygdala emulates the dysregulation of the stress and reproductive axes. *Molecular psychiatry* **14**, 37-50 (2009).
65. E. I. Flandreau, K. J. Ressler, M. J. Owens, C. B. Nemeroff, Chronic overexpression of corticotropin-releasing factor from the central amygdala produces HPA axis hyperactivity and behavioral anxiety associated with gene-expression changes in the hippocampus and paraventricular nucleus of the hypothalamus. *Psychoneuroendocrinology* **37**, 27-38 (2012).
66. M. P. Paulus, J. S. Feinstein, G. Castillo, A. N. Simmons, M. B. Stein, Dose-dependent decrease of activation in bilateral amygdala and insula by lorazepam during emotion processing. *Arch Gen Psychiatry* **62**, 282-288 (2005).
67. A. Etkin, T. D. Wager, Functional neuroimaging of anxiety: a meta-analysis of emotional processing in PTSD, social anxiety disorder, and specific phobia. *Am J Psychiatry* **164**, 1476-1488 (2007).
68. M. A. Lebow, A. Chen, Overshadowed by the amygdala: the bed nucleus of the stria terminalis emerges as key to psychiatric disorders. *Molecular Psychiatry* **21**, 450-463 (2016).
69. K. Itoi *et al.*, Visualization of Corticotropin-Releasing Factor Neurons by Fluorescent Proteins in the Mouse Brain and Characterization of Labeled Neurons in the Paraventricular Nucleus of the Hypothalamus. *Endocrinology* **155**, 4054-4060 (2014).
70. E. Potter *et al.*, Distribution of corticotropin-releasing factor receptor mRNA expression in the rat brain and pituitary. *Proc Natl Acad Sci U S A* **91**, 8777-8781 (1994).
71. J. Kono *et al.*, Distribution of corticotropin-releasing factor neurons in the mouse brain: a study using corticotropin-releasing factor-modified yellow fluorescent protein knock-in mouse. *Brain Struct Funct* **222**, 1705-1732 (2017).

72. K. S. Sink *et al.*, Effects of continuously enhanced corticotropin releasing factor expression within the bed nucleus of the stria terminalis on conditioned and unconditioned anxiety. *Mol Psychiatry* **18**, 308-319 (2013).
73. S. E. Daniel, D. G. Rainnie, Stress Modulation of Opposing Circuits in the Bed Nucleus of the Stria Terminalis. *Neuropsychopharmacology* **41**, 103-125 (2016).
74. J. A. Rinker *et al.*, Extended Amygdala to Ventral Tegmental Area Corticotropin-Releasing Factor Circuit Controls Binge Ethanol Intake. *Biological Psychiatry* **81**, 930-940 (2017).
75. S. N. Avery, J. A. Clauss, J. U. Blackford, The Human BNST: Functional Role in Anxiety and Addiction. *Neuropsychopharmacology* **41**, 126-141 (2016).
76. L. H. Somerville, P. J. Whalen, W. M. Kelley, Human bed nucleus of the stria terminalis indexes hypervigilant threat monitoring. *Biological psychiatry* **68**, 416-424 (2010).
77. T. Straube, H. J. Mentzel, W. H. Miltner, Waiting for spiders: brain activation during anticipatory anxiety in spider phobics. *Neuroimage* **37**, 1427-1436 (2007).
78. M. A. Yassa, R. L. Hazlett, C. E. L. Stark, R. Hoehn-Saric, Functional MRI of the amygdala and bed nucleus of the stria terminalis during conditions of uncertainty in generalized anxiety disorder. *Journal of psychiatric research* **46**, 1045-1052 (2012).
79. O. G. O'Daly *et al.*, Withdrawal-Associated Increases and Decreases in Functional Neural Connectivity Associated with Altered Emotional Regulation in Alcoholism. *Neuropsychopharmacology* **37**, 2267-2276 (2012).
80. L. Islam, A. Franzini, G. Messina, S. Scarone, O. Gambini, Deep Brain Stimulation of the Nucleus Accumbens and Bed Nucleus of Stria Terminalis for Obsessive-Compulsive Disorder: A Case Series. *World Neurosurgery* **83**, 657-663 (2015).
81. A. M. Polter, J. A. Kauer, Stress and VTA synapses: implications for addiction and depression. *Eur J Neurosci* **39**, 1179-1188 (2014).
82. E. N. Holly, K. A. Miczek, Ventral tegmental area dopamine revisited: effects of acute and repeated stress. *Psychopharmacology (Berl)* **233**, 163-186 (2016).

83. P. Belujon, A. A. Grace, Regulation of dopamine system responsivity and its adaptive and pathological response to stress. *Proc Biol Sci* **282**, (2015).

84. K. T. Beier *et al.*, Circuit Architecture of VTA Dopamine Neurons Revealed by Systematic Input-Output Mapping. *Cell* **162**, 622-634 (2015).

85. M. J. Wanat, F. W. Hopf, G. D. Stuber, P. E. M. Phillips, A. Bonci, Corticotropin-releasing factor increases mouse ventral tegmental area dopamine neuron firing through a protein kinase C-dependent enhancement of I (h). *The Journal of Physiology* **586**, 2157-2170 (2008).

86. E. D. Abercrombie, K. A. Keefe, D. S. DiFrischia, M. J. Zigmond, Differential effect of stress on in vivo dopamine release in striatum, nucleus accumbens, and medial frontal cortex. *J Neurochem* **52**, 1655-1658 (1989).

87. J. W. Tidey, K. A. Miczek, Social defeat stress selectively alters mesocorticolimbic dopamine release: an in vivo microdialysis study. *Brain Res* **721**, 140-149 (1996).

88. E. N. Holly *et al.*, Episodic Social Stress-Escalated Cocaine Self-Administration: Role of Phasic and Tonic Corticotropin Releasing Factor in the Anterior and Posterior Ventral Tegmental Area. *J Neurosci* **36**, 4093-4105 (2016).

89. D. J. Barker, D. H. Root, S. Zhang, M. Morales, Multiplexed neurochemical signaling by neurons of the ventral tegmental area. *J Chem Neuroanat* **73**, 33-42 (2016).

90. S. Pupe, A. Wallen-Mackenzie, Cre-driven optogenetics in the heterogeneous genetic panorama of the VTA. *Trends Neurosci* **38**, 375-386 (2015).

91. M. J. Sanchez-Catalan, J. Kaufling, F. Georges, P. Veinante, M. Barrot, The antero-posterior heterogeneity of the ventral tegmental area. *Neuroscience* **282**, 198-216 (2014).

92. T. E. Grieder *et al.*, VTA CRF neurons mediate the aversive effects of nicotine withdrawal and promote intake escalation. *Nat Neurosci* **17**, 1751-1758 (2014).

93. O. George, M. Le Moal, G. F. Koob, Allostasis and Addiction: Role of the Dopamine and Corticotropin-Releasing Factor Systems. *Physiology & behavior* **106**, 58-64 (2012).

94. E. P. Zorrilla, M. L. Logrip, G. F. Koob, Corticotropin releasing factor: a key role in the neurobiology of addiction. *Front Neuroendocrinol* **35**, 234-244 (2014).

95. S. J. Russo, E. J. Nestler, The brain reward circuitry in mood disorders. *Nat Rev Neurosci* **14**, 609-625 (2013).

96. V. Krishnan *et al.*, Molecular adaptations underlying susceptibility and resistance to social defeat in brain reward regions. *Cell* **131**, 391-404 (2007).

97. D. Chaudhury *et al.*, Rapid regulation of depression-related behaviours by control of midbrain dopamine neurons. *Nature* **493**, 532-536 (2013).

98. O. Valenti, K. M. Gill, A. A. Grace, Different stressors produce excitation or inhibition of mesolimbic dopamine neuron activity: response alteration by stress pre-exposure. *Eur J Neurosci* **35**, 1312-1321 (2012).

99. D. Refojo *et al.*, Glutamatergic and dopaminergic neurons mediate anxiogenic and anxiolytic effects of CRHR1. *Science* **333**, 1903-1907 (2011).

100. N. Dedic *et al.*, Chronic CRH depletion from GABAergic, long-range projection neurons in the extended amygdala reduces dopamine release and increases anxiety. *Nature neuroscience*, (2018).

101. J. C. Lemos *et al.*, Severe stress switches CRF action in the nucleus accumbens from appetitive to aversive. *Nature* **490**, 402-406 (2012).

102. E. J. Nestler, W. A. Carlezon, Jr., The mesolimbic dopamine reward circuit in depression. *Biol Psychiatry* **59**, 1151-1159 (2006).

103. T. E. Schlaepfer, B. H. Bewernick, S. Kayser, B. Madler, V. A. Coenen, Rapid effects of deep brain stimulation for treatment-resistant major depression. *Biol Psychiatry* **73**, 1204-1212 (2013).

104. R. L. Hauger, V. Risbrough, O. Brauns, F. M. Dautzenberg, Corticotropin releasing factor (CRF) receptor signaling in the central nervous system: new molecular targets. *CNS Neurol Disord Drug Targets* **5**, 453-479 (2006).

105. T. Alon *et al.*, Transgenic mice expressing green fluorescent protein under the control of the corticotropin-releasing hormone promoter. *Endocrinology* **150**, 5626-5632 (2009).

106. H. Taniguchi *et al.*, A resource of Cre driver lines for genetic targeting of GABAergic neurons in cerebral cortex. *Neuron* **71**, 995-1013 (2011).

107. I. Merchenthaler, M. A. Hynes, S. Vigh, A. V. Shally, P. Petrusz, Immunocytochemical localization of corticotropin releasing factor (CRF) in the rat spinal cord. *Brain Res* **275**, 373-377 (1983).

108. J. P. Gallagher, L. F. Orozco-Cabal, J. Liu, P. Shinnick-Gallagher, Synaptic physiology of central CRH system. *European journal of pharmacology* **583**, 215-225 (2008).

109. J. Vaughan *et al.*, Urocortin, a mammalian neuropeptide related to fish urotensin I and to corticotropin-releasing factor. *Nature* **378**, 287-292 (1995).

110. T. M. Reyes *et al.*, Urocortin II: a member of the corticotropin-releasing factor (CRF) neuropeptide family that is selectively bound by type 2 CRF receptors. *Proc Natl Acad Sci U S A* **98**, 2843-2848 (2001).

111. K. Lewis *et al.*, Identification of urocortin III, an additional member of the corticotropin-releasing factor (CRF) family with high affinity for the CRF2 receptor. *Proc Natl Acad Sci U S A* **98**, 7570-7575 (2001).

112. C. L. Chang, S. Y. Hsu, Ancient evolution of stress-regulating peptides in vertebrates. *Peptides* **25**, 1681-1688 (2004).

113. M. J. Endsin, O. Michalec, L. A. Manzon, D. A. Lovejoy, R. G. Manzon, CRH peptide evolution occurred in three phases: Evidence from characterizing sea lamprey CRH system members. *Gen Comp Endocrinol* **240**, 162-173 (2017).

114. B. Gaszner, V. Csernus, T. Kozicz, Urocortinergic neurons respond in a differentiated manner to various acute stressors in the Edinger-Westphal nucleus in the rat. *J Comp Neurol* **480**, 170-179 (2004).

115. J. C. Bittencourt *et al.*, Urocortin expression in rat brain: evidence against a pervasive relationship of urocortin-containing projections with targets bearing type 2 CRF receptors. *J Comp Neurol* **415**, 285-312 (1999).

116. A. Chen, A. Blount, J. Vaughan, B. Brar, W. Vale, Urocortin II gene is highly expressed in mouse skin and skeletal muscle tissues: localization, basal expression in corticotropin-releasing factor receptor (CRFR) 1- and CRFR2-null mice, and regulation by glucocorticoids. *Endocrinology* **145**, 2445-2457 (2004).

117. C. Li *et al.*, Urocortin III is expressed in pancreatic beta-cells and stimulates insulin and glucagon secretion. *Endocrinology* **144**, 3216-3224 (2003).

118. R. Chen, K. A. Lewis, M. H. Perrin, W. W. Vale, Expression cloning of a human corticotropin-releasing-factor receptor. *Proceedings of the National Academy of Sciences* **90**, 8967-8971 (1993).

119. M. Perrin *et al.*, Identification of a second corticotropin-releasing factor receptor gene and characterization of a cDNA expressed in heart. *Proceedings of the National Academy of Sciences* **92**, 2969-2973 (1995).

120. M. A. Ẓmijewski, A. T. Slominski, Emerging role of alternative splicing of CRF1 receptor in CRF signaling. *Acta biochimica Polonica* **57**, 1-13 (2010).

121. C. P. Chang, R. V. Pearse, S. O'Connell, M. G. Rosenfeld, Identification of a seven transmembrane helix receptor for corticotropin-releasing factor and sauvagine in mammalian brain. *Neuron* **11**, 1187-1195 (1993).

122. T. W. Lovenberg, D. T. Chalmers, C. Liu, E. B. De Souza, CRF2 alpha and CRF2 beta receptor mRNAs are differentially distributed between the rat central nervous system and peripheral tissues. *Endocrinology* **136**, 4139-4142 (1995).

123. B. Martin *et al.*, Class II G Protein-Coupled Receptors and Their Ligands in Neuronal Function and Protection. *Neuromolecular medicine* **7**, 3-36 (2005).

124. A. Bortolato *et al.*, Structure of Class B GPCRs: new horizons for drug discovery. *British Journal of Pharmacology* **171**, 3132-3145 (2014).

125. J. Bender *et al.*, Corticotropin-Releasing Hormone Receptor Type 1 (CRHR1) Clustering with MAGUKs Is Mediated via Its C-Terminal PDZ Binding Motif. *PLoS ONE* **10**, e0136768 (2015).

126. C. Inda *et al.*, Different cAMP sources are critically involved in G protein-coupled receptor CRHR1 signaling. *J Cell Biol* **214**, 181-195 (2016).

127. C. J. Rossant, R. D. Pinnock, J. Hughes, M. D. Hall, S. McNulty, Corticotropin-releasing factor type 1 and type 2alpha receptors regulate phosphorylation of calcium/cyclic adenosine 3',5'-monophosphate response element-binding protein and activation of p42/p44 mitogen-activated protein kinase. *Endocrinology* **140**, 1525-1536 (1999).

128. D. K. Grammatopoulos, Insights into mechanisms of corticotropin ¡releasing hormone receptor signal transduction. *British Journal of Pharmacology* **166**, 85-97 (2012).

129. F. M. Dautzenberg, R. L. Hauger, The CRF peptide family and their receptors: yet more partners discovered. *Trends Pharmacol Sci* **23**, 71-77 (2002).
130. T. Subbannayya *et al.*, An integrated map of corticotropin-releasing hormone signaling pathway. *Journal of Cell Communication and Signaling* **7**, 295-300 (2013).
131. J. Sanders, C. Nemeroff, The CRF System as a Therapeutic Target for Neuropsychiatric Disorders. *Trends Pharmacol Sci* **37**, 1045-1054 (2016).
132. R. L. Hauger *et al.*, Desensitization of human CRF2 (a) receptor signaling governed by agonist potency and βarrestin2 recruitment. *Regulatory Peptides* **186**, 62-76 (2013).
133. M. M. Hammad, H. A. Dunn, S. S. G. Ferguson, MAGI Proteins Regulate the Trafficking and Signaling of Corticotropin-Releasing Factor Receptor 1 via a Compensatory Mechanism. *Journal of Molecular Signaling* **11**, 5 (2016).
134. K. Hollenstein *et al.*, Structure of class B GPCR corticotropin-releasing factor receptor 1. *Nature* **499**, 438-443 (2013).
135. G. Ladds, K. Davis, A. Das, J. Davey, A constitutively active GPCR retains its G protein specificity and the ability to form dimers. *Molecular microbiology* **55**, 482-497 (2005).
136. S. M. Nielsen, L. Z. Nielsen, S. A. Hjorth, M. H. Perrin, W. W. Vale, Constitutive activation of tethered-peptide/ corticotropin-releasing factor receptor chimeras. *Proceedings of the National Academy of Sciences of the United States of America* **97**, 10277-10281 (2000).
137. I. Garcia *et al.*, Local CRH signaling promotes synaptogenesis and circuit integration of adult-born neurons. *Developmental cell* **30**, 645-659 (2014).
138. Y. Yin *et al.*, Rearrangement of a polar core provides a conserved mechanism for constitutive activation of class B G protein-coupled receptors. *J Biol Chem* **292**, 9865-9881 (2017).
139. D. A. Lovejoy, B. S. Chang, N. R. Lovejoy, J. del Castillo, Molecular evolution of GPCRs: CRH/CRH receptors. *J Mol Endocrinol* **52**, T43-60 (2014).
140. A. F. Seasholtz, R. A. Valverde, R. J. Denver, Corticotropin-releasing hormone-binding protein: biochemistry and function from fishes to mammals. *J Endocrinol* **175**, 89-97 (2002).
141. M. O. Huising, W. W. Vale, in *Encyclopedia of Neuroscience*. (Academic Press, Oxford, 2009), pp. 231-237.

142. L. A. Tan, J. M. Vaughan, M. H. Perrin, J. E. Rivier, P. E. Sawchenko, Distribution of corticotropin-releasing factor (CRF) receptor binding in the mouse brain using a new, high-affinity radioligand, [125 I]-PD-Sauvagine. *J Comp Neurol*, (2017).
143. A. Korosi *et al.*, Corticotropin-releasing factor, urocortin 1, and their receptors in the mouse spinal cord. *J Comp Neurol* **502**, 973-989 (2007).
144. O. Berton, E. J. Nestler, New approaches to antidepressant drug discovery: beyond monoamines. *Nat Rev Neurosci* **7**, 137-151 (2006).
145. L. Arborelius, M. J. Owens, P. M. Plotsky, C. B. Nemeroff, The role of corticotropin-releasing factor in depression and anxiety disorders. *J Endocrinol* **160**, 1-12 (1999).
146. M. E. Keck *et al.*, Combined effects of exonic polymorphisms in CRHR1 and AVPR1B genes in a case/control study for panic disorder. *Am J Med Genet B Neuropsychiatr Genet* **147b**, 1196-1204 (2008).
147. E. B. Binder *et al.*, Association of polymorphisms in genes regulating the corticotropin-releasing factor system with antidepressant treatment response. *Arch Gen Psychiatry* **67**, 369-379 (2010).
148. S. Papiol *et al.*, Genetic variability at HPA axis in major depression and clinical response to antidepressant treatment. *J Affect Disord* **104**, 83-90 (2007).
149. D. Wasserman, J. Wasserman, V. Rozanov, M. Sokolowski, Depression in suicidal males: genetic risk variants in the CRHR1 gene. *Genes Brain Behav* **8**, 72-79 (2009).
150. J. W. Smoller, The genetics of stress-related disorders: PTSD, depression, and anxiety disorders. *Neuropsychopharmacology* **41**, 297-319 (2016).
151. S. C. Heinrichs, G. F. Koob, Corticotropin-releasing factor in brain: a role in activation, arousal, and affect regulation. *J Pharmacol Exp Ther* **311**, 427-440 (2004).
152. N. Dedic *et al.*, Assessing behavioural effects of chronic HPA axis activation using conditional CRH-overexpressing mice. *Cell Mol Neurobiol* **32**, 815-828 (2012).
153. G. Liebsch, R. Landgraf, M. Engelmann, P. Lörscher, F. Holsboer, Differential behavioural effects of chronic infusion of CRH 1 and CRH 2 receptor antisense oligonucleotides into the rat brain. *J Psychiatr Res* **33**, 153-163 (1999).

154. G. Laryea, M. G. Arnett, L. J. Muglia, Behavioral Studies and Genetic Alterations in Corticotropin-Releasing Hormone (CRH) Neurocircuitry: Insights into Human Psychiatric Disorders. *Behavioral Sciences* **2**, 135-171 (2012).

155. P. Timpl *et al.*, Impaired stress response and reduced anxiety in mice lacking a functional corticotropin-releasing hormone receptor 1. *Nat Genet* **19**, 162-166 (1998).

156. G. W. Smith *et al.*, Corticotropin releasing factor receptor 1-deficient mice display decreased anxiety, impaired stress response, and aberrant neuroendocrine development. *Neuron* **20**, 1093-1102 (1998).

157. S. M. Korte, Corticosteroids in relation to fear, anxiety and psychopathology. *Neurosci Biobehav Rev* **25**, 117-142 (2001).

158. M. B. Müller *et al.*, Limbic corticotropin-releasing hormone receptor 1 mediates anxiety-related behavior and hormonal adaptation to stress. *Nat Neurosci* **6**, 1100-1107 (2003).

159. X. D. Wang *et al.*, Nectin-3 links CRHR1 signaling to stress-induced memory deficits and spine loss. *Nat Neurosci* **16**, 706-713 (2013).

160. X. D. Wang *et al.*, Forebrain CRHR1 deficiency attenuates chronic stress-induced cognitive deficits and dendritic remodeling. *Neurobiol Dis* **42**, 300-310 (2011).

161. Y. Sztainberg, Y. Kuperman, M. Tsoory, M. Lebow, A. Chen, The anxiolytic effect of environmental enrichment is mediated via amygdalar CRF receptor type 1. *Mol Psychiatry* **15**, 905-917 (2010).

162. Y. Sztainberg, Y. Kuperman, N. Justice, A. Chen, An anxiolytic role for CRF receptor type 1 in the globus pallidus. *J Neurosci* **31**, 17416-17424 (2011).

163. N. A. Chen *et al.*, Knockdown of CRF1 receptors in the ventral tegmental area attenuates cue- and acute food deprivation stress-induced cocaine seeking in mice. *J Neurosci* **34**, 11560-11570 (2014).

164. N. A. Chen *et al.*, Knockdown of corticotropin-releasing factor 1 receptors in the ventral tegmental area enhances conditioned fear. *European Neuropsychopharmacology* **26**, 1533-1540 (2016).

165. J. A. Harris *et al.*, Anatomical characterization of Cre driver mice for neural circuit mapping and manipulation. *Front Neural Circuits* **8**, 76 (2014).

166. Z. J. Huang, H. Zeng, Genetic approaches to neural circuits in the mouse. *Annu Rev Neurosci* **36**, 183-215 (2013).

167. J. Zhang *et al.*, Conditional gene manipulation: Cre-ating a new biological era. *J Zhejiang Univ Sci B* **13**, 511-524 (2012).

168. J. M. Deussing, Targeted mutagenesis tools for modelling psychiatric disorders. *Cell Tissue Res* **354**, 9-25 (2013).

169. S. A. Murray, J. T. Eppig, D. Smedley, E. M. Simpson, N. Rosenthal, Beyond knockouts: cre resources for conditional mutagenesis. *Mammalian genome : official journal of the International Mammalian Genome Society* **23**, 587-599 (2012).

170. M. Schmidt-Supprian, K. Rajewsky, Vagaries of conditional gene targeting. *Nat Immunol* **8**, 665-668 (2007).

171. E. I. Martin *et al.*, A novel transgenic mouse for gene-targeting within cells that express corticotropin-releasing factor. *Biol Psychiatry* **67**, 1212-1216 (2010).

172. G. M. Gafford *et al.*, Cell-type specific deletion of GABA (A) alpha1 in corticotropin-releasing factor-containing neurons enhances anxiety and disrupts fear extinction. *Proc Natl Acad Sci U S A* **109**, 16330-16335 (2012).

173. G. Gafford, A. M. Jasnow, K. J. Ressler, Grin1 receptor deletion within CRF neurons enhances fear memory. *PLoS One* **9**, e111009 (2014).

174. J. Sarkar, S. Wakefield, G. MacKenzie, S. J. Moss, J. Maguire, Neurosteroidogenesis is required for the physiological response to stress: role of neurosteroid-sensitive GABA (A) receptors. *The Journal of Neuroscience* **31**, 18198-18210 (2011).

175. V. Lee, J. Sarkar, J. Maguire, Loss of Gabrd in CRH neurons blunts the corticosterone response to stress and diminishes stress-related behaviors. *Psychoneuroendocrinology* **41**, 75-88 (2014).

176. J. A. Smith *et al.*, Acute hypernatremia promotes anxiolysis and attenuates stress-induced activation of the hypothalamic-pituitary-adrenal axis in male mice. *Physiol Behav* **136**, 91-96 (2014).

177. J. G. McCall *et al.*, CRH Engagement of the Locus Coeruleus Noradrenergic System Mediates Stress-Induced Anxiety. *Neuron* **87**, 605-620 (2015).

178. S. Chung *et al.*, Identification of preoptic sleep neurons using retrograde labelling and gene profiling. *Nature* **545**, 477-481 (2017).
179. M. J. Krashes *et al.*, An excitatory paraventricular nucleus to AgRP neuron circuit that drives hunger. *Nature* **507**, 238-242 (2014).
180. K. E. Pleil *et al.*, NPY signaling inhibits extended amygdala CRF neurons to suppress binge alcohol drinking. *Nat Neurosci* **18**, 545-552 (2015).
181. C. A. Marcinkiewcz *et al.*, Serotonin engages an anxiety and fear-promoting circuit in the extended amygdala. *Nature* **537**, 97-101 (2016).
182. M. B. Pomrenze *et al.*, A Transgenic Rat for Investigating the Anatomy and Function of Corticotrophin Releasing Factor Circuits. *Front Neurosci* **9**, 487 (2015).
183. Y. Shemesh *et al.*, Ucn3 and CRF-R2 in the medial amygdala regulate complex social dynamics. *Nat Neurosci* **19**, 1489-1496 (2016).
184. T. E. Anthony *et al.*, Control of stress-induced persistent anxiety by an extra-amygdala septohypothalamic circuit. *Cell* **156**, 522-536 (2014).
185. M. Henckens *et al.*, CRF receptor type 2 neurons in the posterior bed nucleus of the stria terminalis critically contribute to stress recovery. *Mol Psychiatry* **22**, 1691-1700 (2017).
186. C. Liu, Strategies for Designing Transgenic DNA Constructs. *Methods in molecular biology (Clifton, N.J.)* **1027**, 10.1007/1978-1001-60327-60369-60325_60328 (2013).
187. L. Madisen *et al.*, A robust and high-throughput Cre reporting and characterization system for the whole mouse brain. *Nat Neurosci* **13**, 133-140 (2010).
188. J. J. Nassi, C. L. Cepko, R. T. Born, K. T. Beier, Neuroanatomy goes viral! *Front Neuroanat* **9**, 80 (2015).
189. F. Zhang *et al.*, Optogenetic interrogation of neural circuits: technology for probing mammalian brain structures. *Nat Protoc* **5**, 439-456 (2010).
190. E. Sanz *et al.*, Cell-type-specific isolation of ribosome-associated mRNA from complex tissues. *Proc Natl Acad Sci U S A* **106**, 13939-13944 (2009).
191. H. Bouabe, K. Okkenhaug, Gene Targeting in Mice: a Review. *Methods in molecular biology (Clifton, N.J.)* **1064**, 315-336 (2013).

192. Femi J. Olorunniji, Susan J. Rosser, W. M. Stark, Site-specific recombinases: molecular machines for the Genetic Revolution. *Biochemical Journal* **473**, 673-684 (2016).
193. G. Belteki, M. Gertsenstein, D. W. Ow, A. Nagy, Site-specific cassette exchange and germline transmission with mouse ES cells expressing phiC31 integrase. *Nat Biotechnol* **21**, 321-324 (2003).
194. S. Delic *et al.*, Genetic mouse models for behavioral analysis through transgenic RNAi technology. *Genes Brain Behav* **7**, 821-830 (2008).
195. C.-m. Chen, J. Krohn, S. Bhattacharya, B. Davies, A Comparison of Exogenous Promoter Activity at the ROSA26 Locus Using a PhiC31 Integrase Mediated Cassette Exchange Approach in Mouse ES Cells. *PLoS ONE* **6**, e23376 (2011).
196. B. Tasic *et al.*, Site-specific integrase-mediated transgenesis in mice via pronuclear injection. *Proceedings of the National Academy of Sciences of the United States of America* **108**, 7902-7907 (2011).
197. Cheng, 523. Non-Viral Phi C31 Integrase Mediated In Vivo Gene Delivery to Adult Murine Retinal Pigment Epithelial Cells. *Molecular Therapy* 17, Supplement 1, S200 (2009).
198. E. C. Olivares *et al.*, Site-specific genomic integration produces therapeutic Factor IX levels in mice. *Nat Biotech* **20**, 1124-1128 (2002).
199. A. G. Kotini, M. Sadelain, E. P. Papapetrou, LiPS-A3S, a human genomic site for robust expression of inserted transgenes. *Molecular Therapy - Nucleic Acids* **5**, e394 (2016).
200. C. S. Branda, S. M. Dymecki, Talking about a revolution: The impact of site-specific recombinases on genetic analyses in mice. *Dev Cell* **6**, 7-28 (2004).
201. B. Sauer, J. McDermott, DNA recombination with a heterospecific Cre homolog identified from comparison of the pac-c1 regions of P1-related phages. *Nucleic Acids Res* **32**, 6086-6095 (2004).
202. K. Anastassiadis *et al.*, Dre recombinase, like Cre, is a highly efficient site-specific recombinase in E. coli, mammalian cells and mice. *Dis Model Mech* **2**, 508-515 (2009).
203. L. Madisen *et al.*, Transgenic mice for intersectional targeting of neural sensors and effectors with high specificity and performance. *Neuron* **85**, 942-958 (2015).

204. K. Chuang, E. Nguyen, Y. Sergeev, T. C. Badea, Novel Heterotypic Rox Sites for Combinatorial Dre Recombination Strategies. *G3 (Bethesda)* **6**, 559-571 (2015).

205. V. C. Janbandhu, D. Moik, R. Fässler, Cre recombinase induces DNA damage and tetraploidy in the absence of LoxP sites. *Cell Cycle* **13**, 462-470 (2014).

206. S. Feil, N. Valtcheva, R. Feil, Inducible Cre mice. *Methods Mol Biol* **530**, 343-363 (2009).

207. W. P. Devine, J. D. Wythe, M. George, K. Koshiba-Takeuchi, B. G. Bruneau, Early patterning and specification of cardiac progenitors in gastrulating mesoderm. *eLife* **3**, e03848 (2014).

208. R. Sando *et al.*, Inducible control of gene expression with destabilized Cre. *Nature methods* **10**, 1085-1088 (2013).

209. S. M. Dymecki, R. S. Ray, J. C. Kim, Mapping cell fate and function using recombinase-based intersectional strategies. *Methods Enzymol* **477**, 183-213 (2010).

210. L. E. Fenno *et al.*, INTRSECT: single-component targeting of cells using multiple-feature Boolean logic. *Nature methods* **11**, 763-772 (2014).

211. J. Hirrlinger *et al.*, Split-cre complementation indicates coincident activity of different genes in vivo. *PLoS One* **4**, e4286 (2009).

212. J. Hirrlinger *et al.*, Split-CreERT2: Temporal Control of DNA Recombination Mediated by Split-Cre Protein Fragment Complementation. *PLoS ONE* **4**, e8354 (2009).

213. P. Wang *et al.*, Intersectional Cre driver lines generated using split-intein mediated split-Cre reconstitution. *Sci Rep* **2**, 497 (2012).

214. M. Hermann *et al.*, Binary recombinase systems for high-resolution conditional mutagenesis. *Nucleic Acids Research* **42**, 3894-3907 (2014).

215. G. D. Van Duyne, Cre Recombinase. *Microbiol Spectr* **3**, Mdna3-0014-2014 (2015).

216. R. M. Quadros *et al.*, Easi-CRISPR: a robust method for one-step generation of mice carrying conditional and insertion alleles using long ssDNA donors and CRISPR ribonucleoproteins. *Genome Biology* **18**, 92 (2017).

217. D. Atasoy, Y. Aponte, H. H. Su, S. M. Sternson, A FLEX switch targets Channelrhodopsin-2 to multiple cell types for imaging and long-range circuit mapping. *J Neurosci* **28**, 7025-7030 (2008).

218. I. Dragatsis, S. Zeitlin, A method for the generation of conditional gene repair mutations in mice. *Nucleic Acids Research* **29**, e10-e10 (2001).

219. N. J. Justice, Z. F. Yuan, P. E. Sawchenko, W. Vale, Type 1 corticotropin-releasing factor receptor expression reported in BAC transgenic mice: implications for reconciling ligand-receptor mismatch in the central corticotropin-releasing factor system. *J Comp Neurol* **511**, 479-496 (2008).

220. R. Petryszak *et al.*, Expression Atlas update—an integrated database of gene and protein expression in humans, animals and plants. *Nucleic Acids Research* **44**, D746-D752 (2016).

221. J. L. Quintanar, I. Guzmán-Soto, Hypothalamic neurohormones and immune responses. *Frontiers in Integrative Neuroscience* **7**, 56 (2013).

222. S. M. Baigent, P. J. Lowry, mRNA expression profiles for corticotrophin-releasing factor (CRF), urocortin, CRF receptors and CRF-binding protein in peripheral rat tissues. *J Mol Endocrinol* **25**, 43-52 (2000).

223. K. A. Paschos *et al.*, The corticotropin releasing factor system in the liver: expression, actions and possible implications in hepatic physiology and pathology. *Hormones (Athens)* **12**, 236-245 (2013).

224. R. E. Nappi, S. Rivest, Stress-induced genetic expression of a selective corticotropin-releasing factor-receptor subtype within the rat ovaries: an effect dependent on the ovulatory cycle. *Biol Reprod* **53**, 1417-1428 (1995).

225. M. Simard, M. Cote, P. R. Provost, Y. Tremblay, Expression of genes related to the hypothalamic-pituitary-adrenal axis in murine fetal lungs in late gestation. *Reprod Biol Endocrinol* **8**, 134 (2010).

226. Y. Wu, Y. Xu, H. Zhou, J. Tao, S. Li, Expression of urocortin in rat lung and its effect on pulmonary vascular permeability. *J Endocrinol* **189**, 167-178 (2006).

227. A. Mo *et al.*, Epigenomic Signatures of Neuronal Diversity in the Mammalian Brain. *Neuron* **86**, 1369-1384 (2015).

228. G. N. Smagin, S. C. Heinrichs, A. J. Dunn, The role of CRH in behavioral responses to stress. *Peptides* **22**, 713-724 (2001).

229. Y. Chen, K. L. Brunson, M. B. Muller, W. Cariaga, T. Z. Baram, Immunocytochemical distribution of corticotropin-releasing hormone receptor type-1 (CRF(1))-like immunoreactivity in the mouse brain: light

microscopy analysis using an antibody directed against the C-terminus. *J Comp Neurol* **420**, 305-323 (2000).

230. D. F. Aschauer, S. Kreuz, S. Rumpel, Analysis of transduction efficiency, tropism and axonal transport of AAV serotypes 1, 2, 5, 6, 8 and 9 in the mouse brain. *PLoS One* **8**, e76310 (2013).
231. A. Watakabe *et al.*, Comparative analyses of adeno-associated viral vector serotypes 1, 2, 5, 8 and 9 in marmoset, mouse and macaque cerebral cortex. *Neuroscience Research* **93**, 144-157 (2015).
232. E. N. McDowell *et al.*, A transcriptome-wide screen for mRNAs enriched in fetal Leydig cells: CRHR1 agonism stimulates rat and mouse fetal testis steroidogenesis. *PLoS One* **7**, e47359 (2012).
233. J. Tao *et al.*, Separate Locations of Urocortin and its Receptors in Mouse Testis: Function in Male Reproduction and the Relevant Mechanisms. *Cellular Physiology and Biochemistry* **19**, 303-312 (2007).
234. G. Wypior, U. Jeschke, M. Kurpisz, J. Szekeres-Bartho, Expression of CRH, CRH-related peptide and CRH receptor in the ovary and potential CRH signalling pathways. *Journal of Reproductive Immunology* **90**, 67-73 (2011).
235. J. L. Cazemier, F. Clascá, P. H. E. Tiesinga, Connectomic Analysis of Brain Networks: Novel Techniques and Future Directions. *Frontiers in Neuroanatomy* **10**, 110 (2016).
236. L. Madisen *et al.*, A toolbox of Cre-dependent optogenetic transgenic mice for light-induced activation and silencing. *Nat Neurosci* **15**, 793-802 (2012).
237. F. W. Farley, P. Soriano, L. S. Steffen, S. M. Dymecki, Widespread recombinase expression using FLPeR (flipper) mice. *Genesis* **28**, 106-110 (2000).
238. F. G. Wouterlood, B. Bloem, H. D. Mansvelder, A. Luchicchi, K. Deisseroth, A fourth generation of neuroanatomical tracing techniques: Exploiting the offspring of genetic engineering. *Journal of Neuroscience Methods* **235**, 331-348 (2014).
239. A. Uribe-Mariño *et al.*, Prefrontal Cortex Corticotropin-Releasing Factor Receptor 1 Conveys Acute Stress-Induced Executive Dysfunction. *Biological Psychiatry* **80**, 743-753 (2016).

240. J. M. Tepper, F. Tecuapetla, T. Koós, O. Ibáñez-Sandoval, Heterogeneity and Diversity of Striatal GABAergic Interneurons. *Frontiers in Neuroanatomy* **4**, 150 (2010).
241. C. R. Gerfen, D. J. Surmeier, Modulation of striatal projection systems by dopamine. *Annual review of neuroscience* **34**, 441-466 (2011).
242. L. Kuan *et al.*, Neuroinformatics of the Allen Mouse Brain Connectivity Atlas. *Methods* **73**, 4-17 (2015).
243. D. Pinault, The thalamic reticular nucleus: structure, function and concept. *Brain Res Brain Res Rev* **46**, 1-31 (2004).
244. J. L. Lanciego, N. Luquin, J. A. Obeso, Functional Neuroanatomy of the Basal Ganglia. *Cold Spring Harbor Perspectives in Medicine* **2**, a009621 (2012).
245. N. Rajakumar, K. Elisevich, B. A. Flumerfelt, The pallidostriatal projection in the rat: a recurrent inhibitory loop? *Brain Research* **651**, 332-336 (1994).
246. W. R. Marchand, P. J. Bennett, D. V. Dilda, Evidence for Frontal-Subcortical Circuit Abnormalities in Bipolar Affective Disorder. *Psychiatry (Edgmont)* **2**, 26-33 (2005).
247. T. van Groen, P. Miettinen, I. Kadish, The entorhinal cortex of the mouse: organization of the projection to the hippocampal formation. *Hippocampus* **13**, 133-149 (2003).
248. A. Bjorklund, S. B. Dunnett, Dopamine neuron systems in the brain: an update. *Trends Neurosci* **30**, 194-202 (2007).
249. D. M. Vogt Weisenhorn, F. Giesert, W. Wurst, Diversity matters - heterogeneity of dopaminergic neurons in the ventral mesencephalon and its relation to Parkinson's Disease. *Journal of Neurochemistry* **139**, 8-26 (2016).
250. A. Aransay, C. Rodríguez-López, M. García-Amado, F. Clascá, L. Prensa, Long-range projection neurons of the mouse ventral tegmental area: a single-cell axon tracing analysis. *Frontiers in Neuroanatomy* **9**, (2015).
251. J. Roeper, Dissecting the diversity of midbrain dopamine neurons. *Trends in Neurosciences* **36**, 336-342 (2013).
252. S. A. Sharples, K. Koblinger, J. M. Humphreys, P. J. Whelan, Dopamine: a parallel pathway for the modulation of spinal locomotor networks. *Frontiers in Neural Circuits* **8**, 55 (2014).

253. S. Qu *et al.*, Projections of diencephalic dopamine neurons into the spinal cord in mice. *Exp Brain Res* **168**, 152-156 (2006).
254. L. Li *et al.*, Visualizing the distribution of synapses from individual neurons in the mouse brain. *PLoS One* **5**, e11503 (2010).
255. J. F. Lopez, H. Akil, S. J. Watson, Neural circuits mediating stress. *Biol Psychiatry* **46**, 1461-1471 (1999).
256. D. Chaudhury, H. Liu, M.-H. Han, Neuronal Correlates of Depression. *Cellular and molecular life sciences : CMLS* **72**, 4825-4848 (2015).
257. J. J. Walsh, M. H. Han, THE HETEROGENEITY OF VENTRAL TEGMENTAL AREA NEURONS: PROJECTION FUNCTIONS IN A MOOD-RELATED CONTEXT. *Neuroscience* **282**, 101-108 (2014).
258. L. E. Trudeau *et al.*, The multilingual nature of dopamine neurons. *Prog Brain Res* **211**, 141-164 (2014).
259. G. D. Stuber, A. M. Stamatakis, P. A. Kantak, Considerations when using cre-driver rodent lines for studying ventral tegmental area circuitry. *Neuron* **85**, 439-445 (2015).
260. S. Lammel *et al.*, Unique Properties of Mesoprefrontal Neurons within a Dual Mesocorticolimbic Dopamine System. *Neuron* **57**, 760-773 (2008).
261. J. H. Jennings, G. D. Stuber, Tools for resolving functional activity and connectivity within intact neural circuits. *Curr Biol* **24**, R41-50 (2014).
262. G. Miyoshi, G. Fishell, Directing neuron-specific transgene expression in the mouse CNS. *Curr Opin Neurobiol* **16**, 577-584 (2006).
263. H. Mizuguchi, Z. Xu, A. Ishii-Watabe, E. Uchida, T. Hayakawa, IRES-dependent second gene expression is significantly lower than cap-dependent first gene expression in a bicistronic vector. *Mol Ther* **1**, 376-382 (2000).
264. R. Gerlai, Gene Targeting Using Homologous Recombination in Embryonic Stem Cells: The Future for Behavior Genetics? *Frontiers in Genetics* **7**, 43 (2016).
265. M. Osterwalder *et al.*, Dual RMCE for efficient re-engineering of mouse mutant alleles. *Nat Meth* **7**, 893-895 (2010).
266. M. Heidenreich, F. Zhang, Applications of CRISPR-Cas systems in neuroscience. *Nat Rev Neurosci* **17**, 36-44 (2016).

267. A. F. Eisener-Dorman, D. A. Lawrence, V. J. Bolivar, Cautionary Insights on Knockout Mouse Studies: The Gene or Not the Gene? *Brain, behavior, and immunity* **23**, 318-324 (2009).
268. R. Peng, G. Lin, J. Li, Potential pitfalls of CRISPR/Cas9-mediated genome editing. *Febs j* **283**, 1218-1231 (2016).
269. Y. Hasegawa *et al.*, Generation of CRISPR/Cas9-mediated bicistronic knock-in ins1-cre driver mice. *Exp Anim* **65**, 319-327 (2016).
270. L. E. Dow, Modeling disease in vivo with CRISPR/Cas9. *Trends in molecular medicine* **21**, 609-621 (2015).
271. W. M. Stark, Making serine integrases work for us. *Current Opinion in Microbiology* **38**, 130-136 (2017).
272. K. Rutherford, G. D. Van Duyne, The ins and outs of serine integrase site-specific recombination. *Current Opinion in Structural Biology* **24**, 125-131 (2014).
273. F. Schnutgen, A. F. Stewart, H. von Melchner, K. Anastassiadis, Engineering embryonic stem cells with recombinase systems. *Methods Enzymol* **420**, 100-136 (2006).
274. L. Ringrose, S. Chabanis, P. O. Angrand, C. Woodroofe, A. F. Stewart, Quantitative comparison of DNA looping in vitro and in vivo: chromatin increases effective DNA flexibility at short distances. *Embo j* **18**, 6630-6641 (1999).
275. L. Ringrose *et al.*, Comparative kinetic analysis of FLP and cre recombinases: mathematical models for DNA binding and recombination. *Journal of Molecular Biology* **284**, 363-384 (1998).
276. S. L. P. Schilit, M. Ohtsuka, R. Quadros, C. B. Gurumurthy, Pronuclear Injection-based Targeted Transgenesis. *Current protocols in human genetics* **91**, 15.10.11-15.10.28 (2016).
277. L. Huang *et al.*, RNA Homeostasis Governed by Cell Type-Specific and Branched Feedback Loops Acting on NMD. *Molecular cell* **43**, 950-961 (2011).
278. R. Kuhn, F. Schwenk, Conditional knockout mice. *Methods Mol Biol* **209**, 159-185 (2003).
279. C. I. Rodriguez *et al.*, High-efficiency deleter mice show that FLPe is an alternative to Cre-loxP. *Nat Genet* **25**, 139-140 (2000).

280. L. Smith, Good planning and serendipity: exploiting the Cre/Lox system in the testis. *Reproduction* **141**, 151-161 (2011).

281. M. A. Magnuson, A. B. Osipovich, Pancreas-specific Cre driver lines and considerations for their prudent use. *Cell Metab* **18**, 9-20 (2013).

282. N. J. Dora, J. M. Collinson, R. E. Hill, J. D. West, Hemizygous Le-Cre transgenic mice have severe eye abnormalities on some genetic backgrounds in the absence of LoxP sites. *PLoS One* **9**, e109193 (2014).

283. C. S. Heffner *et al.*, Supporting conditional mouse mutagenesis with a comprehensive cre characterization resource. *Nature Communications* **3**, 1218 (2012).

284. E. Harno, Elizabeth C. Cottrell, A. White, Metabolic Pitfalls of CNS Cre-Based Technology. *Cell Metabolism* **18**, 21-28 (2013).

285. F. Gofflot *et al.*, in *Current Protocols in Mouse Biology*. (John Wiley & Sons, Inc., 2011).

286. C. Gregg, Known unknowns for allele-specific expression and genomic imprinting effects. *F1000Prime Reports* **6**, 75 (2014).

287. K. Yamasaki *et al.*, Neurons but not glial cells show reciprocal imprinting of sense and antisense transcripts of Ube3a. *Hum Mol Genet* **12**, 837-847 (2003).

288. L. S. Wilkinson, W. Davies, A. R. Isles, Genomic imprinting effects on brain development and function. *Nat Rev Neurosci* **8**, 832-843 (2007).

289. A. V. Gendrel *et al.*, Developmental dynamics and disease potential of random monoallelic gene expression. *Dev Cell* **28**, 366-380 (2014).

290. D. Kawaguchi, S. Sahara, A. Zembrzycki, D. D. M. O ¸ Leary, Generation and analysis of an improved Foxg1-IRES-Cre driver mouse line. *Developmental Biology* **412**, 139-147 (2016).

291. J. D. Perez *et al.*, Quantitative and functional interrogation of parent-of-origin allelic expression biases in the brain. *Elife* **4**, e07860 (2015).

292. Paul J. Bonthuis *et al.*, Noncanonical Genomic Imprinting Effects in Offspring. *Cell Reports* **12**, 979-991 (2015).

293. D. P. Barlow, M. S. Bartolomei, Genomic imprinting in mammals. *Cold Spring Harb Perspect Biol* **6**, (2014).

294. S. Hayashi, A. P. McMahon, Efficient recombination in diverse tissues by a tamoxifen-inducible form of Cre: a tool for temporally regulated gene activation/inactivation in the mouse. *Dev Biol* **244**, 305-318 (2002).

295. J. Liu *et al.*, Non-parallel recombination limits Cre-LoxP-based reporters as precise indicators of conditional genetic manipulation. *Genesis* **51**, 436-442 (2013).

296. H. Y. Chan *et al.*, Comparison of IRES and F2A-Based Locus-Specific Multicistronic Expression in Stable Mouse Lines. *PLoS ONE* **6**, e28885 (2011).

297. G. Trichas, J. Begbie, S. Srinivas, Use of the viral 2A peptide for bicistronic expression in transgenic mice. *BMC Biology* **6**, 40 (2008).

298. G. Milligan, Exploring the dynamics of regulation of G protein-coupled receptors using green fluorescent protein. *British Journal of Pharmacology* **128**, 501-510 (1999).

299. G. A. Luke, *Translating 2A Research Into Practice*. (INTECH Open Access Publisher, 2012).

300. T. Rotolo, P. M. Smallwood, J. Williams, J. Nathans, Genetically-Directed, Cell Type-Specific Sparse Labeling for the Analysis of Neuronal Morphology. *PLoS ONE* **3**, e4099 (2008).

301. T. C. Badea *et al.*, New mouse lines for the analysis of neuronal morphology using CreER (T)/loxP-directed sparse labeling. *PLoS One* **4**, e7859 (2009).

302. D. A. Fortin *et al.*, Live Imaging of Endogenous PSD-95 Using ENABLED: A Conditional Strategy to Fluorescently Label Endogenous Proteins. *The Journal of Neuroscience* **34**, 16698-16712 (2014).

303. G. Aguilera, M. Nikodemova, P. C. Wynn, K. J. Catt, Corticotropin releasing hormone receptors: two decades later. *Peptides* **25**, 319-329 (2004).

304. D. M. Juriloff *et al.*, Investigations of the genomic region that contains the clf1 mutation, a causal gene in multifactorial cleft lip and palate in mice. *Birth Defects Res A Clin Mol Teratol* **73**, 103-113 (2005).

305. A. Ramot *et al.*, Hypothalamic CRFR1 is essential for HPA axis regulation following chronic stress. *Nat Neurosci* **20**, 385-388 (2017).

306. D. T. Chalmers, T. W. Lovenberg, E. B. De Souza, Localization of novel corticotropin-releasing factor receptor (CRF2) mRNA expression to specific

subcortical nuclei in rat brain: comparison with CRF1 receptor mRNA expression. *J Neurosci* **15**, 6340-6350 (1995).

307. M. B. Muller *et al.*, Expression of CRHR1 and CRHR2 in mouse pituitary and adrenal gland: implications for HPA system regulation. *Endocrinology* **142**, 4150-4153 (2001).
308. C. Tsatsanis *et al.*, The corticotropin-releasing factor (CRF) family of peptides as local modulators of adrenal function. *Cell Mol Life Sci* **64**, 1638-1655 (2007).
309. S. P. Chang, J. J. Mullins, S. D. Morley, J. D. West, Transition from organogenesis to stem cell maintenance in the mouse adrenal cortex. *Organogenesis* **7**, 267-280 (2011).
310. M. A. Bruce, D. M. Griffith, R. J. Thorpe, Stress and the Kidney. *Advances in chronic kidney disease* **22**, 46-53 (2015).
311. E. L. Webster, D. E. Tracey, M. A. Jutila, S. A. Wolfe, Jr., E. B. De Souza, Corticotropin-releasing factor receptors in mouse spleen: identification of receptor-bearing cells as resident macrophages. *Endocrinology* **127**, 440-452 (1990).
312. M. Radulovic, F. M. Dautzenberg, S. Sydow, J. Radulovic, J. Spiess, Corticotropin-Releasing Factor Receptor 1 in Mouse Spleen: Expression After Immune Stimulation and Identification of Receptor-Bearing Cells. *The Journal of Immunology* **162**, 3013-3021 (1999).
313. T. Audhya, R. Jain, C. S. Hollander, Receptor-mediated immunomodulation by corticotropin-releasing factor. *Cellular Immunology* **134**, 77-84 (1991).
314. S. Mousa, C. P Bopaiah, C. Stein, M. Schaefer, *Involvement of corticotropin-releasing hormone receptor subtypes 1 and 2 in peripheral opioid-mediated inhibition of inflammatory pain*. (2004), vol. 106, pp. 297-307.
315. A. N. McEvoy, B. Bresnihan, O. FitzGerald, E. P. Murphy, Corticotropin-releasing hormone signaling in synovial tissue from patients with early inflammatory arthritis is mediated by the type 1 alpha corticotropin-releasing hormone receptor. *Arthritis Rheum* **44**, 1761-1767 (2001).
316. P. Feng *et al.*, Immune Cells of the Human Peripheral Taste System: Dominant Dendritic Cells and CD4 T-Cells. *Brain, behavior, and immunity* **23**, 760-766 (2009).

317. P. Feng *et al.*, Interleukin-10 Is Produced by a Specific Subset of Taste Receptor Cells and Critical for Maintaining Structural Integrity of Mouse Taste Buds. *The Journal of Neuroscience* **34**, 2689-2701 (2014).

318. R. Pabst, T. Tschernig, Lymphocytes in the lung: an often neglected cell. Numbers, characterization and compartmentalization. *Anat Embryol (Berl)* **192**, 293-299 (1995).

319. P.-Q. Yuan *et al.*, Expression of corticotropin releasing factor receptor type 1 (CRF (1)) in the human gastrointestinal tract and upregulation in the colonic mucosa in patients with ulcerative colitis. *Peptides* **38**, 62-69 (2012).

320. C. Porcher, A. Juhem, A. Peinnequin, V. Sinniger, B. Bonaz, Expression and effects of metabotropic CRF1 and CRF2 receptors in rat small intestine. *Am J Physiol Gastrointest Liver Physiol* **288**, G1091-1103 (2005).

321. G. E. Hodes, C. Ménard, S. J. Russo, Integrating Interleukin-6 into depression diagnosis and treatment. *Neurobiology of Stress* **4**, 15-22 (2016).

322. B. E. Leonard, The concept of depression as a dysfunction of the immune system. *Current immunology reviews* **6**, 205-212 (2010).

323. M. Nezi, G. Mastorakos, Z. Mouslech, in *Endotext,* L. J. De Groot *et al.*, Eds. (MDText.com, Inc., South Dartmouth (MA), 2000).

324. Y. Sun, S. F. Grieco, T. C. Holmes, X. Xu, Local and Long-Range Circuit Connections to Hilar Mossy Cells in the Dentate Gyrus. *eNeuro* **4**, (2017).

325. S. Jinde, V. Zsiros, K. Nakazawa, Hilar mossy cell circuitry controlling dentate granule cell excitability. *Frontiers in Neural Circuits* **7**, 14 (2013).

326. S. Willadt, M. Canepari, P. Yan, L. M. Loew, K. E. Vogt, Combined optogenetics and voltage sensitive dye imaging at single cell resolution. *Frontiers in Cellular Neuroscience* **8**, 311 (2014).

327. N. B. Danielson *et al.*, In Vivo Imaging of Dentate Gyrus Mossy Cells in Behaving Mice. *Neuron* **93**, 552-559.e554 (2017).

328. N. Tamamaki, K. Nakamura, T. Furuta, K. Asamoto, T. Kaneko, Neurons in Golgi-stain-like images revealed by GFP-adenovirus infection in vivo. *Neurosci Res* **38**, 231-236 (2000).

329. T. Furuta *et al.*, In vivo transduction of central neurons using recombinant Sindbis virus: Golgi-like labeling of dendrites and axons with membrane-targeted fluorescent proteins. *J Histochem Cytochem* **49**, 1497-1508 (2001).

330. N. Kataoka, H. Hioki, T. Kaneko, K. Nakamura, Psychological stress activates a dorsomedial hypothalamus-medullary raphe circuit driving brown adipose tissue thermogenesis and hyperthermia. *Cell Metab* **20**, 346-358 (2014).
331. A. V. Kravitz, K. Devarakonda, A. C. Kreitzer, in *Handbook of Behavioral Neuroscience,* H. Steiner, K. Y. Tseng, Eds. (Elsevier, 2017), vol. 24, pp. 689-706.
332. W. R. Marchand *et al.*, Aberrant functional connectivity of cortico-basal ganglia circuits in major depression. *Neuroscience Letters* **514**, 86-90 (2012).
333. B. Zięba *et al.*, The behavioural and electrophysiological effects of CRF in rat frontal cortex. *Neuropeptides* **42**, 513-523 (2008).
334. J. I. Kim *et al.*, Aldehyde dehydrogenase 1a1 mediates a GABA synthesis pathway in midbrain dopaminergic neurons. *Science* **350**, 102-106 (2015).
335. N. X. Tritsch, W. J. Oh, C. Gu, B. L. Sabatini, Midbrain dopamine neurons sustain inhibitory transmission using plasma membrane uptake of GABA, not synthesis. *Elife* **3**, e01936 (2014).
336. J. H. Jennings *et al.*, Distinct extended amygdala circuits for divergent motivational states. *Nature* **496**, 224-228 (2013).
337. A. Adhikari, Distributed circuits underlying anxiety. *Frontiers in Behavioral Neuroscience* **8**, 112 (2014).
338. D. F. Cardozo Pinto, S. Lammel, Viral vector strategies for investigating midbrain dopamine circuits underlying motivated behaviors. *Pharmacol Biochem Behav*, (2017).
339. S. Gong *et al.*, A gene expression atlas of the central nervous system based on bacterial artificial chromosomes. *Nature* **425**, 917-925 (2003).

11 Appendix

11.1 Buffers and Solutions

With some exceptions (indicated) all reagents were purchased from Sigma-Aldrich (Taufkirchen, Germany), Roche Life Science (Mannheim, Germany), Carl Roth (Karlsruhe, Germany), Merck Millipore (Darmstadt, Germany) and prepared using purified water (H_2O_{bidest}).

Tris acetate EDTA (TAE) buffer

4.84g TRIS
1.142ml acetic acid
20ml 0.5M EDTA, pH 8.0
800ml H_2O
adjust pH to 8.3 with acetic acid, adjust volume to 1 liter with H_2O_{bidest}

6x DNA Loading buffer Orange

1g Orange G
10ml 2M Tris/HCL, pH 7.5
150ml glycerol
adjust volume to 1 liter with H_2O_{bidest}

1x Phosphate buffered saline (PBS)

137mM NaCl
2.7mM KCl
20mM Na_2HPO_4
2mM KH_2PO_4
adjust to pH 7.4, adjust volume to 1 liter with H_2O_{bidest}

RNase free water (DEPC-H_2O)

1 liter H_2O_{bidest}
add 1ml diethylpyrocarbonate (DEPC) and shake well
incubate overnight (ON)/room temperature(RT) (lid unscrewed); autoclave twice

20x Saline Sodium Citrate (SSC)

3M NaCl
0.3M sodium citrate
adjust to pH 7.4 with 1M HCL, adjust volume to 1 liter with H_2O_{bidest}

0.2M Hydrogen chloride (HCL), RNase free for ISH

492ml DEPC-H_20
add 8ml 37% HCL

10x Phosphate buffered saline (PBS), RNase free for ISH

1.37M NaCl
27mM KCl
200mM Na_2HPO_4
20mM KH_2PO_4
adjust to pH 7.4
adjust volume to 1 liter with H_2O_{bidest}
add 1ml DEPC/liter, incubate ON/RT (lid unscrewed); autoclave twice

10x Triethanolamine (TEA)

1M TEA, pH 8.0
adjust volume to 1 liter with H_2O_{bidest}
add 1ml DEPC/liter, incubate ON/RT (lid unscrewed); autoclave twice

20% Paraformaldehyde (PFA), RNase free for ISH

20% w/v PFA
dissolve in 1x PBS under constant stirring (hood)
adjust to pH 7.4

5M Dithiothreitol (DTT), RNase free for ISH

7.715g DTT
4ml DEPC-H_2O_{bidest}
dissolve under constant shaking until powder is nearly solved
adjust volume to 10ml with DEPC-$H_2O_{bidest;}$ aliquot and store at -20°C

0.5M Ethylendiamintetraacetic acid (EDTA

186.1g Na_2EDTA
add 800ml H_2O_{bidest}
adjust to pH 8.0 with NaOH
adjust volume to 1 liter with H_2O_{bidest}
stir vigorously on a magnetic stirrer
sterilize by autoclaving; store at room temperature

3M Ammonium acetate (NH_4OAc)

49.22g NH_4OAc
adjust volume to 100ml with H_2O_{bidest}
adjust to pH 5.2 with glacial acetic acid
adjust volume to 200ml with H_2O_{bidest}
sterilize by autoclaving; store at 4°C

dNTP-Mix

10mM of each deoxynucleoside triphosphate (dATP, dCTP, dGTP, dTTP)

NEN-TNB blocking buffer

0.5% blocking reagent (NEL700A Kit; Perkin Elmer)
dissolve in 1x TNT buffer

5x NTE

146.1g NaCl
50ml 1M TRIS/HCL, pH 8
50ml 0.5M EDTA, pH 8
adjust volume to 1 liter with H_2O_{bidest}
add 1ml DEPC/liter, incubate ON/RT (lid unscrewed); autoclave twice

1x TNT

0.1M TRIS/HCL
0.15M NaCl
0.05% Tween 20
adjust volume to 800ml with $H_2O_{bidest;}$ adjust to pH 7.6
adjust volume to 1 liter with H_2O_{bidest}

***LacZ* fix (for *LacZ* staining)**

4% PFA/PBS, pH 7.4 (dilute the 20% PFA/PBS)
0.005M EGTA (dilute the 0.1M stock solution)
0.001M $MgCl_2$ (dilute the 1M stock solution)

***LacZ* wash buffer**

0.002M $MgCl_2$ (dilute the 1M stock solution)
0.01% deoxycholate (dilute the 5% stock solution)
0.02% NP40 (dilute the 10% stock solution)
PBS, pH 7.4

***LacZ* stain**

0.1% X-Gal (Stock-solution in DMF)
0.005M potassium-ferrocyanide
0.005M potassium-ferricyanide
diluted in lacZ wash buffer
Prepare fresh: for 120ml: solve completely 120mg X-Gal + 4ml DMF in glassware and give this dropwise to the ferro-/ferricyanide-lacZ-wash-solution

Chamber fluid for ISH incubation chambers

250ml Formamide
50ml 20x SSC
200ml H_2O_{bidest}

Hybridization mix for *in situ* Hybridization (ISH)

50ml Formamide (final concentration 50%)
1ml 2M Tris/HCL, pH 8 (final concentration 20mM)
1.775g NaCl (final concentration 300mM)
1ml 0.5M EDTA, pH 8 (final concentration 5mM)
10g dextran sulphate (final concentration 10%)
0.02g Ficoll 400 (final concentration 0.02%)
0.02g Polyvinylpyrrolidone 40 (PVP 40; final concentration 0.02%)
0.02 g Bovine Serum Albumin (BSA; final concentration 0.02%)
5ml tRNA (10mg/ml)
1ml Salmon Sperm (10mg/ml)
4ml 5M DTT (final concentration 200mM)
aliquot and store at -80°C

Lysogeny Broth (LB Medium)

10g Bacto-Tryptone
5g Bacto-Yeast extract
10g NaCl
adjust to 800ml with H_2O_{bidest}
adjust to pH 7.5 with NaOH
adjust volume to 1000ml with H_2O_{bidest}
sterilize by autoclaving, store at 4°C

LB Agar

10g Bacto-Tryptone
5g Bacto-Yeast extract
10g NaCl
adjust to 800ml with H_2O_{bidest}
adjust to pH 7.5 with NaOH
add 15g Agar, adjust volume to 1000ml with H_2O_{bidest}
sterilize by autoclaving, store at 4°C

Ampicillin/Kanamycin

100mg/ml salt in 75% Ethanol (storage -20°C)

Culture medium for embryonic stem (ES) cells

500ml Dulbecco's Modified Eagle Medium (DMEM)
75ml Fetal Calf Serum (FCS, heat inactivated 56°C/30minutes)
1ml β-Mercaptoethanol (50mM)
5ml L-Glutamine (200mM)
5ml non-essential amino acids (100x MEM)
90µl Leukaemia Inhibitory Factor (LIF10^7U/ml)

Culture medium for feeder cells

500ml Dulbecco's Modified Eagle Medium (DMEM)
50ml Fetal Calf Serum (FCS, heat inactivated 56°C/30minutes)
5ml L-Glutamine (200mM)
6ml non-essential amino acids (100x MEM)

2x Freezing medium for feeder and ES cells

3ml DMEM
5ml FCS
2ml Dimethylsulfoxid (DMSO)

Lysis buffer for ES cells

5ml 1M Tris HCL
10ml 0.5M EDTA
1ml 5M NaCl
12.5ml 20% N-Lauroylsarcosine
prior to use: add 0.6ml Proteinase K (20mg/ml)/12ml buffer

Precipitation mix for isolation of genomic DNA from ES cells

10ml cold 100% Ethanol
0.15ml 5M NaCl

Cryoprotection solution

125ml Glycerin
125ml Ethylenglycol
250ml 1xPBS

12 Acknowledgments

I am very grateful to Prof. Dr. Alon Chen for giving me the opportunity to realize my doctoral thesis in his department.

I would also like to express my very special thanks to Prof. Dr. Kaspar Matiasek for supervising my thesis.

Above all, I want to express my deepest gratitude to Dr. Jan Deussing. It was him who shared his profound knowledge and expertise about molecular biology and mouse genetics with me. Without his support and patience, it would not have been possible for me to realize this thesis.

A heartful gratitude also goes to Dr. Nina Dedic. Thank you for all your help in the past years and especially the successful cooperation regarding our joint paper.

I am also greatly indebted to the following members of our laboratory: Dr. Rosa Eva Hüttl, Dr. Mira Jakovcevski and Anna Mederer for help with the virus-studies; Dr. Martin Ableitner and Max Pöhlmann for assistance with the behavioral experiments.

My gratitude also goes to all our collaborators: Dr. Ralf Kühn and the IDG mouse facility staff (for the provision of ES cells and EMFI feeder cells and for blastocyst injections); Dr. Valery Grinevich and Dr. Arenkiel for adenovirus preparations and plasmid supply.

My warm thanks for technical assistance go to all technicians within the department Chen: Carola Eggert, Cornelia Flachskamm, Maria Holzapfel, Markus Nußbaumer, Andrea Parl, Andrea Reßle, Marcel Schieven, Bianca Schmid, Rainer Stoffel, Lisa Tietze and furthermore to all members of the animal facility and to the technical personnel of the institute. My special thanks go to Daniela Harbich for the constructive and collegial cooperation. In addition, I would especially like to thank all the colleagues that I have had the pleasure to work with from the very beginning: Stephanie Alam, Sabrina Bauer, Steffi Unkmeir and Barbara Wölfel.

I want to express special thanks to Tanja Siart for her encouragement and friendship over the years.

Finally, I would like to thank my parents for their continuous support, constant faith and love.